

POLITECNICO DI TORINO

Department of Mechanical and Aerospace Engineering

MSc Thesis
in Automotive Engineering

Finite Element Simulation of Impact of Autonomous Vehicle with Human Body Model in Out-of-Position Configuration



**POLITECNICO
DI TORINO**

Tutors

Prof. Eng. Giovanni Belingardi

Prof. Eng. Alessandro Scattina

Eng. Francesco Cappellino

Candidate

Filippo Germanetti

December 2019

Index

INDEX	5
PREFACE	9
THESIS INTRODUCTION	9
CHAPTER 1	11
HUMAN BODY MODELS (HBMs)	11
1.1 SCENARIO	11
1.1.1 Time History of Human Body Models	12
1.2 TOTAL HUMAN MODEL FOR SAFETY (THUMS)	14
1.2.1 THUMS Version 1.0	15
1.2.2 THUMS Advances in 2002-2005: THUMS Version 1.x and Version 2.0 ^[4]	17
1.2.3 THUMS Advances in 2007	20
1.2.4 THUMS Version 3.0	22
1.2.5 THUMS Version 4.0	22
1.2.6 THUMS Version 5.0 ^{[8][9]}	36
1.2.7 THUMS Version 6.0 ^[12]	41
1.3 GLOBAL HUMAN BODY MODELS CONSORTIUM (GHBMC) ^[13, 14]	43
1.4 VIRTUAL VEHICLE-SAFETY ASSESSMENT PROJECT (ViVA) ^[15, 16, 17]	46
1.4.1 ViVa Model – The development	47
1.4.2 ViVa Model II – Advances in 2018	48
1.5 HUMOS HBM ^[20, 21]	49
1.5.1 HUMOS FE model	49
1.5.2 HUMOS2 FE model	51
CHAPTER 2	53
OCCUPANTS’ POSTURE IN AUTONOMOUS VEHICLES (AVs)	53
2.1 AUTONOMOUS VEHICLES DEVELOPMENT ^[22, 23, 24, 25]	53
2.1.1 Automation Levels ^[30]	54
2.1.2 Autonomous Vehicles challenges - Safety and security ^[24]	57
2.2 DRIVER BEHAVIOUR DURING HIGHLY AUTOMATED DRIVING	58
2.2.1 Driving and non-driving related tasks and postures ^[31, 32, 35]	58
2.2.2 Future seating positions in Highly Automated Vehicles ^[35, 36]	63
CHAPTER 3	65
VEHICLE MODEL AND THUMS HBM POSITIONING	65
3.1 VEHICLE MODEL	65
3.2 THESIS WORK ROADMAP	69
3.3 ORIGINAL THUMS OCCUPANT MODEL AND POSITIONING TOOL ^[37]	70
3.3.1 Scaling and Positioning of the HBM Model – the PIPER Tool ^[37, 38]	71
3.3.2 PIPER Tool – Advantages, disadvantages and considerations	74

CHAPTER 4	77
SIMULATIONS SET-UP: CONVENTIONAL DRIVING AND OUT-OF-POSITION CONFIGURATIONS	77
4.1 THUMS POSITIONED FE MODEL IN CONVENTIONAL DRIVING POSTURE	77
4.2 THUMS POSITIONED FE MODEL IN OUT-OF-POSITION (OOP) CONFIGURATION.....	80
4.2.1 Investigation of the possible THUMS Out-of-Position Postures.....	80
4.2.2 THUMS OOP configuration – Positioned FE model.....	83
4.3 THUMS MODEL - ADDITIONAL FE COMPONENTS	85
4.3.1 Creation of the THUMS model footprint on the undeformed FE vehicle seat	85
4.3.2 Creation of the THUMS shoe soles	87
4.3.3 Creation of the THUMS Seatbelt.....	90
4.3.4 Implementation of the central tunnel FE component in the vehicle model	93
4.4 SIMULATION SET UP – HBM IMPLEMENTED SENSORS.....	95
4.4.1 THUMS Positioned model – first version of sensors	95
4.4.2 THUMS Positioned model – Sensors improvement.....	98
4.4.3 THUMS Positioned model – Sensors implemented in the impact simulations	103
4.5 INJURY CRITERIA (IC) DESCRIPTION	104
4.5.1 Head Injury Criteria (HIC) ^[43]	104
4.5.2 Brain Injury Criteria (BrIC) ^[44]	105
4.5.3 Tibia Index (TI) ^[45]	105
CHAPTER 5	107
THUMS IN CONVENTIONAL DRIVING POSTURE - IMPACT TEST SIMULATIONS RESULTS....	107
5.1 IMPACT TESTS DESCRIPTION.....	107
5.2 THUMS IN CONVENTIONAL DRIVING POSTURE	108
5.2.1 Results of the THUMS impact simulations and comparison with the THOR dummy FE model - Full Width Rigid Barrier (FWRB) Impact case.....	109
5.2.2 Results of the THUMS impact simulations and comparison with the THOR dummy FE model – Offset Deformable Barrier (ODB) Impact case	127
CHAPTER 6	145
THUMS IN OUT-OF-POSITION CONFIGURATION - IMPACT TEST SIMULATIONS RESULTS ...	145
6.1 THUMS IN OUT-OF-POSITION CONFIGURATION	145
6.2 RESULTS OF THE THUMS OOP AND COMPARISON WITH THE HBM IN CONVENTIONAL DRIVING POSTURE - FULL WIDTH RIGID BARRIER (FWRB) IMPACT CASE	146
6.3 RESULTS OF THE THUMS OOP AND COMPARISON WITH THE HBM IN CONVENTIONAL DRIVING POSTURE – OFFSET DEFORMABLE BARRIER (ODB) IMPACT CASE.....	162
THESIS FINAL CONSIDERATIONS	179
APPENDIX A	181
SIGNALS FILTERING - SAE FILTER J211, MAR 1995 ^[48]	181
BIBLIOGRAPHY	183

Preface

Thesis Introduction

The aims of this Thesis work, done in collaboration with the Centro Ricerche Fiat (CRF) – an FCA Company - are the following:

- To investigate the opportunities opened by the use of the Human Body Models (HBMs) for the occupant protection evaluation and to analyze the occupant behavior and response in crashes for a Level 3 Autonomous Vehicle, both in standard driving and in Out-of-Position (OOP) configurations
- To highlight the differences and the advantages/disadvantages in the use of HBMs for occupant protection with respect to the traditional crash dummy models
- To identify and draw up the main possible guidelines for the operational use of HBMs within occupant protection numerical simulations

In particular, the Finite Element Human Body Model used in this work to represent the vehicle occupant is the Total HUMAN Model for Safety (THUMS) 4.02 Academic Version (Figure 0.0), developed by Toyota Motor Corporation (Toyota Central R&D Labs. Inc.) and available at Politecnico di Torino. The results of the conventional driving posture simulations are compared with the ones of the traditional THOR dummy, whose data were delivered by the CRF.

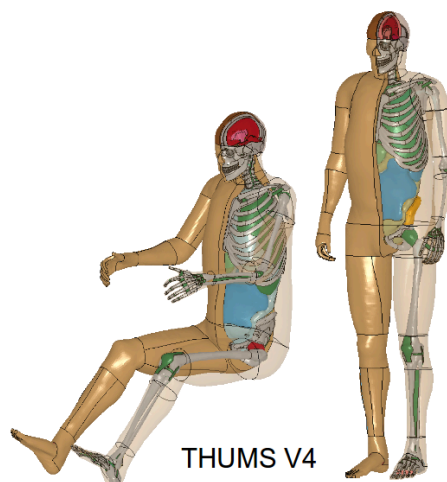


Figure 0.0. FE Models - THUMS V.4.02 – occupant (left) and pedestrian (right)

The vehicle used in the simulations (Jeep Renegade®) consists in a simplified model, and it is supposed to be equipped with the technologies enabling the Level 3 Autonomous Driving.

Moreover, two different frontal impacts were considered in the analyses: Full Width Rigid Barrier (FWRB) and Offset Deformable Barrier (ODB).

The first chapter is thought to be a summary of the Human Body Models actual State of the Art, and it contains a detailed description of their main features.

In the second chapter, entitled “Occupants’ posture in Autonomous Vehicles (AVs)”, the description of the different Autonomous Driving SAE levels is found, together with the presentations of some studies regarding the possible future innovations of the vehicle environment.

In Chapter 3, the vehicle model used in the simulations is reported and described. In addition, the positioning phases of the used THUMS HBM are there explained.

The proper simulation set-up, needed to achieve the desired results, is instead reported in Chapter 4. Great attention is given to the different sensors implemented in the HBM.

The results of this Thesis work are shown in Chapters 5 and 6. In particular, the former contains the results of the simulations involving the THUMS in conventional driving posture and their comparison with the traditional THOR dummy, while the latter includes the results obtained from the OOP simulations and a comparison with the THUMS in standard driving configuration.

Chapter 1

Human Body Models (HBMs)

1.1 Scenario

In order to reduce the number of casualties in real-world road accidents, it is necessary to investigate every possible situation through accident reconstruction (e.g. analysing impact speed, impact angle, etc.). This approach, however, is not always enough to deeply understand the relationship between accident situations and occupant injuries.

Over the last century, human surrogates such as volunteers or cadaver tests, crash dummies and computer simulations have been exploited to analyse the occupant's response in traffic accidents.

Even if crash dummies are accurate anthropomorphic test devices used to evaluate crash safety measures for vehicles, they are built for repeated use and they show different response with respect to the real human body. For these reasons, human modelling approach using the Finite Element (FE) method was introduced and it is now being adopted in different disciplines. In particular, for what the automotive field is considered, even if Human Body Models (HBMs) are still not expected to be employed in homologation tests, the number of carmakers studying them is nowadays increasing. Moreover, HBMs will be likely to be introduced in the near future in EuroNCAP® rating tests.

Many researchers developed FE models of each human body part, representing the real human anatomy by means of simplified or detailed structures. Moreover, since many and various inputs may often cause multiple injuries to several body parts, especially in fatal accidents, it is necessary and important to simulate both the gross motion and the overall multiple injuries of the whole human body at the same time.

The main purposes in the development of real Human Body Models can be related, therefore, to the injury's investigation and locations of bone fractures during impacts and to the effect of active muscles in pre-crash instants.

In this Chapter, the main development steps and a detailed description of the different HBMs are reported. Greater attention is given to the THUMS model, since it is the one used in the simulations performed for this study.

1.1.1 Time History of Human Body Models

The most relevant HBMs are listed here in the following and reported in Figure 1.0. Each modelling approach has its own advantages and disadvantages for what computational costs and injury predictions are concerned.

- 1997-2001: First phase of the HUMOS FE model project, sponsored by the European Community; the resulting HBM was presented in 2001 at the ESV Conference.
- 2000-2002: Iwamoto et al. developed and released the first versions of the FE human body called “THUMS” (Total Human Model for Safety) - AM50
- 2002-2006: Second phase of the HUMOS FE model project, sponsored by the European Community; the new FE human model was presented in 2006 at the ESV Conference.
- 2003: Iwamoto et al. developed a human body FE occupant model with individual internal organs, a 2D brain model, a small female model and a pedestrian model. However, those models had some problems on computational stability and accuracy in geometry, anatomic structure and material properties
- 2007: Iwamoto et al. developed the human body FE called “THUMS Ver. 3.0” (LS-DYNA version), which included a 3D detailed head/brain model, based on Kimpara one (2006)
- 2008: Toyota Motor Corporation released the THUMS Version 3.0, containing both rigid and deformable bodies but without active muscles
- 2010: Toyota Motor Corporation, together with Toyota Central R&D Labs, Inc. released the THUMS Version 4.0 (addition of detailed modeling of internal organs)
- 2012: Osth et al. developed a human body FE model with some muscles in the neck and trunk; they included the muscle models into the THUMS Ver. 3.0 FE model and they achieved the prediction of occupant behaviors during deceleration with Autonomous Emergency Braking (AEB)
- 2012: Gayzik et al. developed the FE model of an adult mid-size male occupant, called Global Human Consortium model (GHBMC), validated against several cadaver data.
Advantage: good/acceptable impact responses
Disadvantage: computational costs and consideration of muscular tone effects

- 2013: Meijer et al. created a multibody human model with active muscles to investigate the muscular tone effects on occupant motions during frontal impacts:
 - Muscles were modelled using bar elements with Hill-type muscle material properties
 - Joints were modelled by mechanical joint structure
 - Each human body part was modelled as rigid body

Advantage: computational cost and prediction of overall occupant motion with muscle activation

Disadvantage: model cannot be used for injury predictions in bones, ligaments and internal organs
- 2013-2016: ViVA HBM project – development of 50th percentile female Open Source Human Body Model
- 2015: Toyota released the THUMS Version 5.0 (addition of body muscles to THUMS Version 3.0)
- 2017: The PIPER Child HBM (seated configuration) was released – EU PIPER Project
- 2018: ViVA HBM advances – addition of muscle activation on the 50th percentile female HBM
- 2018: The PIPER Child model (standing configuration) was released – EU PIPER Project
- 2019: Toyota released the THUMS Version 6.0, combining the features of THUMS Versions 4.0 and 5.0

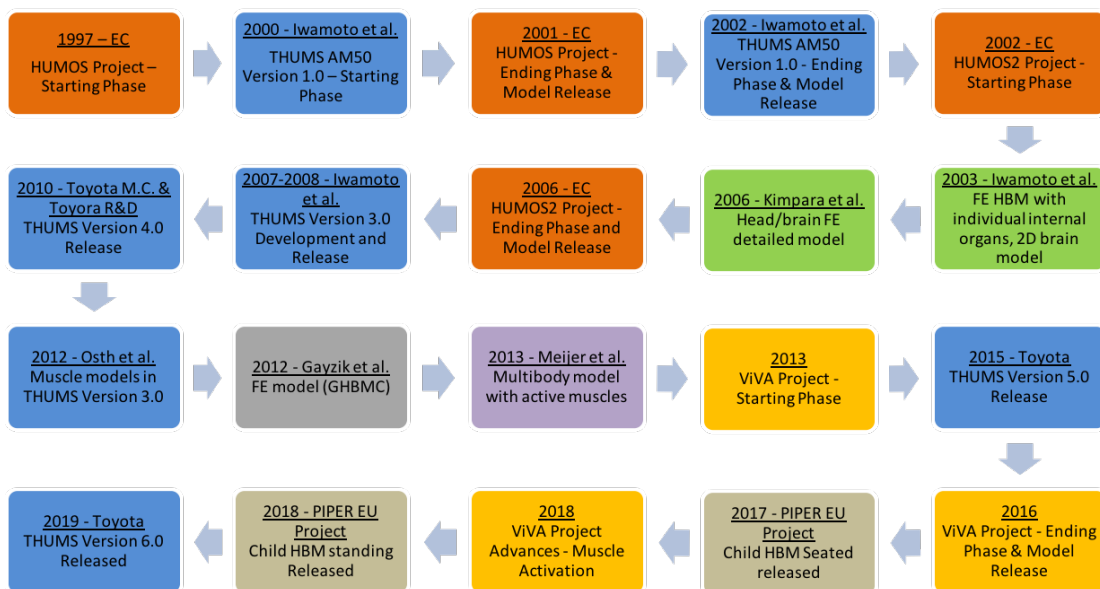


Figure 1.0. FE HBMs – Time History

1.2 Total Human Model for Safety (THUMS)

In order to predict the gross motions and to estimate the overall multiple skeletal injuries of a whole human body during traffic impacts, a finite element model called “*Total Human Model for Safety*” (*THUMS*) was developed by Toyota and presented in 2000. The original THUMS base model reproduces a mid-size adult male occupant and it includes all the deformable human body parts with anatomical geometry and biomedical properties. This original model has then been modified and improved in the subsequent years: the overview of the THUMS different versions is reported in Figure 1.1.

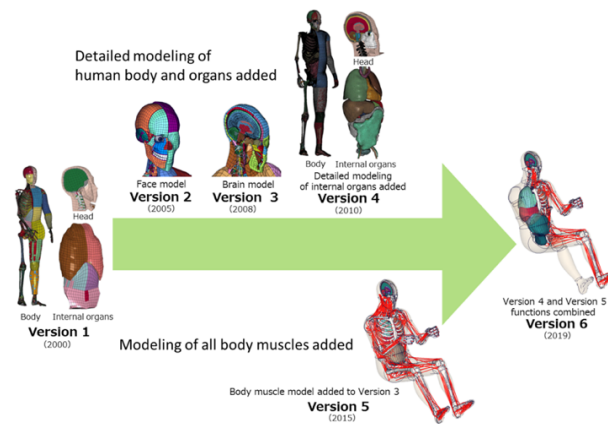


Figure 1.1. THUMS versions overview [1]

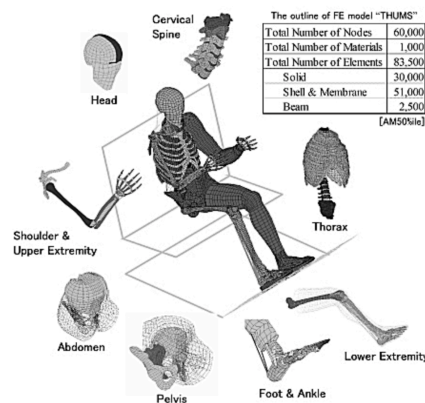


Figure 1.2. THUMS Base Model [2]

The basic geometrical information was based on commercial data packages and anatomical texts of the human body. The model THUMS AM50 (reported in Figure 1.2) was then scaled to fit a 50th percentile American male occupant in a sitting posture, basing on the data described by Schneider et al. (1983): 175 cm height and 77 kg weight.

1.2.1 THUMS Version 1.0

Main characteristics

This first version (Version 1) includes the models of the major bones and ligaments, but the brain and the internal organs are simplified as solid parts. The motions around body joints are simulated as relative motion between bones without implementing any kinematic joint element. The total number of elements is around 80.000. The model is able to simulate bony fractures and ligament ruptures in car crashes.

Bones

In the THUMS model each bone (except the thoracic and lumbar vertebrae) consists of outer cortical bone, modelled as isotropic elastic plastic material using shell elements, and inner spongy bone, modelled as solid elements associated with the same material. The bones are modelled without any strain dependency, while strain rate dependency or nonlinear property is represented in soft tissues. Moreover, it was assumed that bone fractures could occur when stress or strain in any element of each bone exceeds the ultimate stress or strain of each bone as obtained from literature.

Soft tissues and muscles

Soft tissues (e.g. brain, internal organs, abdomen, flesh and fat) are modelled as viscoelastic material using solid elements, whereas the skin is modelled as elastic material using shell elements. Muscles and tendons, instead, are modelled as tension-only elastic material using bar elements. The muscles around the neck can be flexed in order to simulate the effects of an occupant's neck muscles for rear-end impacts.

Material properties of density, Young's modulus, Poisson ratio, stress-strain curve, stiffness, ultimate stress and strain of the bone and soft tissues in THUMS were based on available literature. The model can then simulate deformations caused by contacts with objects and stress or strain distribution on the bones and soft tissues in any part of the human body.

More in details, the THUMS consists of a *base model* and specially developed *detailed models*:

- The *base model* includes a detailed structure for the cervical spine, thorax, spine, pelvis and lower extremity and simple structure for the head/brain, shoulder/upper extremity and internal organs

- The *detailed models* of the head/face, shoulder and individual internal organs can be integrated with the THUMS base model and used according to the user's purpose:
 - The head/face model includes facial and cranial bones, ligaments and muscles with the simple brain model (Figure 1.3)
 - The shoulder model consists of bones (the scapula, clavicle, humerus), ligaments, muscles, fat and skin
 - The internal organ models consist of the heart, lungs, liver, kidneys, pancreas, spleen, stomach, diaphragm, intestine and blood vessels; the geometry was derived using data from the Visible Human Project (National Library of Medicine)

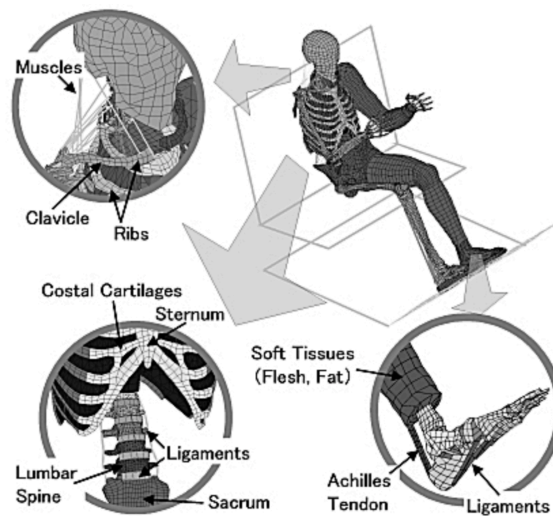


Figure 1.3. THUMS Modelling [2]

Model Validation

In FE human models like THUMS, the *bio-fidelity verification* is one of the most important activities to be accomplished. Each body part has to be, in fact, selectively validated against published test data based on human cadavers in more than one situation, such as frontal, side or rear impacts.

Torso

The thorax and spine models are validated for frontal and side impacts (Figure 1.4) using cadaver test data published, respectively, by Kroell et al. (1971-1974) and Bouquet et al. (1994). Simulation show good agreement with test data.

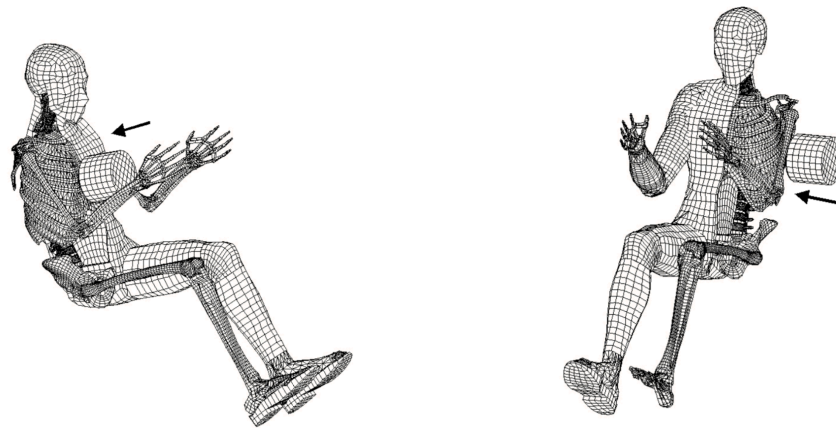


Figure 1.4. THUMS Thoracic impact simulation – verification against frontal (left) and side (right) impacts ^[3]

Lower extremities

The lower extremity model is validated for cadaver test data published by Manning et al. (1998). The simulation result respects the test data. In addition, the lower extremity model was also used to evaluate the effectiveness of the Tibia Index (T.I.) under dynamic axial load (Iwamoto et al. 2000).

Detailed models

The head/face model is validated for cadaver test data published by Nyquist et al. (1986).

The shoulder model, instead, is validated for cadaver test data published by Bendjellal et al. (1989). Simulation results fall within cadaver test corridors.

The internal organ models are validated for cadaver test data published by Cavanaugh et al. (1986).

The results for each body part indicate that THUMS has adequate biofidelity to simulate human body responses during impacts.

1.2.2 THUMS Advances in 2002-2005: THUMS Version 1.x and Version 2.0 ^[4]

The first version of the mid-size adult male occupant model of THUMS is validated, as already introduced, for frontal and/or lateral impacts to the thorax, abdomen and hip. However, the internal organs and the brain are simplified with continuum bodies and homogeneous material properties.

Therefore, the model is not able to show motions and injuries of the individual internal organs and brain during impact situations.

In the study presented in the occasion of the 4th European LS-DYNA Users' Conference (Ulm, 2003), the models of individual internal organs and of a detailed brain were presented: they reproduce their complicated structures as faithfully as possible and define necessary connections and sliding interfaces associating each component with the others.

Moreover, in the same occasion, a female occupant model was released (developed and validated), since females and males are different both in geometry and material property of some skeletal parts and soft tissues.

Additionally, a mid-size male pedestrian model was developed (by modifying the posture of the occupant model) and presented.

Internal Organs

The individual internal organ FE models (about 30.000 nodes and 73.000 elements) include heart, lung, stomach, liver, spleen, pancreas, kidney, intestine, aorta and vena cava.

The respiratory, circulatory and digestive system models are shown in Figure 1.5.

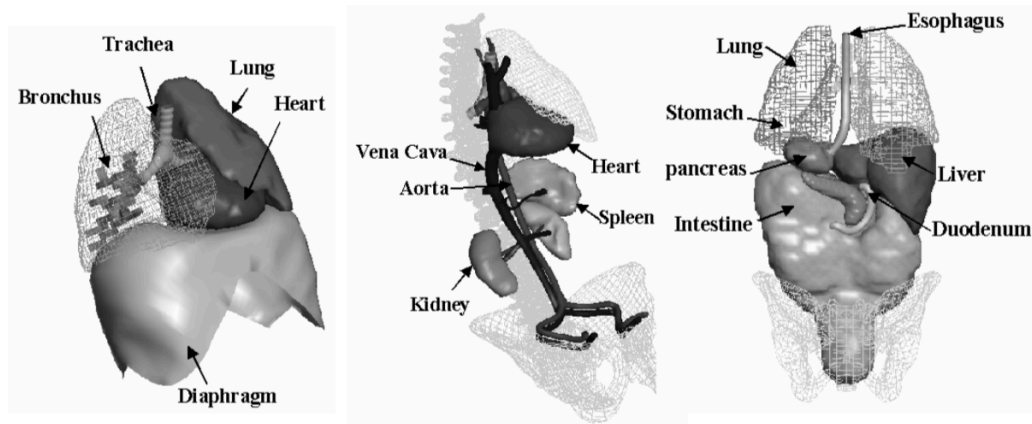


Figure 1.5. THUMS Internal organ models: Respiratory (left), Circulatory (middle) and Digestive (right) systems ^[4]

Solid organs (e.g. liver, spleen, pancreas and kidney) are modelled using solid elements.

The heart, lung, stomach, duodenum and intestine are not solid organs, but they are filled with solid elements, in order to reproduce blood, air and other contents.

The trachea, bronchus, diaphragm, aorta, vena cava and esophagus are instead modelled using shell elements. In addition, bar elements are used to model the bronchioles of the lungs, the interlobularis of the liver and the capillary of kidneys.

The upper part of the trachea and esophagus are fixed with shell elements to the upper part of the cervical spine. The lower part of the intestine is fixed with soft tissues of buttock while the rear part of it is fixed with the lumbar spine using bar elements.

Most organs are modelled using non-linear elastic materials; different material properties, which are obtained from Yamada and Ishihara, were assigned to these organs.

Detailed brain model

Brain injury is one of the major issues: in brain, in particular, two different types of injuries can be verified:

- Focal injury due to direct contact
- Diffuse injury due to inertial loading (Diffuse Axonal Injury – DAI – is the severest form of the diffuse injuries and one of the major causes of death)

However, the injuries due to direct impacts have been often investigated using the models, while DAI had not been deeply investigated.

The purpose of the study presented in the 4th European LS-DYNA Users' Conference was to develop a brain FE model useful to predict the DAI occurrence.

The model was used to simulate a human head sustaining angular acceleration applied on the skull with the mass center of the head coincident with center of rotation (i.e. skull rotating in axial plane – Figure 1.6).

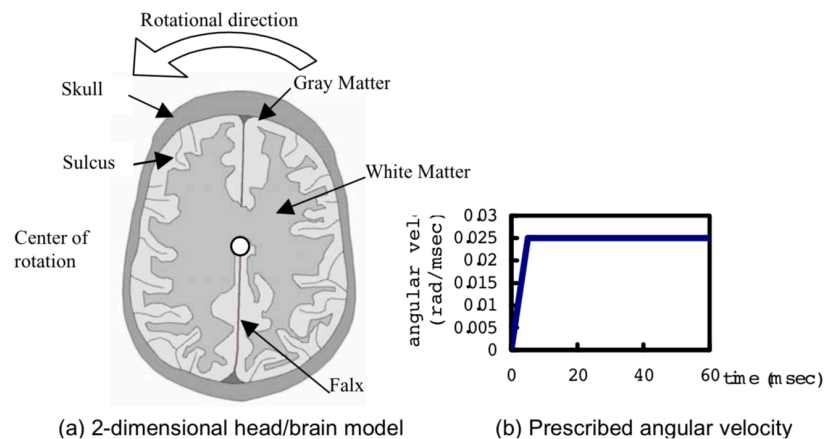


Figure 1.6. 2-D head model and simulation set-up with prescribed angular velocity ^[4]

In the subsequent years, further studies have been performed to develop a 3-D model of the brain, basing on those simulation results.

In Figure 1.7, the Small Female Model announced at the beginning of this section is reported. This THUMS version is a FE model of a female occupant with 152 cm height and 46.4 kg; it was called THUMS-AF05.

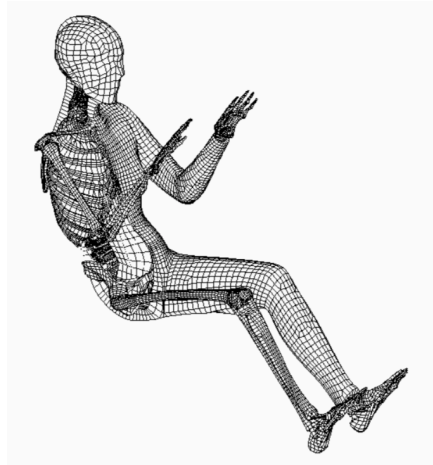


Figure 1.7. THUMS AF05 occupant model ^[4]

The model is validated for frontal impact cadaver test data conducted by Kroell et al. (1971): the simulation result show good agreement with cadaver test data.

In the following years, further development of internal organs for a female and pregnant human body model would be realized.

All those model improvements were then introduced in the THUMS Version 2 (generated in 2004 and released in 2005), which also include modified facial bone parts able to simulate fracture.

1.2.3 THUMS Advances in 2007

In the paper presented in occasion of the 6th European LS-DYNA User's Conference (Gothenburg, 2007), advanced developments in THUMS model were reported: 3D brain model, improvement of internal organs and different types of human body models such as American Female 5th percentile and 6-years-old child.

Head/Brain model (4,39 kg, 49.700 elements upon solid, shell and seatbelt elements)

The improved head/brain model (reported in Figure 1.8) was developed to investigate head/brain injury mechanisms during impacts. It includes the skull, the brain and the skin: basic anthropometric data of the skull and brain model were partially obtained from available

anatomical data sets and modified based on anatomical reference. The brain is constituted by hexagonal solid elements with distinct grey and white matter and cerebral spinal fluid (CSF). In order to represent those entities, viscoelastic material with incompressibility was used.

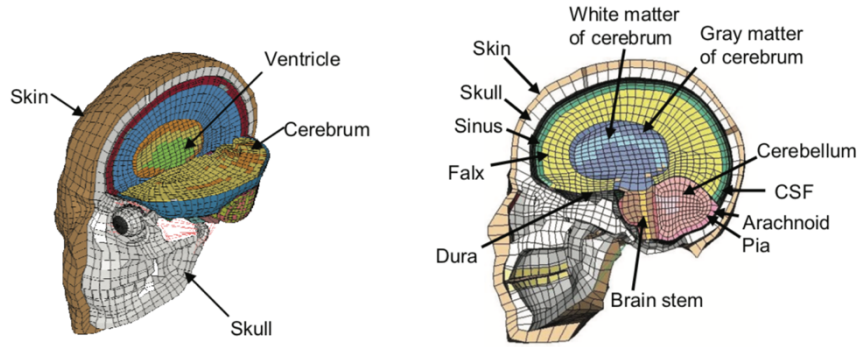


Figure 1.8. THUMS Head/Brain model – oblique view (left) and lateral view (right) [6]

This model was then also implemented into the THUMS-AM50 pedestrian model and used for the brain injury predictions in SUV-to-pedestrian impacts.

Internal organs model (30.000 nodes and 73.000 elements)

The individual internal organs were developed to predict injuries of lungs, heart, liver, spleen, kidney and aorta. In particular, solid organs of the liver, spleen, pancreas and kidney are modelled using solid elements. On the other hand, the heart, lungs, stomach, duodenum and intestine, which are not solid organs, are filled with solid elements to represent blood, air and other contents. The trachea, bronchus, diaphragm, aorta, vena cava and esophagus are modelled using shell elements. The sliding interfaces are defined on the contact surfaces of adjacent organs. The internal organs (Figure 1.9) were also integrated in the THUMS-AM50 occupant model. They are validated against test data and simulation results suggest that the internal organ models have adequate biofidelity and computational stability.

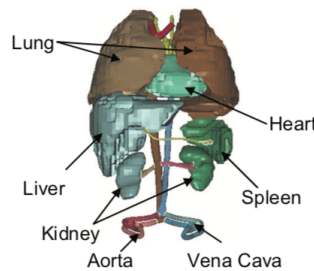


Figure 1.9. THUMS Individual Internal organ models [6]

1.2.4 THUMS Version 3.0

The THUMS AM50 Version 3.0 is a whole-body FE HBM released by Toyota Motor Corporation in 2008. As its previous versions, it is based on the anthropometry of a 50th percentile male. It contains approximately 147.200 elements. The model consists in an improvement of THUMS Version 2 and it includes both rigid and deformable bodies (i.e. bones, vertebrae, intervertebral disks, ribs, skin and internal organs) but it does not have any active muscles. However, an even more detailed brain model was introduced to more precisely simulate brain injury.

1.2.5 THUMS Version 4.0

The THUMS Version 4.0, which is the one used in this Project, has been jointly developed by Toyota Central R&D Labs, Inc. and Toyota Motor Corporation and it was released in 2010.

This version includes three body sizes (Figure 1.10): AM50, AF05 and AM95. As previous versions, the AM50 model represents a 50th percentile American male person with a weight of 77 kg and an height of 175 cm. The other two body sizes, instead, represent:

- A 5th percentile American female person with 152 cm and 52 kg
- A 95th percentile American male person with 188 cm and 101 kg



Figure 1.10. THUMS Academic Version 4 Models ^[5]

The models are all available in two different postures: a standing position (to be used for car-to-pedestrian collision simulations) and a sitting posture used to simulate the occupant in a vehicle.

In this THUMS version, completely new FE meshes were generated to accurately represent the human body geometry. The model is able, then, to simulate brain and internal organ injury at a tissue level, as well as skeletal and ligamentum injuries.

The geometry of bones and internal organs (Figure 1.11) was precisely described basing on the one obtained through high-resolution CT scans, able to digitalize the body interior. The anatomical features of the internal organs, instead, were carefully duplicated referring to the anatomy books (Abe et al. 1996 and Yamada et al. 1970). The material properties of the body parts in the model were defined so as to represent those of a male person in the thirties or forties referring to the research data in the literature. The FE code compatibility and the detailed model description is reported in the User's Manual [5]. Here in the following, only the most relevant characteristics are described. The total number of elements is around 2 millions.

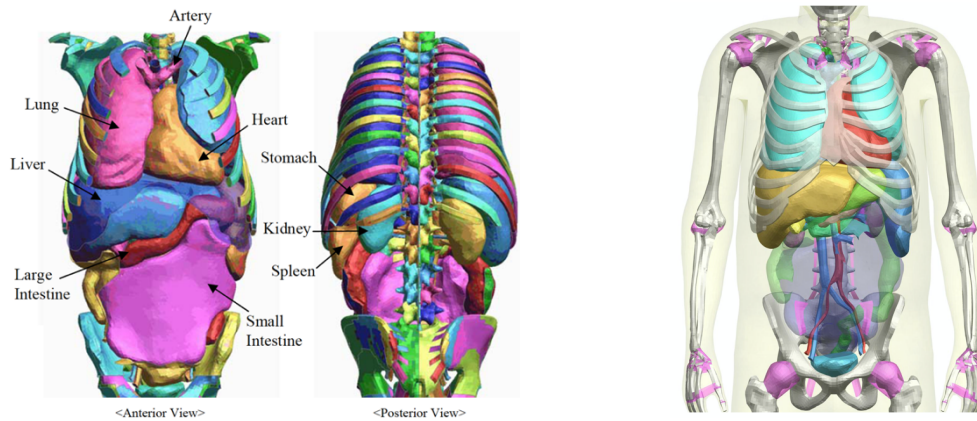


Figure 1.11. THUMS Version 4 – Internal organs representation [8]

1.2.5.1 THUMS Version 4.0 – Model description

The concept of modelling followed to develop the THUMS was to accurately represent the human body without any geometrical simplification.

The internal upper body structure was built in cooperation with the University of Michigan, which holds large quantities of data obtained through high-precision CT scans: a data set of a 39-years old male with a height of 173 cm, a weight of 77.3 kg and a BMI of 25.8 was selected for the AM50 THUMS model.

The considered organs were heart, lungs, liver, kidneys, spleen, pancreas, gall, bladder, esophagus, stomach, duodenum, small intestine and large intestine. Moreover, also the geometries of the most important arteries, veins and membrane tissues surrounding the organs were extracted.

The CT scans data were used for the torso part only: the data of the head and extremities were defined based on the Version 3, but they were refined for thinner mesh.

Material modelling [5]

Skeletal parts are assumed to have elasto-plastic properties. Hyperelastic material is instead assumed for soft tissues. Ligaments and tendons generally show low stiffness for small elongations but high stiffness in case of large elongations.

Skin and flesh parts are also represented by the hyperelastic materials. Hollow organs such as the lungs and the intestine have compressive mechanical properties. The hearth is a hollow organ, but it has thick muscular walls and blood inside. The mechanical property of the hearth is very incompressive. The property data input into each material model was selected from literature data.

FE components numbering criteria [5]

The entity IDs in THUMS Version 4 AM50 are defined as reported in Figure 1.12.

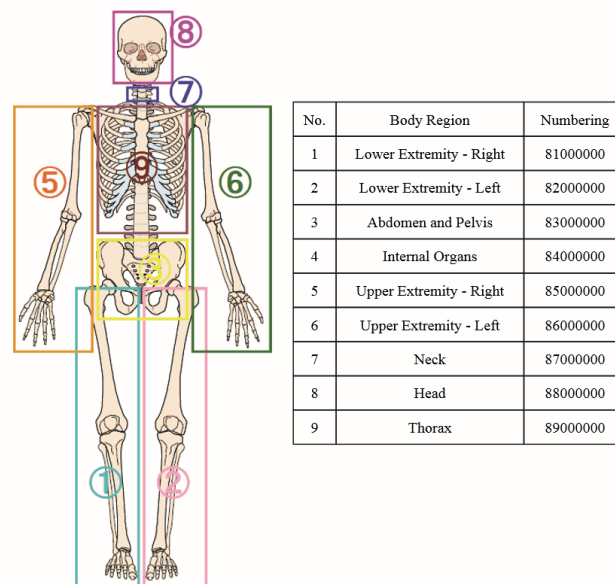


Figure 1.12. THUMS Version 4 – Numbering of entities [8]

Head model [5]

The model (Figure 1.13) includes the epidermis (skin), skull, mandible, eyeballs, teeth, meninges, cerebrum, cerebellum, brainstem, CSF etc. The brain parts include the white matter and the grey matter. The inferior part of the head model is connected to the torso model through the neck.

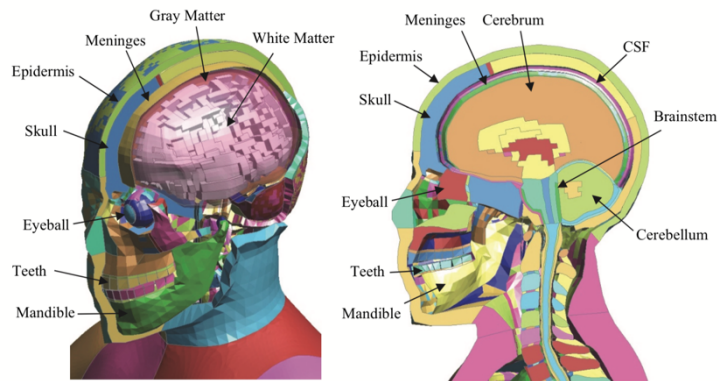


Figure 1.13. THUMS Version 4 – Head model ^[5]

Torso model ^[5]

The model includes all skeletal parts (Figure 1.14), and the major soft tissues. The hard tissues, instead, are ribs, sternum, spine (vertebrae), clavicles, scapulae, sacrum and pelvis. The connective tissues such as costal cartilages, intervertebral disks, pubic symphysis and ligaments are also modelled.

In Figure 1.15, on the opposite, the major soft tissue parts are shown.

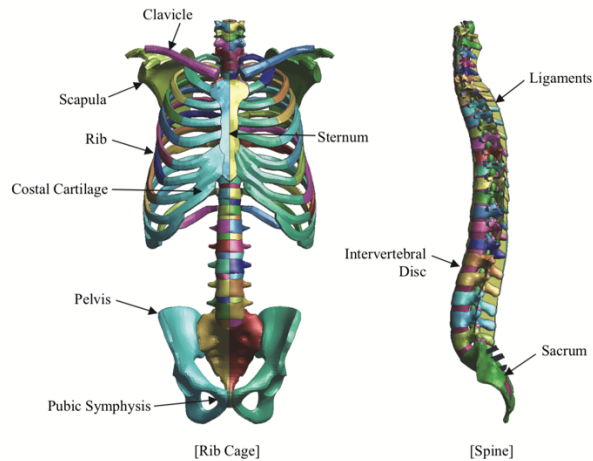


Figure 1.14. THUMS Version 4 – Skeletal Parts in Torso model including the neck ^[5]

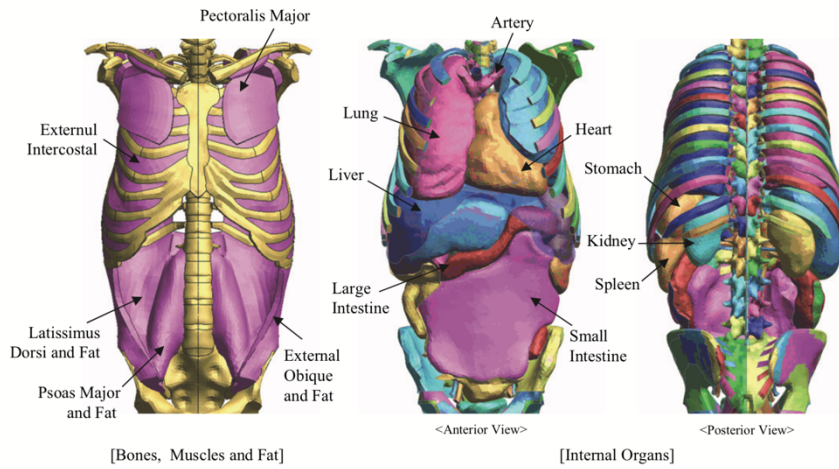


Figure 1.15. THUMS Version 4 – Soft Tissue parts in Torso model ^[5]

Extremity model ^[5]

The extremity models include all the skeletal parts and the major soft tissues. The major components are reported in Figure 1.16. The skeletal parts are surrounded by flesh parts, which are divided in subgroups, mostly corresponding to extensor and flexor muscles. Shell elements are used to model the skin, which fully covers the flesh parts sharing the nodes.

Joints models ^[5]

Joints are modelled as bone-to-bone connection with ligaments: no kinematic joint element is used. The knee joint and the ankle joint are represented in Figure 1.17.

Full-Body model ^[5]

The whole-body model was then generated by combining the different component models (head, torso and extremity models). The connections between component models were carefully realized so as to match the meshes without making geometrical discontinuity. The full body model of the standing version is reported in Figure 1.18: the skin and flesh parts fully cover the body. The skeletal/muscular view is shown in Figure 1.19, whereas Figure 1.20 is the deeper view.

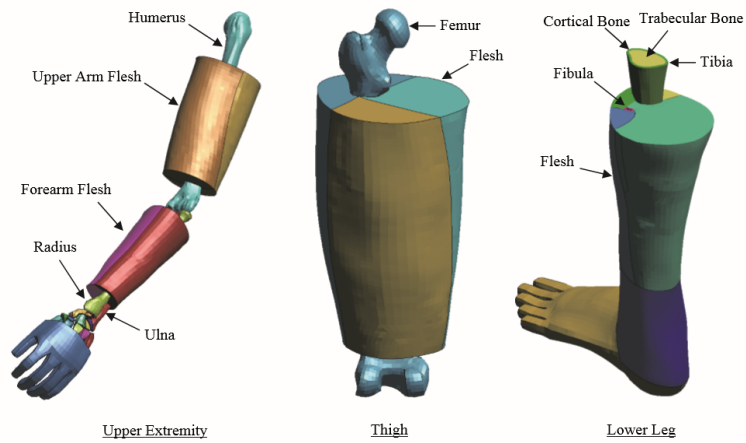


Figure 1.16. THUMS Version 4 – Extremity models [5]

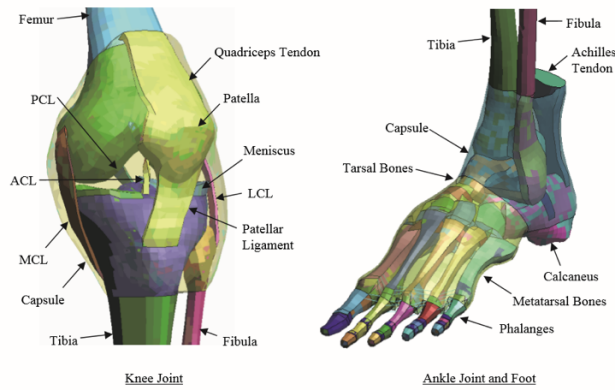


Figure 1.17. THUMS Version 4 – Joint model [5]

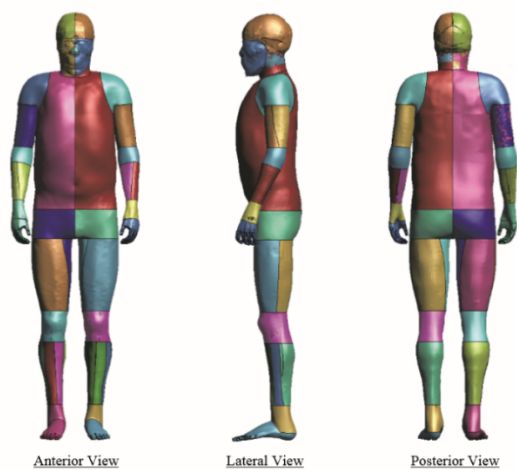


Figure 1.18. THUMS Version 4 – Whole Body Pedestrian model [5]

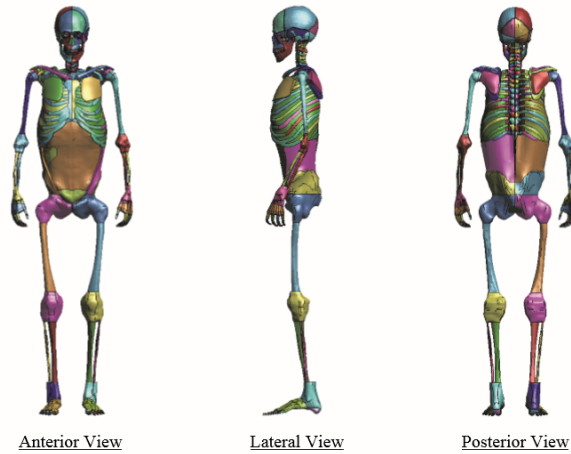


Figure 1.19. THUMS Version 4 – Whole Body Pedestrian model (skeletal/muscular view) ^[5]

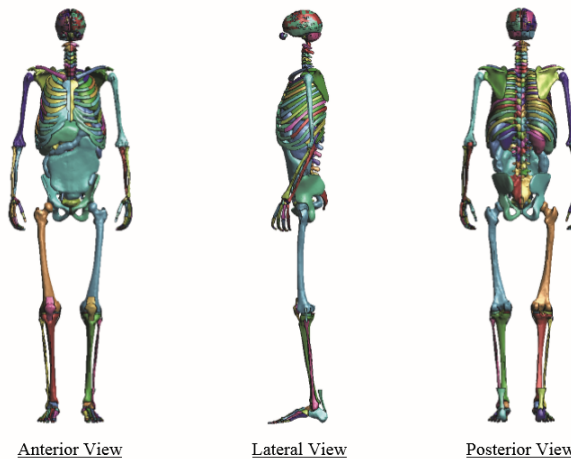


Figure 1.20. THUMS Version 4 – Whole Body Pedestrian model (deeper view) ^[5]

From Pedestrian to Occupant model ^[5]

The sitting model has been generated by changing the posture of the standing (pedestrian) model.

The torso was rotated of about 20° in the direction reclining against the seatback.

The head was rotated so that the face looked forward. The upper extremities were moved simulating the driving posture holding the steering wheel with the hands. The thigh angle was rotated 90° from its original position. The model was checked and corrected after changing posture; the skin and flesh parts around the rotated joints were then remeshed.

The comparison between the standing (pedestrian) and the sitting (occupant) postures is shown in Figure 1.21.

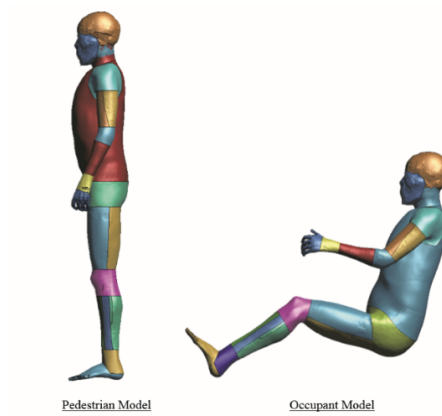


Figure 1.21. THUMS Version 4 – Pedestrian and occupant models [5]

1.2.5.2 THUMS Version 4.0 – Validation at component level and fully-body level

The bio fidelity of THUMS Version 4 is verified by comparing its impact responses against those of post-mortem human subjects (PMHS) reported in the literature.

Body Region		Target Impact Response
Head		Translational Impact (Anterior)
		Translational/Rotational Impact (Sagittal)
		Translational Impact (Parietal)
Neck		Dynamic Axial Loading
Torso	Thorax	Cylindrical Impact (Anterior)
		Belt Loading (Anterior)
		Cylindrical Impact (Lateral)
	Abdomen	Bar Impact (Anterior)
		Belt Loading (Anterior)
	Pelvis	Knee-Thigh-Hip Impact (Anterior)
Dynamic Hip Loading (Lateral)		
Extremity	Humerus	Quasi-static-3-point Bending
		Dynamic Lateral Compression
	Femur	Quasi-static-3-point Bending
	Knee Joint	Dynamic Lateral Loading
		Dynamic 4-point Bending
	Tibia	Dynamic 3-point Bending
Ankle and Foot	Dynamic Axial Loading	

Table 1.0. THUMS Version 4 – Validation list [5]

The validation tests of the major THUMS components are resumed in this chapter. The complete list of validations for component models is instead reported in the Table 1.0.

Head model validation ^[5,7]

Figure 1.22 shows the head and neck models simulating the impact test conducted by Nahum et al. (1997). This test was performed to measure the acceleration and pressure responses of the brain. Both the forces and pressure peaks resulting from the simulation show a good agreement with the test data.

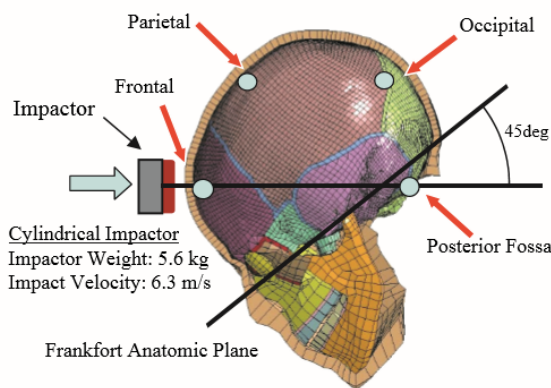


Figure 1.22. THUMS Version 4 – Head Validation model (Translational impact) ^[5]

The brain kinematics in the head model is validated with respect to the tests conducted by Hardy et al. (2001) and Kleiven et al. (2002). The head was rotated in the posterior and anterior directions at velocities ranging from 2 to 4 m/s. The test conditions are shown in Figure 1.23.

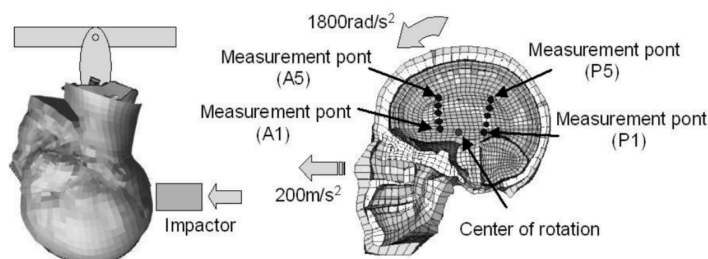


Figure 1.23. THUMS Version 4 – Head Validation model (Rotational test) ^[7]

In Figure 1.24, instead, the model simulating the test conducted by Yoganandum et al. (1995) is shown. The calculated peak forces are within the range of the test data at all the impact speeds compared.

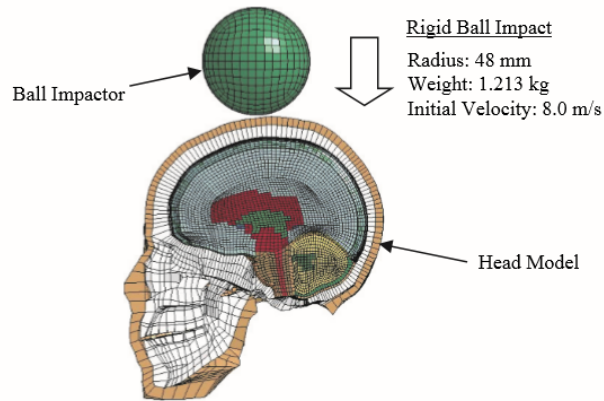


Figure 1.24. THUMS Version 4 – Head Validation model (Parietal impact) ^[5]

Neck model validation ^[5]

The setting simulating the test conducted by Nightingale et al. (1997) to validate the neck model is reported in Figure 1.25. The purpose of the test was to observe and measure the neck buckling. Forces were measured at the contact surface and the neck supporting part.

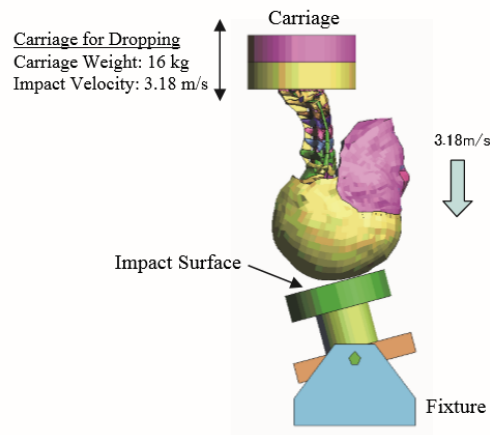


Figure 1.25. THUMS Version 4 – Neck Validation model (Axial Loading) ^[5]

Thorax model validation ^[5]

The model used to validate the thorax region against an anterior cylindrical impact is reported in Figure 1.26. The model simulated a series of tests conducted by Kroell et al. (1974). A

cylindrical impactor loaded the anterior thorax of the subject, placed on a test bench in a sitting posture.

Figure 1.27 shows the force-deflection curve calculated by the thorax part of THUMS.

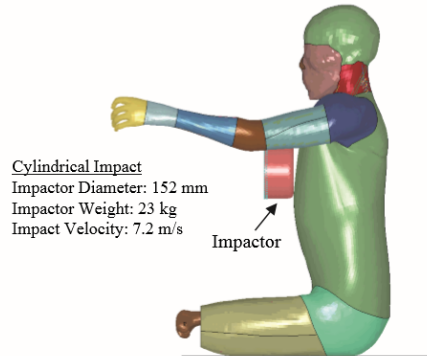


Figure 1.26. THUMS Version 4 – Thorax Validation model against Cylindrical Impact (Anterior) [5]

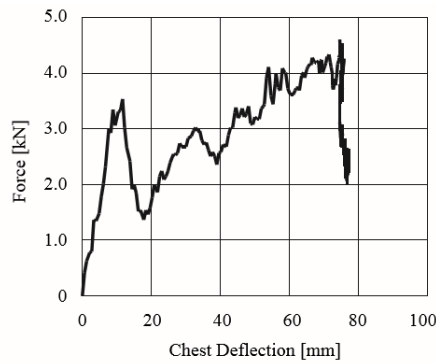


Figure 1.27. THUMS Version 4 – Calculated Force-deflection curve of Thorax (Anterior Impact) [5]

The model is also verified against an anterior belt loading, simulating a series of tests performed by Cesari et al. (1990). The belt-shaped loading device was placed diagonally across the anterior thorax. The ends of the belt were pulled by an impactor. The test model is reported in Figure 1.28.

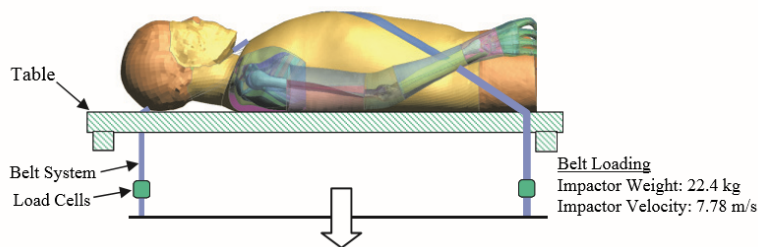


Figure 1.28. THUMS Version 4 – Thorax Validation model against Belt Loading (Anterior) [5]

Figure 1.29 shows the model simulating the loading test to the lateral thorax with a cylindrical impactor conducted by Shaw et al. (2006).

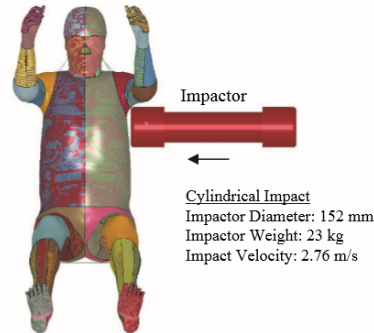


Figure 1.29. THUMS Version 4 – Thorax Validation model against Cylindrical Lateral Impact ^[5]

Figure 1.30 reports, instead, the model used to validate the abdominal response against an anterior impact, simulating a series of tests conducted by Cavanaugh et al. (1986).

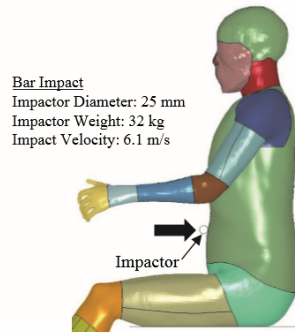


Figure 1.30. THUMS Version 4 – Abdomen Validation model against Bar Impact (Anterior) ^[5]

The model simulating the abdominal belt compression tests conducted by Foster et al. (2006) is described in Figure 1.31. The tests were conducted compressing the anterior abdomen of subjects at various speed range from 4.0 to 13.3 m/s. The considered belt width was 50 mm.

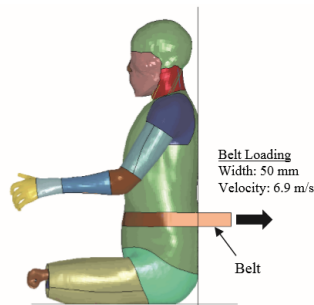


Figure 1.31. THUMS Version 4 – Abdomen Validation model against Belt Impact (Anterior) ^[5]

Extremity models validation ^[5]

For what the extremities are concerned, the impact responses of the humerus, femur, knee and tibia regions were examined.

The validation model against the 3-point bending test performed on the humerus by Kemper et al. (2005) is shown in Figure 1.32.

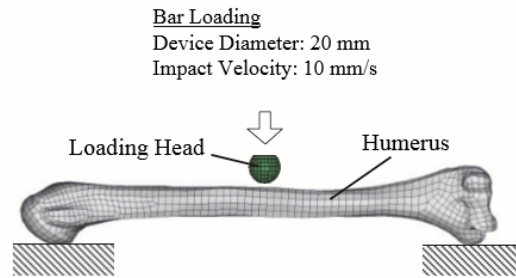


Figure 1.32. THUMS Version 4 – Humerus Validation model against quasi-static 3-points Bending ^[5]

The dynamic lateral compression test conducted by Kemper et al. (2005) is simulated by the model of Figure 1.33. The test was done by removing the flesh. The humerus was placed on a circular table and compressed by a circular impactor with the same dimensions of the table, at a velocity of 4m/s.

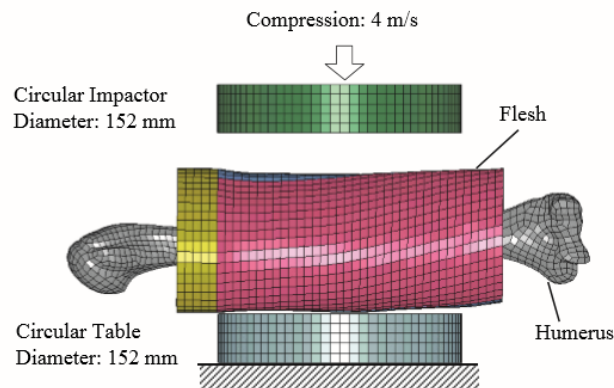


Figure 1.33. THUMS Version 4 – Humerus Validation model against Dynamic Lateral Compression ^[5]

Figure 1.34 shows the femur validation model against the static 3-point bending test performed by Yamada et al. (1970).

The model knee extracted from the THUMS Version 4 to simulate the knee joint bending test conducted by Bose et al. (2004) is illustrated in Figure 1.35.

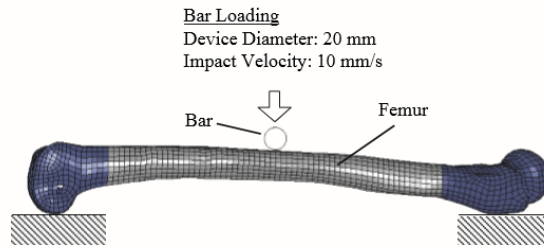


Figure 1.34. THUMS Version 4 – Femur Validation model against quasi-static 3-point Bending ^[5]

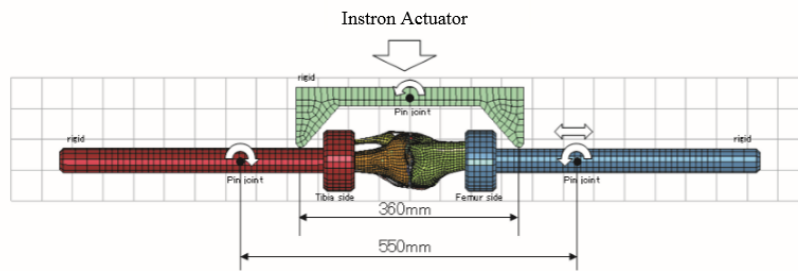


Figure 1.35. THUMS Version 4 – Knee Validation model against 4-point Bending ^[5]

Figure 1.36 shows the ankle and foot complex model used for the validation against dynamic axial loading. The tests were conducted by Kitagawa et al. (1998). In the tests, the Achilles tendon was pulled by a cable simulating the driver's foot stepping on the brake pedal.

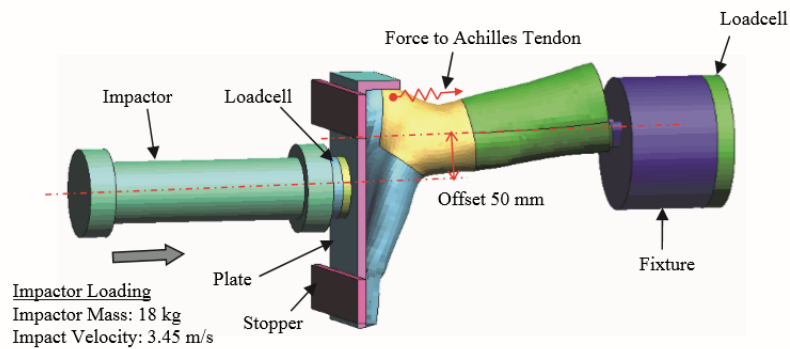


Figure 1.36. THUMS Version 4 – Ankle and Foot Validation Model against Dynamic Axial Loading ^[5]

1.2.6 THUMS Version 5.0 [8][9]

Quite recent researches indicate that muscle tone could have significant effects on human body kinematics both in precrash and during crash instants (ref. Ejima et al. 2009 and Kemper et al. 2001). Moreover, it was demonstrated that muscle activations, especially in neck region, can affect occupant head kinematics. A (FE) human body model which takes into account muscle activation can be therefore useful to predict the occupant head kinematics in real-world automotive accidents.

Different finite element human body models with active muscles have been developed in recent years to investigate muscular effects on body kinematics. In 2012, Osth et al. developed a human body FE model with active muscle, containing PID (Proportional Integral Derivative) controllers in the neck and trunk: in the tests, it was proved that the model could capture passenger pre-crash kinematics. In 2013, Dibb et al. developed a 50th percentile male computational head-neck model with active muscles and it was found that the head kinematics during low-speed frontal impacts could be reproduced with muscle activation schemes.

In those previous studies, however, not all human body muscles were considered.

For this reason, in 2015, the THUMS Version 5 was released by Toyota. This model (here reported in Figure 1.37) includes multiple 1D muscles over the entire body.

This THUMS model is validated against 36 series of Post Mortem Human Surrogate – PMHS – and cadaver test data for frontal, side and rear impacts. The muscular effects on occupant kinematics and injury outcome during frontal impact can then be investigated.



Figure 1.37. THUMS Version 5 - Occupant model (left) [8] and seated in a passenger car FE model (right) [9]

As its previous versions, THUMS Version 5 is a finite element human body model scaled to fit a 50th percentile adult male occupant (AM50) according to the data reported by Schneider et al. (1983). The height and the weight of the model are, respectively, 175 cm and 77 kg.

The basic material properties of bones and soft tissues have been obtained from Yamada (1970) and Abe et al. (1996).

The skeletal part of THUMS Version 5 includes major bones such as the skull, ribs, spine, femur, tibia, pelvis, humerus, ulna and radius and major anatomical points such as the ankle, knee, hip, shoulder, elbow and hand. Also in this Version, the bones are modelled in two parts: cortical and spongy bones.

Each joint is modeled using bone-to-bone contacts with major ligaments and deformable cartilages or disks.

THUMS Version 5 also includes skin, flesh, brain and internal organs such as the lungs, heart, esophagus, aorta, vena cava, liver, kidney, spleen, stomach and bowel.

The head/brain model (Figure 1.38) was modified, gaining in computational stability, with respect to the one of the previous models.

In order to verify the applicability of those modified head/brain models in the skull and brain injury predictions, they are validated against:

- One head translational impact (Nahum et al. 1977)
- One head translational and rotational impact (Troseille et al. 1992)
- Three head translational and rotational impacts (Hardy et al. 2001)
- Five skull or face impacts (Yoganandan et al. 1995, Allsop et al. 1988, Nyquist et al. 1986, Melvin et al. 1989)

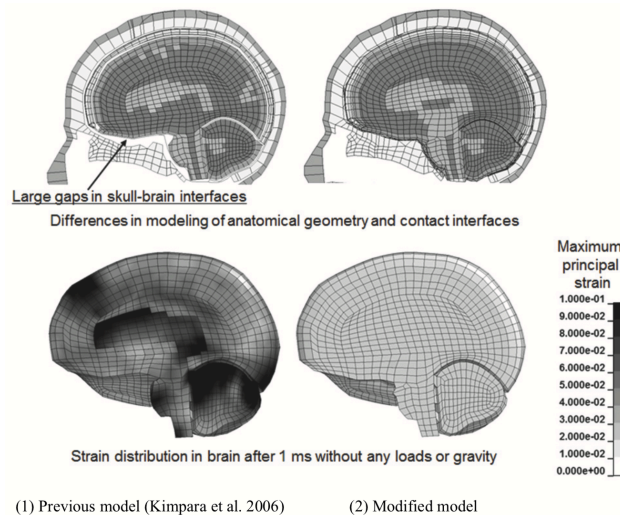


Figure 1.38. THUMS Version 5 - Modified Head/Brain FE model [9,10]

Each muscle is modelled as a muscle-tendon complex and they have an active part that can contract with increasing activation level and a passive part that can have nonlinear elastic properties only in tension (Figure 1.39). The total number of elements and nodes included in the whole body of the THUMS Version 5 are, respectively, 281.260 and 184.600.

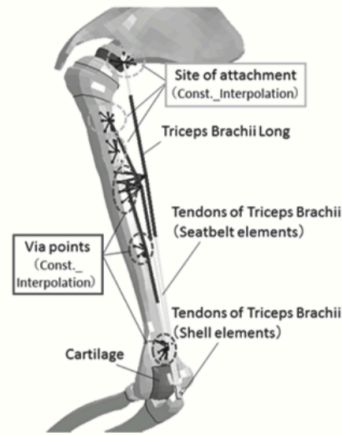


Figure 1.39. THUMS Version 5 – Muscle modelling of muscle-tendon complex ^[9]

1.2.6.1 THUMS Version 5.0 – Muscle activation

Carlsson and Davidsson in 2011 conducted volunteer tests in a Volvo XC60 with an automatic gearbox driving on ordinary roads: the passengers, generally, showed larger head-neck-torso motions than drivers. This suggested that the drivers tend to hold their postures by their upper and lower extremities with muscle activity. Moreover, Ejima et al. (2009) conducted volunteer tests using a mini-sled with a brake deceleration of 0.8g and they found that head-neck-torso kinematics were strongly influenced by muscle activity and the volunteers tended to hold their postures in tensed muscle conditions. The same applies for the lateral flexion of head-neck-torso. In conclusion, drivers or passengers can activate their muscles to hold their driving or sitting postures just before and after impacts. In order to represent the posture maintenance, some muscle control methods such as Proportional Integral Derivative (PID) control (e.g. Figure 1.40), optimal algorithm, and reinforcement learning are used. Rooij (2011) developed the MADYMO FE model with some muscles in the neck and controlled the muscles by using three PID controllers for joint motions in the neck, thorax, and lumbar to hold driver's head-neck postures during a deceleration of automatic emergency braking (AEB). Osth et al. also developed a human FE model with some muscles using THUMS Version 3. Dibb et al. (2013) developed a human head-neck FE model, and controlled the muscles via an optimization method to hold occupant head-neck postures during low-speed frontal impacts with peak sled accelerations of 3.6g and 3.8g. Iwamoto et al.

(2012) developed a human FE model with 3D geometry of muscles in the whole body and controlled the muscles by using reinforcement learning to hold occupant head-neck postures during a low-speed frontal impact with peak sled acceleration of 16g.

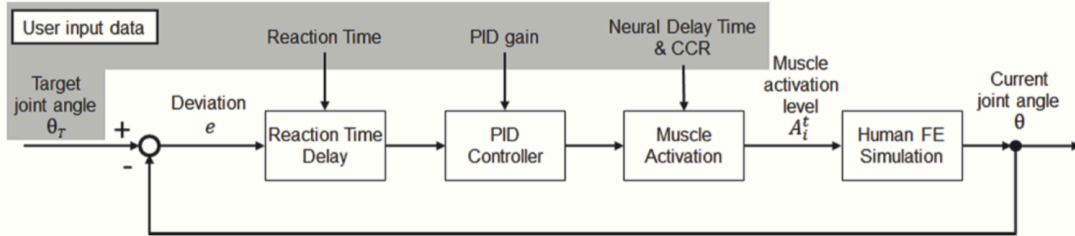


Figure 1.40. THUMS Version 5 – Example of muscle controller using PID for an anatomical joint [9]

In THUMS Version 5, therefore, PID controllers are used to hold driving and passenger postures during side impacts. Figure 1.40 shows a diagram of the muscle control system using a PID controller for an anatomical joint. THUMS Version 5.0 includes a total of 262 skeletal muscles: 23 neck muscles, 47 arm muscles, 9 trunk muscles, and 52 leg muscles on one-side.

A frontal crash simulation with Automatic Emergency Braking (AEB) was assumed to investigate the driver’s kinematics and injury outcomes during pre-collision braking and a crash event with a vehicular sled model, as shown in Figure 1.41. The deceleration of AEB was set to a magnitude of 0.8g with a time duration of 300 ms followed by an impact deceleration ΔV of 50 km/h [11].

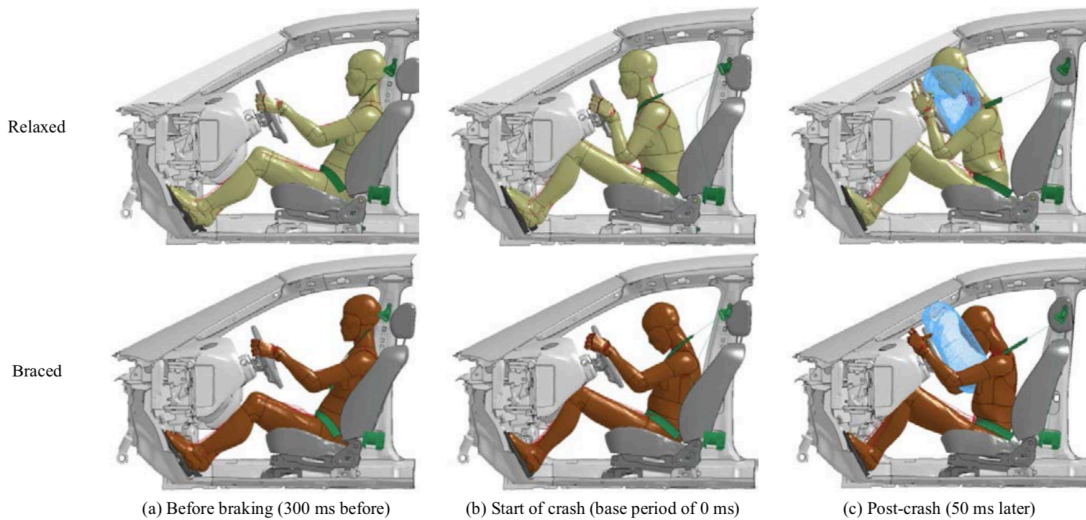


Figure 1.41. Impact response of the occupant during pre-collision braking and frontal crash [10]

Two driver conditions were assumed:

- The relaxed condition was assumed to be constantly defined as consistent activation levels of 1% in order to obtain numerical stabilities
- The braced condition was generated by using the inputs of muscular activation levels into THUMS version 5.

The time when the crash started was set as the base period for the simulation results. The head of the relaxed driver moved forward by 340 mm more than that of the braced one at the start of the crash. In addition, the upper body kinematics of the relaxed and braced drivers were different under the post-crash condition. The Von Mises stress distribution on the skeletal parts of THUMS Version 5 is reported in Figure 1.42. The relaxed driver had greater stress on the ribs, while the braced driver had greater stress on the upper and lower extremities, especially the forearms and the right foot.

Therefore, complete ribs fracture, represented by mesh elimination, only appeared in the relaxed case (ref. Figure 1.43), while severe compression strain was conserved in the internal organs of the relaxed drivers.

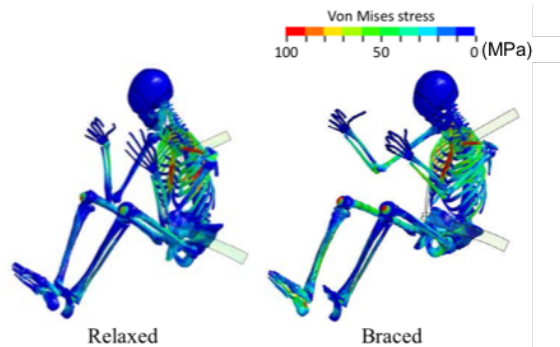


Figure 1.42. Stress distribution on the skeletal parts ($t=50$ ms) ^[10]

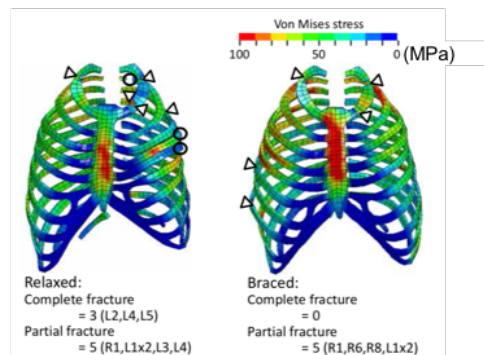


Figure 1.43. Stress distribution and locations of rib fractures – rib fracture (mesh elimination) are highlighted in Figure ($t=62.5$ ms) ^[10]

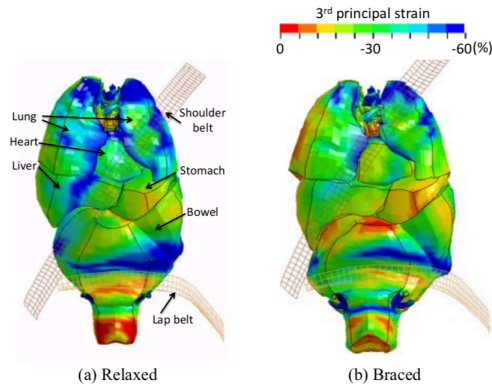


Figure 1.44. Compressional strain distributions around internal organs ($t=112.5$ ms) ^[10]

The relaxed driver sustained more damage to the thorax than the braced driver. This is due to the fact that the braced driver first received impact loadings on the extended upper and lower extremities after the crash, whereas the relaxed driver received minor support from the extremities. Therefore, the braced driver sustained less thorax deformation than the relaxed driver in this simulation setup.

1.2.7 THUMS Version 6.0 ^[12]

The THUMS Version 6 was developed and presented in 2018, including both a detailed human-body structure and activable muscles, for predicting occupant injury risks in frontal collisions with deceleration before the crash and to apply the developed model to injury analysis in such conditions.

This THUMS Version was released in three different body sizes (Figure 1.45), corresponding to a 50th percentile adult male (AM50, with a height of 179 cm and weight of 79 kg), a 5th percentile adult female (AF05, with a height of 153 cm and weight of 49 kg) and a 95th percentile adult male (AM95, with a height of 188 cm and weight of 106 kg).

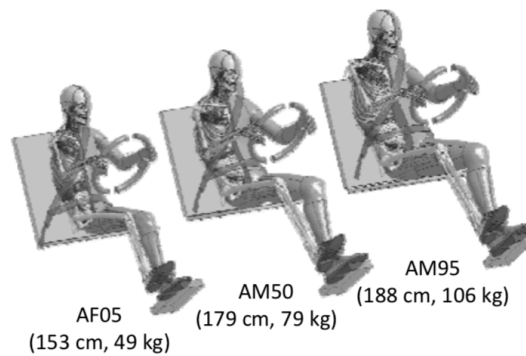


Figure 1.45. Occupant models of THUMS Version 6 ^[12]

THUMS Version 4 included detailed body-part models based on a high-precision CT-scan dataset and it was used to predict bone fractures, ligament ruptures and damage to the brain and internal organs. On the other hand, THUMS Version 5 was developed by updating THUMS Version 3 with major modifications including the implementation of whole-body skeletal muscles. THUMS Version 6 was developed by incorporating the muscle models of Version 5 into Version 4. The total numbers of elements in AM50, AF05, and AM95 of THUMS Version 6 are approximately 1.9, 2.5, and 2.0 million, respectively. The models can generate muscular forces based on given activation levels of muscles. THUMS Version 6 has both a detailed human-body structure and activated muscles.

The muscle parameters of AF05 are set differently from those of the male models.

1.2.7.1 THUMS Version 6.0 – Muscle activation ^[12]

When a driver is exposed to deceleration due to braking or impact, he is supposed to have several reactions to changes in velocity. As already introduced, in other words, if a driver does not anticipate the braking or impact, he may unconsciously perform some reflective action to reverse the posture changes due to the deceleration (relaxed condition). If, on the opposite, a driver anticipates the braking or impact, he may brace himself by pushing the steering wheel and pressing the pedal or footrest (braced condition).

An example of diagram of muscle-activation controller is reported in Figure 1.46. This controller decides the activation levels of muscles based on the displacement and force obtained from the FE analysis in each time step.

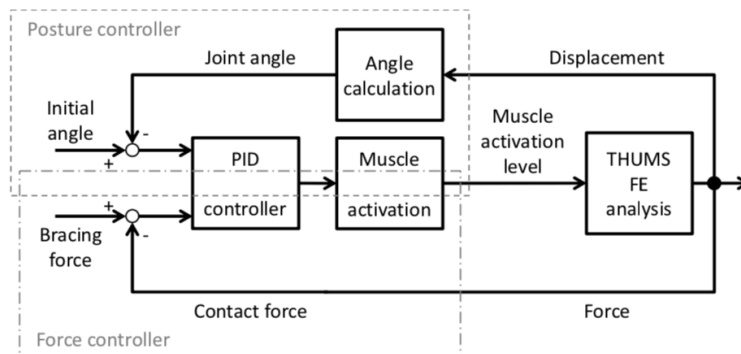


Figure 1.46. Muscle activation controller for THUMS Version 6 ^[12]

The controller consists of two closed-loop feedback controls – one for posture control and the other for force control – and uses the Proportional-Integral-Derivative (PID) control method. The posture control works to maintain the initial one, and the force control works to reproduce the

forces exerted by braced drivers to support their body. The muscle condition for the relaxed driver is represented using only the posture control, while that for the braced driver is represented using both the posture and force control.

1.3 Global Human Body Models Consortium (GHBMC) [13, 14]

The Global Human Body Models Consortium is an international consortium of automakers and suppliers working with research institutes and government agencies to advance human body modelling (HBM) technologies for crash simulations. The objective is to consolidate world-wide human body model research and development into a single global effort.

The result is a M50 seated FE model intended for use in simulations of vehicle crash. It was created to simulate kinematic and kinetic responses of the body in the blunt loading regime.

The template for the M50 model was a 26-years-old male in excellent health, with a weight of 78.6 kg and a height of 174.9 cm. Three different methods were used to collect the necessary human body data:

- Magnetic Resonance Imaging (MRI)
- Upright MRI
- Computed Tomography (TM)

The external anthropometry was instead collected in the seated posture using a 3D digitalizer.

Once that the data have been acquired, the CAD development of the human body has taken place. In the M50 CAD (shown in Figure 1.47) model there are 418 individual parts including bones, organs, muscles, vessels and ligaments.

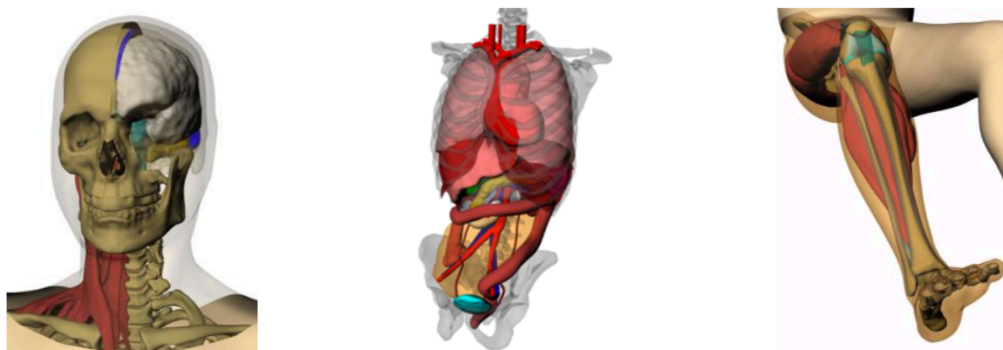


Figure 1.47. GHBMC M50 - CAD of head (left), thorax & abdomen (middle) and lower extremity (right) [13]

The five Body Region Models (BRMs) reported in Figure 1.48 were developed by partner research institutions in the GHBMC. The CAD parts were meshed and regional models were then validated.



Figure 1.48. GHBMC M50 - BRMs: Head, Neck, Thorax, Abdomen and Plex (Pelvis + Lower extremity) ^[13]

Head-to-Neck interface

Fifty-two 3D muscles are modeled in the neck and attached to the skull and cervical vertebrae via tied contacts. Ligaments, fibers and 1D elements are connected to the head model via nodal connections as well.

Neck-to-Thorax interface

All 1D neck muscles, 1D neck ligaments and 3D neck muscles are attached to the corresponding thoracic body landmarks. Tied contacts are used for the 3D muscles. The thorax and neck flesh components are connected through shared nodes.

Thorax-to-Abdomen interface

Tied contacts between thoracic and abdominal muscles to their neighboring regions are established. Abdominal ligaments are connected via shared nodes to the inferior surface of the diaphragm. The thoracic and abdominal great vessels are attached through shared nodes. Superior lumbar kinematic constraints are confirmed; both the thoracic and lumbar spinal vertebrae are modeled as rigid bodies.



Figure 1.49. GHBMCM50 - Head-neck interface ^[13]



Figure 1.50. GHBMCM50 - Thorax and abdomen ^[13]

Number of elements / nodes	$1,95 \times 10^6 / 1,30 \times 10^6$
Number of parts	847
Number of materials	557
Model mass (kg)	75

Table 1.1. GHBMCM50 – Model specifics

The detailed summary of the M50 is reported in Table 1.1, while the mass distribution region is shown in Figure 1.51.

The M50 HBM contains detailed anatomy in each body region. The model has been tested in nearly 20 impact simulations in frontal and lateral loading.

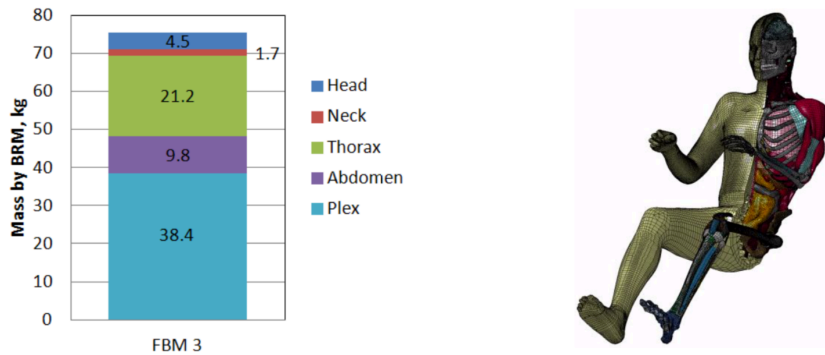


Figure 1.51. GHBMC M50 – Model mass distribution by BRM (left) and oblique view of M50 (right) [13]

1.4 Virtual Vehicle-safety Assessment Project (ViVa) [15, 16, 17]

The Virtual Vehicle-safety Assessment (ViVa) Project took place from 1/11/2013 to 31/12/2016: even if significant progresses had been made in the development of FE Human Body Models and in their introduction in the advance of automotive safety systems, the average female model was not studied in the previous projects.

The ViVa project aimed to describe the development of a 50th percentile female Open Source HBM, to validate its kinematics and compare the effect of having a detailed or simplified neck model. Whiplash Associated Disorder (WAD) is the common name for a range of symptoms associated with cervical spine soft tissue injury commonly resulting from low severity vehicle collisions. The risk for females to sustain WAD symptoms is, on average, double than in males (and even higher) in similar crash conditions, as demonstrated by previous studies (Carlsson et al. (2014), O’Neil et al. (1972), Morris et al. (1996), Temming et al. (1998), Krafft et al. (2003), Jakobsson et al. (2004) and Carstensen et al. (2012)).

In addition, for more severe injuries, studies have shown that females are at higher risk than males of sustaining severe injuries in comparable crashes (Bose et al. (2011)). This was the driving force behind the development of a 50th percentile female HBM.

The project started from data of a 50th percentile female, using rigid bones, kinematic joints and deformable tissues for the whole-body model, together with an existing detailed model and a new simplified neck model.

A great number of partners took part to the Project, both from the research and industrial sides.

1.4.1 ViVa Model – The development

The developed female HBM is reported in Figure 1.52. The model was created from Stereolithography (STL) surfaces of the skeleton and outer surface of a 31-years-old female subject of 161.6 cm stature and 60.8 kg weight.

Extremities

The bones of the upper and lower extremities are modelled as rigid bodies and soft tissues with hexahedral solid elements, connected to the bones by nodal constraints. The joints are modelled as spherical, saddle or revolute joints.

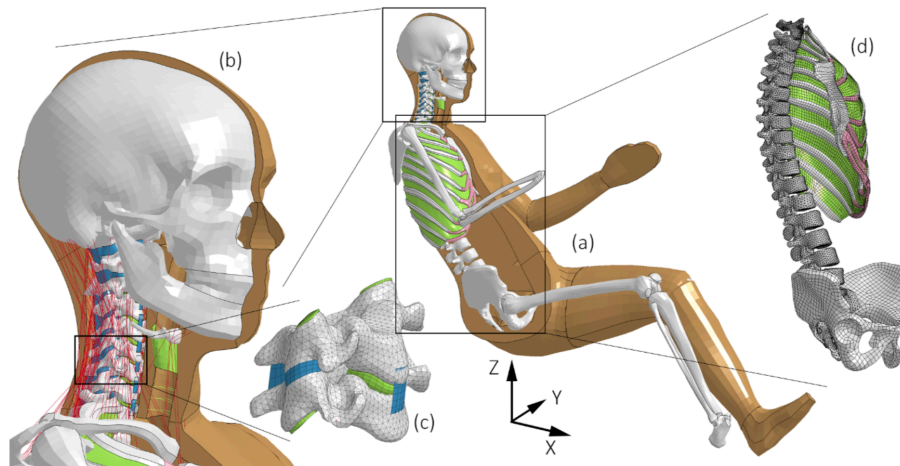


Figure 1.52. Overview of ViVa HBM (a), view of cervical spine (b), C5C6 vertebral segment (c) and axial skeleton, pelvis and left side of thoracic cage (d) ^[15]

Torso

The torso is modelled as a combination of rigid and deformable bodies. The external soft tissue and skin layer extends continuously from the neck to the superior portion of the femur. The spine, from T1 to sacrum and pelvis, is modelled with rigid bodies, connected with compliant kinematical joints. The ribcage is modelled with rigid costae and sternum, connected by linear elastic hexahedral elements representing the costal cartilage. The costae are then connected to each other by the intercostal muscles, modelled with linear elastic quadrilateral shell elements. In addition, the costae are attached to the thoracic vertebrae by spherical joints. The external soft tissues are connected to the skeletal rigid bodies by nodal constraints. The thoracic and abdominal cavities are modelled with tetrahedral elements, separated by a quadrilateral shell representing the diaphragm.

Head and neck

The cervical spine had previously been described and validated (by Östh et al. (2016)) for quasistatic loading on both segment and whole ligamentous spine level, as well as in dynamic rear-impact simulations. It consists of a rigid body head, linear elastic vertebrae, intervertebral discs and orthotropic membranes (intervertebral ligaments). In the simplified neck model, the intervertebral soft tissue structures are removed and kinematic compliant joints are implemented at the instantaneous centres of rotation for each vertebral joint of the model.

1.4.2 ViVa Model II – Advances in 2018

During the Nordic LS-DYNA Users' Conference (2018), a further development of the earlier created ViVA Model was presented: to increase the model biofidelity, the muscles responses had to be included (Figure 1.53).

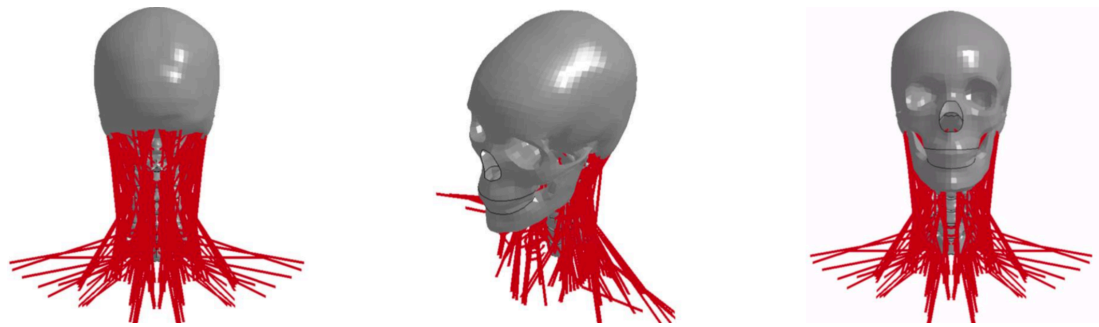


Figure 1.53. Implementation, calibration of LS-DYNA PID Feedback control of the FE models of cervical muscles ^[17]

The previously validated open-source head-neck model (VIVA Open HBM) was enhanced by the addition of muscle activation. The previous model contained 129 beam elements on both the left and right side of the neck. However, these muscles were defined as passive muscles model without any active tensile forces.

The first goal of the study presented in 2018 was to implement the LS-DYNA PID (Proportional Integral Derivative) feedback control mechanism on Finite Element models of cervical muscles. The second goal was to calibrate the PID control gains by conducting a parameter identification using LS-OPT with published-volunteer data in rear impact collisions being used as reference performance data. To activate these muscles, the closed-loop control strategy was applied. This method of controlling muscles activation with reflexive feedback control was adopted from Östh et al. [18] and Olafsdottir [19].

1.5 HUMOS HBM [20,21]

The HUMOS HBM Project was sponsored by the European Community (EC): the development involved fourteen different partners from automotive industry, research institutes, universities, software providers and public research organizations. The primary job phase started in 1997 and the first FE model was presented at the ESV Conference in 2001.

The second project phase started in 2002 and the improved HUMOS2 FE model was then released in 2006, together with an associated scaling and positioning tool.

1.5.1 HUMOS FE model

HUMOS program was a first step towards the development of commonly accepted models and computer methods since, even if computer methods were more and more widely used to optimize the safety devices, no biofidelic numerical tool was available.

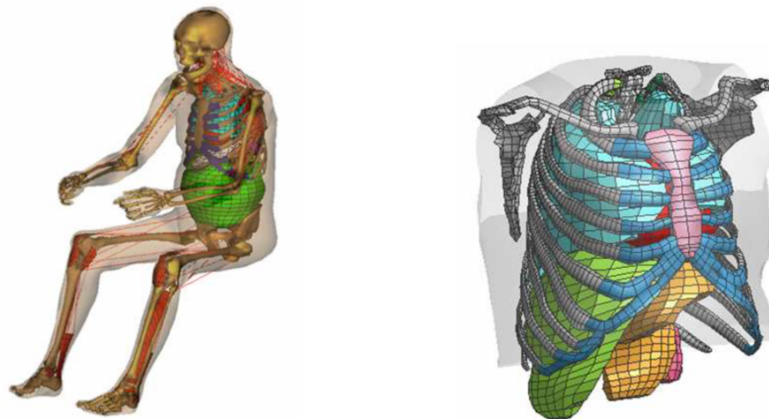


Figure 1.54. Overall view of Radioss HUMOS 50th male model (left) and detail of HUMOS thorax (right) [20]

The main aims of the HUMOS program were:

- To synthesize and complete the available knowledge of human body in terms of geometry, kinematics behavior, injury threshold and risk
- To implement this knowledge in the new human body materials

A wide bibliographical research supported those major goals. The geometry of the model is based on the one of a mid-sized male (50th percentile) in a car driver seated position and the main human body structures are then reconstructed using a CAD software and delivered to the so-called “modelling partners”. The meshing is based on the CAD definition and leads to models accounting for skin, bones, muscles as well as the main organs (lungs, heart, liver, kidneys, etc.).

The validation process was carried out on a segment basis. The final part of this program consisted in the assembly of the whole model. A correct representation of the main human body structures, together with most of the bones, muscles and internal organs and the assignment of satisfactory mechanical behaviour in a car crash simulation were needed to realize a biofidelic model structurally close to the real human body. This program led to a primary definition of a refined FE model of the human body in a driving sitting posture. It was implemented in three main dynamic computer codes: MADYMO, RADIOSS and PAM-CRASH.

Geometry acquisition

The main external dimensions of the human body were taken from commercially available databases, while some information concerning the geometry of the different organs and the position of the different structures in the seated position were missing. The choice was then to physically slice a frozen cadaver.

3D Geometrical reconstruction

The step consisted in the point-by-point transformation of the geometrical data previously generated in the CAD files. The main organs are reconstructed using available mathematical surface definitions (see Figure 1.55).

Meshing process

This step was carried out by different partners of the program, depending upon their experience. Some assumptions based on the anatomical description were also made to add some more muscle parts and some more ligaments. The decision was to keep the deformable elements number lower than 50.000 (Figure 1.56).



Figure 1.55. 3D Representation of the bony parts (left) and main organs (right) acquisition result ^[20]

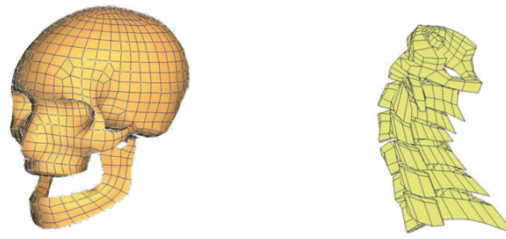


Figure 1.56. Mesh of the bony part of the skull (left) and of the cervical vertebrae (right) ^[20]

1.5.2 HUMOS2 FE model

The HUMOS2 project was the evolution of the HUMOS one. As in the previous case, the basic assumption of the project was to build a biofidelic model structurally close to the real human body. The second assumption was, instead, that all road users need to be correctly protected by the safety devices during the collision and it is consequently needed to develop personalized models able to represent all the population.

The HUMOS2 program was organized around different tasks.

The first two tasks aimed at providing meshes representative of the 5th percentile female and the 50th and 95th percentile male in sitting and standing positions, basing on European anthropometry measurements databases.

The statistical data were then used to develop a software which allows the scaling of the existing HUMOS Version 1 mesh (50th percentile) towards any other percentile from a set of main external dimensions. Before being scaled, the existing mesh (HUMOS) had been improved.

The third task dealt with the improvement of biomechanical behaviour knowledge, specifically concerning the mechanical properties of biological tissues, the effect of muscle tone and the whole-body response to realistic impact conditions. This knowledge was fundamental for the improvement and validation of the FE model.

The fourth task consisted, instead, in the improvement of the developed models by simulating the injury mechanisms and in the assessing of their biofidelity and injury prediction capabilities by referring to the PMHS sled tests previously performed.

The last task was dedicated to the extensive use of the HUMOS validated models in different impact conditions. A further objective of the project was to compare these capabilities with dummies in view to complete the regulations by numerical simulations.

Chapter 2

Occupants' posture in Autonomous Vehicles (AVs)

2.1 Autonomous Vehicles Development ^[22, 23, 24, 25]

Two emerging trends in personal transportation (automated vehicles –AVs– and on-demand mobility) may provide important alternatives to conventional ones (private vehicles and public transit). The so-called Automated/Autonomous vehicles consist in high-tech cars able to recognize the external environment and drive through it without the intervention of the human as a driver.

Even though now the AVs are only living the first phase of their development, several analyses have foreseen possible changes to personal transport, with potentially nearly all vehicles becoming autonomous by mid-century. Autonomous cars (also known as self-driving or driverless vehicles) are currently under development and have attracted growing research interest over the last years. More in particular, the technology implemented in AVs had a rapid development with the improvement, for example, of sensor capabilities and machine learning. The advances reached in communications, controls and embedded system fields are making it possible for the vehicle to take decisions in place of the drivers, such as steering, acceleration or deceleration.

Self-driving or autonomous vehicles are expected to deliver several key advantages over traditional human-driven vehicles. The main benefits of such solutions are thought to be linked with safety, increased mobility and travel convenience, more efficient road use, decreased congestion and reduced travel time, increased driver productivity, fuel economy and lower emissions.

However, to finally reach those goals, people have to accept and adopt the new technologies.

Even if it is not yet possible to know the effects on mobility and traffic congestion until large number of self-driving vehicles take to the roads, it is anyway possible to analyse their various safety aspects. The transition from human to machine, indeed, can be potentially disruptive both technologically and socially, opening new possibilities such as dispatching, parking and refuelling

vehicles without the human intermediation and providing mobility for people currently unable to drive.

2.1.1 Automation Levels ^[30]

Autonomous or Automated Vehicles (AVs) can be roughly defined as transports to move passengers or merchandise without human intervention. AV technology development began in 1977 in Japan [26] and it has successively included Germany, Italy, the European Union and the USA [27-29].

It is fully believable that *“AVs will become an emergent phenomenon in 2020, an accepted technology by the 2030s, and come to dominate personal transportation by 2050, as much as mobile phones have come to dominate personal telecommunications”* [30]. Moreover, on-demand mobility (as also enabled by smartphone apps) could become much more widespread by 2020s and grow to occupy a large share of personal transportation by 2050.

Even if the highest level of automation is represented by the completely unmanned vehicle, different steps in the development and introduction processes can be recognized before complete automation is achieved. For this reason, the International Society of Automotive Engineers (SAE) and the National Highway Traffic Safety Administration (NHTSA) defined five different automation levels, reported in Table 2.0 and explained here in the following.

A full set of parameters, referring to the operating environment and system function, are described as reported in the NHTSA website.

With reference to the SAE Levels of Automation reported in Table 2.0:

- DDT = Dynamic Driving Tasks
 - Sustained lateral and longitudinal vehicle motion: sequence of execution of manoeuvres to laterally and longitudinally control the vehicle (steering and acceleration/deceleration)
 - OEDR = Object and Event Detection and Response (monitoring of driving environment)
- DDT fallback = Dynamic Driving Task fallback (remedy action)
- ODD = Operational Design Domain

Level	Name	Narrative definition	DDT		DDT fallback	ODD
			Sustained lateral and longitudinal vehicle motion control	OEDR		
Driver performs part or all of the DDT						
0	No Driving Automation	The performance by the <i>driver</i> of the entire DDT, even when enhanced by <i>active safety systems</i> .	Driver	Driver	Driver	n/a
1	Driver Assistance	The <i>sustained</i> and <i>ODD-specific</i> execution by a <i>driving automation system</i> of either the <i>lateral</i> or the <i>longitudinal vehicle motion control</i> subtask of the DDT (but not both simultaneously) with the expectation that the <i>driver</i> performs the remainder of the DDT.	Driver and System	Driver	Driver	Limited
2	Partial Driving Automation	The <i>sustained</i> and <i>ODD-specific</i> execution by a <i>driving automation system</i> of both the <i>lateral</i> and <i>longitudinal vehicle motion control</i> subtasks of the DDT with the expectation that the <i>driver</i> completes the OEDR subtask and <i>supervises</i> the <i>driving automation system</i> .	System	Driver	Driver	Limited
ADS ("System") performs the entire DDT (while engaged)						
3	Conditional Driving Automation	The <i>sustained</i> and <i>ODD-specific</i> performance by an ADS of the entire DDT with the expectation that the DDT fallback-ready user is <i>receptive</i> to ADS-issued requests to <i>intervene</i> , as well as to DDT performance-relevant system failures in other vehicle systems, and will respond appropriately.	System	System	Fallback-ready user (becomes the driver during fallback)	Limited
4	High Driving Automation	The <i>sustained</i> and <i>ODD-specific</i> performance by an ADS of the entire DDT and DDT fallback without any expectation that a user will respond to a request to <i>intervene</i> .	System	System	System	Limited
5	Full Driving Automation	The <i>sustained</i> and unconditional (i.e., not <i>ODD-specific</i>) performance by an ADS of the entire DDT and DDT fallback without any expectation that a user will respond to a request to <i>intervene</i> .	System	System	System	Unlimited

Table 2.0. SAE Levels of Automation - Information report J3016

Level 0 (L0) – No Automation

The driver is the only one able to control the primary vehicle dynamics (brake, steering, throttle, etc.) at all times, and he is the only one responsible for monitoring the roadway and for safe operation of all vehicle controls. Vehicles including systems which only provide warnings (e.g. forward collision warning - FCW, lane departure warning – LDWS, blind spot monitoring), as well as systems providing automated secondary controls (e.g. wipers, headlight, turn signals, hazard lights, etc.) are still considered as belonging to the L0 automation level. Although a vehicle implementing vehicle-to-vehicle (V2V) warning technology alone would still be considered at this level, that technology is capable of providing warnings in several scenarios where sensors and cameras alone cannot.

Level 1 (L1) – Driver Assistance or Function-Specific Automation

At this level, automation technologies can involve one or more control functions: if multiple functions can be automatically performed, they operate independently from each other. The driver has overall vehicle control and he is the only responsible for safe operations, but:

- It is possible to cede limited authority over a primary control (e.g. adaptive cruise control - ACC)
- The vehicle can automatically assume limited authority over a primary control (e.g. electronic stability control ESC)
- The automated system can provide added control to aid the driver in certain normal driving or crash-imminent situations

The vehicle may implement multiple capabilities combining individual driver support and crash avoidance technologies, but it does not replace driver vigilance or assume driving responsibility. The vehicle's automated systems may only assist the driver in operating one of the primary controls. Therefore, there is no combination of the vehicle automated features working together that can enable the driver to disengage from physically operating the vehicle (i.e. contemporary removing the hands from the steering wheel and the feet from the pedals).

The L1 automation technologies are mainly represented by the so-called "ADAS" (Advanced Driver Assistance Systems), such as cruise control - CC, automatic emergency braking – AEB and lane keeping.

Level 2 (L2) – Combined Function Automation or Partial Driving Automation

Level 2 involves automation of at least two primary control functions designed to work together to discharge the driver of controlling those functions. However, the driver is still responsible for monitoring the roadway and safe operation and he is expected to be available for control at all times and on short notice. An example of combined functions enabling an L2 system is adaptive cruise control in combination with lane keeping.

The main difference between L1 and L2 automation levels is that in L2 an automated operating mode is enabled such that the driver is disengaged from physically operating the vehicle.

Level 3 (L3) – Conditional Driving Automation or Limited Self-Driving Automation

At this automation level, vehicles enable the driver to cede full control of all safety-critical functions under certain traffic or environmental conditions and, in those conditions, to rely heavily

on the system to monitor for changes of those circumstances requiring transition back to driver control.

In any case, the driver is expected to be available for occasional control, but with sufficiently comfortable transition time. The vehicle is designed to ensure safe operation during the automated driving mode. An example can be an automated vehicle that can determine when the system is no longer able to support automation and then alerts the driver to reengage in the driving task, in an appropriate amount of transition time.

The main difference between L2 and L3 is that a L3 vehicle is designed so that the driver is not expected to constantly monitor the road.

Level 4 (L4) – Full Self-Driving Automation or High Driving Automation

The L4 automated vehicle is designed to perform all safety-critical driving functions and monitor roadway conditions for an entire trip. The driver can therefore provide destination or navigation input, but he is not expected to be available for control at any time during the trip. This includes both occupied and unoccupied vehicles and, by design, safe operations are only relying on the automated vehicle system. However, the vehicle ODD is still limited.

Level 5 (L5) – Full Driving Automation

The only difference between L4 and L5 automated vehicles is that L5 ones have no limit of Operational Design Domain: the automated manoeuvres can be performed in any place and with any traffic condition.

2.1.2 Autonomous Vehicles challenges - Safety and security ^[24]

“A typical prediction of the future Autonomous Vehicles includes people being relieved from the stress of daily driving, perhaps even taking a nap on the way to work. This is expected to be complemented by a dramatic reduction in driving fatalities, due to replacing imperfect human drivers with (presumably) better computerized autopilots” [24]. However, there are a number of areas presenting significant challenges in creating acceptably safe, fully autonomous vehicles compared to the conventionally human-driven vehicles. Therefore, it is not easy to develop a safe fully-AV. On the opposite, there is a set of problems that must be solved in a coordinated and inter-disciplinary manner (e.g. technology implementation and improvement, environments for testing, etc).

Moreover, even automotive computing security has been now receiving increased attention: security measures will be than necessary not only to counteract attacks on specific vehicles, but also to avoid system-level attacks and failures. As an example, it will be necessary to blindly trust in the computer security of other vehicles or roadside infrastructures during autonomous driving tasks. A possible solution could be to encrypt vehicle-to-vehicle (V2V) communications, but it is essential to be sure that the vehicle you are communicating with is delivering correct information.

The communication and cooperation between vehicles and humans, then, is becoming more and more relevant: AVs will have to interact with the human drivers of the near vehicles, bicycles, scooters and with general human road users. In urban areas, moreover, vehicles should also deal with pedestrians, which are less likely to strictly follow road rules.

As a consequence, even the social impact and acceptance of autonomous vehicles will be a complex process.

2.2 Driver behaviour during Highly Automated Driving

As already introduced in the previous section, occupants of future highly automated vehicles are not supposed to pay attention to the road conditions anymore. On the contrary, they are only expected to relax and enjoy the journey.

However, the technology to enable complete automation, especially from Level 3 to Level 5, is extremely sophisticated and, moreover, currently very expensive.

Different studies have been already conducted in order to analyse the behaviour of vehicle occupants during automated manoeuvres.

2.2.1 Driving and non-driving related tasks and postures ^[31, 32, 35]

An important concept, mentioned by Kun et al. [33], is referred to the so-called Non-Driving-Related Tasks or Activities (NDRTs or NDRAs). More in details, when considering AVs, the driver (or, better, occupant) can “*perform a multitude of activities and can fully concentrate on those, without taking care of vehicle controls*” [32]. It is therefore useful and interesting to understand which activities can be more likely to be performed inside the vehicle and how the driver posture and space can be adapted to better accomplish those tasks. Automotive manufacturers may then provide the possibility to recline or relax the driver’s seating position, withdraw or collapse the steering wheel or provide additional interior lighting to enhance comfort, space and visibility.

Actually, as also declared in the study conducted by Yucheng Yang et al. [34], drivers already handle Non-Driving-Related Tasks (NDRTs) in the current manual driving condition, such as talking to the other occupants, using technological devices, tune radio channels and volume etc.

In Level 3 automated vehicles, a sort of intermediate step between the manual and automated driving is achieved: the driver is, by definition, “*expected to be available for occasional control, but with sufficiently comfortable transition time*”. Furthermore, from Level 3 on, the driver is more and more expected to conduce NDRA, without being interrupted by the driving tasks.

For the same research [34], 122 participants between 18 and 79 years old were interviewed through an online questionnaire with reference to:

- NDRTs performed during manual driving
- NDRTs and their associated NDRPs (Non-Driving-Related Postures) in AD conditions

However, most of them had never used the Advanced Driving Assist Systems (ADAS), like the automated parking assistant (83%), active cruise control (70%) and lane-keeping assistant (75%).

In Figure 2.0, the statistical results of the test comparing the NRDTs in today and future (automated) vehicles are reported:

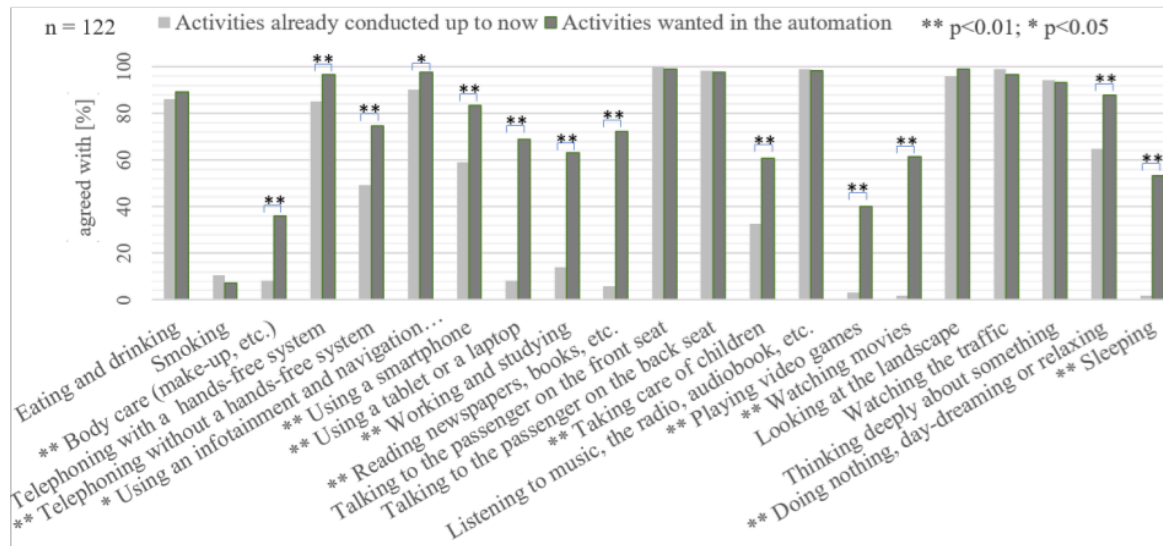


Figure 2.0. Comparison of NRDTs today and in automated vehicles [32]

In addition, based on the results obtained from the online questionnaire, the main human body posture angles were also obtained (ref. Figure 2.1). As an example, the reclined posture could be one of the most preferred in Highly Automated Vehicles (HAVs). The distributions and

descriptive statistics of torso, thigh, knee and seat back angles of four supervised postures are reported in Figure 2.2.

The participants expressed also their favourite posture in relation to the performed NRDT (Figure 2.3). For instance, the “seated facing the driving direction” is still the most preferred posture by 10 activities, except for “sleeping”, for which the “reclined posture facing the driving direction” is generally chosen.

Furthermore, Figure 2.4 shows the same results of Figure 2.2 for six different defined NDRTs.

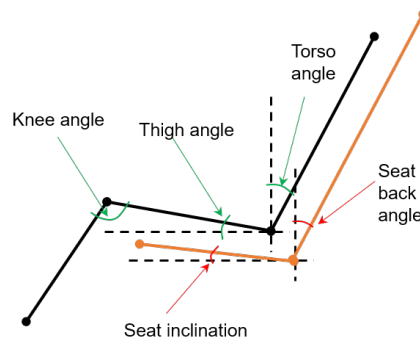


Figure 2.1. Main driver posture angles

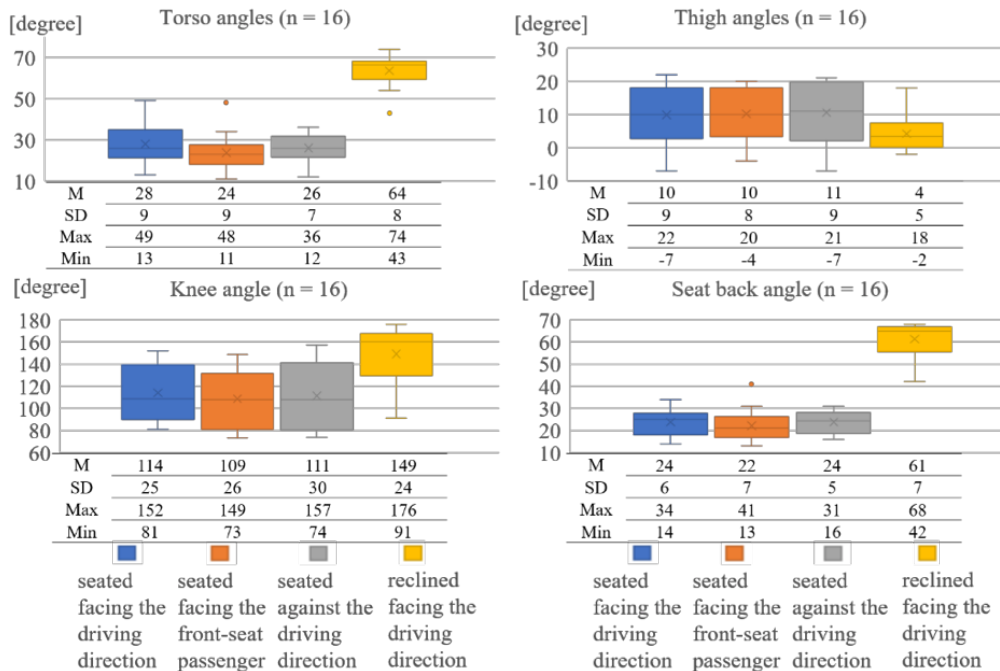


Figure 2.2. Relationships between NDRTs and Non-Driving-Related-Postures (NDRPs)^[32]

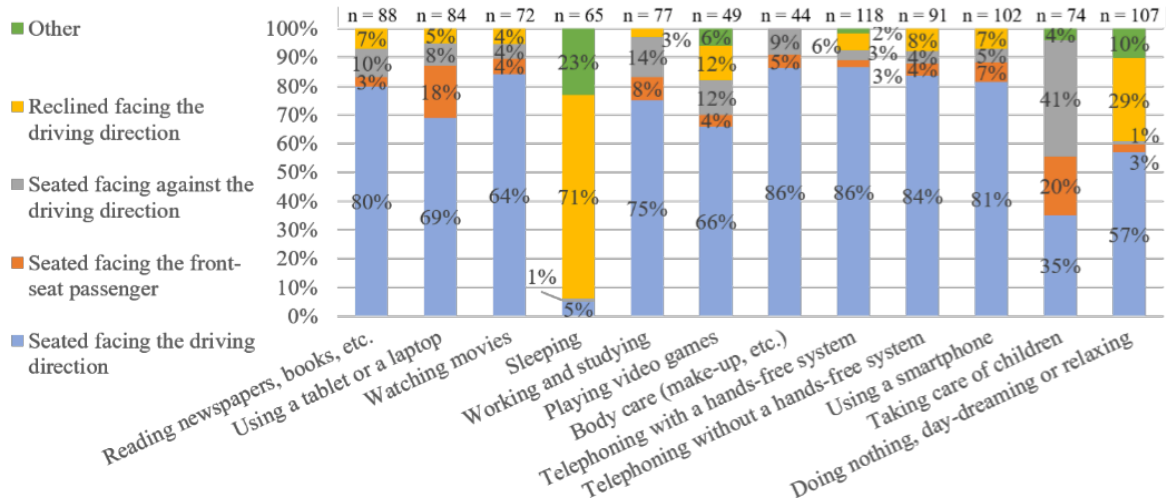


Figure 2.3. Postures and seat back adjustments without NDRTs^[32]

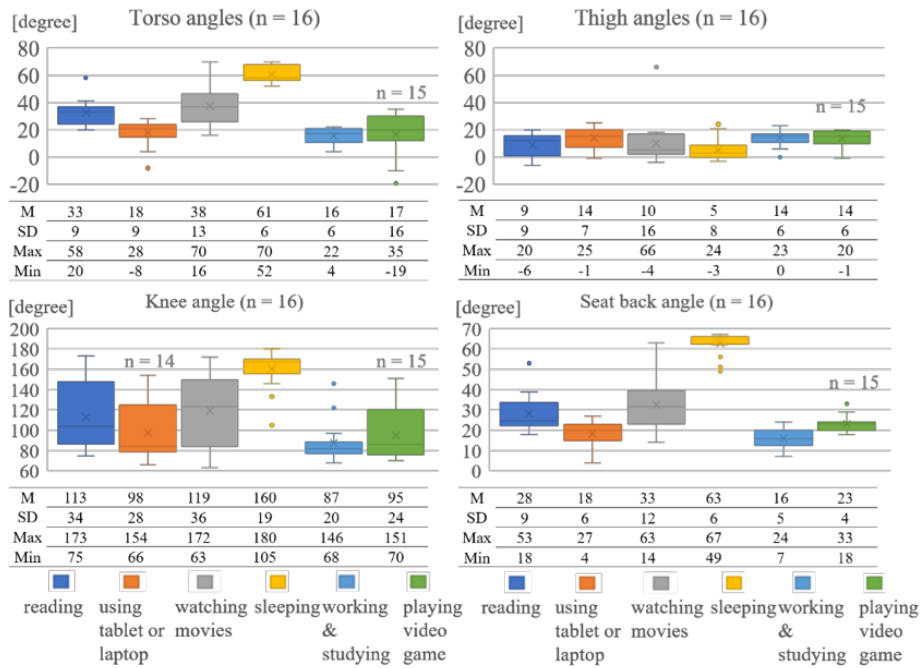


Figure 2.4. Postures and seat back adjustments with NDRTs^[32]

Another relevant study in this field is the one conducted in 2017 by Large et al. [35], based on a social experiment. The aims were to understand the nature of the activities performed by the drivers/occupants during automated control and to appreciate the possible innovations that could be implemented in future vehicles with respect to interior design and packaging.

A realistic driving L3 AV simulator (Figure 2.5) was built and participants were asked to complete, for five consecutive weekdays, the same 30 minutes of highway, bringing with them

items and devices (e.g. paper documents and computing devices) to be freely used during periods of automation (Figure 2.6).



Figure 2.5. Driving Simulator showing motorway scenario ^[35]

In some cases, particularly when small items such as books, papers, smartphones or tablets were used, the vehicle steering wheel provided good support for the object and the driver were also able to easily have a look on the road situation.

In other cases, on the opposite, when using larger items (e.g. laptops), the steering wheel hindered the activities and drivers were required to recline or adjust their seating position or place the larger items elsewhere (e.g. passenger seat).

The drivers regularly changed their posture (Figure 2.7) throughout periods of automated control due to the adoption of new tasks or as a strategy to alleviate discomfort, boredom, fatigue, etc.



Figure 2.6. Occupants performing NRDTs in AV Driving Simulator ^[35]



Figure 2.7. Different postures adopted during periods of automated driving^[35]

2.2.2 Future seating positions in Highly Automated Vehicles^[35, 36]

Until now, only the most frequent postures taken by the occupants of AVs still equipped by standard internal layout and packaging were considered. However, as mentioned before, the higher the level of automation, the higher the possibility for the occupant to adopt different postures.

In particular, in Level 4 and Level 5 vehicles, in which humans do not have to care about driving activities at all, new configurations for the vehicle interior can be designed.

As an example, the seat could have the possibility to be rotated and/or to be fixed at different angles after rotating, in order to re-create a sort of “living-room atmosphere” between the different vehicle occupants. However, those new and innovative postures, apart from potentially causing motion sickness, raise critical safety issues in crash tests. The aim of the research study computed by Larsson et al. [36] was exactly to identify future seating positions and activities in Highly Automated cars and to explore new attitudes towards extra restraint systems.

The different layouts among which 52 users had to choose are reported in Figure 2.8. The most preferred position for longer family drives is the C configuration, then followed by E and D. In addition, participants showed positive attitude towards extra restraint systems, if they allowed new seating positions.

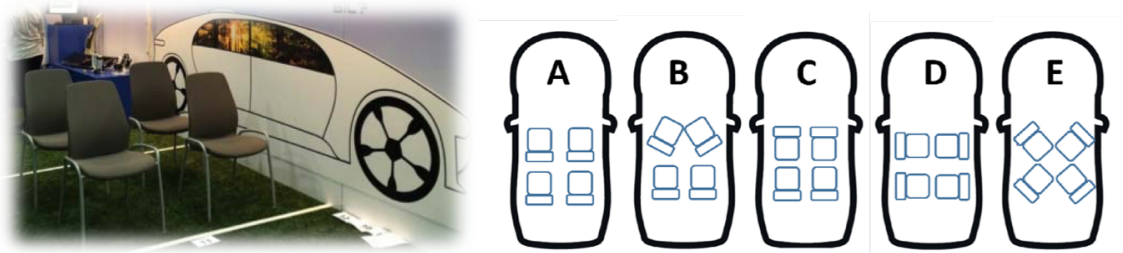


Figure 2.8. Test scenario (left) and different possible seat configurations^[36]

Chapter 3

Vehicle Model and THUMS HBM Positioning

3.1 Vehicle Model

In this Thesis work, carried out in cooperation with the Centro Ricerche Fiat (CRF), the model of a traditional Internal Combustion Engine (ICE) based vehicle is considered. However, as already anticipated in the Preface Chapter, it is supposed to be equipped by the Level 3 Autonomous Vehicle technologies. The driver may therefore compute secondary tasks while the vehicle is in control.

The FE model of the vehicle, delivered by the CRF, is reported in Figures 3.0 and 3.1:

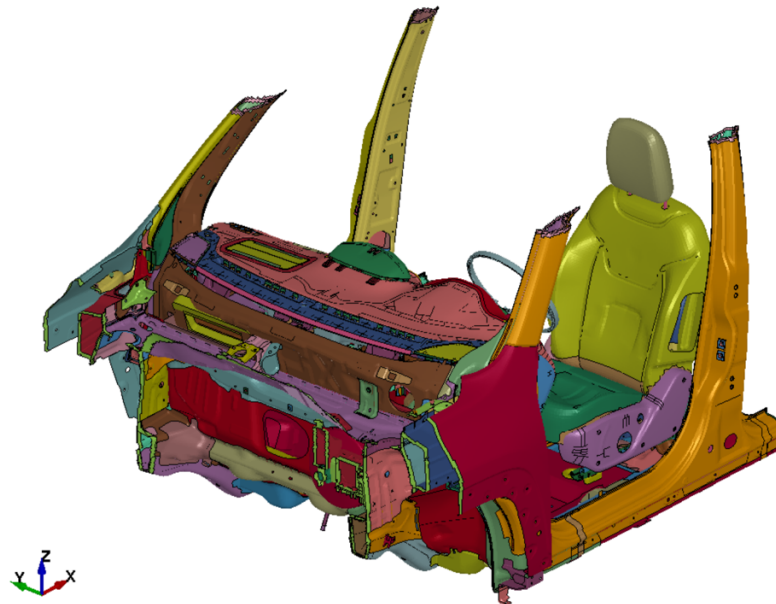


Figure 3.0. Simplified SLED Model of the vehicle – Isometric view

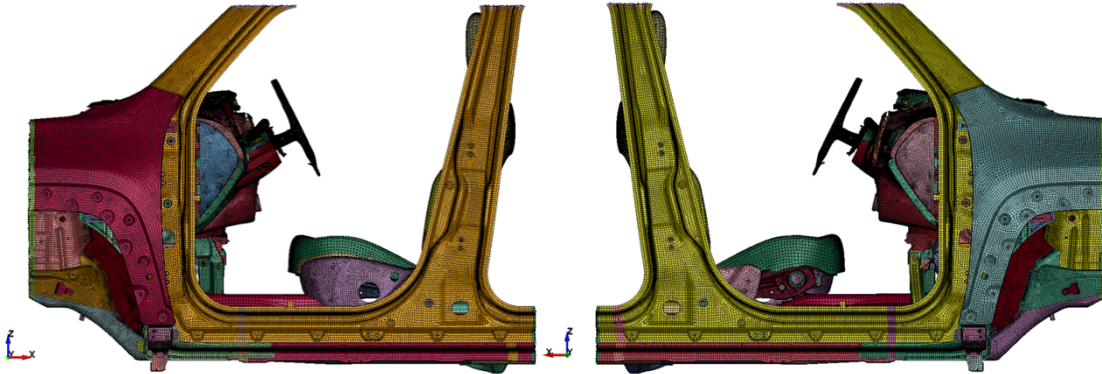


Figure 3.1. Simplified SLED Model of the vehicle – Lateral xz left plane (left) and xz right plane (right) views

The model includes the main components of the frontal part of the vehicle Body in White (BiW) and of the internal cabin. In particular, the anterior part of the vehicle floor, the A and B pillars, the complete dashboard with the steering wheel and the Driver Air Bag (DAB), the firewall and the driver seat are included. On the opposite, the engine compartment has been omitted, as well as the passenger seat, the roof and the rear part of the vehicle. The choice to consider this simplified Multi Degrees-of-Freedom SLED has been taken with the aim of reducing both the computational effort of the model itself during the simulations and the risk of errors. For these reasons, actually, it is of common practice to implement those simplified models in this kinds of safety studies.

However, in order to represent the reality as faithfully as possible, the equations of motions, implemented in the code as pulses, are the ones obtained during the real crash tests, involving the full vehicle. Those deceleration pulses, defined as velocities in input, are directly applied to the vehicle body (in four points: two in the front and two in the rear); the only necessary assumption is that the vehicle floor deforms as a rigid body.

The pulses (in Figures 3.2-3.7 the ones for FWRB) are coming from two reference frontal impacts (ref. §5.1):

- Full Width Rigid Barrier (FWRB) at 50 km/h
- Offset Deformable Barrier (ODB) at 56 km/h

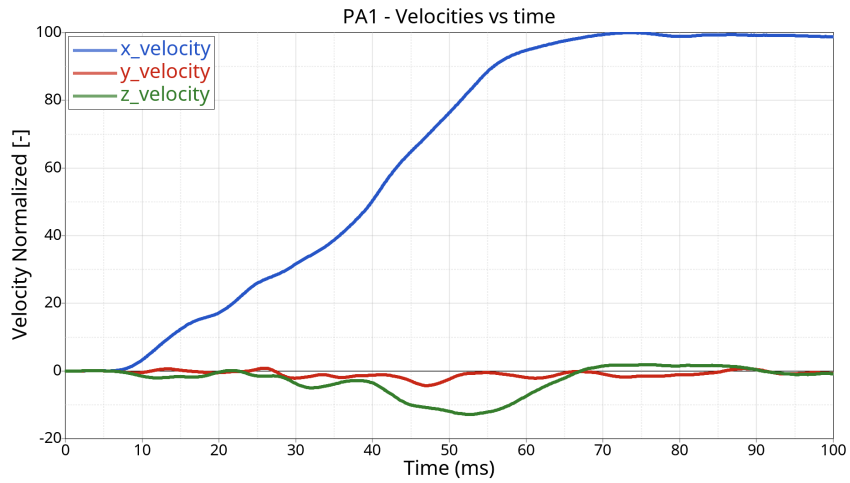


Figure 3.2. Velocity Pulse at point PA1 (anterior-left point of vehicle frame)

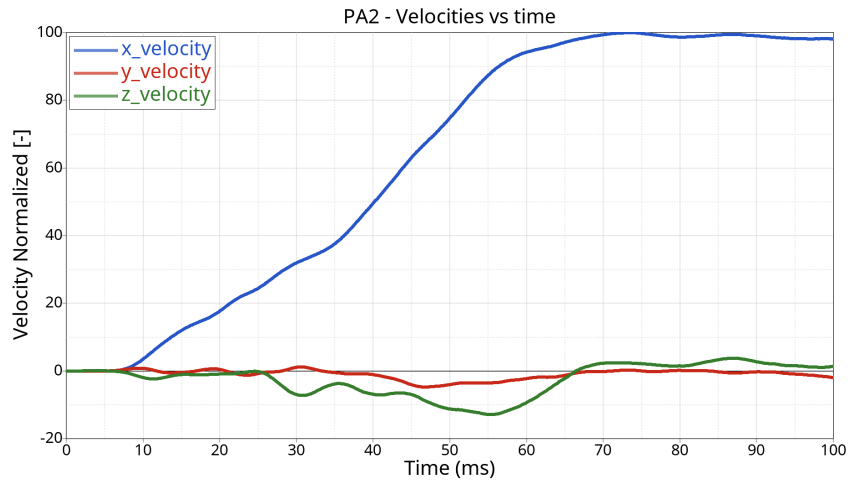


Figure 3.3. Velocity Pulse at point PA2 (anterior-left point of vehicle frame)

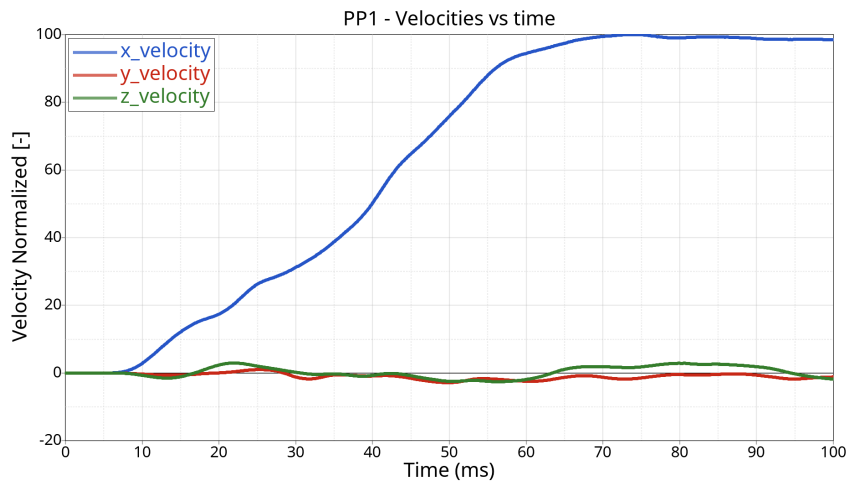


Figure 3.4. Velocity Pulse at point PP1 (posterior-left point of vehicle frame)

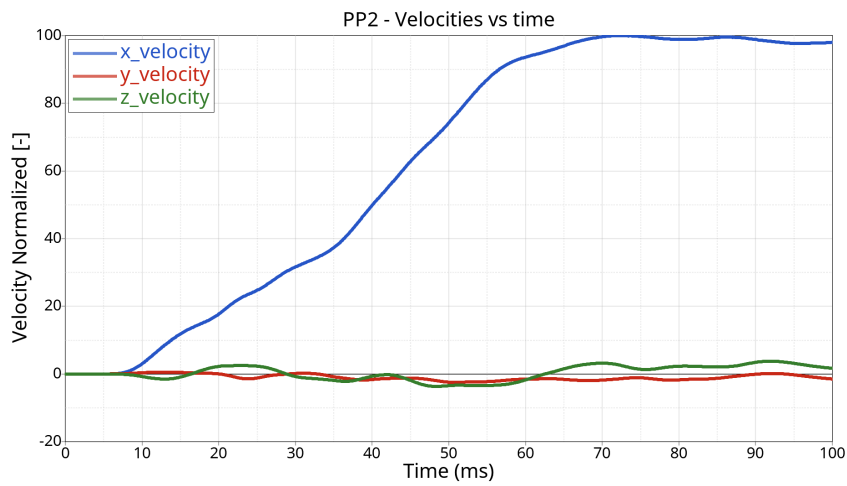


Figure 3.5. Velocity Pulse at point PP2 (posterior-right point of vehicle frame)

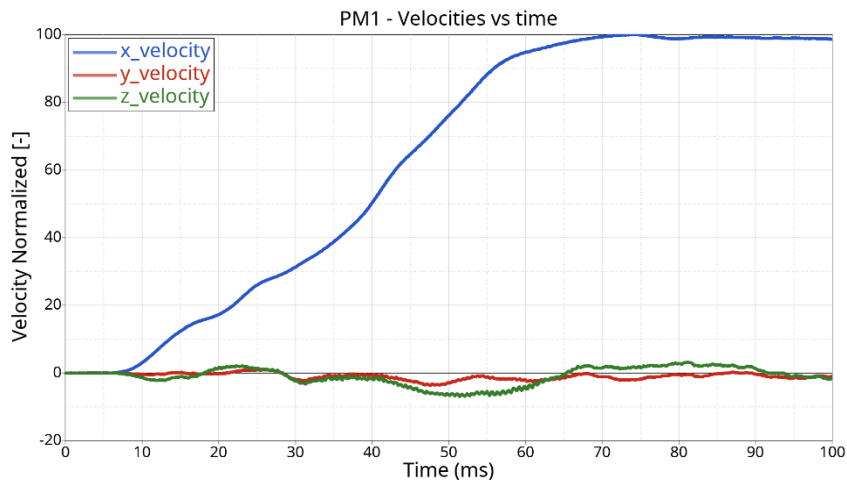


Figure 3.6. Velocity Pulse at point PM1 (anterior-middle point of vehicle frame)

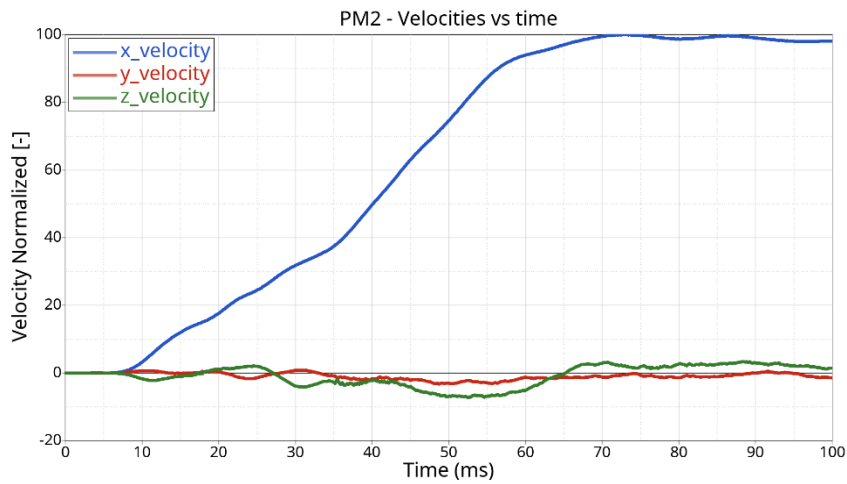


Figure 3.7. Velocity Pulse at point PM2 (posterior-middle point of vehicle frame)

3.2 Thesis work roadmap

The main Thesis steps are represented in Figure 3.8 and they can be shortly summarized as follows:

- Simulation set-up
- Definition of impact configurations (FWRB and ODB)
- THUMS HBM in Conventional driving posture configuration - Modelling and simulations of the two impact cases:
 - THUMS positioning (PIPER Tool - §3.2) in vehicle environment
 - Creation of the HBM footprint on the vehicle seat undeformed model (§4)
 - Creation of the shoes for the THUMS HBM positioned model (§4)
 - Seatbelt and sensors implementation (§4)
- Comparison of results with the conventional THOR dummy FE model (§5)
- THUMS HBM in Out-of-Position (OOP) posture - Modelling and simulations of the two impact cases
 - Repeat previous points a-d for the OOP posture configuration (§4)
- Analysis of OOP results and comparison with the conventional driving posture simulation (§6)
- Final considerations

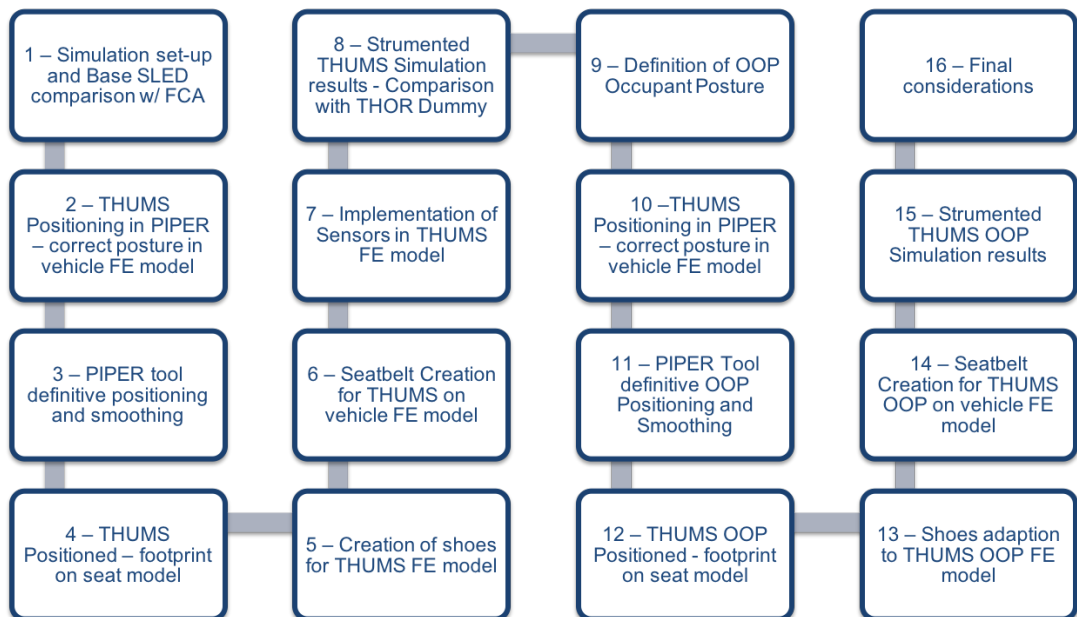


Figure 3.8. Thesis Project Roadmap – Main steps

3.3 Original THUMS Occupant model and Positioning Tool [37]

Once that the simulation set-up is completed, the THUMS Occupant model can be positioned in the vehicle environment. The original THUMS model (in the following, also, “non-positioned”) is reported in Figure 3.9.

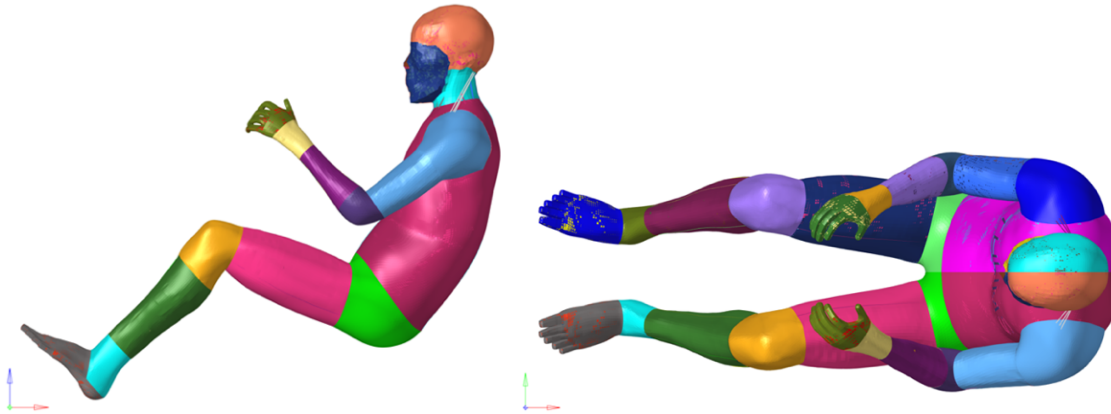


Figure 3.9. Original (non-positioned) THUMS V. 4.02 FE model – side xz (left) and top xy (right) views

The non-positioned FE model inserted in the vehicle environment is shown in Figures 3.10 and 3.11. Its posture has to be modified, in order to be similar to the THOR dummy model one.

This is done to reduce to the minimum the number of variables between the two models and to better compare their simulation results. To this purpose, the geometrical approaches used to position conventional FE dummy models cannot be directly used, mainly due to the presence of soft tissues. *“The most common approach used for positioning FE HBMs is to perform a full FE simulation [...], between the original and target position. Among alternative approaches, a constraint-based simplified simulation approach was recently proposed and implemented in the PIPER open source software”* [37].



Figure 3.10. Original THUMS in vehicle FE model – side xz (left) and section (right) views



Figure 3.11. Original THUMS in vehicle FE model – isometric (above) and frontal (below) views

3.3.1 Scaling and Positioning of the HBM Model – the PIPER Tool ^[37, 38]

In this Thesis work, the PIPER (Position and Personalized Advanced Human Body Models for Injury Prediction) open-source Scaling and Positioning Tool, developed within a European Commission Project, is used.

Since it is not yet possible, in FE format, to link an entity to an anatomical structure (i.e to indicate that something is a bone, a muscle, etc.), “*it is desirable to associate some of the FE entities to anatomical concepts as these are useful for scaling or positioning*” [38]. This association has been implemented in the PIPER software through the use of metadata. The latter are used to describe anatomical structure and functional constraints of the finite element model. In this way, the software only captures the anatomical entities to be transformed and the HBMs are converted into a simplified model with limited number of degrees of freedom.

The original HBM is imported in the software, together with the necessary environmental models (e.g. steering wheel, lower part of the dashboard, etc.), as reported in Figure 3.12. By doing this, the main dimensions and obstructions can be previously detected. To this purpose,

only the strictly necessary models of the vehicle environment are considered (e.g. steering wheel only, instead of entire dashboard), so that high computational cost is avoided.

The adjustment of the HBM posture is performed by following geometrical considerations.

As also reported in [37], “*the simulation is driven by positional and/or angular targets defined for the bones and joints, and can be interfaced with a priori knowledge [...]*”. Furthermore, “*the simulation is interactive [...] and helps to quickly adjust and define a plausible target [...] which can be used for positioning by full FE simulation [...] or to transform directly the original model*” [37].

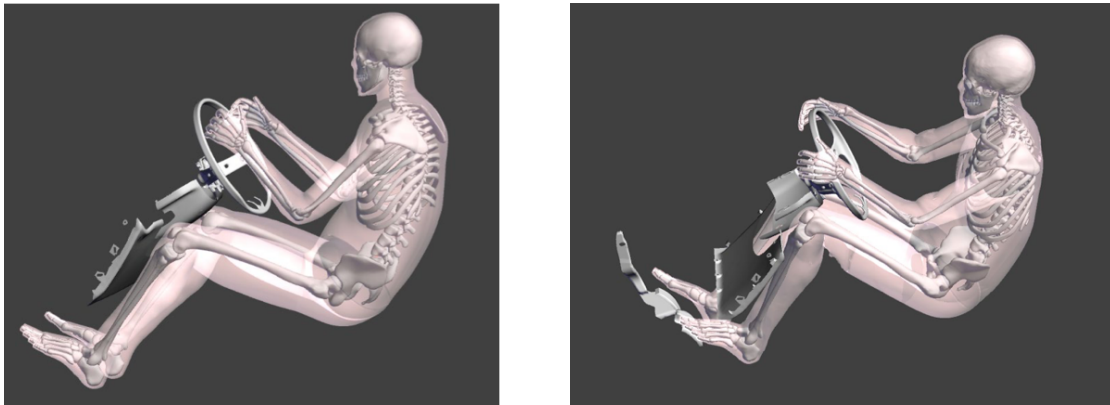


Figure 3.12. PIPER software – HBM Positioning: THUMS and necessary environmental models

In particular, three main software functions are used in order to move the different human body parts:

- *Landmarks positioning*: the landmarks, mainly corresponding to the nodes of the different bones’ extremities, are defined in the PIPER through an appropriate file, editable by the user; they can be moved either by manually changing their coordinates or by physically moving the landmark symbols (yellow points in Figure 3.13); in addition, once positioned, they can be exported in a dedicated file, so that it is possible to save the desired posture;
- *Joint rotations*: the angles of the main human body joints can be directly modified
- *Fixed bones*: if the imposed motion does not involve some specific bones, or their desired location has already been achieved, they can be fixed in order to maintain their position (Figure 3.14)

“*However, when the simplified simulation is used to transform the original model directly, the simplifications often produce surface (shape) and volume (internal) artefacts which can lead to degraded element quality and inverted elements*” [37]. This issue is solved in the last positioning step (Smoothing phase).

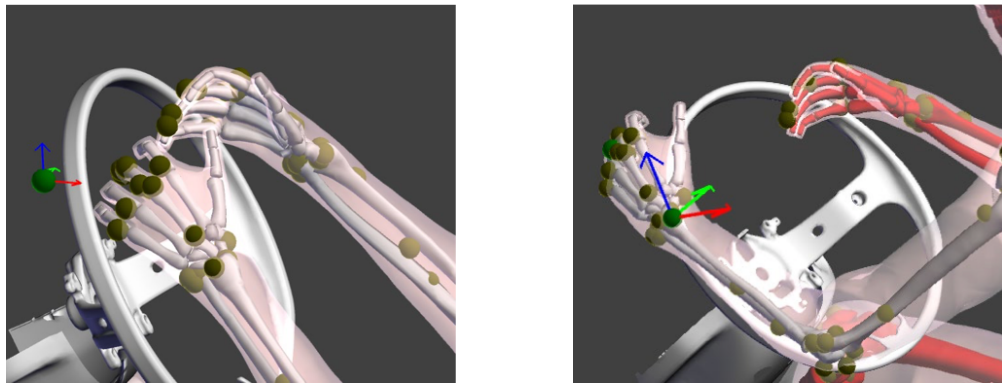


Figure 3.13. PIPER software – HBM Positioning: Landmarks before (left) and after (right) positioning phase



Figure 3.14. PIPER software – HBM Positioning: Fixed Bones represented in red – The reported configuration is the one used, for instance, to correctly position the legs, without moving the other bones

The main positioning phases to be executed in the PIPER tool, therefore, after having imported the HBM model, are:

- In the “Pre-Positioning” Module window, the landmarks and the joints can be modified to reach the final desired position
- In the same Module, by means of the “Positioning” button, the model moves and reaches the desired, manually imposed configuration
- In the “Smoothing Module”, the quality of the model mesh, usually degraded due to the body motion, is improved, so that the final positioned FE model can be exported and read by the solver code

3.3.2 PIPER Tool – Advantages, disadvantages and considerations

By using the PIPER tool in this Thesis, some advantages and disadvantages have been recognized. Moreover, an easy and straight-forward strategy to overcome the major software issues is here reported.

Advantages

- The positioning of the different human body parts by means of landmarks and joints motion results to be clear, easy, intuitive and very flexible, since the whole x , y and z coordinates can be separately imposed
- Low computational cost for model positioning is observed
- The metadata files are available for different HBMs

Disadvantages

- During the main positioning steps, when the body angles undergo big variations, high elements distortion and degraded mesh result
- The computational time needed for the steps for the improvements of the mesh quality (performed in the “Smoothing module”) is quite high
- If the smoothing action is applied at global scale (without acting on the single entities), low quality result can be achieved

Hints and suggestions

The basic procedure to position a generic HBM, indicated also in the PIPER Tool User’s Manual, consists in importing the model, moving the body parts towards the desired posture and smoothing the positioned HBM in order to improve the mesh quality.

However, in light of the several trials made during this job, an easier and more effective procedure has been experimented. In particular, the positioning phase is not done in a single step, then followed by a single smoothing phase, but those two phases are alternately performed. Therefore, once having defined the desired global position and exported the Landmarks list, a step-by-step positioning process is suggested.

The scheme of the procedure is reported in Figure 3.15. The overall timing needed to complete the whole steps (on a simple laptop) is between three and four hours.

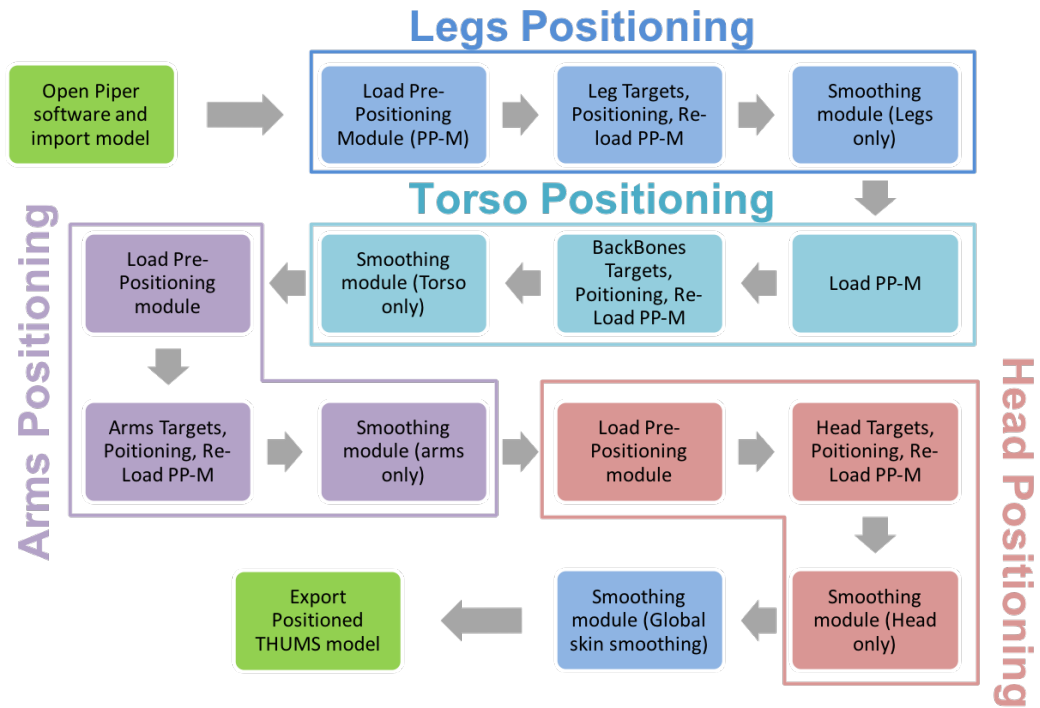


Figure 3.15. PIPER software – HBM (THUMS) Positioning steps

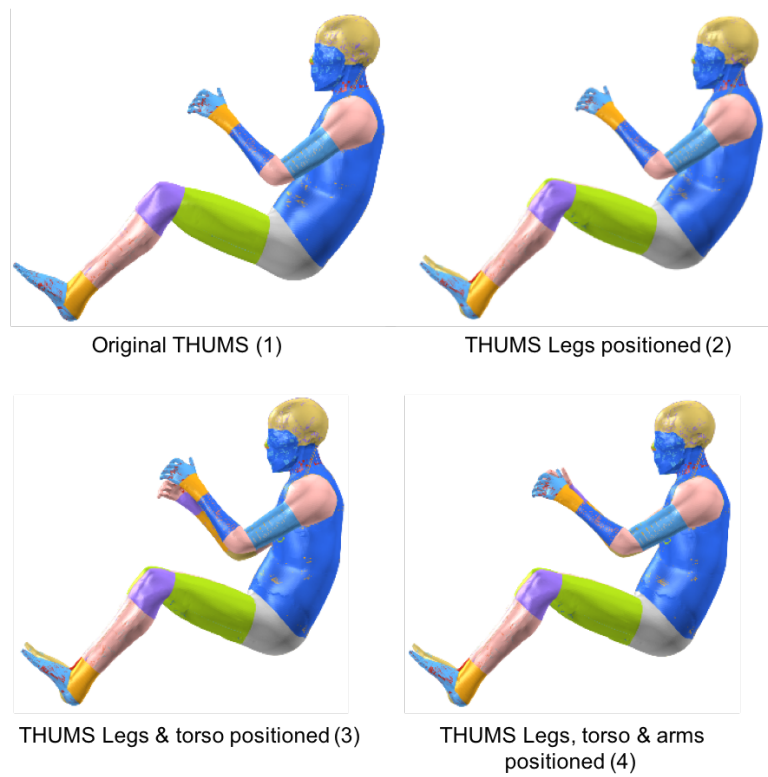


Figure 3.16. PIPER software – HBM (THUMS) different steps of the positioning process

Moreover, in order to have a clearer idea of the mesh quality of the model, the HBM can be exported from the PIPER tool after each smoothing phase and imported in a generic Pre-Post Processing software to perform the necessary element checks. In this way, if the mesh quality is acceptable, the following positioning step can be performed. On the contrary, an additional smoothing step in the PIPER environment should be carried on before moving to the subsequent human body motion step.

This procedure helps to obtain an higher mesh quality and lower computational time is required rather than applying a single and global smoothing action at the end of the different positioning phases.

The different configurations of the THUMS model during the different positioning steps, illustrated in the flowchart of Figure 3.15, are reported in Figure 3.16.

Chapter 4

Simulations Set-up: Conventional Driving and Out-of-Position Configurations

4.1 THUMS Positioned FE Model in Conventional Driving Posture

In the first step of this Thesis, as introduced in §3.2, the crash simulations are performed by positioning the THUMS Finite Element HBM in a typical driving posture. In this case, therefore, the vehicle is assumed to be controlled by the human driver, as a conventional one.

In order to be as similar as possible to the one of the THOR dummy, as anticipated in §3.3, the driver posture has, therefore, to fulfil the following requirements:

- The backbone must be arranged in a straighter configuration, with respect to the original model
- The left foot is placed on the specific footrest, located on the left side of the pedals
- The right foot is positioned in such a way that the heel point lies on the vehicle ground and the tip is in contact with the accelerator pedal
- Both the hands are kept on the steering wheel

The THUMS model used in the simulations, positioned by means of the PIPER Tool (§3.3), is reported in Figure 4.0:

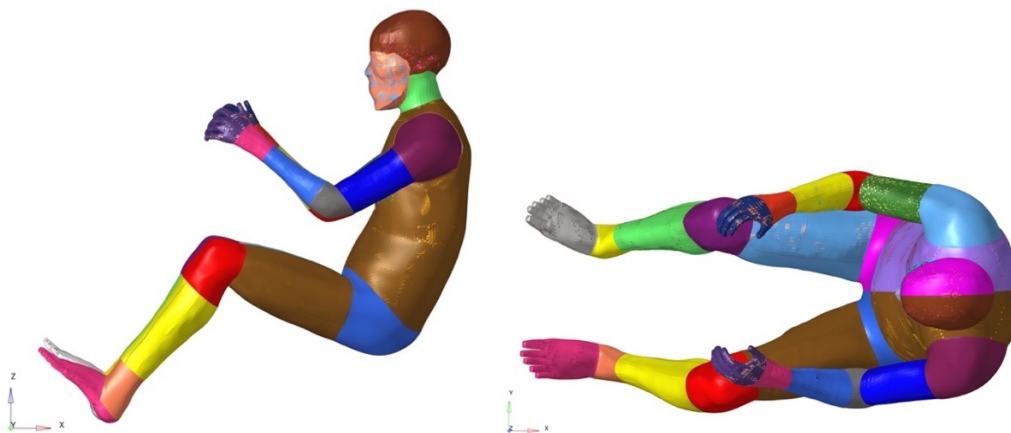


Figure 4.0. Positioned THUMS V. 4.02 FE model – side xz (left) and top xy (right) views

Here in the following, the comparison between the original and the positioned THUMS models is reported: in particular, Figure 4.1 shows the main human body angles of the non-positioned configuration, whereas Figure 4.2 shows the same data for the HBM obtained at the end of the PIPER Tool positioning process.

The torso angle α is decreased, so that the back of the driver becomes straighter. The knee angle γ , additionally, is reduced to correctly position the feet as previously described. The shoulder angle ε and the elbow angle δ are then increased to properly adjust the hands on the steering wheel of the vehicle model used for the simulations.

The final configuration of the positioned THUMS and the comparison between the two models in the vehicle environment are reported, respectively, in Figures 4.3 and 4.4.

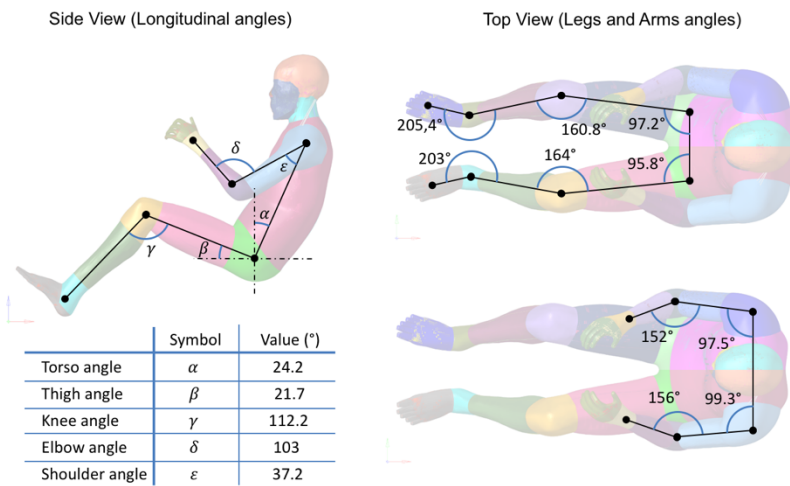


Figure 4.1. Original (non-positioned) THUMS V. 4.02 FE model – Main Body angles

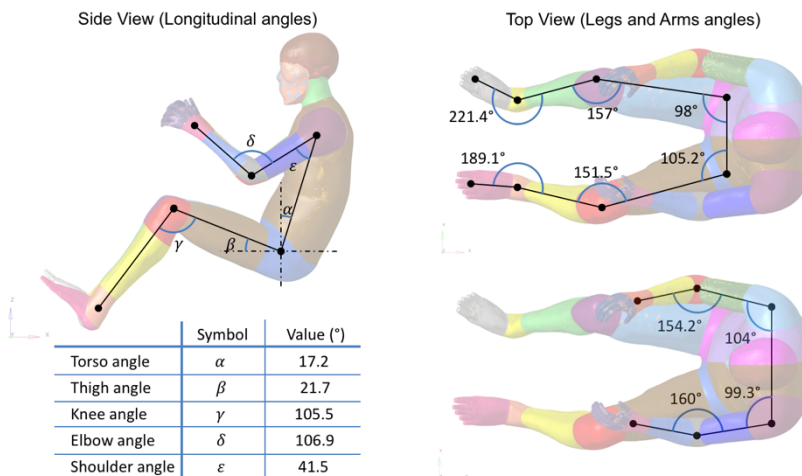


Figure 4.2. Positioned THUMS V. 4.02 FE model – Main Body angles

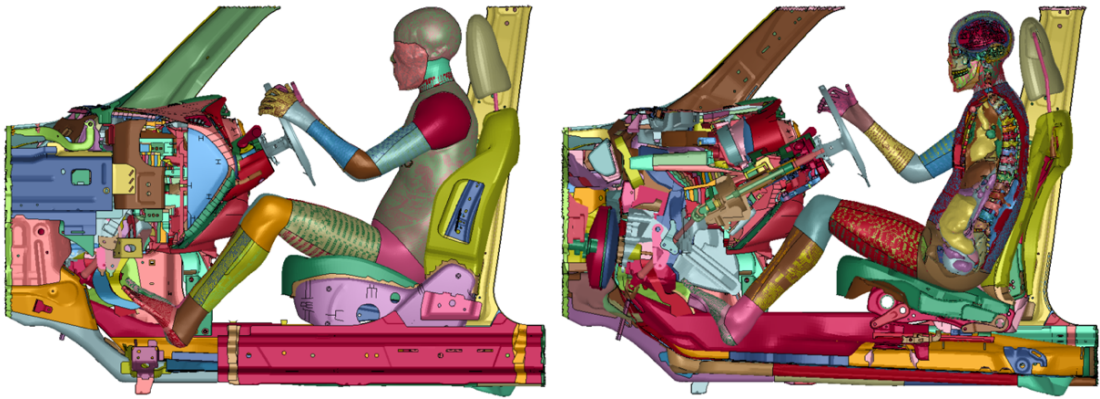


Figure 4.3. Positioned THUMS in vehicle FE model – side xz (left) and section (right) views

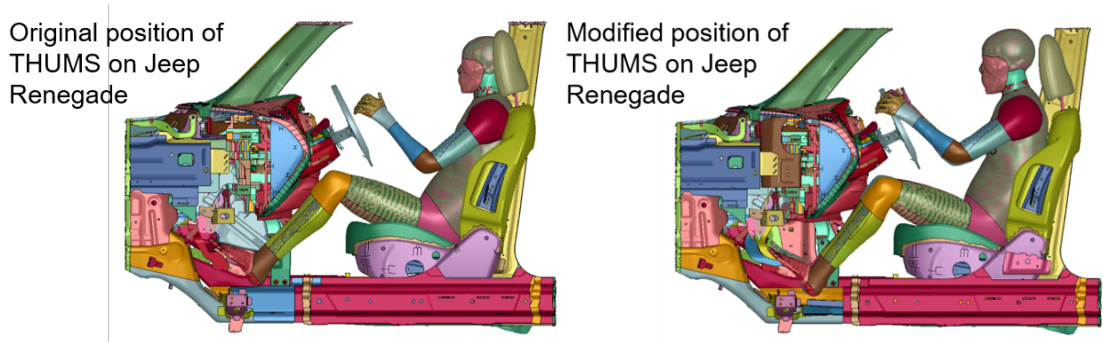


Figure 4.4. Original (left) vs Positioned (right) THUMS in vehicle FE model – side xz views

A further comparison, by overlapping the original and the positioned THUMS models, is shown in Figure 4.5.

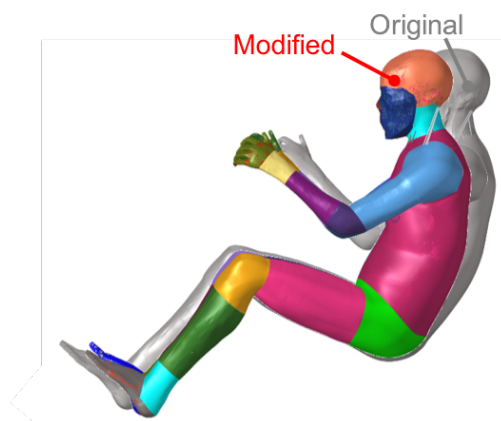


Figure 4.5. Positioned vs original – overlapped THUMS models

Some details of the model final posture are instead shown in Figure 4.6.

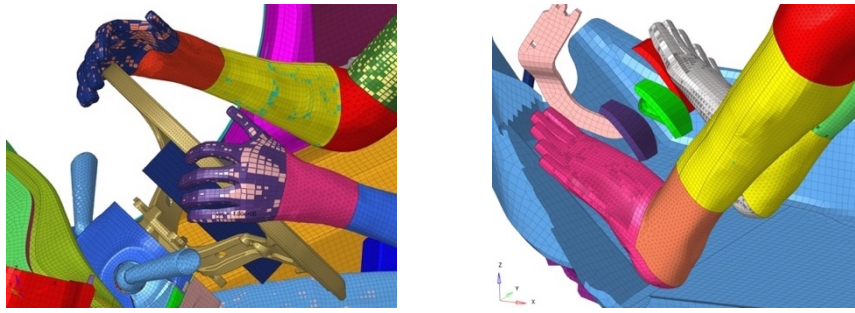


Figure 4.6. Positioned THUMS in vehicle FE model – hands on steering wheel (left) and foot (right) views

4.2 THUMS Positioned FE Model in Out-of-Position (OOP) Configuration

4.2.1 Investigation of the possible THUMS Out-of-Position Postures

Since the used vehicle model is supposed to be equipped by the Level 3 Autonomous Vehicles technology, the simulations performed in the second part of this Thesis are carried out under the assumption that it is possible, for the driver, to take a more relaxed posture during the automated manoeuvres.

In this section, therefore, a possible Out-of-Position configuration for the THUMS HBM driver is hypothesized and, then, created, by using the PIPER Positioning Tool (§3.3).

Basing on the statistical researches and the previous studies [31], [32] and [35] presented in §2.2, the two preferred seat configurations that are generally chosen by the drivers in a L3 Autonomous Vehicle are (see Table 4.0 with reference to Figure 4.7):

- Seated facing the driving direction (blue)
- Reclined facing the driver direction (yellow)

	Seated Facing the driving direction	Reclined facing the driving direction
Torso angle	28°	64°
Thigh angle	10°	4°
Knee angle	114°	149°
Seat back angle	24°	61°

Table 4.0. Summary of the preferred driver posture configurations in AVs (ref. Figure 2.2)^[34]

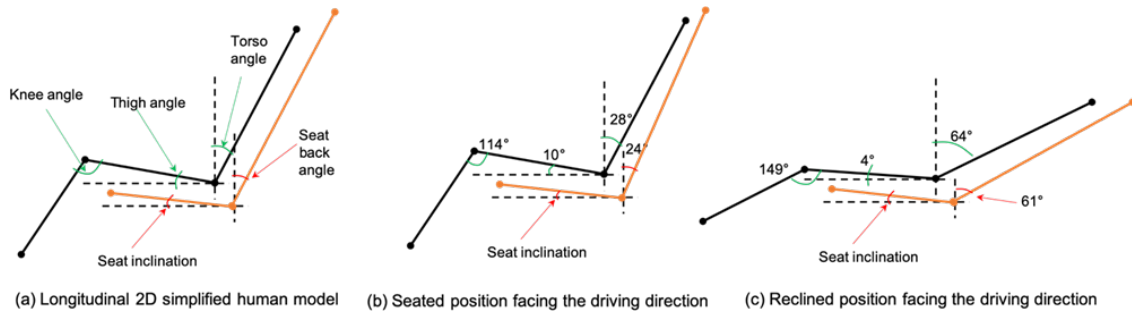


Figure 4.7. Driver preferred postures in AVs and related seat back adjustment [34]

In addition, the relevant human body angles corresponding to the most frequent Non-Driving-Related Tasks (NDRTs) [34] are shown in Table 4.1:

	Reading	Using tablet / Laptop	Watching movies	Sleeping	Working/ Studying	Playing video games
Torso angle	33°	18°	38°	61°	16°	17°
Thigh angle	9°	14°	10°	5°	14°	14°
Knee angle	113°	118°	119°	160°	87°	95°
Seat back angle	28°	18°	33°	63°	16°	23°

Table 4.1. Postures and seat back angles for specific NDRTs (ref. Figure 2.2) [34]

In this Thesis work, however, the seat inclination and the steering wheel position are supposed to be fixed (i.e. unchanged with respect to the ones used for the simulations of the THUMS in the conventional driving posture).

The investigation of the possible THUMS OOP posture to be used for the simulations is based, also, on the internal environment of vehicle (Figure 4.8) and on the main anthropometric data reported in Table 4.2 and in Figure 4.9. The occupant is supposed to be seated in a more relaxed posture with respect to the conventional driving one. Furthermore:

- A different knee angle is assumed for the left and right legs of the THUMS HBM: the left foot remains on the specific footrest, located on the left side of the pedals, while the right foot is placed on the vehicle floor
- The hands are not placed on the steering wheel: in particular, the right elbow is considered to be laid on the central tunnel support.

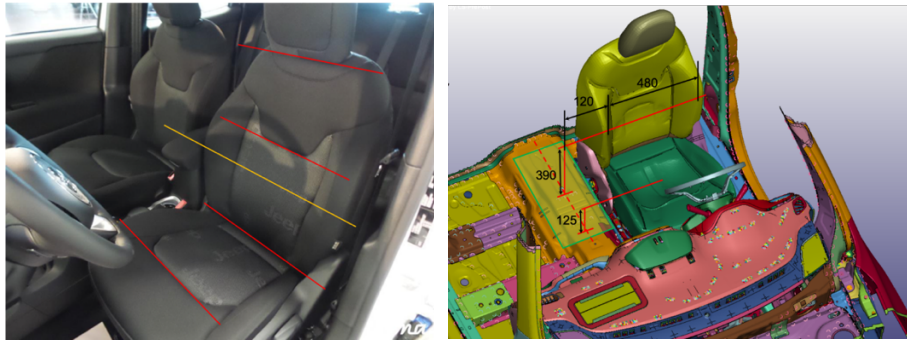


Figure 4.8. Vehicle seat and internal environment: real vehicle (left) and FE model (right)

# of Body part	Dimension	50 th [cm]
17	Sitting height	90.7
19	Shoulder height	59.2
20	Shoulder-elbow	36.3
21	Forearm-hand	48
27	Shoulder breadth	45.5

Table 4.2. Anthropometric data – useful quotes – with reference to Figure 5.2 [44]

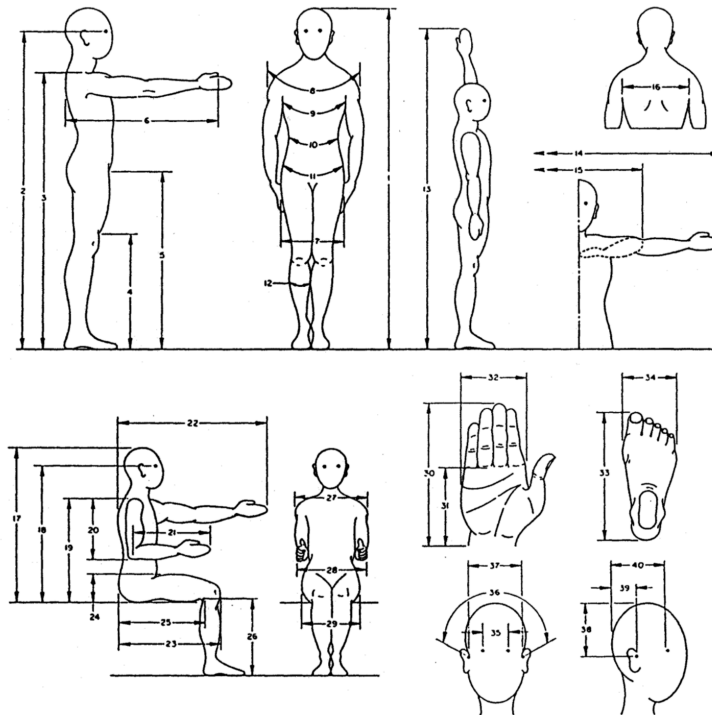


Figure 4.9. Anthropometric data [40]

A first attempt result of the THUMS OOP investigation is based on the combination of the data reported in Figure 4.8 and in Table 4.2: the front and the lateral views of the driver posture in the vehicle are represented in Figure 4.10.

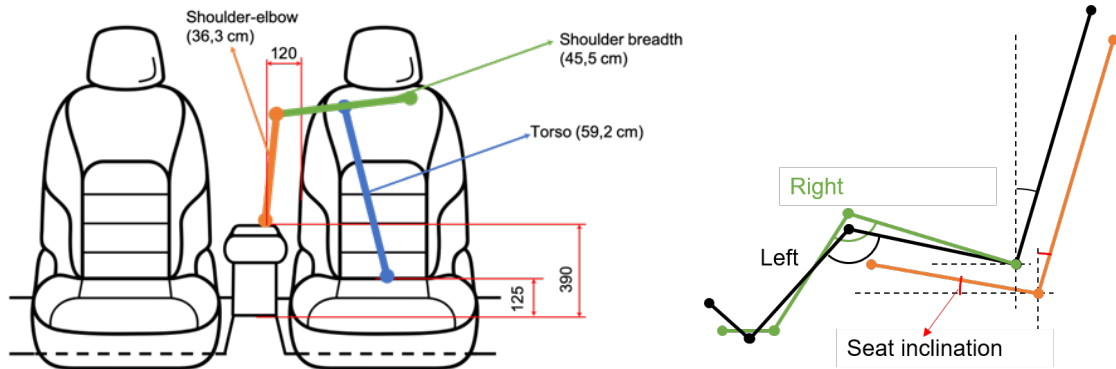


Figure 4.10. First attempt concept of THUMS OOP Posture – front (left) and lateral (right) views

4.2.2 THUMS OOP configuration – Positioned FE model

The final THUMS model in the Out-of-Position (OOP) configuration used in the simulations is reported in Figure 4.11:

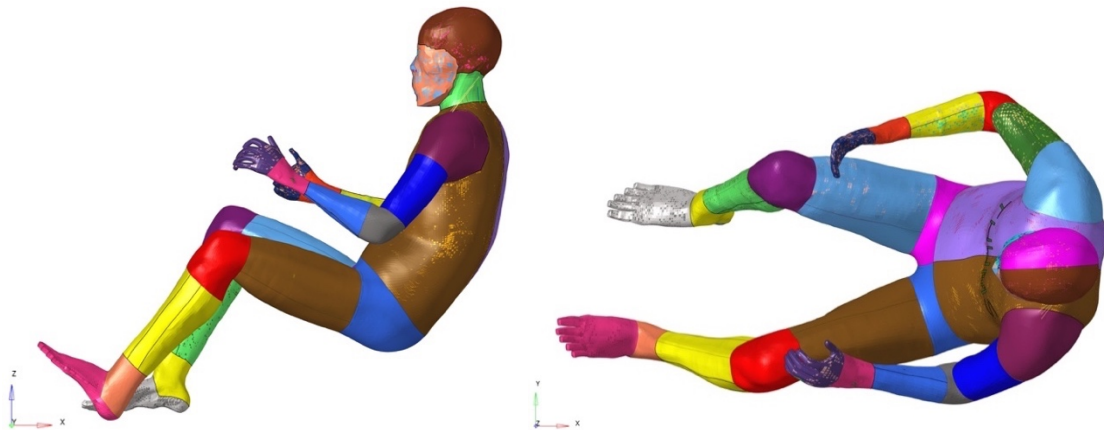


Figure 4.11. Positioned THUMS V. 4.02 FE in OOP configuration – side xz (left) and top xy (right) views

The final configuration of the HBM in the Jeep Renegade® vehicle environment and its comparison with the conventional driving posture are shown, respectively, in Figures 4.12 and 4.13.

The main human body angles of the THUMS in the realized Out-of-Position configuration are reported in Figure 4.14. Those data can be easily be compared with the ones of the Positioned HBM in conventional driving posture and of the original one (ref. *Figures 4.1 and 4.2 - §4.1*).

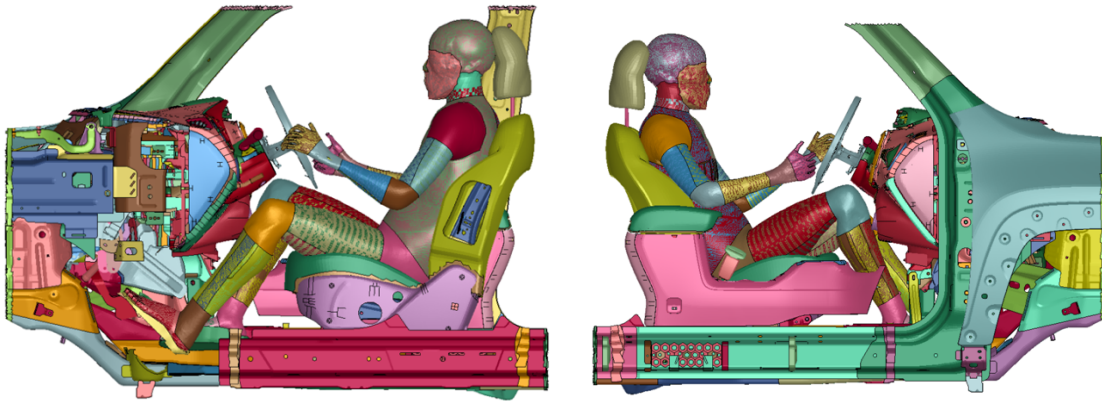


Figure 4.12. THUMS OOP in vehicle FE model – side xz left plane (left) and side $-xz$ right plane (right) views

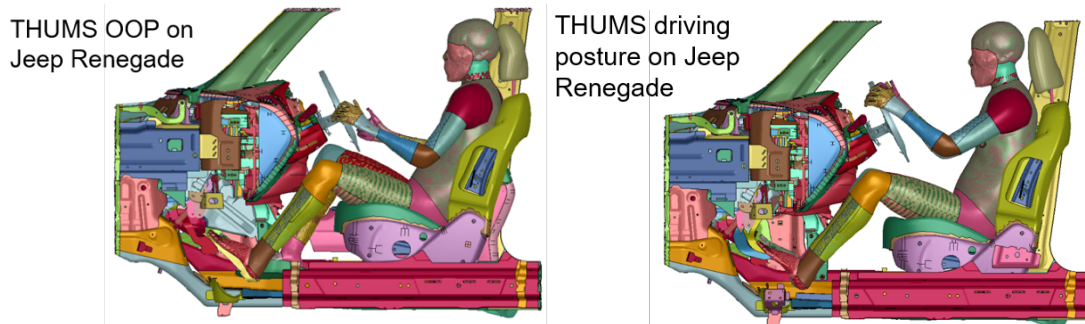


Figure 4.13. THUMS in driving posture (left) vs THUMS OOP (right) in vehicle FE model – side xz views

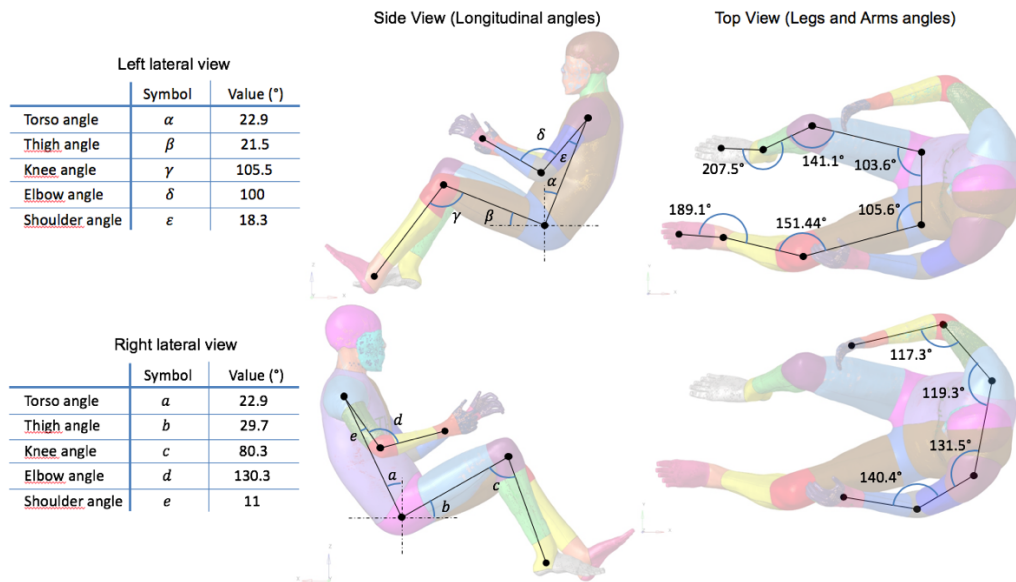


Figure 4.14. THUMS V. 4.02 FE model in OOP configuration – Main Body angles

4.3 THUMS Model - Additional FE components

In order to correctly represent the reality and to properly set the simulations according to the ones carried out with the THOR dummy model, some additional actions need to be performed and new components have to be done. Their creation process is described in this paragraph.

In particular, the supplementary finite element components *ad hoc* created for the positioned HBM are a pair of shoe soles and the vehicle restraint system for the driver (safety belt). Moreover, a supplementary component is needed for the simulations with the THUMS in the OOP configuration: in order to correctly lean the right elbow of the occupant on the vehicle armrest, the central tunnel has to be added to the vehicle model.

4.3.1 Creation of the THUMS model footprint on the undeformed FE vehicle seat

In order to avoid penetrations and/or intersections between the driver and the seat, and to correctly represent the pressure of the driver body on the seat foams, a preparatory simulation is performed, with the aim of reproducing the THUMS model footprint on the used vehicle seat.

The undeformed seat model reported in Figure 4.15 includes a stiff structure and deformable foam covers (seat cushion and seat back). The frame is fixed to the vehicle floor. The same seat angles adopted for the THOR dummy model simulations are maintained.



Figure 4.15. Undeformed vehicle seat FE model

Due to the aim of this preliminary simulation, the skin components of the positioned THUMS model are extrapolated and considered only. Moreover, even if their original thickness and property are maintained, a rigid material is assigned to this shell component, so that, by contact, it is able to deform the seat foams. Since the deformations of the human body lying on the seat can be considered as negligible, this procedure allows to run a lighter and faster simulation. The “full” and the skin shell models of the modified THUMS driver are shown in Figure 4.16.

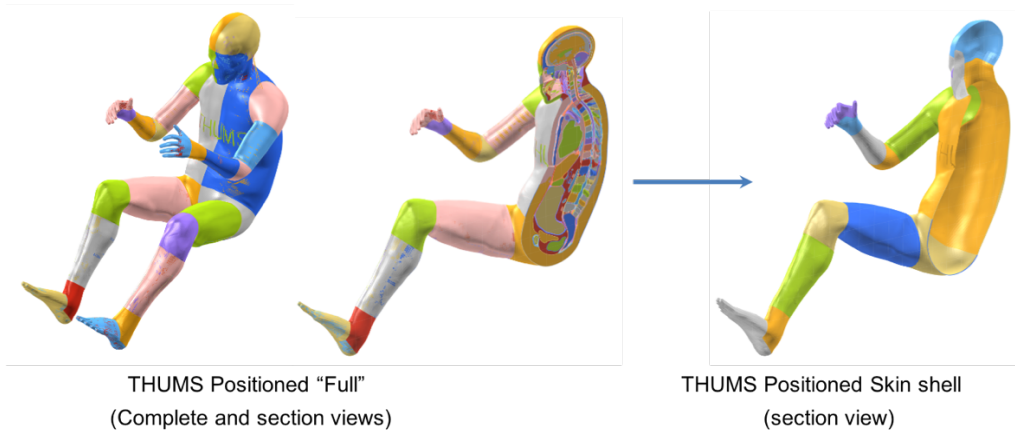


Figure 4.16. Positioned THUMS model – Seat creation simulation – Full (left) and skin shell (right) FE models

The HBM footprint is created by means of a rigid translation (imposed motion) of the THUMS model against the seat, whose rigid frame is constrained in all of his six degrees of freedom. At the beginning of the simulation, the driver initial position in the space is translated, with respect to its final one on the seat, along the x and z axes of quantities equal to, respectively, 50 and 80 mm. Those values are the ones usually used for those kinds of activities in the CRF company.

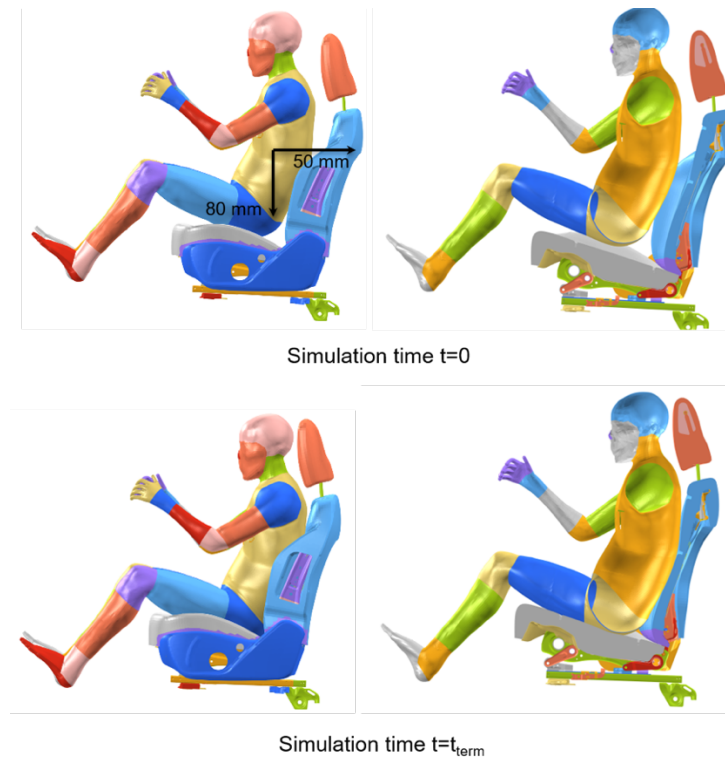


Figure 4.17. Positioned THUMS model – Footprint creation – Initial (upper) and final (lower) simulation steps – side xz and section views

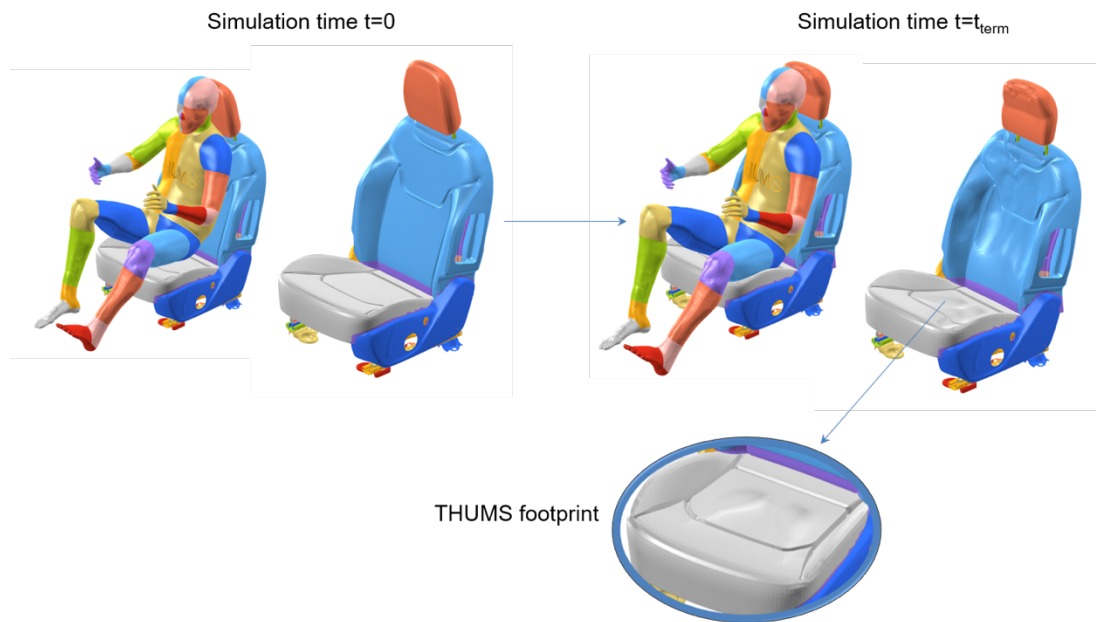


Figure 4.18. Positioned THUMS model – Footprint creation – Undeformed (left) and deformed (right) seats

The starting and ending phases of the seat creation simulation are represented in Figure 4.17. The original and final models are instead reported in Figure 4.18, in which the THUMS prints can be noticed (in the deformed configuration) on both the seat back and the seat cushion.

By means of this procedure, however, the residual stresses of the deformed seat are not considered. The preloads contribution on the deformed components has, in fact, negligible influence on the obtained biomechanical signals.

As a result, the deformed FE model of the driver seat can then be exported and included in the vehicle environment to be used for simulations.

4.3.2 Creation of the THUMS shoe soles

Additionally, a pair of shoe soles for the HBM in the conventional driving posture configuration has to be realized, with the purposes of:

- Reproducing, in a more correct way, the real driving situation: the bare foot impact on the vehicle pedals would not be realistic
- Introducing some additional friction material between the human driver feet and the surfaces of the vehicle pedals, as prescribed in the safety regulations

The first version of the created shoe sole, corresponding to the left foot, is represented in Figure 4.19. The upper surface of the shoes is created by reproducing the lower one of the THUMS feet.

Subsequently, by considering both the final smoothed version of the HBM and his definitive position inside the vehicle environment, the shoe soles components are transformed, and their final version, with a modified rear part and lower thickness, is reported in Figure 4.20.

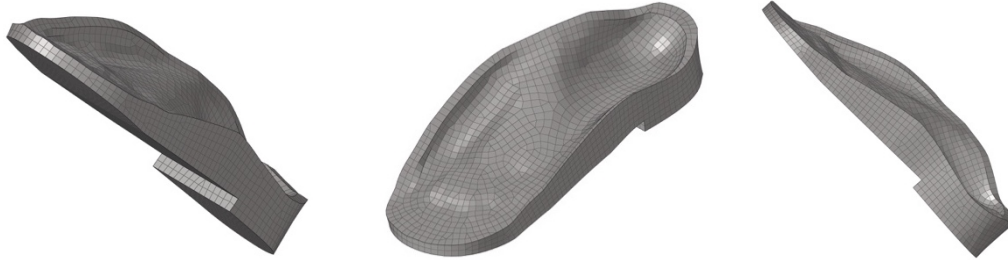


Figure 4.19. Positioned THUMS model – Shoe soles creation – First version (left foot)

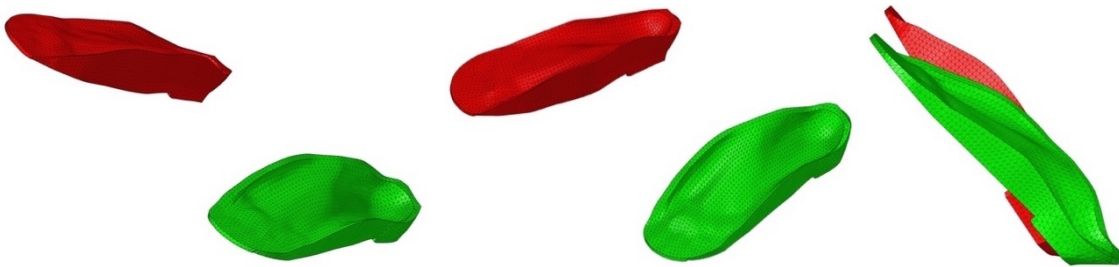


Figure 4.20. Positioned THUMS model – Shoe soles creation – Definitive version (left, green and right, red)

The final version components are meshed with 3D tetra elements. A simple rubber material, whose properties are listed in the Table 4.3, is associated to the shoes. Furthermore, it is necessary to check that there are no geometrical penetration and/or intersection between the shoes and the feet or the shoes and the vehicle environment during the setting of the simulations. The shoes on the THUMS Positioned model are shown in Figure 4.21.

The shoes weight, which is around 900 g, complies with the one reported in the EuroNCAP® document requirements about Pedestrian HBMs (≤ 1300 g) [41]. Moreover, the contact between the shoes and the THUMS feet is achieved by means of a tied contact: according to [41], “the pair of shoes can consist of a sole only [...]; in the latter case, the sole has to be tied – without failure – to the foot”.

Simple Rubber – Shore A (material name M-SHORE_A50)	
E = Young’s modulus	0.5244275 GPa
ρ = Density	$9.7E^{-7}$ kg/mm ³
LS-Dyna Material Keyword	*MAT_ELASTIC

Table 4.3. Positioned THUMS model – Shoe soles creation – Shoes material

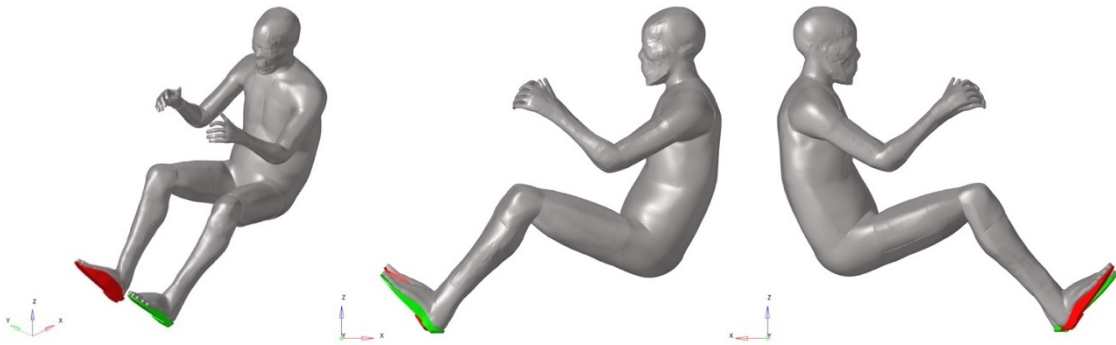


Figure 4.21. Positioned THUMS model – Shoe soles creation – THUMS with Shoe soles: isometric (left), side left plane xz (middle) and side right plane $-xz$ (right)

The shoe soles created for the THUMS model in the conventional driving posture are then adapted to the model in the OOP configuration. In particular, since the left foot is placed in the same position in both the THUMS configurations, only the right shoe sole has to be rotated and translated to be compatible with the right foot, which is placed on the vehicle floor.

With this goal in mind, during the positioning process of the HBM in the PIPER Tool, enough space has to be left between the skin of the right foot and the vehicle floor trims. The final version of implemented shoes is reported in the Figures 4.22 and 4.23.

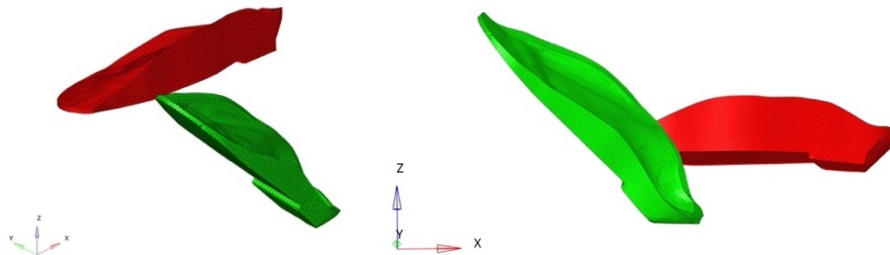


Figure 4.22. THUMS OOP – Shoe soles creation – Final implemented version (left, green and right, red)

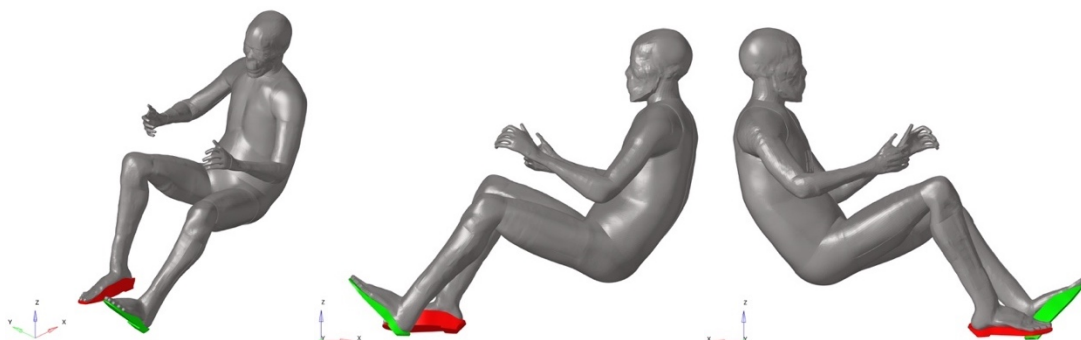


Figure 4.23. THUMS OOP – Shoe soles creation – THUMS with Shoe soles: isometric (left), side left plane xz (middle) and side right plane $-xz$ (right)

4.3.3 Creation of the THUMS Seatbelt

The seatbelts are defined as passive safety devices which, together with the Air Bags, are activated, in case of crash, with the aim of maintaining the occupant's body in contact with the vehicle seats, possibly reducing or avoiding the injuries.

The main seatbelt components of a standard “*three-points belt*” (constituted by sub-abdominal and diagonal body segments) are described here in the following and represented in Figure 4.24:

- The *belt*: it is a flexible component in contact with the occupant's body; the materials used to realize the belts are, generally, soft but highly resistant to cuts and scratches
- The *retractor*: it allows to unroll the belt till the desired length and it is able to block the unrolling phase if the belt extraction velocity exceeds a threshold value (e.g. during hard braking, crash, etc.)
- The *anchor points*: they are the linkages between the seatbelt restraint system and the vehicle structure
- The *D-ring*: it is fixed to the upper anchor point and the belt passes through it
- The *buckle*: it links the belt with the lower vehicle anchor point
- The *pretensioner*: it is a mechanic and pyrotechnic device which, in case of crash, acts on a plunger and rewinds the belt (if applied on the retractor) or pulls the buckle (if it is applied to it).

The seatbelt components used in the THUMS driver impact simulations are created in the ANSA® Pre-Post Processor software environment, by exploiting the automatic Seatbelt Tool.

The necessary components are:

- The THUMS Positioned FE model
- The deformed seat (exported at the end of the seat creation process - §4.2.1)
- The seatbelt anchor points and devices actually mounted on the vehicle used in the simulation;

In the case of this Thesis, they are delivered by the CRF; they include:

- The buckle system (buckle cover, buckle tongue, buckle head, cable and anchor)
- The D-ring anchor point, with its proper connection to the B-pillar of the vehicle
- The pretensioner (in this case applied on the retractor – sill side)
- The retractor

The procedure followed to create the seatbelt component is described in this section; in Figure 4.25 the starting point of the modelling process is reported.

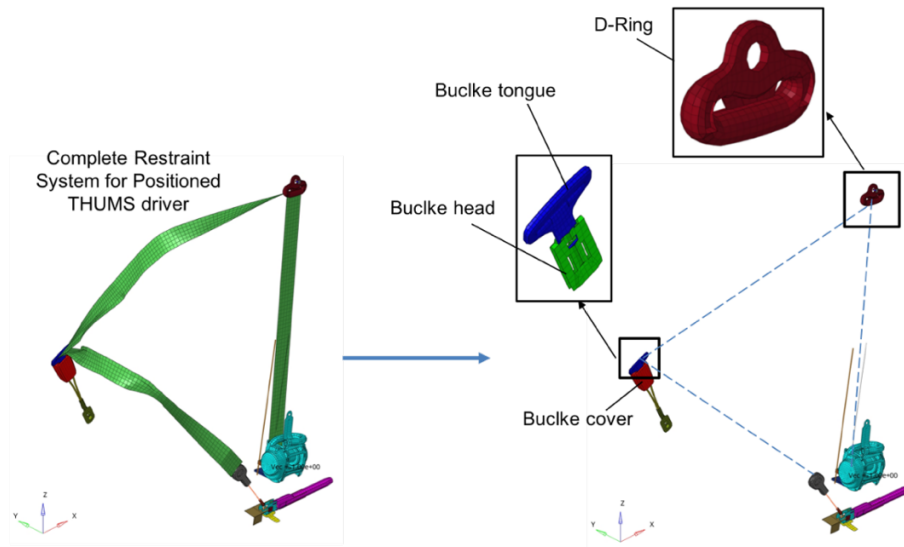


Figure 4.24. Positioned THUMS model – Seatbelt creation – Complete system (left) and components (right)



Figure 4.25. Positioned THUMS model – Seatbelt creation – Starting point of the realization process – isometric (left), side left plane, xz (middle) and side right plane $-xz$ (right)

The ANSA® Seatbelt Tool has the purpose to correctly create the different belt elements, providing that the anchor points are available. The user interface window is shown in Figure 4.26. A *Component* represents a part of the complete seatbelt. As an example, the shoulder belt and the lap belt are two different components of the complete driver’s seatbelt.

By means of the *Parts to Wrap* command, the selection of the entities to be restrained is performed. For instance, in the case of the THUMS driver, the wrapped parts are (in the proper selection order): the seat back foam, the left shoulder, the torso, the first part of the upper legs (right and left) and the seat cushion.

In the *Component Parameters* area, all the necessary settings to properly set up a seatbelt component are present. In the case of this Thesis, the 2D type elements are used for every single component. In order to create a seatbelt, the path of the belt and the Component Parameters are needed.

In the *Main Part – 2D* section of the *Component Parameters*, the *Entry* and *Exit Vectors* (red contour of Figure 4.26) define the axis about which the belt is folded when it passes through the slipping.

In LS-DYNA, the keyword **ELEMENT_SEATBELT* allows the 2D elements to pass through the slippings, here constituted by the D-ring and the buckle tongue.

At the end of the creation process, when all the fields are compiled, it is furthermore possible, with the aid of the *Interactive Edit* button, to manually adjust the belt path by directly dragging the desired points. The resulting seatbelt model created for the Positioned THUMS is shown in Figure 4.27.

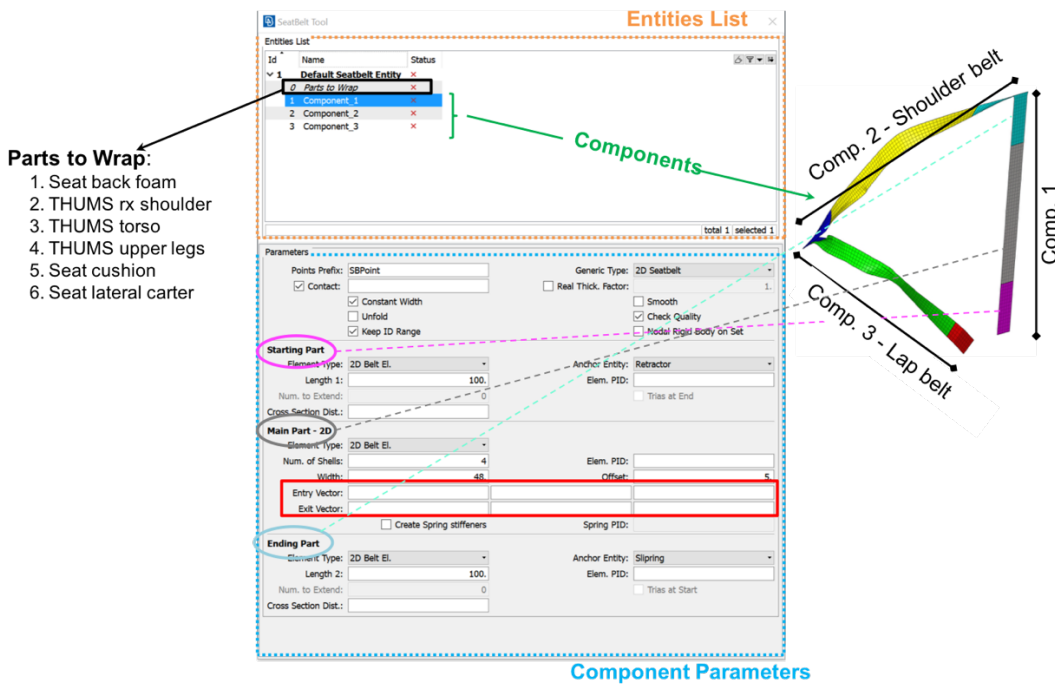


Figure 4.26. Positioned THUMS model – Seatbelt creation – ANSA® V.20.0.0 SeatBelt Tool User Interface window



Figure 4.27. Positioned THUMS model – Seatbelt creation – Definitive Seatbelt on Positioned THUMS process – isometric (left), side left plane, *xz* (middle) and side right plane *-xz* (right)

The seatbelt for the THUMS in Out-of-Position configuration is reported, on the opposite, in Figure 4.28.



Figure 4.28. THUMS OOP – Seatbelt creation – Definitive Seatbelt on Positioned THUMS process – isometric (left), side left plane, xz (middle) and side right plane $-xz$ (right)

When the finished seatbelt component is exported from the ANSA® Pre-Post Processing software, the Tool automatically creates all the necessary slipping nodes and elements sets and their proper definitions needed for the LS-DYNA Solver. The materials of the belt and the pre-tensioning system characteristics are the same of the ones used for the THOR dummy FE model simulations.

4.3.4 Implementation of the central tunnel FE component in the vehicle model

As it is possible to notice by looking at the Figures 4.10 and 4.12, the central tunnel components have to be included in the vehicle model for the OOP simulations. The CAD file of the Jeep Renegade® tunnel, delivered by the CRF, is reported in Figure 4.29, whereas the available FE components are shown in Figure 4.30.

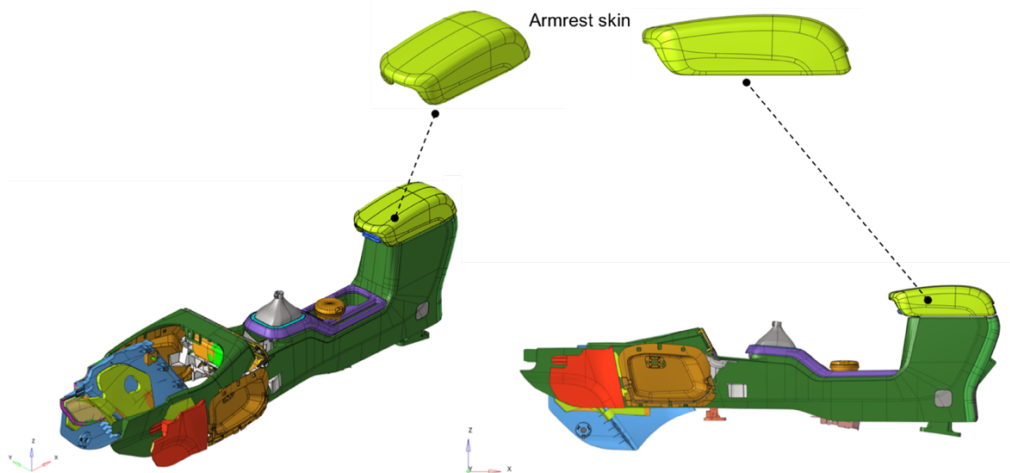


Figure 4.29. Jeep Renegade® central tunnel – CAD model (provided by CRF)

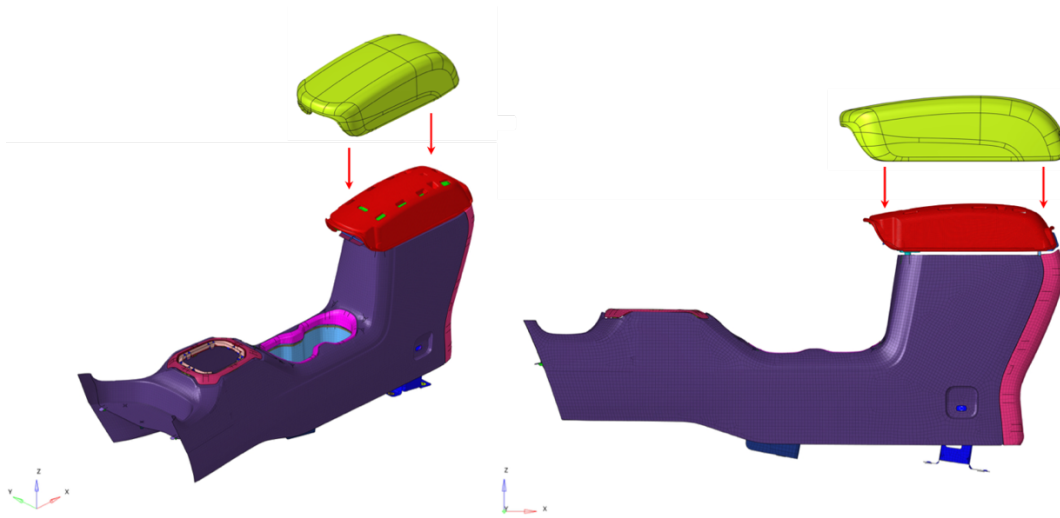


Figure 4.30. Jeep Renegade® central tunnel – no armrest skin - FE model (provided by CRF)

As reported in the Figures 4.29 and 4.30, the armrest skin, useful for the THUMS model to lean its right elbow, is not present in the central tunnel FE model and it has, therefore, to be meshed and included. The components of the central tunnel situated in front of the gear-lever housing, reported in Figure 4.29, can instead be neglected for the studies presented in this Thesis.

The CAD component of the armrest skin is, therefore, meshed with solid tetra elements by using the Hypermesh® Pre-Post software. The final FE component to be included in the vehicle model, together with the ones reported in Figure 4.30, is shown in Figure 4.31.

The assigned material is a *MAT_LOW_DENSITY_FOAM one (LS-DYNA® material *Keyword).

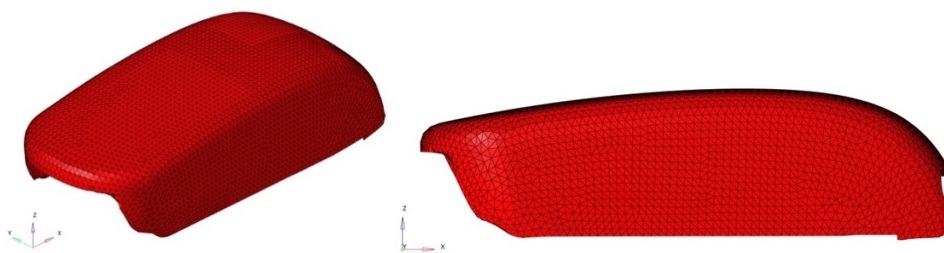


Figure 4.31. Jeep Renegade® central tunnel – armrest skin – FE meshed component: isometric (left) and lateral xz (right) views

Once that the complete central tunnel FE model is obtained, the proper interface between the vehicle BiW and the tunnel itself has to be set.

In other words, the new components have to be properly constrained to the vehicle frame.

4.4 Simulation Set up – HBM implemented sensors

4.4.1 THUMS Positioned model – first version of sensors

In order to extrapolate the necessary biomechanical values from the performed crash simulations and to correctly compare the behaviours of the THUMS and the THOR FE models, a sensor system has to be implemented in the HBM. The THUMS model developed by the Toyota Motors Corporation, actually, does not include any database definition and, as also reported in [5], the “users need to specify the entities for output such as nodes, elements, materials and cross sections, in order to output data such as acceleration, velocity, displacements, force, stress, strain and energy”.

As a first attempt, an existing example of sensors system, already realized for previous activities (Lateral impact simulations) at the Politecnico di Torino, is introduced and adapted to the positioned THUMS used in the vehicle crash simulations.

Those kinds of implemented accelerometers are, mainly, constituted by an additional rigid body (i.e. a 10 mm-sided cube), which is inserted in the different body areas and constrained to a certain number of the existing nodes of the body part to be analysed.

This system, shown in Figures 4.32 and 4.33, includes:

- One head accelerometer, positioned in the proximity of the head Centre of Gravity (H.C.G.)
- One torso accelerometer, positioned between the T4 and the T5 vertebrae
- One pelvis accelerometer, positioned near the pubic bone arch of the THUMS model
- The femur and tibia accelerometers for both the left and right legs
- Six human body cross sections, allowing to analyze the forces passing through:
 - The Upper and Lower right tibia
 - The Upper and Lower left tibia
 - The C1 vertebra and the Upper neck

The results obtained with the implementation of those first sensors are reported in the plots of Figures 4.34 – 4.36:

- The green lines show the THUMS output filtered by means of the SAE J211 CFC 60 filter (*see Appendix A*)
- The blue lines show the HBM output filtered by means of the SAE J211 CFC 180 filter
- The red dashed lines show the reference THOR dummy model accelerations

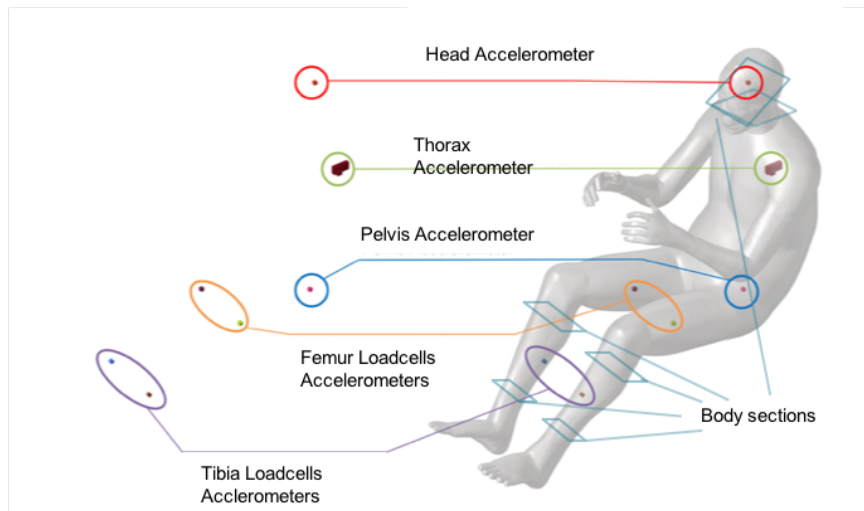


Figure 4.32. First version of implemented sensors on original THUMS HBM

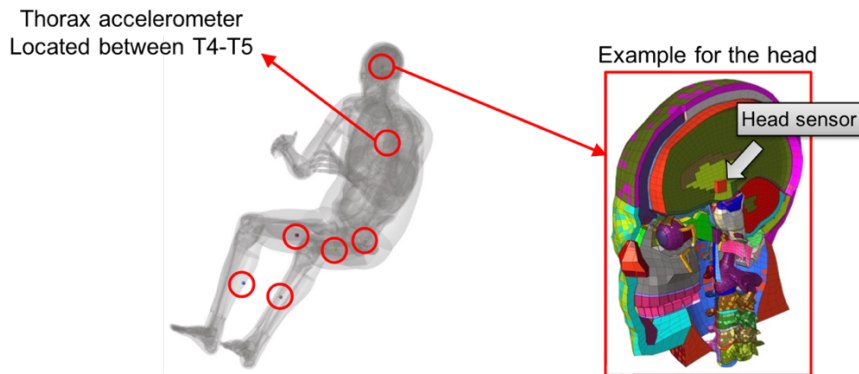


Figure 4.33. Positioned THUMS model - First version of implemented sensors – Head example

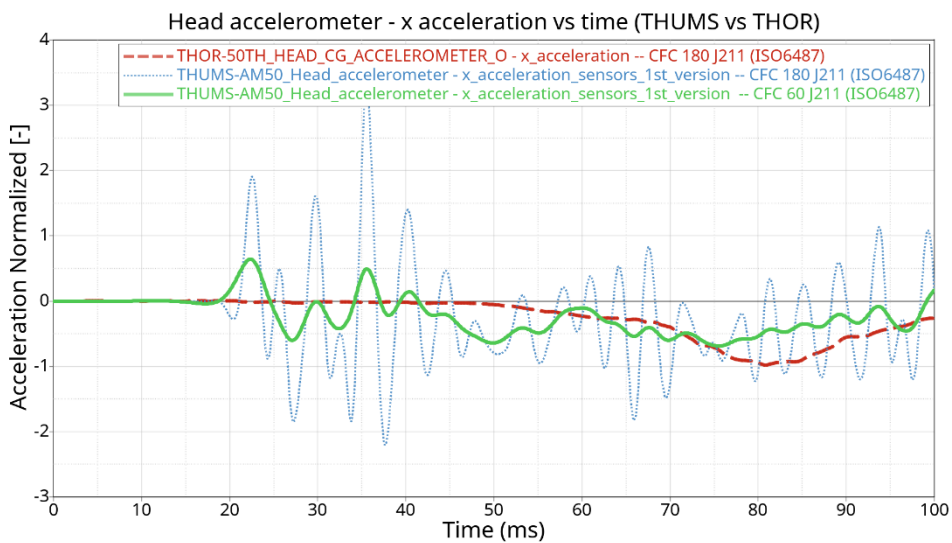


Figure 4.34. Positioned THUMS vs THOR - Head x acceleration – First version of sensors - FWRB

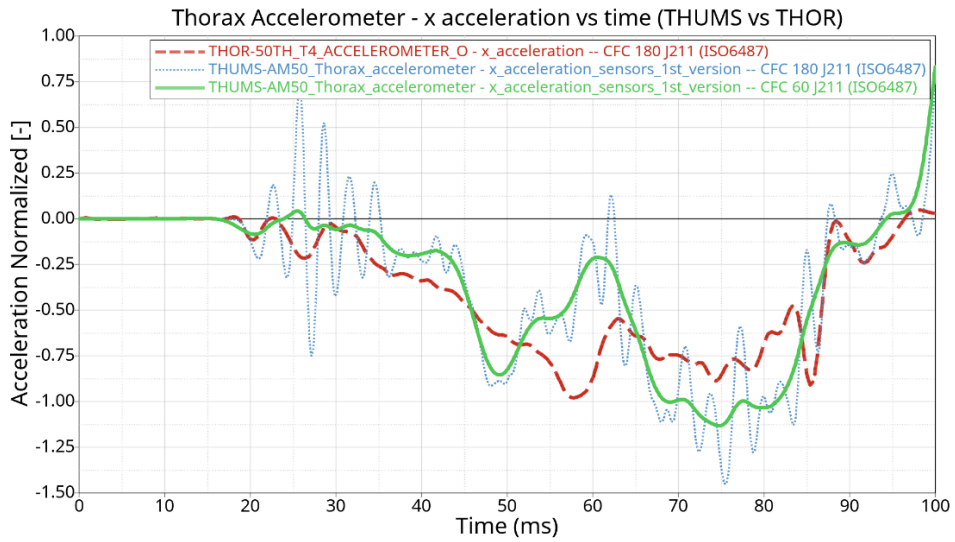


Figure 4.35. Positioned THUMS vs THOR - Thorax x acceleration – First version of sensors - FWRB

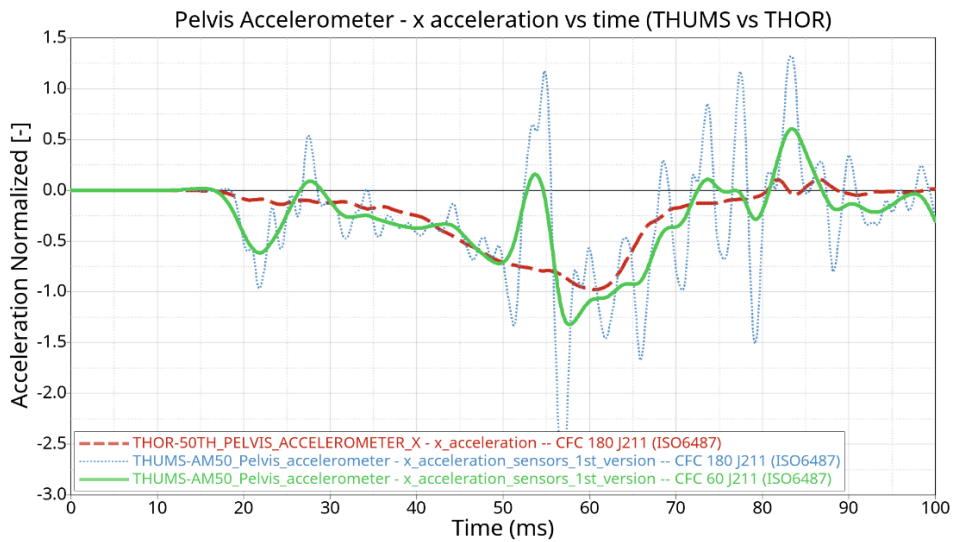


Figure 4.36. Positioned THUMS vs THOR - Pelvis x acceleration – First version of sensors - FWRB

As it is likely to be noticed from the plots reported here above, even if a certain correlation between the THUMS and THOR acceleration trends is present, the HBM outputs result to be affected by very high numerical excitations. In this way, it is difficult to obtain a “cleaned” signal, easily comparable with the THOR dummy one. This is the reason why two different filters are applied to the THUMS signals.

Those oscillations are probably due to the high complexity of the THUMS model, for what both material properties and number of components are concerned. In addition, since it consists in a reliable reproduction of an actual human, it is believable that the soft parts present inside the

body move in a different way (i.e. vibrations and oscillations) with respect to the ones of a dummy made up of rigid materials and already built-in sensors. In order to try to improve the quality of the output signals obtained from the THUMS FE HBM, other versions of sensors are investigated and reported here in the following.

4.4.2 THUMS Positioned model – Sensors improvement

Head sensor – Version 2 ^[41]

As a first trial to improve the sensors implemented in the THUMS HBM model, the head accelerometer is considered and investigated. In particular, starting from a study developed by the Politecnico di Milano [41], the rigid cube accelerometer (representing an additional body with its own – even if limited - mass), previously introduced, is now removed. On the opposite, an already existing small part of the original THUMS model is in this case converted to rigid and used as accelerometer. In particular, the inner part of the brain near the head centre of gravity is chosen (Figure 4.37 - “*third_ventricle_right*” part) and the accelerations are directly read on this head component. The material formulation assigned to the chosen brain element is quite simple (LS-DYNA *MAT_VISCOELASTIC material card), thus allowing a rapid conversion to a rigid body. This action is necessary since, from the solver point of view, the implemented accelerometer elements (*ELEMENT_SEATBELT_ACCELEROMETER) must be fixed to a rigid part. However, in the conversion, the thickness and density properties of the components of interest are not changed. In this way, the total weight of the HBM is unaffected and the minimum necessary variations are applied on the overall model.

The effect of this second version of implemented sensor in the THUMS head is reported in Figure 4.38. The obtained *x* acceleration results now to be fully comparable with the THOR dummy one. The oscillations observed in Figure 4.34 are now disappeared, even by applying the same filtering action to both signals. This good outcome is, probably, also favored by the presence of a big amount of soft tissues and components around the brain part chosen as sensor. This may provide a sort of oscillations dumping (e.g. spring-mass-damper system), which results in a cleaner output signal.

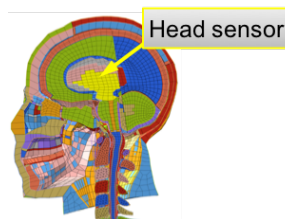


Figure 4.37. Positioned THUMS – Head accelerometer (ref. [41]) - Second version of implemented sensors

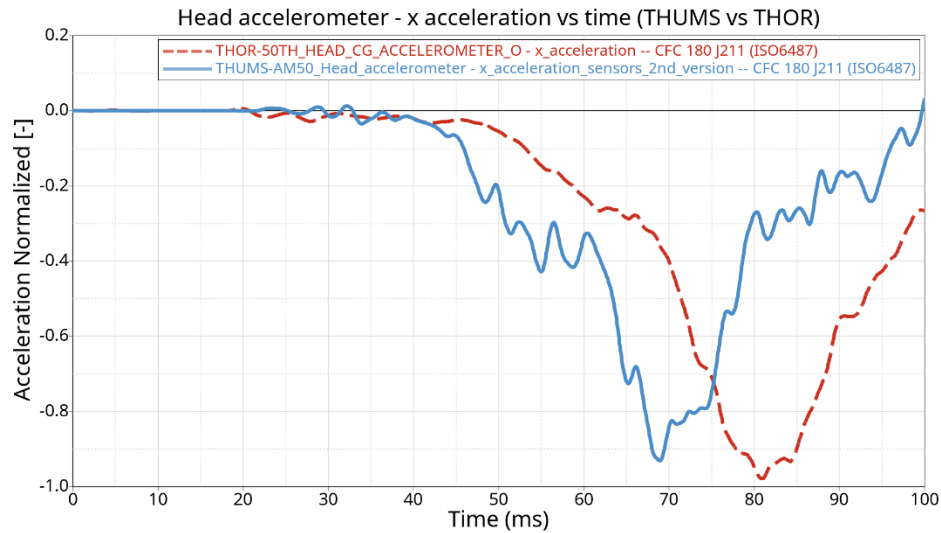


Figure 4.38. Positioned THUMS vs THOR - Head x acceleration – Second version of sensors - FWRB

Head sensor – Version 3 – inspired by Research Paper [42]

To be sure to extrapolate the correct head acceleration of the THUMS HBM generated during the impact tests, a further trial version of the head accelerometer is realized.

This solution is based on previous studies performed on Post-Mortem Human Subjects (PMHS) and presented in [42], in which a rigid metal plate is fixed on the cadaver head to read the displacements and accelerations. The upper surface of the THUMS skull is therefore stiffened by means of a set of rigid elements connecting the upper part of the head with its centre of gravity (Figure 4.39).

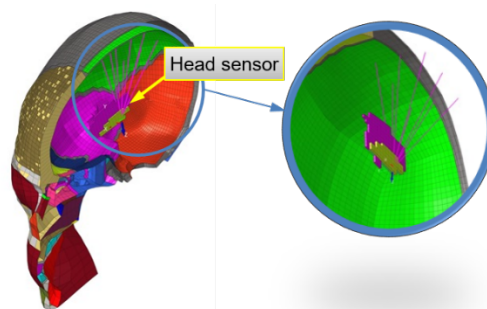


Figure 4.39. Positioned THUMS - Third version of implemented sensors – Head accelerometer (ref. [41])

However, the results obtained by means of this sensor are similar to the ones of the first version accelerometers: the oscillations, even if lower than the ones reported in Figure 4.34, are always present in the output signal.

The output is reported in Figure 4.40:

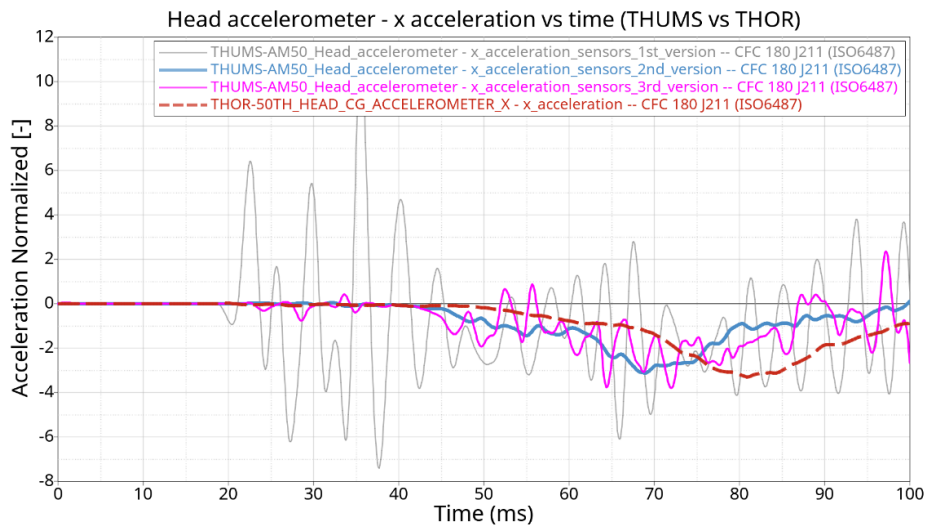


Figure 4.40. Positioned THUMS vs THOR - Head *x* acceleration – Third version of implemented sensors - FWRB

Thorax sensor – Version 2

Basing on the results obtained with the second version of the head sensor (ref. “*Head sensor – Version 2* and *Figure 4.38*”), a further improvement of the thorax sensor is then investigated.

In particular, the same procedure followed for the head accelerometer is repeated: the rigid cube constituting the thorax accelerometer is removed and a component already present in the original THUMS model - i.e. vertebra - (Figure 4.41 - “*R/L_T4_SPON*” part) is used as sensor.

Moreover, in order to compare in a more accurate way the obtained results with the signals deriving from the THOR FE model, the same accelerometer is also implemented in the vertebrae T1 and T12, by converting to rigid, respectively, the parts: “*R/L_T1_SPON*” and “*R/L_T12_SPON*” (Figure 4.41).

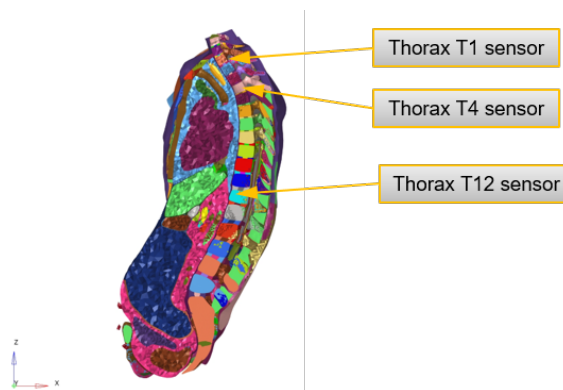


Figure 4.41. Positioned THUMS sect. view - Second version of implemented sensors – Thorax accelerometer

The comparison between the first and second version of the thorax accelerometers is reported in the plot of Figure 4.42:

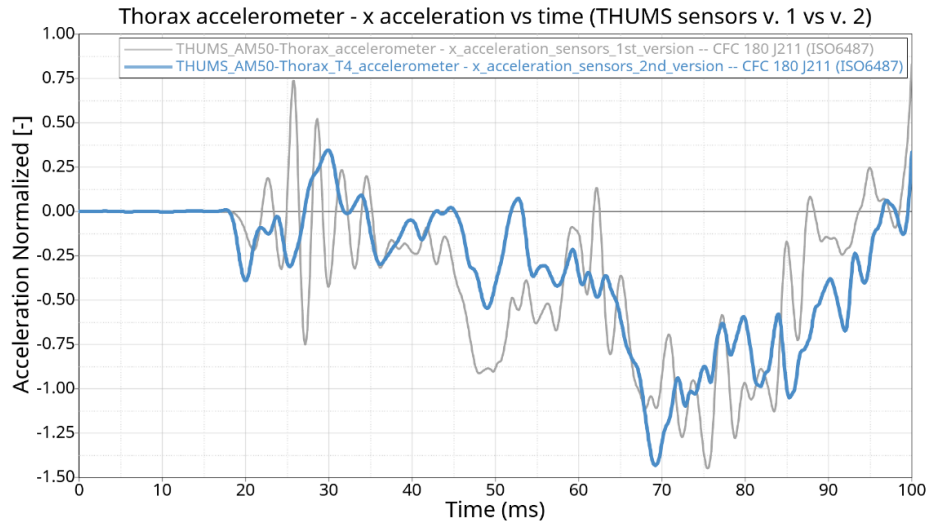


Figure 4.42. Positioned THUMS - Thorax *x* acceleration – First vs Second version of sensors - FWRB

As it is possible to notice from Figure 4.42, the trend of the curve obtained by converting to rigid the T4 vertebra is improved. However, the oscillations, even if reduced, are still present.

Pelvis sensor – Version 2

The improvement of the pelvis accelerometer is done basing on the second version of the head and the thorax sensors.

In this case, however, only part of the pelvis bone is converted to rigid. The conversion of the whole bone component would result, in fact, in an excessive stiffening of the THUMS model.

The sensor implemented in the HBM is reported in Figures 4.43 and 4.44: the accelerometer is constituted by the number of elements highlighted in green.

The comparison between the first and second version of the pelvis accelerometers is reported in the plot of Figure 4.44. In this case, even if lower than the ones obtained with the cubic accelerometers, some numerical instabilities (signal oscillations) are also present in the output data.

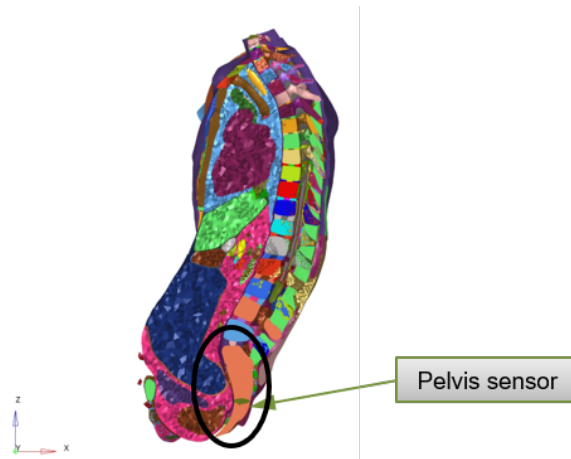


Figure 4.43. Positioned THUMS sect. view - Second version of implemented sensors – Pelvis accelerometer

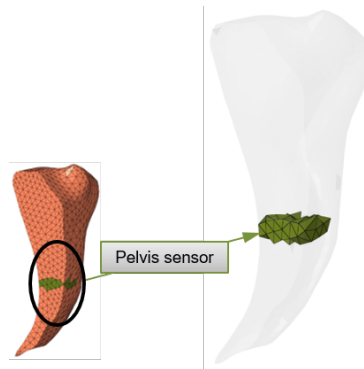


Figure 4.44. Positioned THUMS sect. view - Second version of implemented sensors – Pelvis accelerometer

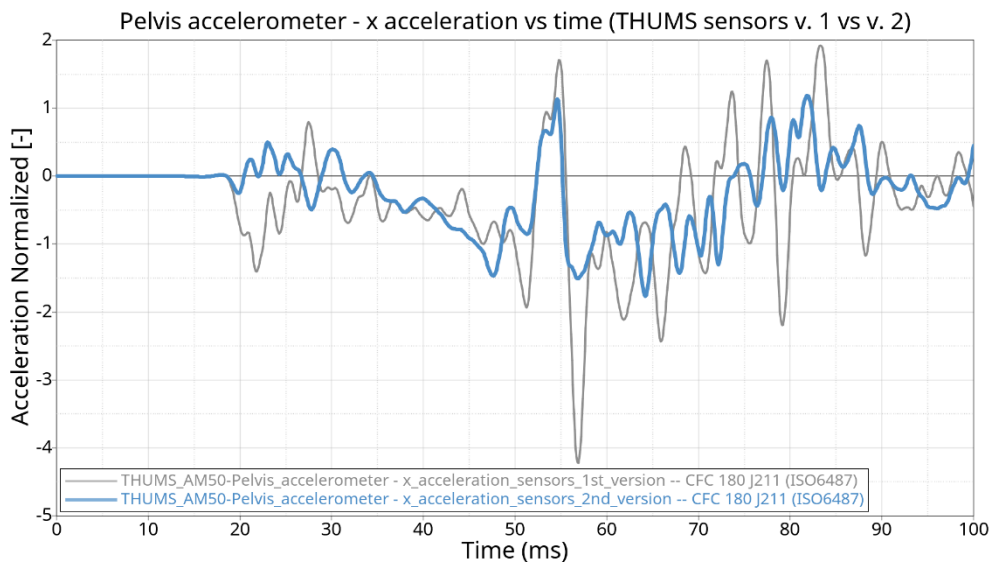


Figure 4.45. Positioned THUMS - Pelvis x acceleration – First vs Second version of implemented sensors

4.4.3 THUMS Positioned model – Sensors implemented in the impact simulations

The different versions of sensor improvements (§4.3.2) are summarized in Figure 4.46.

The final sensors implemented in the Full Width Rigid Barrier (FWRB) and in the Offset Deformable Barrier (ODB) impact simulations, together with the measurable data, are shown in Figure 4.47. In particular:

- To measure the head accelerations and displacements, the second version of the head accelerometer is included in the model
- The accelerations and displacements of the vertebrae T1, T4 and T12 are computed by means of the second version of thorax sensors
- The pelvis acceleration of the THUMS is measured introducing in the model the second version of pelvis accelerometer
- The accelerations and displacements of both the right and left femur and tibia are measured by means of the accelerometers included in the first version of sensor system
- The forces of the tibia and the neck bones are measured through the sections included in the first version of sensor systems

With the implemented sensors, therefore, the x , y and z displacements, linear/rotational velocities and linear/rotational accelerations can be measured.

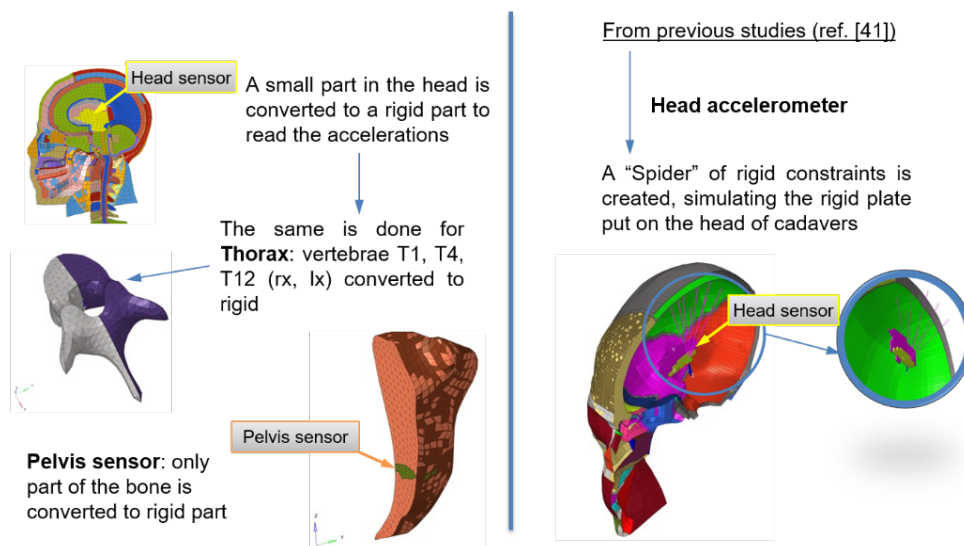


Figure 4.46. Positioned THUMS – Versions of implemented sensors in impact simulations

Final Version of Implemented Sensors in FWRB/ODB Impact Simulations - Measured data

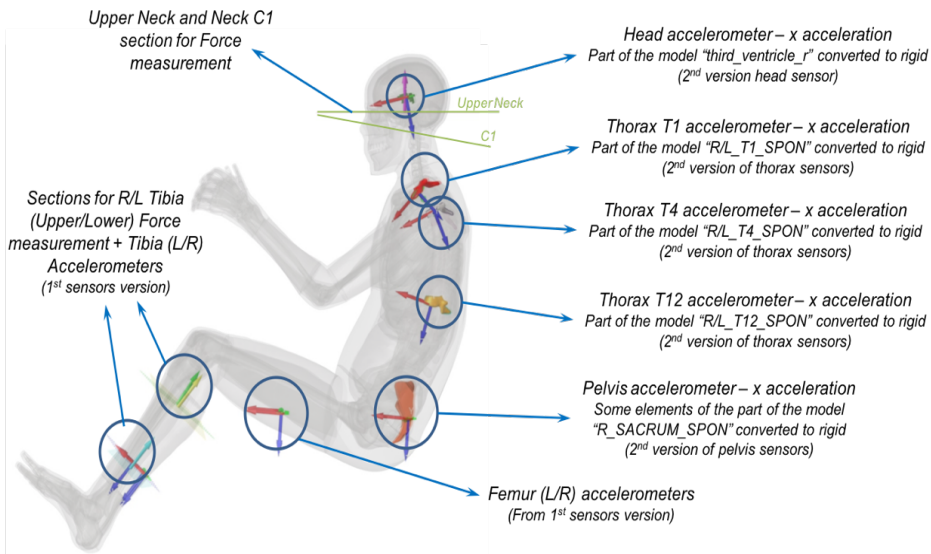


Figure 4.47. Positioned THUMS – Final Versions of implemented sensors in impact simulations

4.5 Injury Criteria (IC) Description

In this section, the main Injury Criteria are introduced.

4.5.1 Head Injury Criteria (HIC) ^[43]

The Head Injury Criteria (HIC) is one of the main parameters used to compute the head equivalent damage on the traditional dummies. It is computed as:

$$HIC_{15} = (t_2 - t_1) \left(\left(\frac{1}{t_2 - t_1} \right) \int_{t_1}^{t_2} a_r \cdot dt \right)^{2.5}$$

where a_r is the head resultant acceleration.

4.5.2 Brain Injury Criteria (BrIC) ^[44]

The Brain Injury Criteria is obtained using critical values of maximum resultant angular velocity. The directional dependence of the critical velocity is considered by computing the BrIC as:

$$BrIC = \sqrt{\left(\frac{\omega_x}{\omega_{xC}}\right)^2 + \left(\frac{\omega_y}{\omega_{yC}}\right)^2 + \left(\frac{\omega_z}{\omega_{zC}}\right)^2}$$

where the numerators are the maximum angular velocities and the denominators are the critical angular velocities in their directions.

4.5.3 Tibia Index (TI) ^[45]

The Tibia Index parameter, which takes into account the axial force and the bending moment to which the bone undergoes, is computed as:

$$TI(t) = \left| \frac{M_{R(t)}}{(M_R)_C} \right| + \left| \frac{F_{z(t)}}{(F_z)_C} \right|$$

where:

- $M_{R(t)} = \sqrt{M_x(t)^2 + M_y(t)^2}$
- M_x is the filtered bending moment (Nm)
- F_x is the filtered force along the z axis (kN)
- $(M_R)_C$ is the critical bending moment
- $(F_z)_C$ is the critical compression force in the z direction

Chapter 5

THUMS in Conventional Driving Posture - Impact Test Simulations Results

5.1 Impact tests description

Full Width Rigid Barrier (FWRB) ^[46]

This test was introduced in the EuroNCAP® tests in 2015. In the recent vehicle structures, which are stiffer than the old ones, higher compartment decelerations are experienced. This must be taken into account in designing the restraint systems of the front and rear passengers, since *“those decelerations can lead to severe injuries, especially to the chest of the more vulnerable, smaller or elderly occupants”* [46].

In this impact test, the vehicle is crashed against a rigid barrier with full overlap (Figure 5.0) at a speed of 50 km/h. The LS-DYNA simulation performed for this work has a total duration of 100 ms.

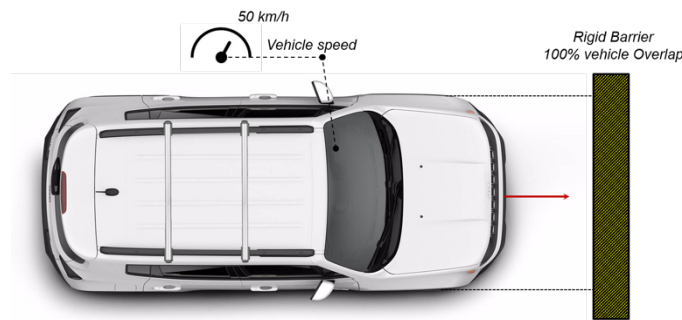


Figure 5.0. Full Width Rigid Barrier (FRWB) impact case representation

Offset Deformable Barrier (ODB) ^[47]

“A typical scenario is a head-on collision between two oncoming cars at moderately high speeds. In most collisions of this type, only a part of the vehicle front width structure is involved i.e. the two colliding vehicles are offset” [47].

In the tests performed in this Thesis work, the vehicle is driven at 56 km/h and with 40% overlap into a deformable barrier, which represents the oncoming vehicle (Figure 5.1). The

performed LS-DYNA simulation has a total duration of 130 ms. The speed at which the vehicle is crashed in the official EuroNCAP® ODB tests is, on the other hand, 64 km/h. This “replicates a crash between two cars of the same weight, both travelling at a speed of 50 km/h” [47].

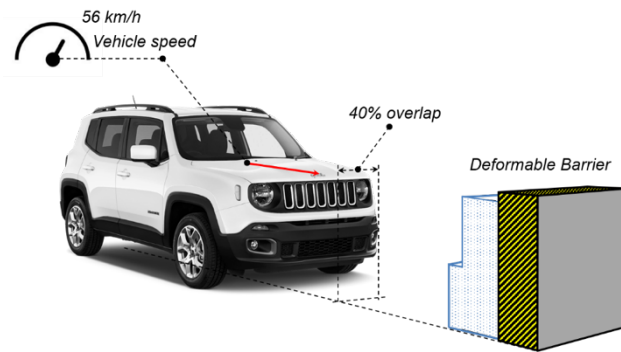


Figure 5.1. Offset Deformable Barrier (ODB) impact case representation

5.2 THUMS in Conventional Driving Posture

In the Figure 5.2, the complete model used for both the FWRB and ODB impact simulations is shown. This includes the previously created components (§4).

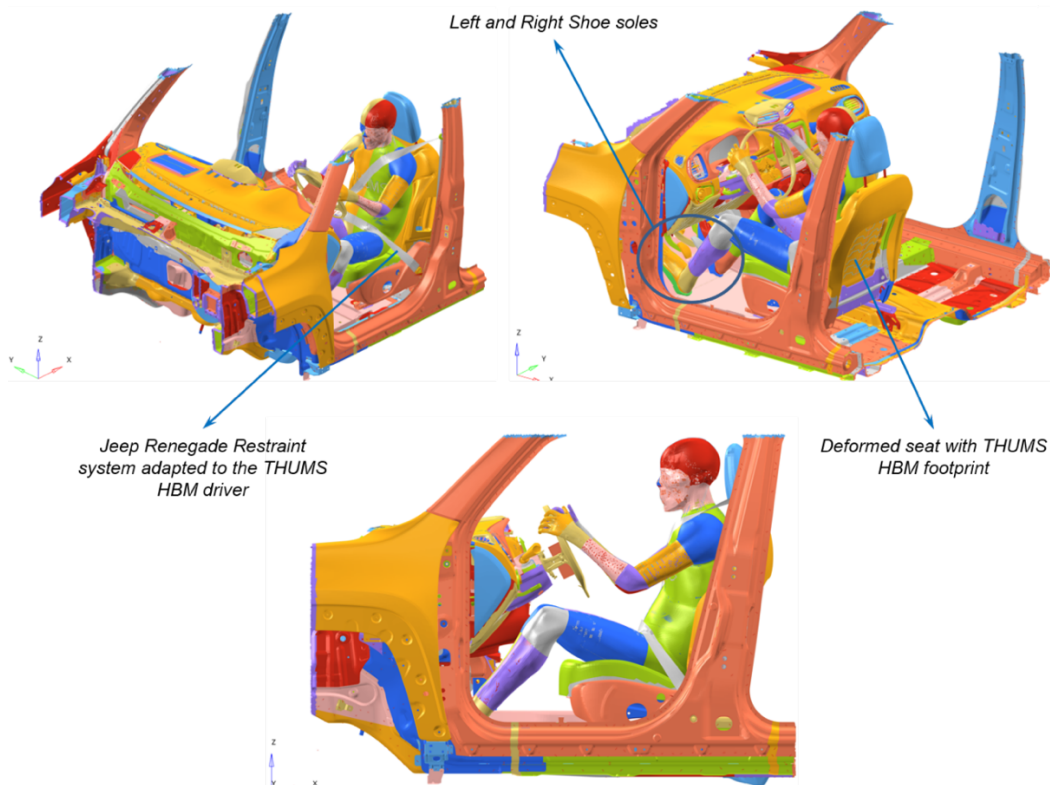


Figure 5.2. THUMS on vehicle FE model – Final simulation setting – Conventional driving posture

5.2.1 Results of the THUMS impact simulations and comparison with the THOR dummy FE model - Full Width Rigid Barrier (FWRB) Impact case

Global Energies

The comparison between the base SLED simulation (vehicle only – ref. *Figure 3.0*) and the one with the Positioned THUMS seated in the vehicle is shown in *Figure 5.3*.

The difference between the red and the blue curves is due to the presence of the HBM components. The total energy curve includes the contributions of all the other energies. In particular, the ones here considered are:

- The hourglass energy
- The internal energy
- The kinetic energy
- The sliding interface energy

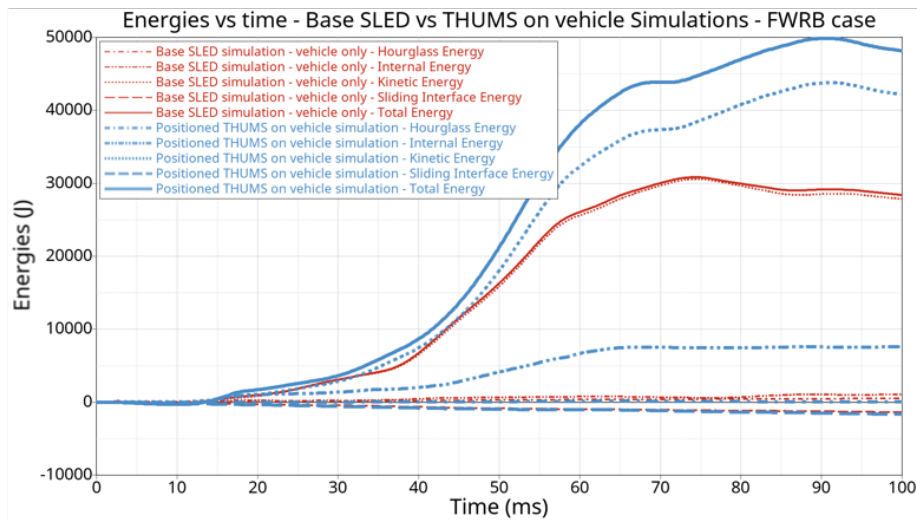


Figure 5.3. Positioned THUMS on vehicle vs Base SLED simulations – Global Energies – FWRB

THUMS Simulation Frames

Here in the following, the time frames of the simulation of the Positioned THUMS driver on the vehicle FE model during the FWRB impact are reported.

In *Figures 5.4* and *5.5*, the lateral xz (left plane) and the isometric views are, respectively, shown.

The THUMS model correctly behaves inside the vehicle during the impact, as well as the created driver restraint system (ref. §4.3.3).

In the following sections, the analysis of the extrapolated biomechanical and physical values and the comparison with the traditional THOR dummy model are reported. A different behaviour is expected to be observed in the two models.

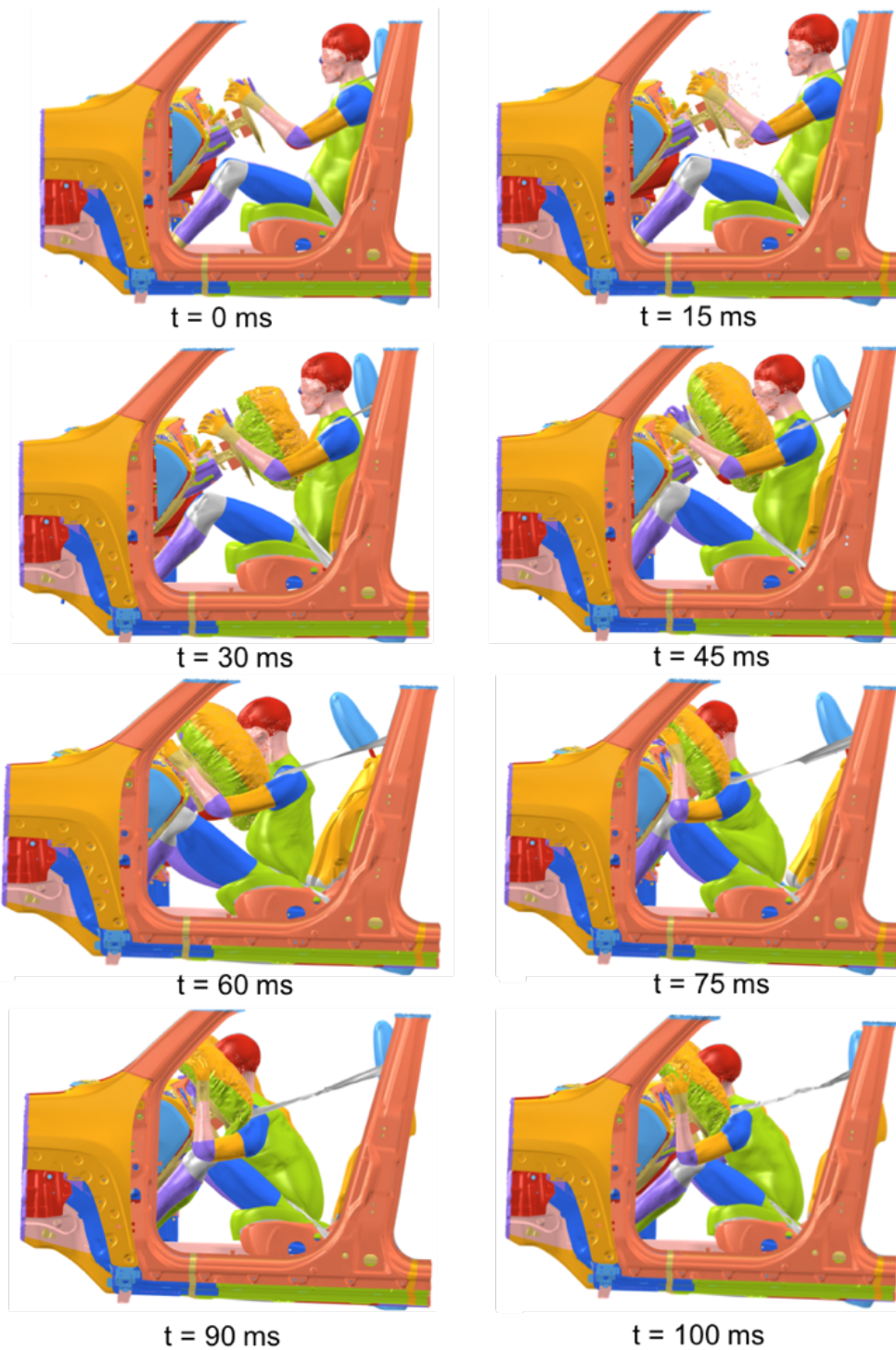


Figure 5.4. Positioned THUMS on vehicle – side xz view - FWRB

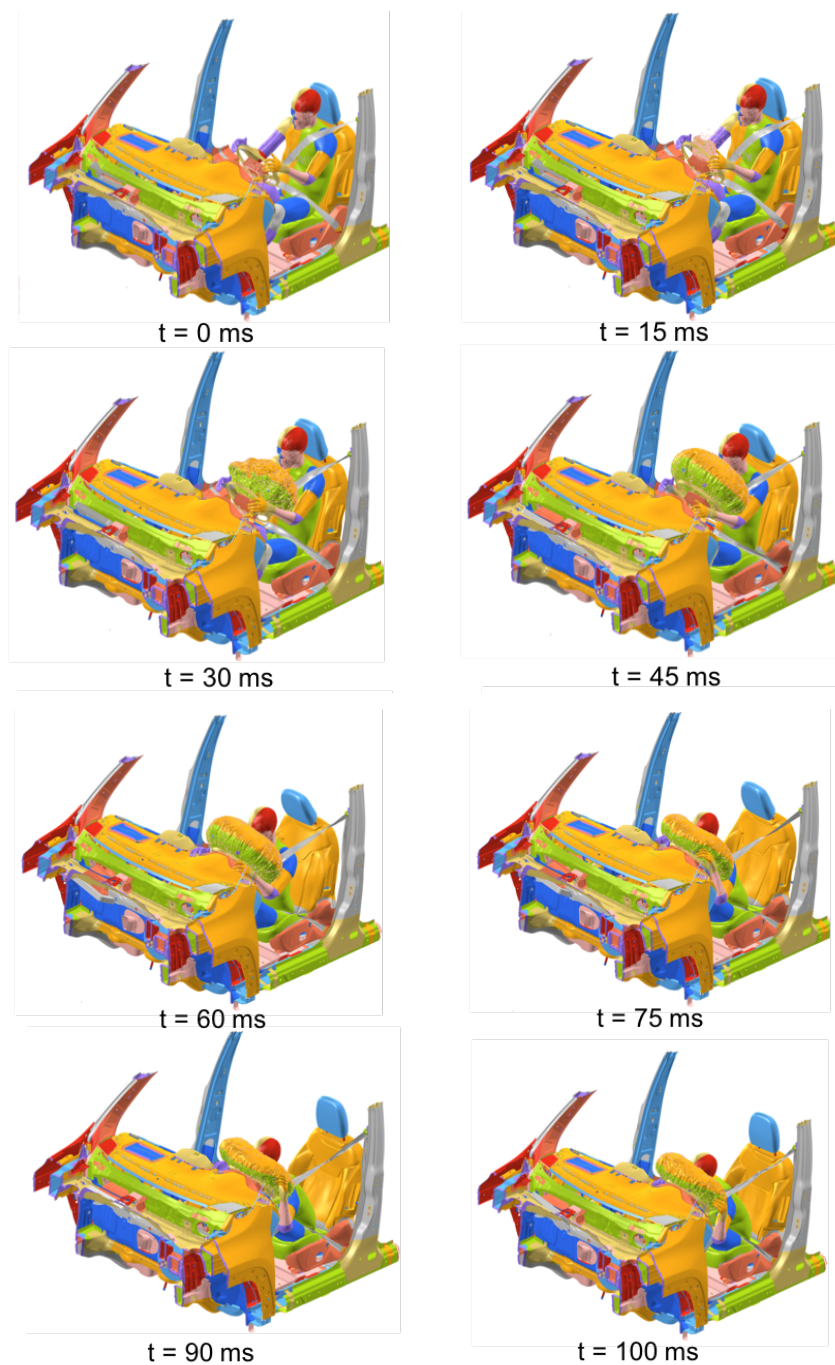


Figure 5.5. Positioned THUMS on vehicle – isometric view - FWRB

In order to properly understand the differences between the traditional THOR dummy and the Positioned HBM, a visual comparison is reported in Figures 5.6 – 5.15. In particular, the two models are represented and compared in the same simulation time instants. The time step used to capture the simulation frames is equal to 15 ms. As it can be noticed in the Figures 5.6 - 5.8, the initial posture of the two FE driver models is very similar. However, the hands of the THUMS

model are placed in the upper part of the steering wheel, whereas the hand of the THOR are positioned in the central part of the steering wheel. Moreover, it is here possible to notice how much the two models differ from each other's, especially in their inner parts.

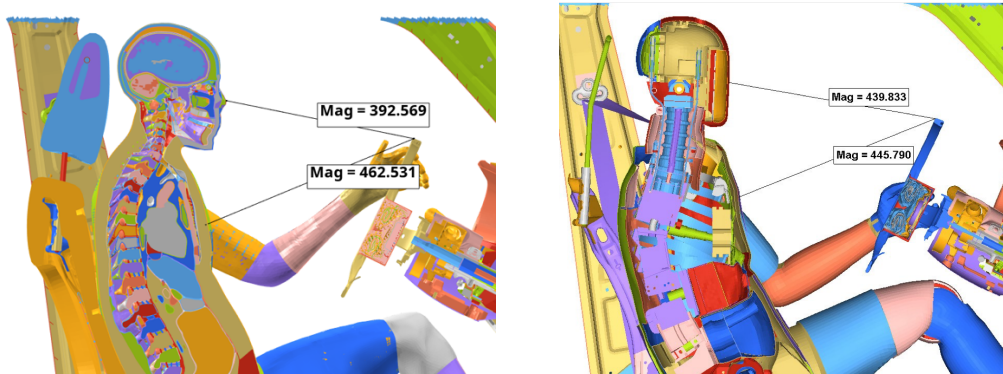


Figure 5.6. Positioned THUMS (left) vs THOR (right) - side -xz section view – FWRB – 0 ms – distance to steering wheel

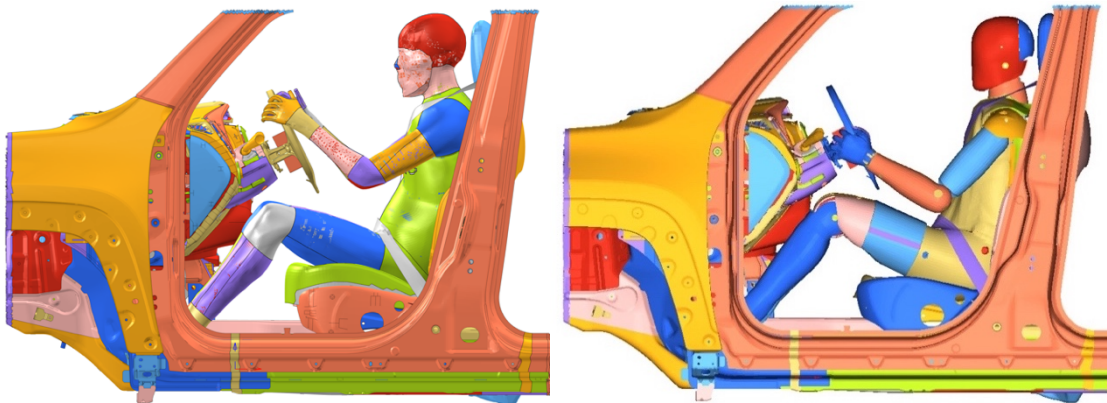


Figure 5.7. Positioned THUMS (left) vs THOR (right) - side xz view – FWRB – 0 ms



Figure 5.8. Positioned THUMS (left) vs THOR (right) - side xz section view – FWRB – 0 ms



Figure 5.9. Positioned THUMS (left) vs THOR (right) - side xz section view – FWRB – 15 ms



Figure 5.10. Positioned THUMS (left) vs THOR (right) - side xz section view – FWRB – 30 ms



Figure 5.11. Positioned THUMS (left) vs THOR (right) - side xz section view – FWRB – 45 ms



Figure 5.12. Positioned THUMS (left) vs THOR (right) - side *xz* section view – FWRB – 60 ms

The first difference in the behaviour of the two models can be already appreciated between 30 and 45 ms (Figures 5.10 and 5.11): even if the Driver Air Bag (DAB) apparently gets in contact with the thorax of the two models in the same time instant, the head of the HBM touches the DAB when the THOR one is still detached from it. This is due to the different volumes of the two objects and to position of the hands previously described: in the THOR simulation, the hands are slowing down the body motion by initially resting on the steering wheel. As a consequence, the whole upper body motion of the traditional dummy is retarded with respect to the one of the HBM. The observed delay between the THUMS and the THOR models is, mainly, the reason why a discrepancy between the peaks of the output curves (Figures 5.16 – 5.32) is obtained.

Moreover, the head of the THUMS model does not remain straight when touching the DAB: by comparing the Figures 5.11 and 5.12, it is possible to notice that the head negatively rotates around its *y* axis. The face is, in this first impact phase, looking down and the chin is able to touch the upper part of the thorax. This rotational motion is not appreciable by looking, instead, to the THOR images, where, furthermore, a completely different behaviour of the backbone can be observed. A similar behaviour of the two models can be observed, on the opposite, in correspondence of the abdominal part of the seatbelt.

Additionally, a counter rotation of the head is experienced in the THUMS FE model: between 75 ms and 100 ms, a positive rotation around its *y* axis can be noticed (Figures 5.13 – 5.15). The maximum distance between the chin and the upper part of the thorax is, in fact, obtained at the end of the simulation.

Further attention can be focused on the motion of the legs of the two models during the simulation. The legs of the THOR dummy tend to stretch, by increasing the knee body angle. On the opposite, position of the ones of the THUMS model do not substantially change from 0 to 100 ms.



Figure 5.13. Positioned THUMS (left) vs THOR (right) - side *xz* section view – FWRB – 75 ms



Figure 5.14. Positioned THUMS (left) vs THOR (right) - side *xz* section view – FWRB – 90 ms



Figure 5.15 Positioned THUMS (left) vs THOR (right) - side *xz* section view – FWRB – 100 ms

THUMS Head signals

The obtained velocities and accelerations of the head of the Positioned THUMS HBM during the crash simulation are here shown. In particular, the linear quantities are presented in Figures 5.16 – 5.23, whereas the rotational ones are included in Figures 5.24 – 5.32.

When a comparison between the THOR and THUMS value is reported in the graphs, the curves are here normalized with respect to the THOR values. This rule is valid for all the plots contained in §5.2.

The difference between the two models, shown in the output signal of the linear velocity along the y axis (Figure 5.17) is due to a different rotation of the head when getting in contact with the DAB. However, the velocity and acceleration components along the x axis are, in a full overlap frontal crash, generally neglected when dealing with the traditional dummies.

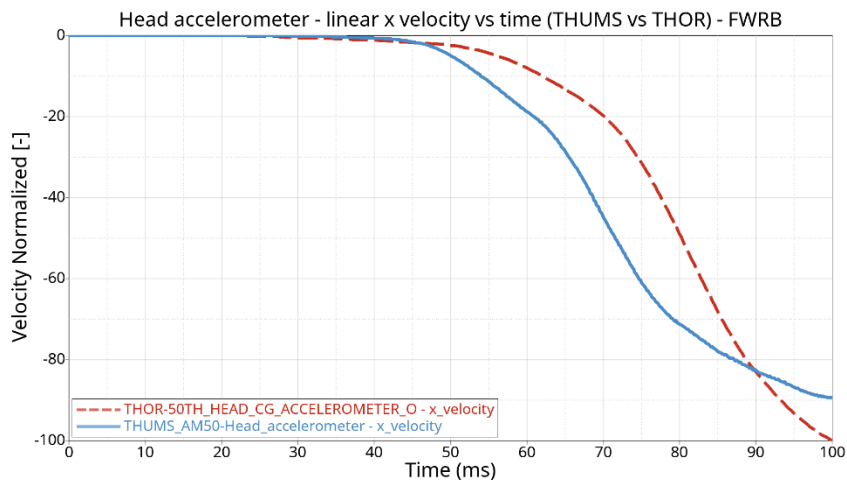


Figure 5.16. Positioned THUMS vs traditional dummy- Head - x linear velocity - FWRB

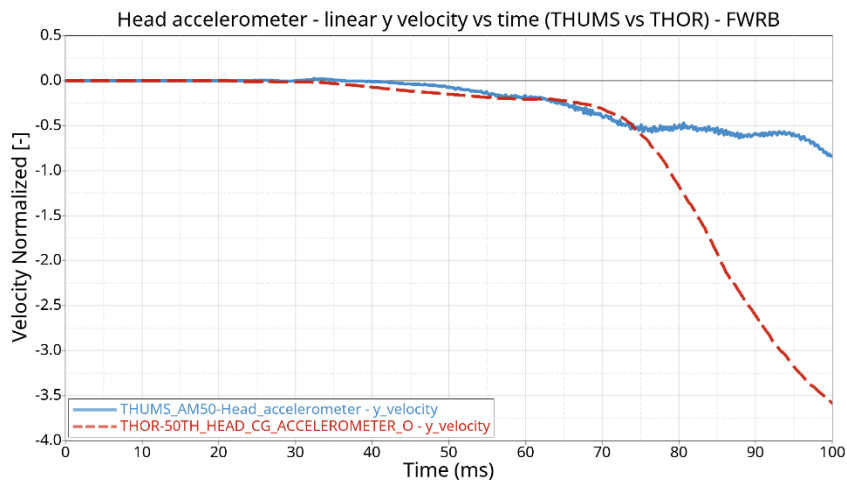


Figure 5.17. Positioned THUMS vs traditional dummy- Head – y linear velocity - FWRB

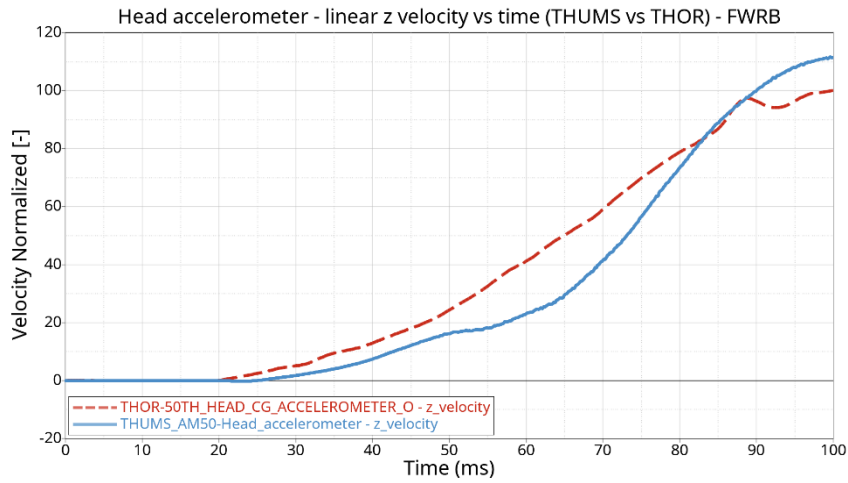


Figure 5.18. Positioned THUMS vs traditional dummy- Head – z linear velocity - FWRB

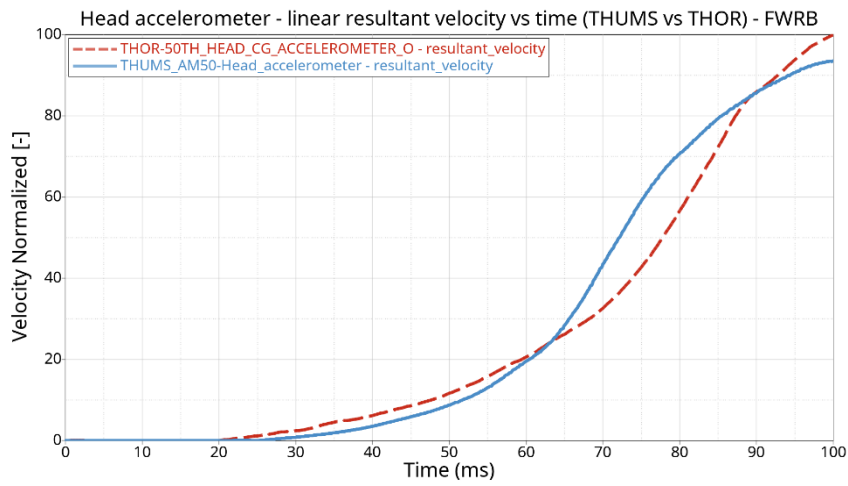


Figure 5.19. Positioned THUMS vs traditional dummy- Head – resultant linear velocity - FWRB

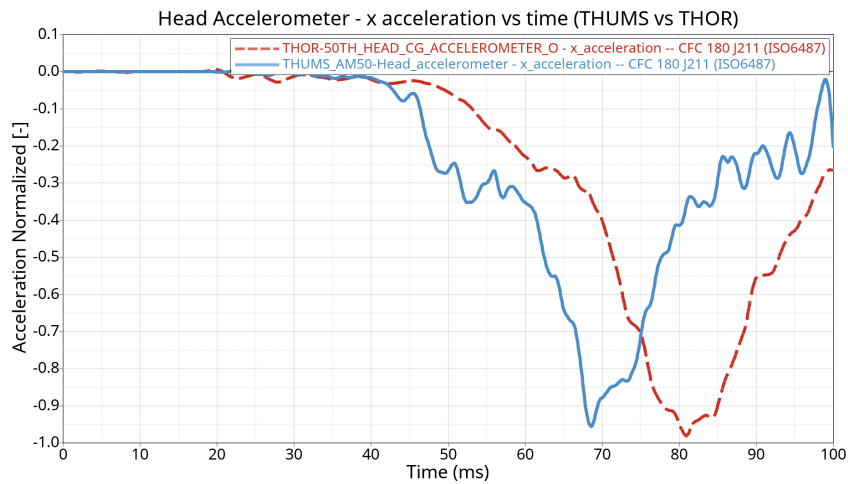


Figure 5.20. Positioned THUMS vs traditional dummy- Head - x linear acceleration - FWRB

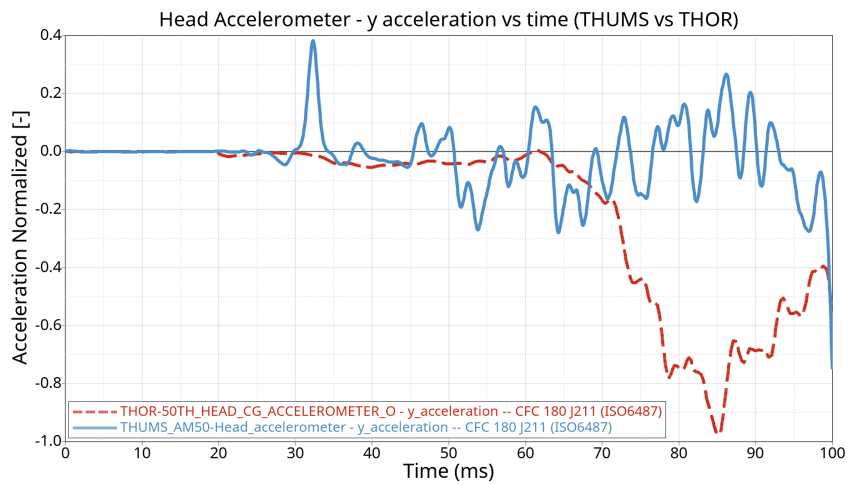


Figure 5.21. Positioned THUMS vs traditional dummy- Head - y linear acceleration – FWRB

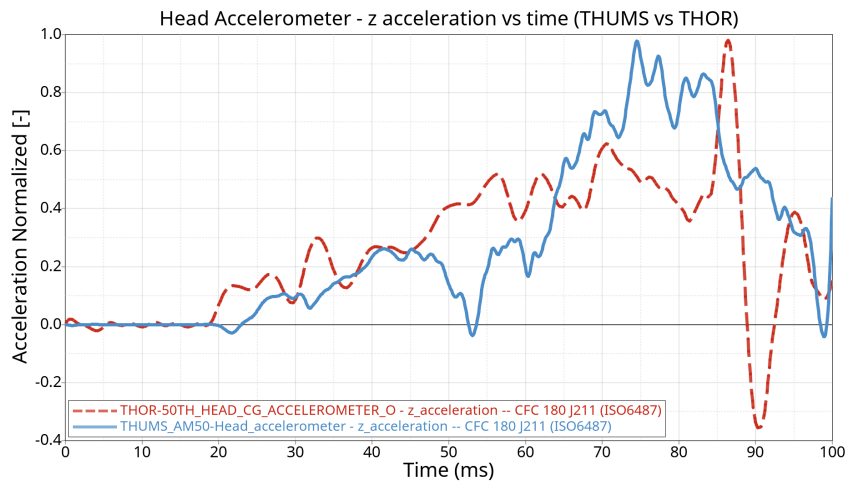


Figure 5.22. Positioned THUMS vs traditional dummy- Head - z linear acceleration – FWRB

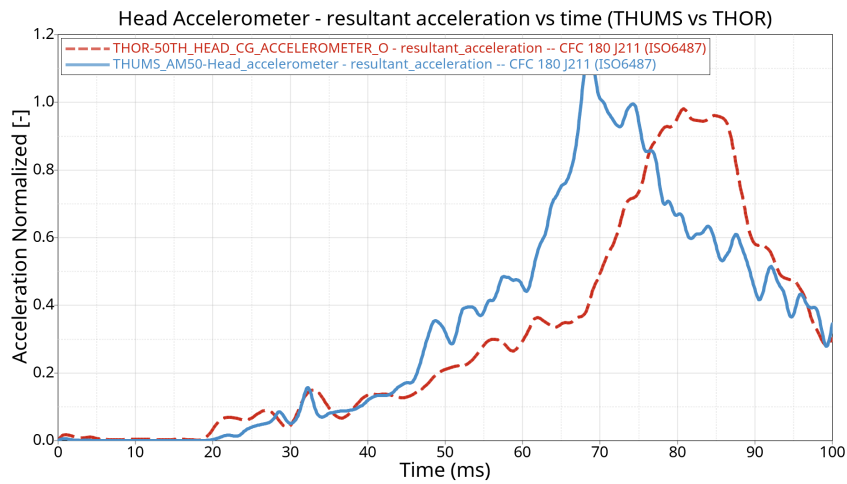


Figure 5.23. Positioned THUMS vs traditional dummy- Head – resultant linear acceleration - FWRB

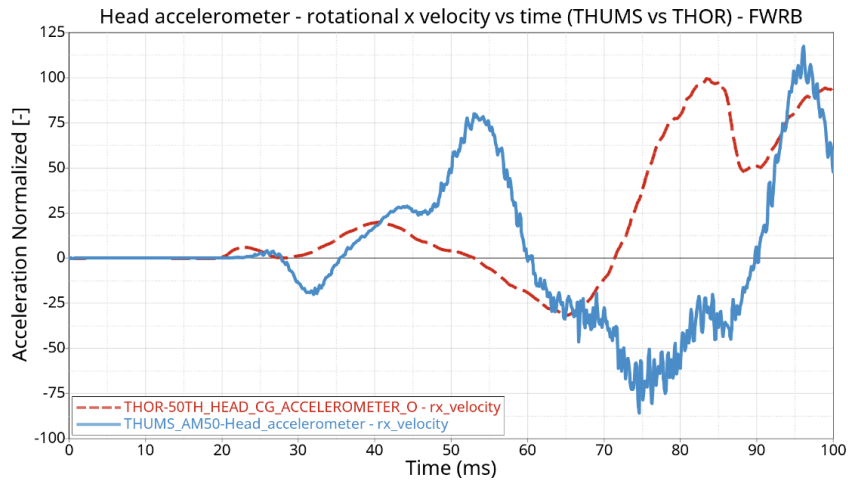


Figure 5.24. Positioned THUMS vs traditional dummy – Head – rot. x velocity – FWRB

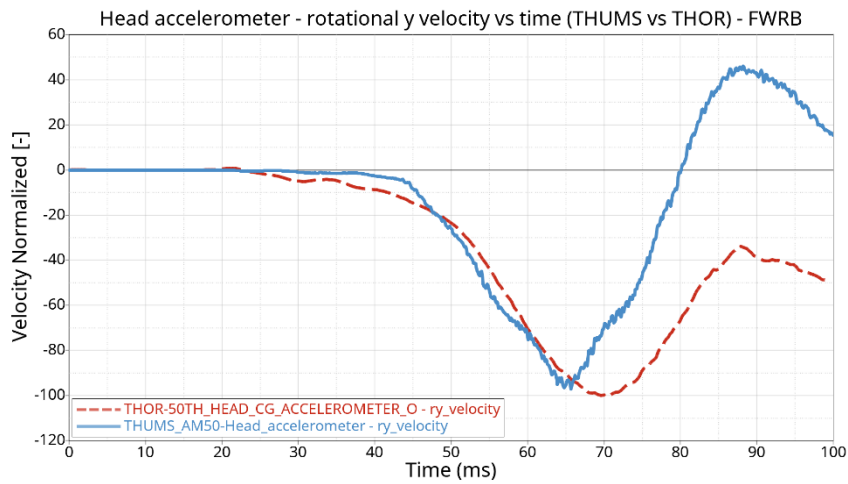


Figure 5.25. Positioned THUMS vs traditional dummy – Head – rot. y velocity – FWRB

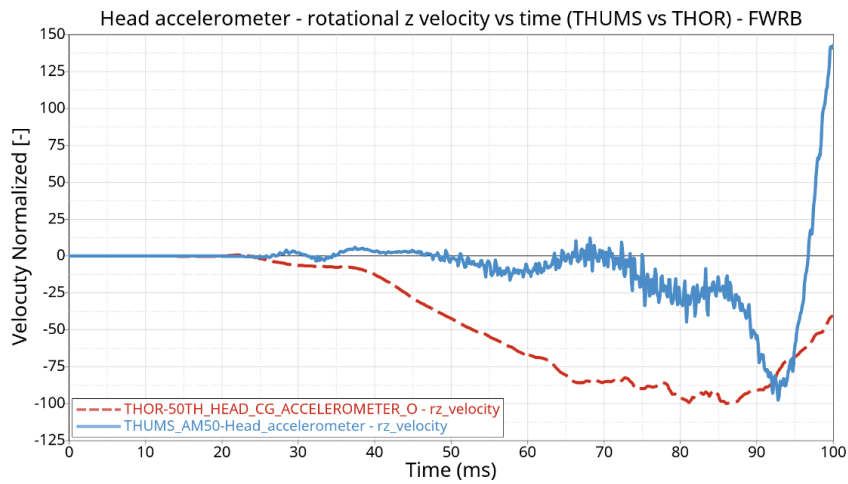


Figure 5.26. Positioned THUMS vs traditional dummy – Head – rot. z velocity – FWRB

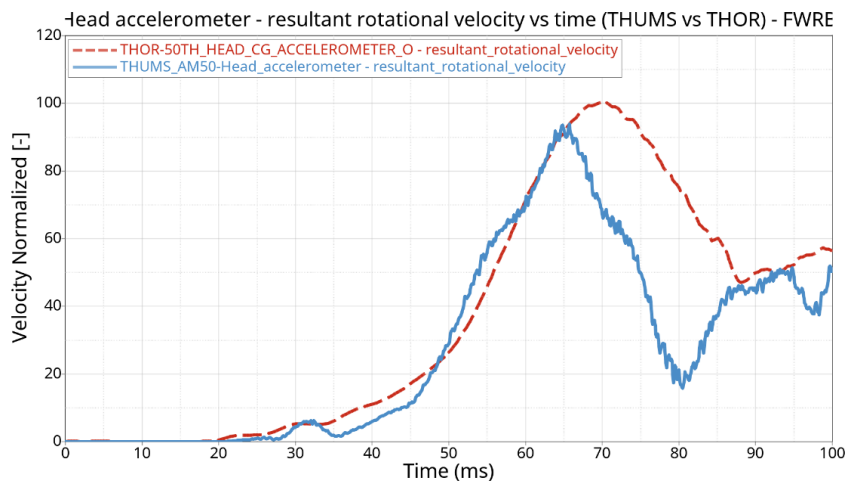


Figure 5.27. Positioned THUMS vs traditional dummy – Head – resultant rot. z velocity – FWRB

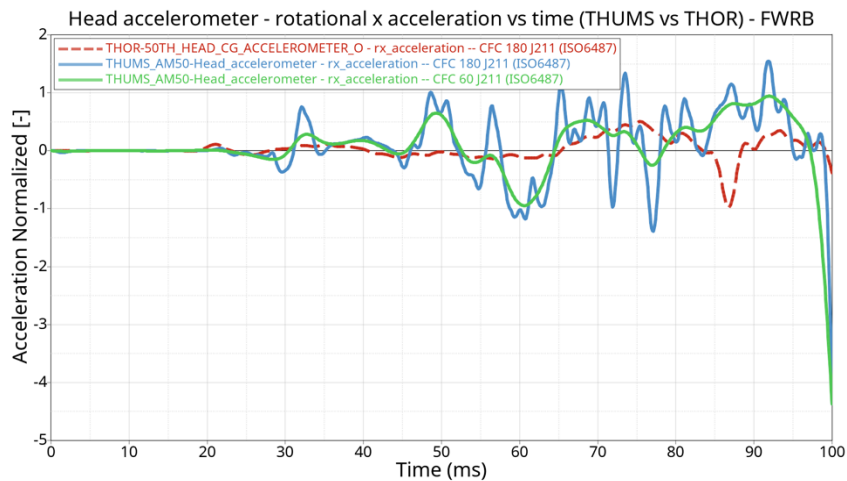


Figure 5.28. Positioned THUMS vs traditional dummy – Head – rot. x acceleration – FWRB

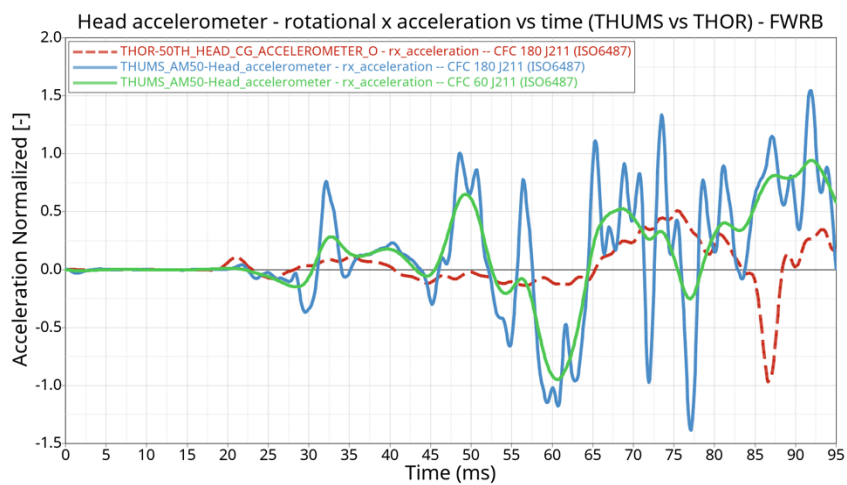


Figure 5.29. Positioned THUMS vs traditional dummy – Head – rot. x acceleration – 95 ms – FWRB

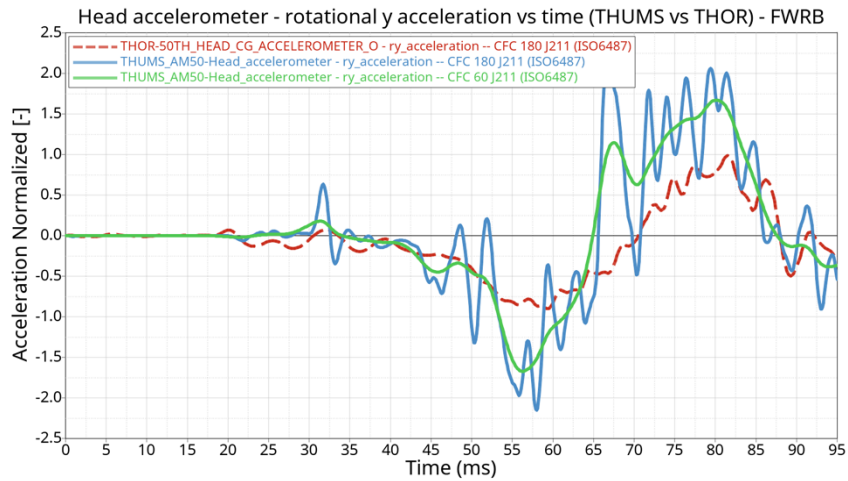


Figure 5.30. Positioned THUMS vs traditional dummy – Head – rot. y acceleration – 95 ms – FWRB

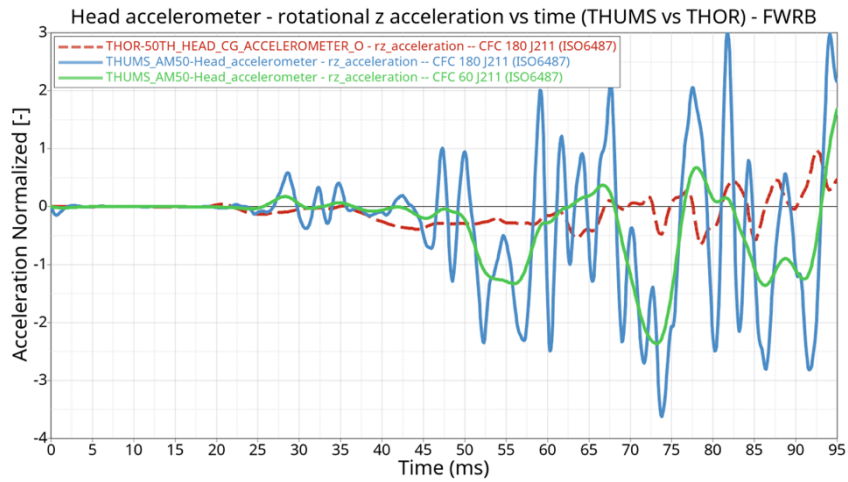


Figure 5.31. Positioned THUMS vs traditional dummy – Head – rot. z acceleration – 95 ms – FWRB

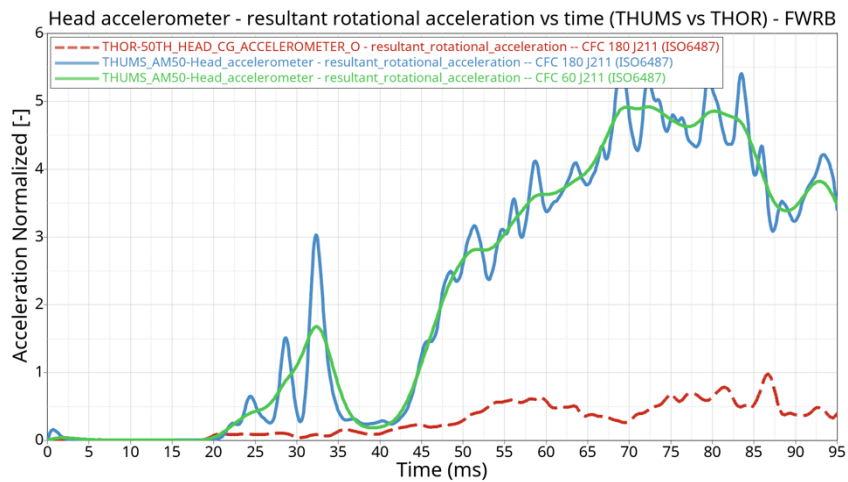


Figure 5.32. Positioned THUMS vs traditional dummy – Head – resultant rot. x acceleration – 95 ms – FWRB

By referring to the curves of Figure 5.20, the THUMS FE model reaches the negative peak before the THOR traditional dummy since, as also anticipated in the previous pages with reference to the Figures 5.10 – 5.11, the head of HBM is the first to get in contact with the DAB and it is, as a consequence, the first to stop and invert its motion.

Since, in the rotational accelerations, the filtering action can cause numerical oscillations at the end of the curves (e.g. in Figure 5.28), in the Figures 5.29 – 5.32 the abscissa axis representing the time (ms) is cut at 95 ms. In this way, it is possible to better appreciate the ordinate values of the curves.

Head Injury Criteria (HIC)

Basing on the head resultant acceleration, computed as

$$a_r = \sqrt{a_x^2 + a_y^2 + a_z^2}$$

The HIC can be calculated, as described in §4.5.1 both for the THUMS and THOR model.

In this Thesis work, as done for the curves reported in the plots, also the injury criteria values are expressed in relative form and normalized with respect to the THOR ones: if the THOR HIC is assumed to be equal to 100, the computed THUMS HIC value is 105,04. The reference time interval window is 63.8 – 78.9 ms.

Brain Injury Criteria (BrIC)

Basing on the formula reported in §4.5.2, the BrIC can be computed for both the traditional dummy and the THOR model. If the THOR BrIC is assumed to be equal to 100, the computed THUMS BrIC is 106.34.

Neck Forces

The comparison between the THUMS and THOR neck forces is reported in Figure 5.33.

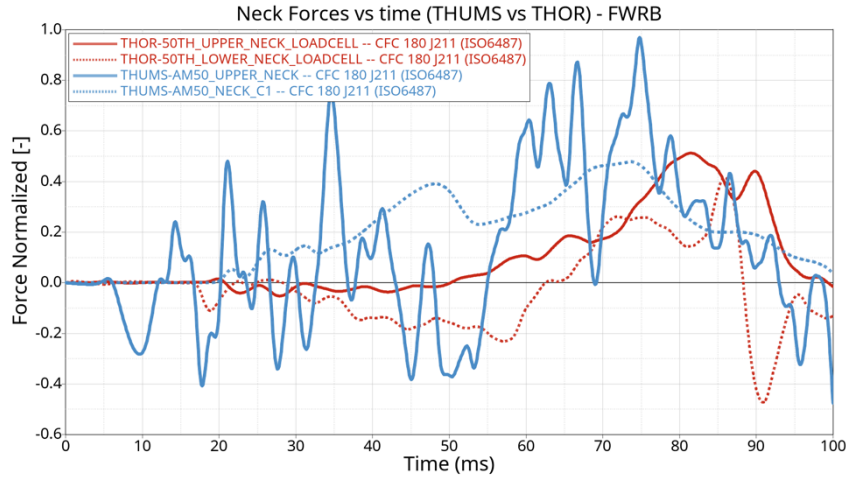


Figure 5.33. Positioned THUMS vs traditional dummy – Upper and Lower (C1) Neck Forces – FWRB

As it is possible to notice, the trends of the two curves are comparable. However, the upper neck force obtained from the THUMS model simulation is higher than the THOR one. This is due to the model complexity in terms of assigned soft materials and to the different number of components present in the neck region. Still, the high signal oscillations could suggest that the force measured by means of those sections is not the best parameter to be examined in a HBM. The maximum values of the THUMS neck forces (between 60 and 80 ms) coincide with the maximum head rotation and minimum distance between the chin and the thorax i.e. maximum elongation of the neck cervical part (ref. Figures 5.12 – 5.14).

THUMS Thorax signals

In the plots of Figures 5.34 – 5.36, the thorax accelerations, obtained by means of the sensors positioned in correspondence of the vertebrae T1, T4 and T12, as in the THOR dummy model, are shown. As for the head signals, the red dashed lines show the outputs obtained from the THOR model simulation, whereas the blue and the green lines refer to the THUMS signals with different filtering actions.

In the case of the thorax signals, the different peaks and timings detected in the comparison of the two models are, also, generally due to the:

- Complexity of the HBM structure with respect to the traditional THOR dummy
- Different shape and volumes of the two observed objects

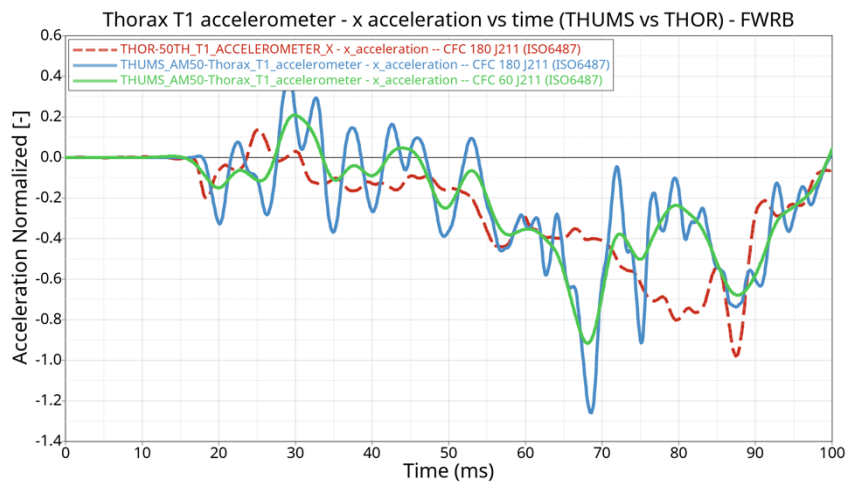


Figure 5.34. Positioned THUMS vs traditional dummy – Thorax T1 – linear x acceleration –FWRB

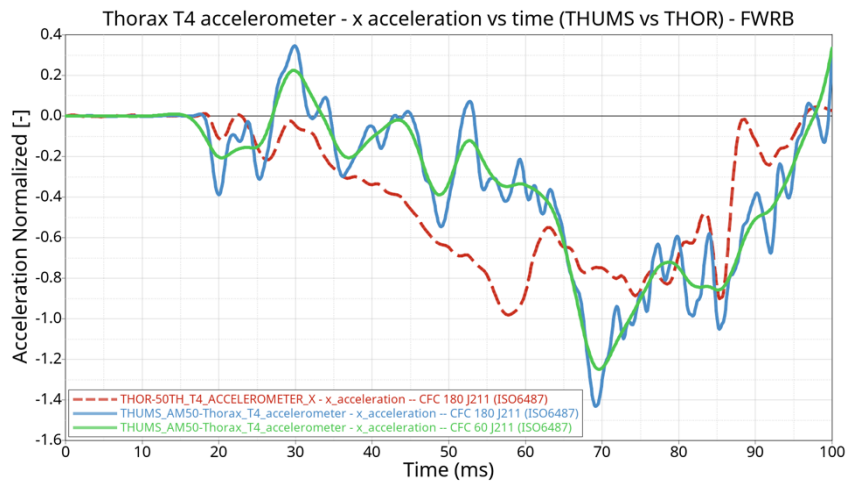


Figure 5.35. Positioned THUMS vs traditional dummy – Thorax T4 – linear x acceleration –FWRB

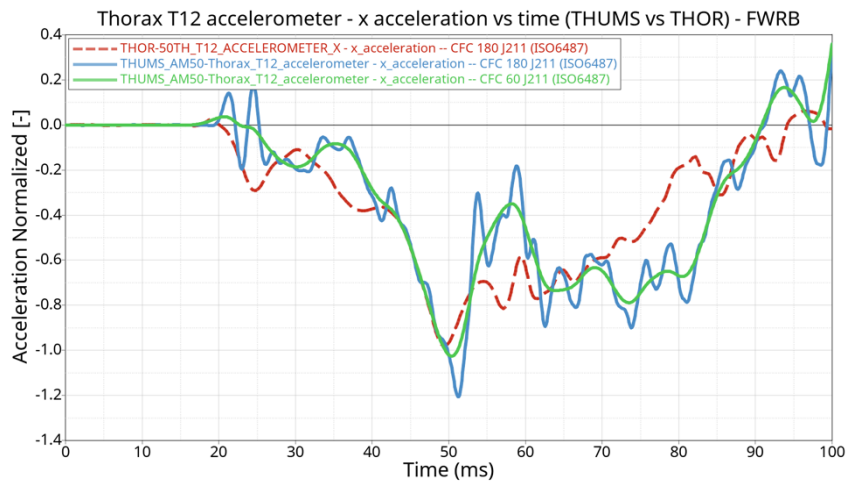


Figure 5.36. Positioned THUMS vs traditional dummy – Thorax T12 – linear x acceleration –FWRB

THUMS Pelvis signal

In Figure 5.37, it is possible to notice that the x acceleration of the pelvis of the THUMS model highly oscillates in the time interval 45 – 55 ms. The confirmation of this behaviour can be explained by observing the animation frames shown in the Figures 5.10 – 5.12.

The pelvis undergoes a rotation around its y axis and a translation towards the $+z$ and $-x$ directions. This behaviour, on the opposite, is not appreciable if looking at the THOR simulation frames, in which a more linear motion of the pelvis is achieved.

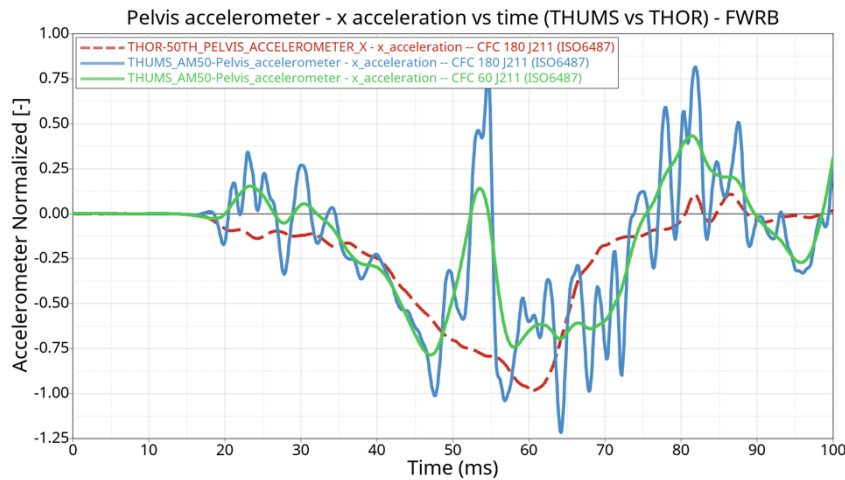


Figure 5.37. Positioned THUMS vs traditional dummy – Pelvis – linear x acceleration –FWRB

THUMS Legs – forces

In Figures 5.38 and 5.39, the comparison of the THUMS and THOR models in terms of Upper and Lower Tibia forces during the FWRB impact simulation is reported.

The peak forces measured on the right tibia (Figure 5.38) of the conventional THOR dummy are comparable to the ones of the THUMS model. In particular, the maximum value of the upper tibia force is slightly higher in the THOR model, while the one of the lower tibia results to be higher in the outcomes obtained from the HBM simulation.

As it is possible to notice by looking at the Figures 5.11 – 5.13, in the time interval between 50 and 75 ms, the minimum distance between the THOR model and the vehicle surfaces is achieved. This explains the force peaks that can be observed in Figure 5.38.

If the left tibia forces are instead considered, the HBM values are much smaller than the THOR ones. Since there is no contact between the left foot and the pedals, the obtained divergence between the curves is due to the different interaction between the two models and the vehicle.

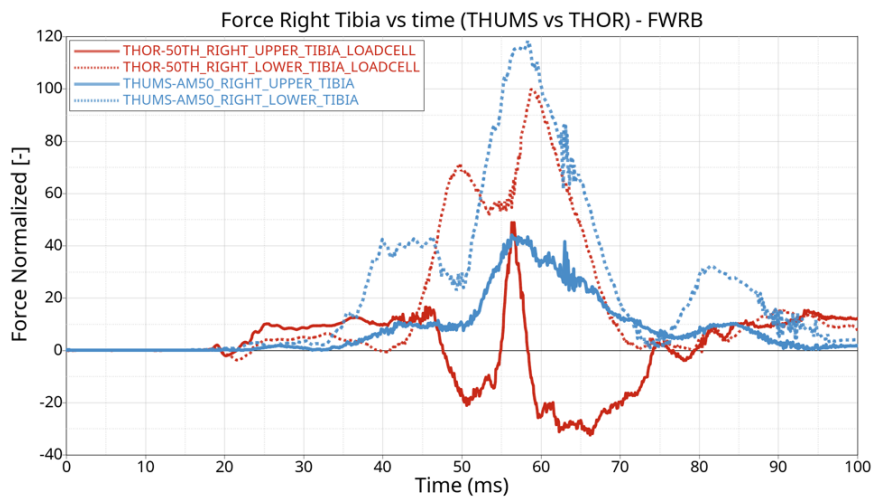


Figure 5.38. Positioned THUMS vs traditional dummy – Right Tibia – Force –FWRB

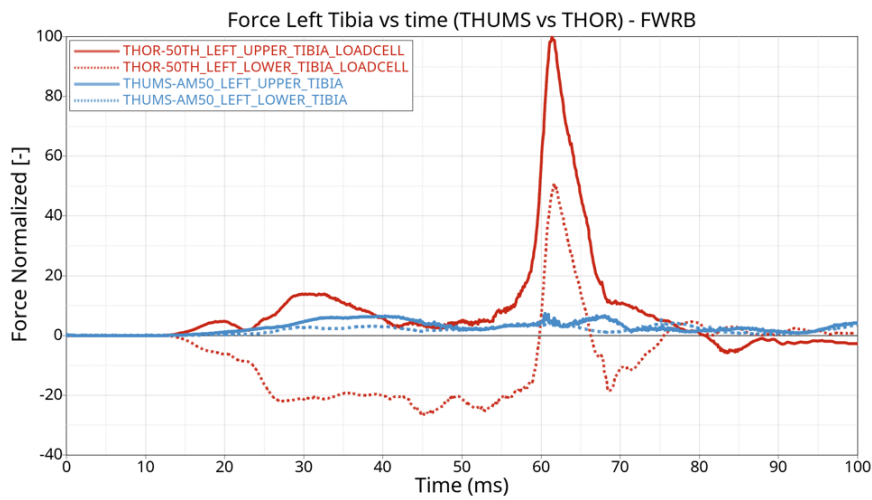


Figure 5.39. Positioned THUMS vs traditional dummy – Left Tibia – Force –FWRB

5.2.2 Results of the THUMS impact simulations and comparison with the THOR dummy FE model – Offset Deformable Barrier (ODB) Impact case

Global Energies

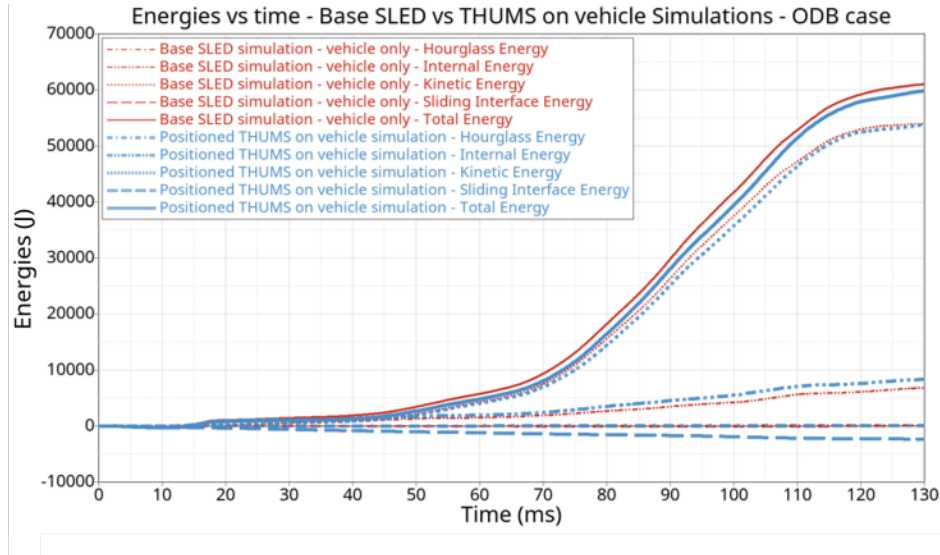


Figure 5.40. Positioned THUMS on vehicle vs Base SLED simulations – Global Energies – ODB

As for the FWRB impact case (§5.2.1), the comparison between the base SLED simulation (vehicle only – ref. *Figure 3.0*) and the one with the Positioned THUMS as driver is shown in *Figure 5.40*.

Even in the ODB case, the difference between the red and the blue curves is due to the contribution of the HBM components present in the model.

THUMS Simulation Frames

The time frames of the Positioned THUMS on vehicle for the Offset Deformable Barrier simulation are reported in the following.

As for the FWRB impact case, in the *Figures 5.41* and *5.42*, the lateral *xz* (left plane) and the isometric views are, respectively, shown.

Subsequently, the comparison with the traditional THOR dummy model is reported, both in terms of simulation frames and obtained signals.

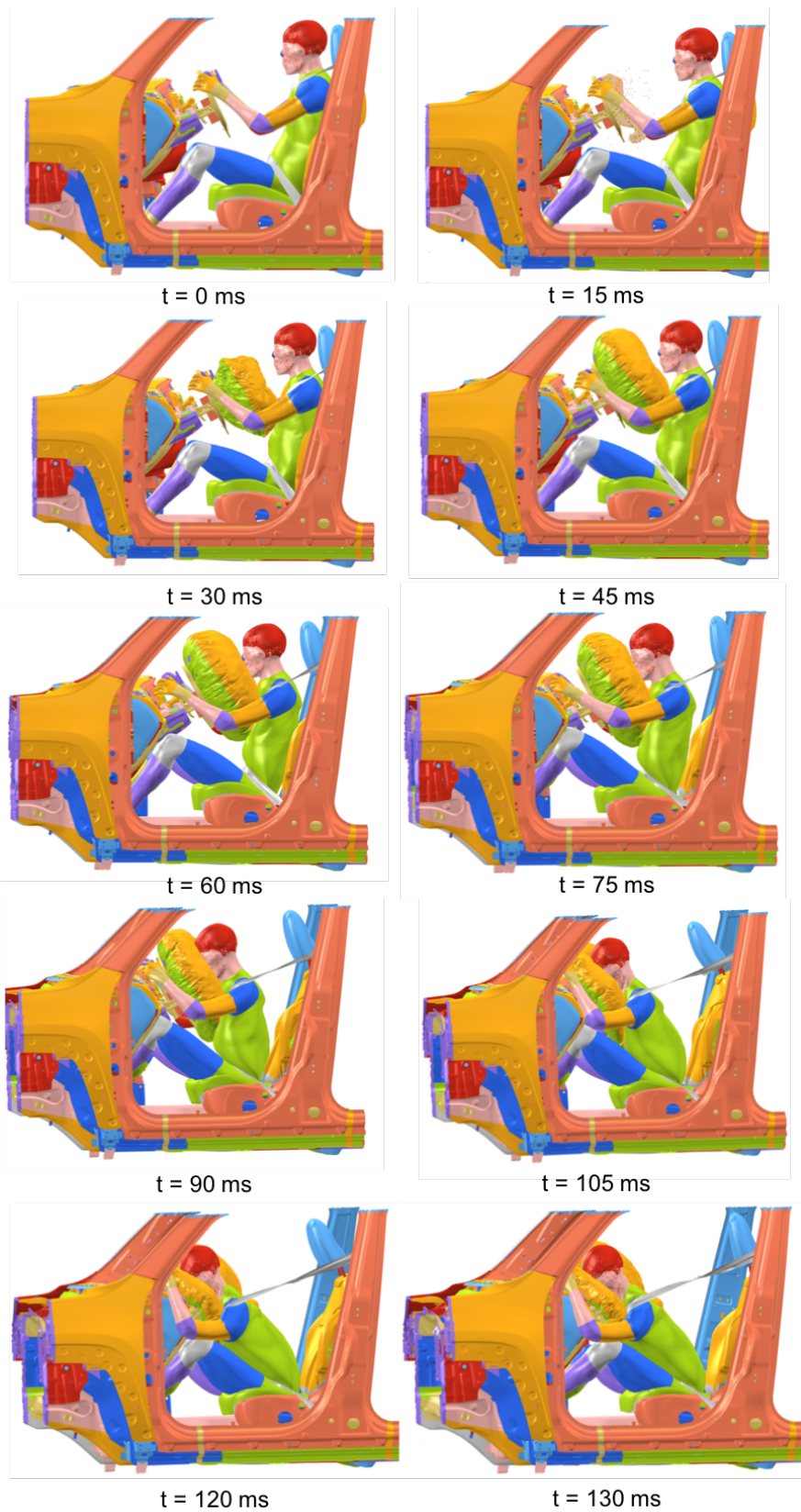


Figure 5.41. Positioned THUMS on vehicle – side xz view - ODB

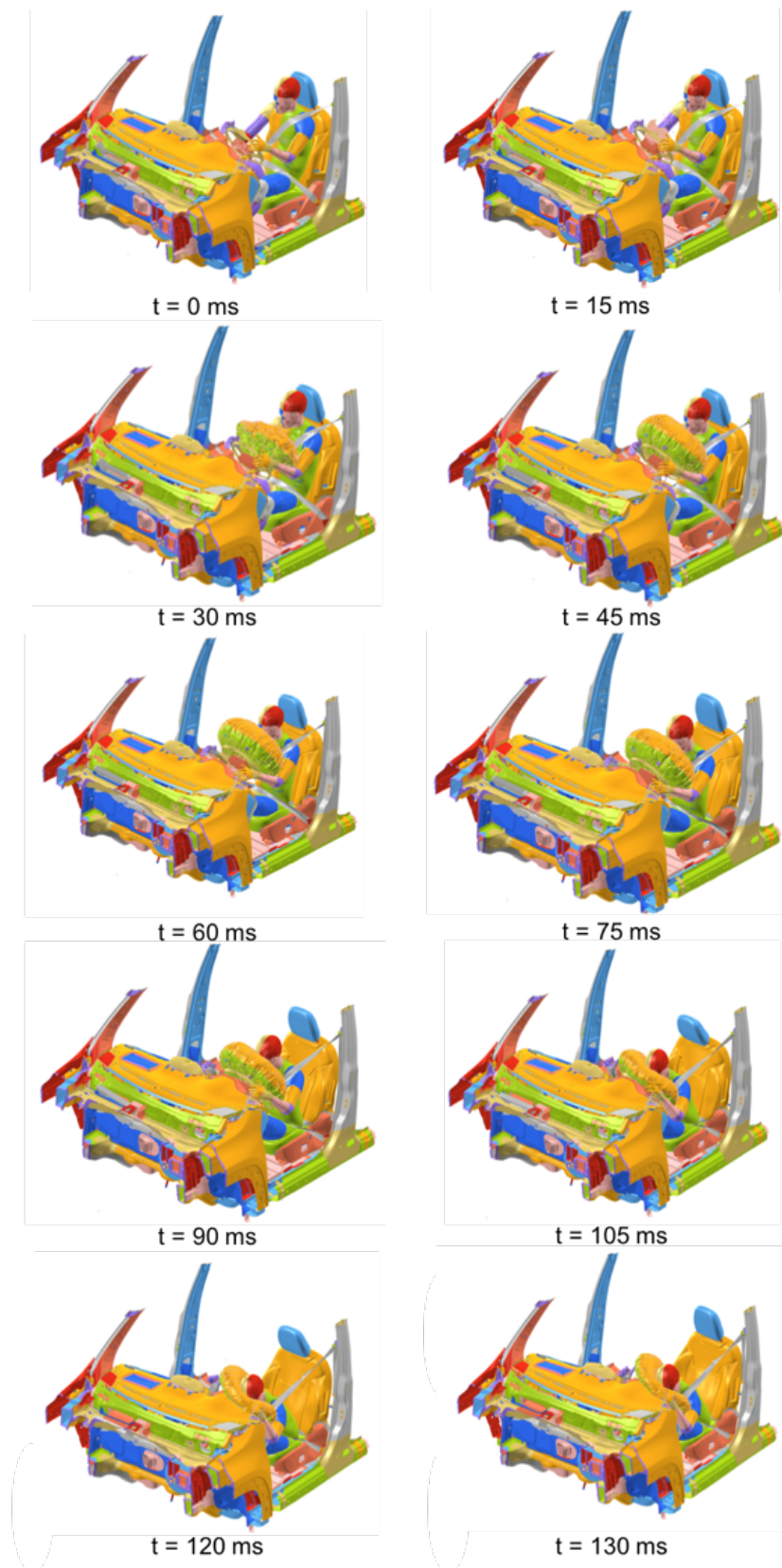


Figure 5.42. Positioned THUMS on vehicle – side xz view - ODB

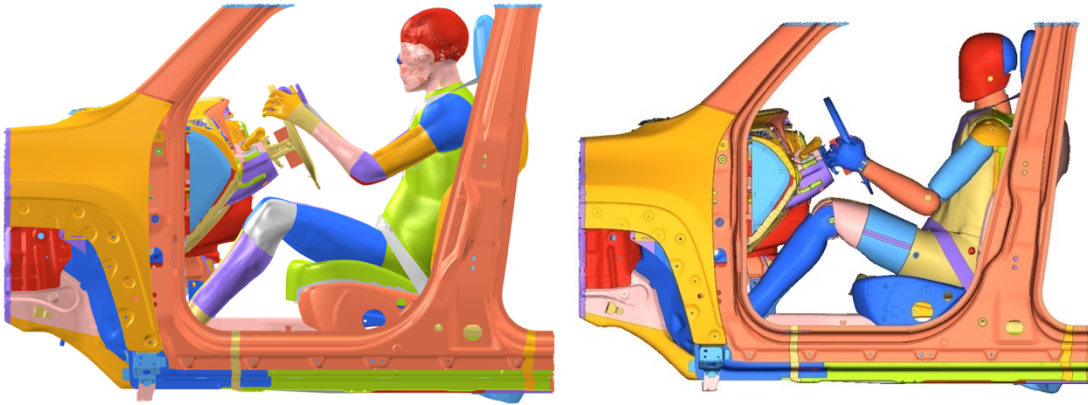


Figure 5.43. Positioned THUMS (left) vs THOR (right) - side xz view – ODB– 0 ms



Figure 5.44. Positioned THUMS (left) vs THOR (right) - side xz section view – ODB– 0 ms



Figure 5.45. Positioned THUMS (left) vs THOR (right) - side xz section view – ODB – 15 ms



Figure 5.46. Positioned THUMS (left) vs THOR (right) - side xz section view – ODB – 30 ms



Figure 5.47. Positioned THUMS (left) vs THOR (right) - side xz section view – ODB – 45 ms



Figure 5.48. Positioned THUMS (left) vs THOR (right) - side xz section view – ODB – 60 ms



Figure 5.49. Positioned THUMS (left) vs THOR (right) - side xz section view – ODB – 75 ms

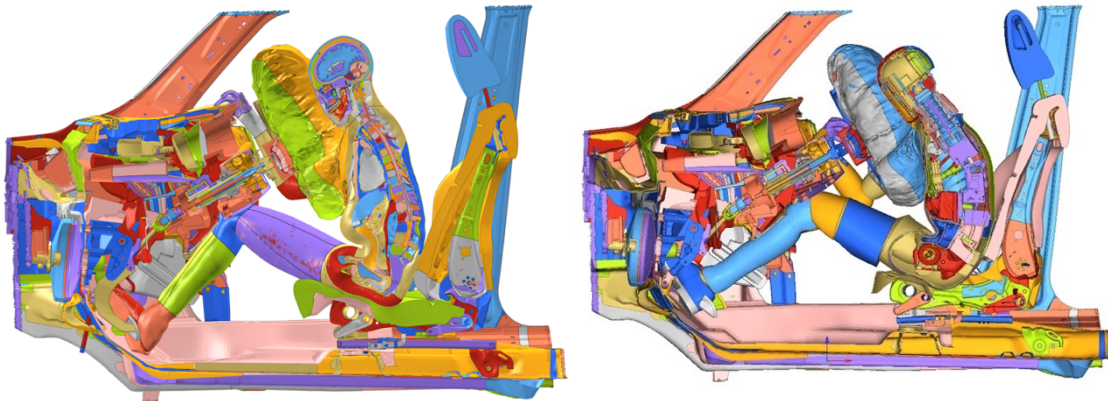


Figure 5.50. Positioned THUMS (left) vs THOR (right) - side xz section view – ODB – 90 ms



Figure 5.51. Positioned THUMS (left) vs THOR (right) - side xz section view – ODB – 105 ms



Figure 5.52. Positioned THUMS (left) vs THOR (right) - side xz section view – ODB– 120 ms



Figure 5.53. Positioned THUMS (left) vs THOR (right) - side xz section view – ODB – 130 ms

As it can be noticed in the Figures 5.44 and 5.45, the initial posture of the two FE driver models is the same of the one included in the FWRB impact case simulation.

The same first difference in the behaviour of the two models, previously illustrated for the FWRB case, can be also appreciated in this case between 30 and 45 ms (Figures 5.46 and 5.47: the head of the HBM goes in contact with the DAB before the one of the THOR dummy).

In the ODB simulation (Figures 5.47 and 5.50), the head negatively rotates also, around its y axis but, in this case, does not rotate back to reach a straighter neck configuration as in the FWRB case. In Figures 5.50 – 5.52, a different inclination of the backbone of the THOR dummy model can be appreciated, with respect to one of the THUMS HBM.

Further attention can be focused on the motion of the legs of the two models during the ODB simulation. The legs of the THOR dummy tend to stretch, by increasing the knee body angle. On the opposite, position of the ones of the THUMS model do not substantially change from 0 to 100 ms.

THUMS Head signals

The obtained velocities and accelerations of the head of the Positioned THUMS HBM during the ODB crash simulation are reported in this section.

In particular, the linear quantities are presented in Figures 5.54 – 5.61, whereas the rotational ones are included in Figures 5.62 – 5.70.

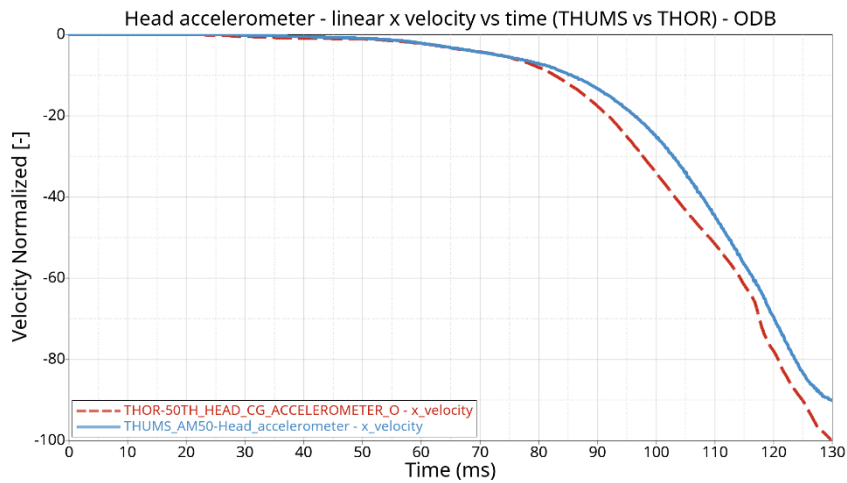


Figure 5.54. Positioned THUMS vs traditional dummy- Head - x linear velocity - ODB

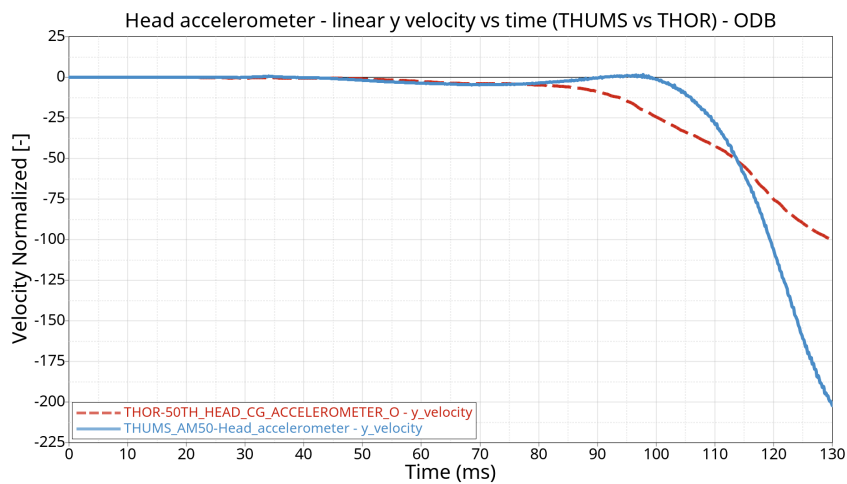


Figure 5.55. Positioned THUMS vs traditional dummy- Head – y linear velocity - ODB

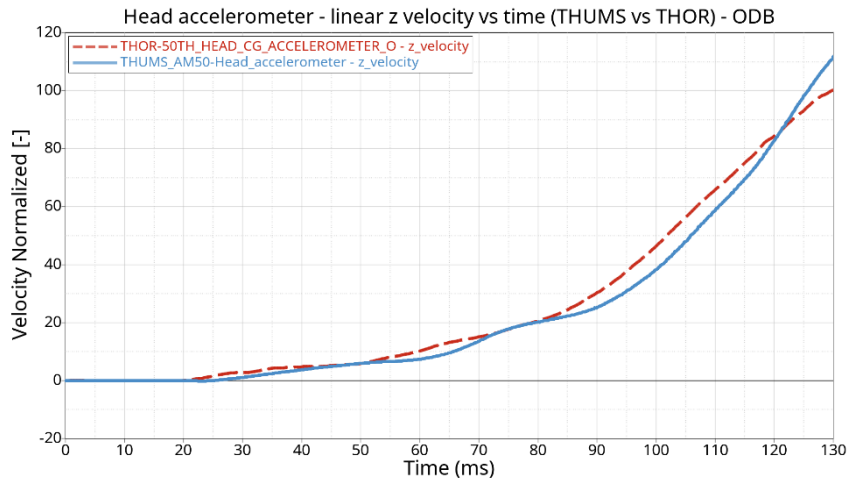


Figure 5.56. Positioned THUMS vs traditional dummy- Head – z linear velocity - ODB

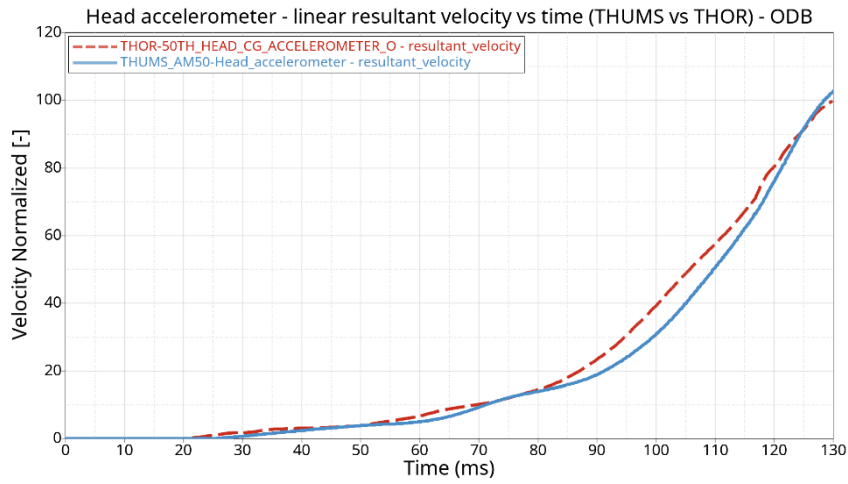


Figure 5.57. Positioned THUMS vs traditional dummy- Head – resultant linear velocity - ODB

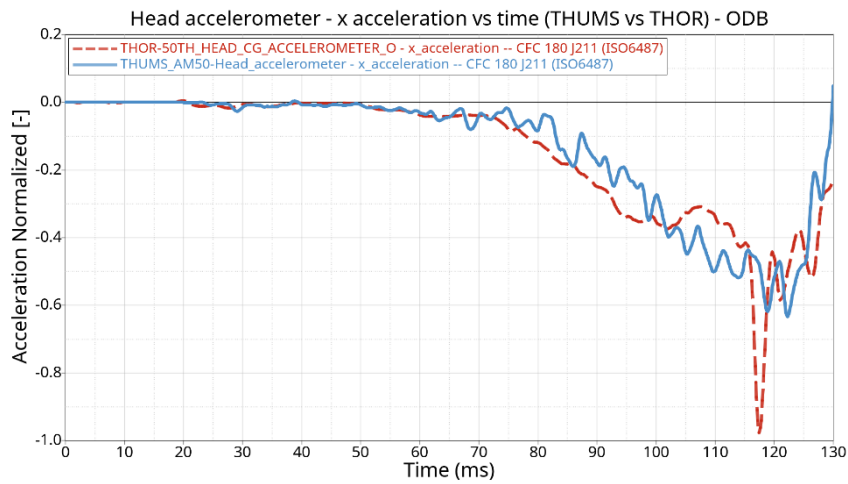


Figure 5.58. Positioned THUMS vs traditional dummy- Head - x linear acceleration - ODB

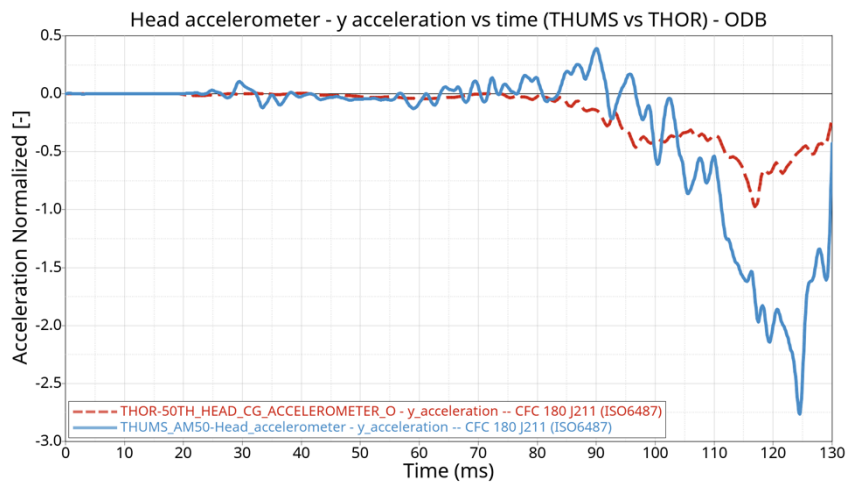


Figure 5.59. Positioned THUMS vs traditional dummy- Head - y linear acceleration – ODB

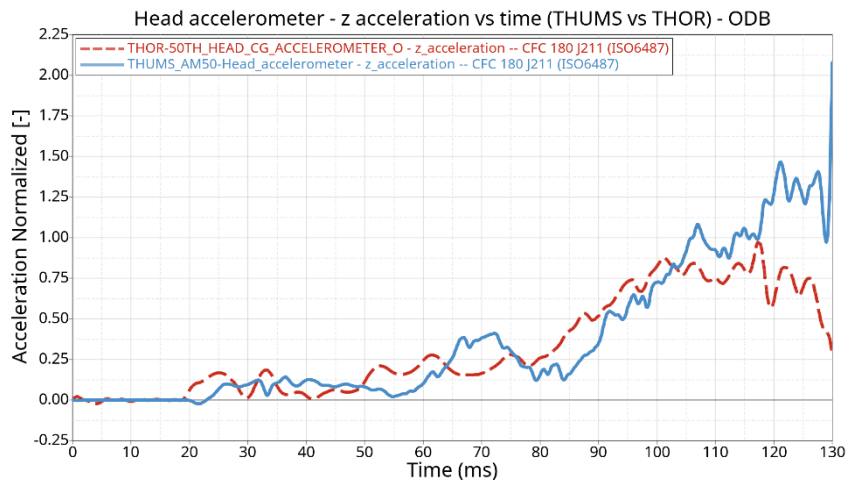


Figure 5.60. Positioned THUMS vs traditional dummy- Head - z linear acceleration – ODB

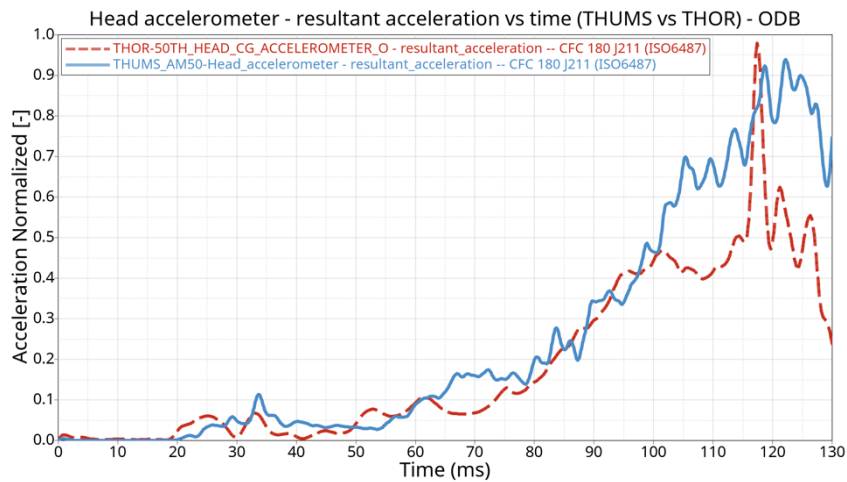


Figure 5.61. Positioned THUMS vs traditional dummy- Head – resultant linear acceleration - ODB

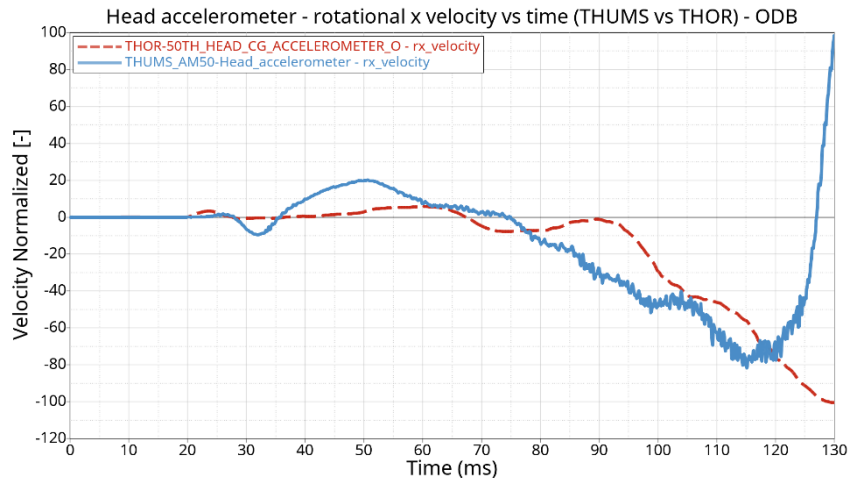


Figure 5.62. Positioned THUMS vs traditional dummy – Head – rot. x velocity – ODB

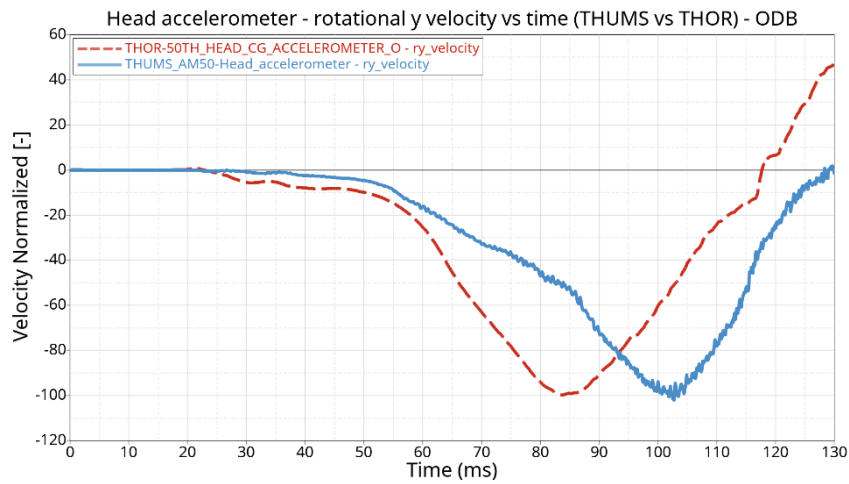


Figure 5.63. Positioned THUMS vs traditional dummy – Head – rot. y velocity – ODB

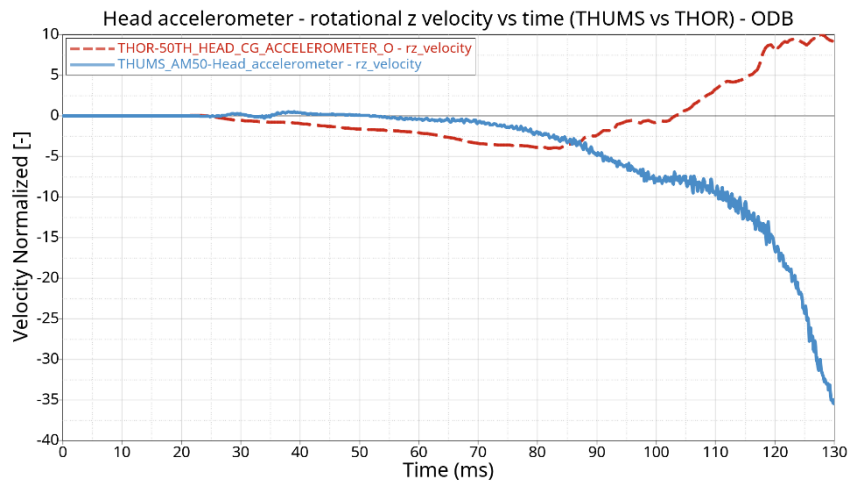


Figure 5.64. Positioned THUMS vs traditional dummy – Head – rot. z velocity – ODB

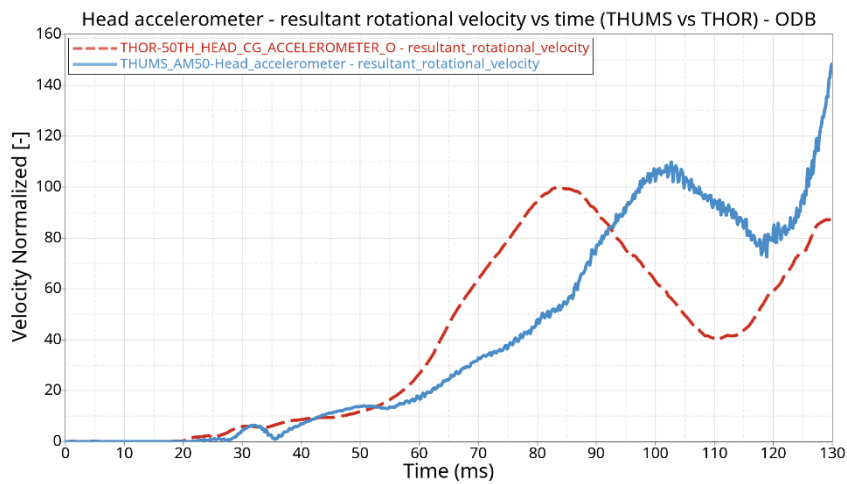


Figure 5.65. Positioned THUMS vs traditional dummy – Head – resultant rot. z velocity – ODB

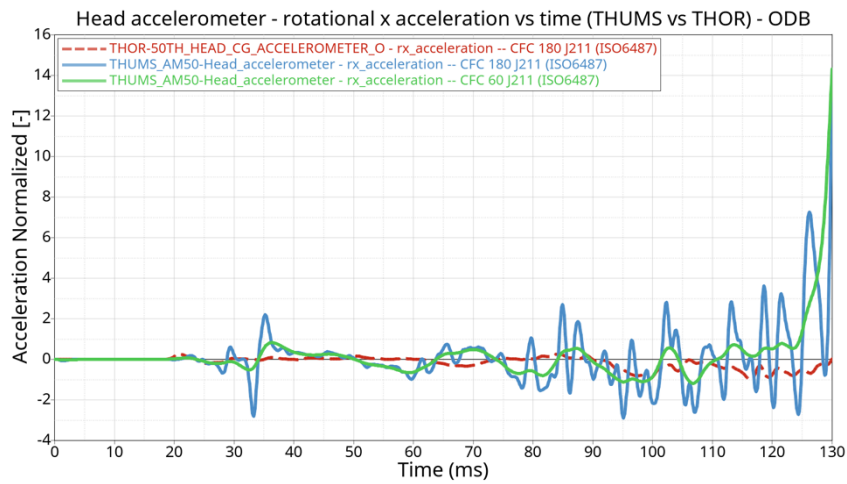


Figure 5.66. Positioned THUMS vs traditional dummy – Head –rot. x acceleration – ODB

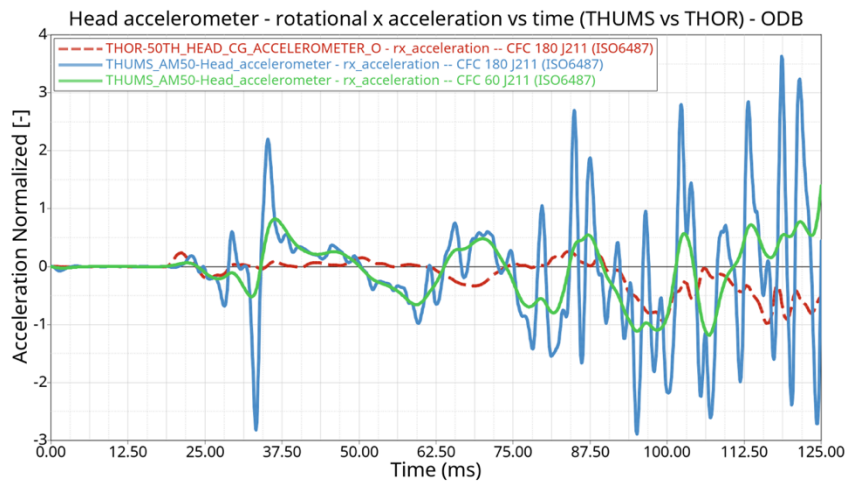


Figure 5.67. Positioned THUMS vs traditional dummy – Head –rot. x acceleration – 95 ms – ODB

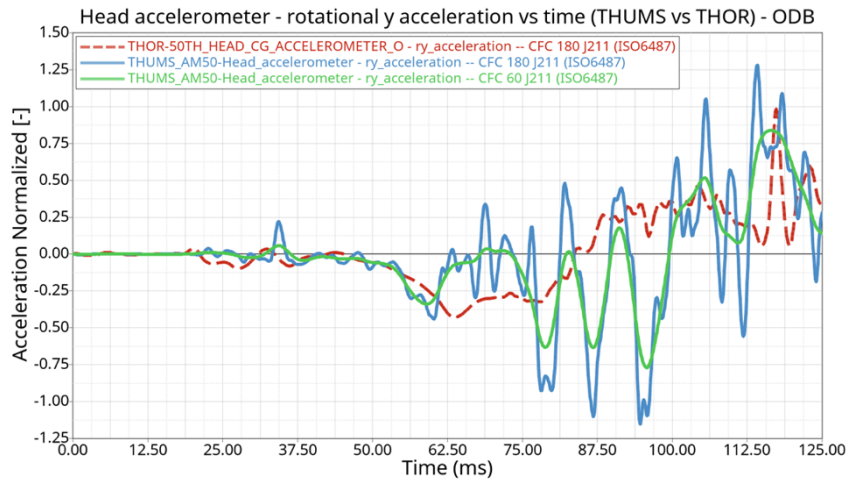


Figure 5.68. Positioned THUMS vs traditional dummy – Head –rot. y acceleration – 95 ms – ODB

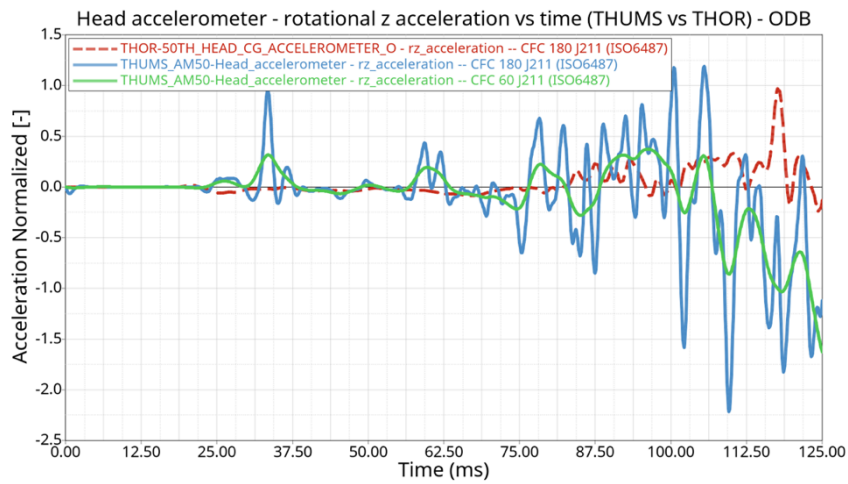


Figure 5.69. Positioned THUMS vs traditional dummy – Head –rot. z acceleration – 95 ms – ODB

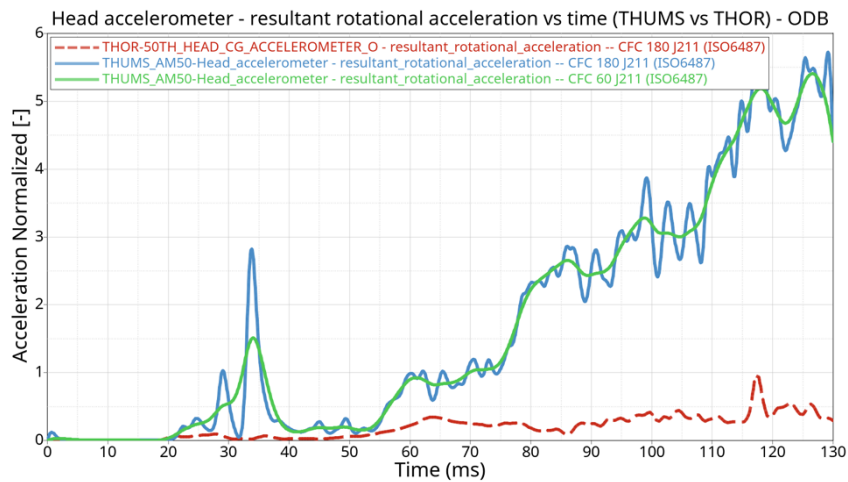


Figure 5.70. Positioned THUMS vs traditional dummy – Head –res. rot. x acceleration – 95 ms – ODB

As in the case of the FWRB signals, especially in the rotational accelerations, the filtering action can cause numerical oscillations at the end of the curves (e.g. in Figure 5.66). In the Figures 5.67 – 5.69, therefore, the abscissa axis reporting the time (ms) is cut at 125 ms. In this way, it is easier to appreciate the ordinate values of the curves.

Head Injury Criteria (HIC)

Also in the ODB impact case, the HIC can be calculated, as described in §4.5.1 both for the THUMS and THOR model.

Therefore, if the THOR HIC is assumed to be equal to 100, the computed THUMS HIC value in the ODB case is 259.6. The reference time interval window is 113.1 – 128.1 ms.

Brain Injury Criteria (BrIC)

If the THOR BrIC is assumed to be equal to 100, the computed THUMS BrIC, computed by following the formula reported in §4.5.2, is value in the ODB case is 169,55.

Neck Forces

The comparison between the THUMS and THOR neck forces is reported in Figure 5.71.

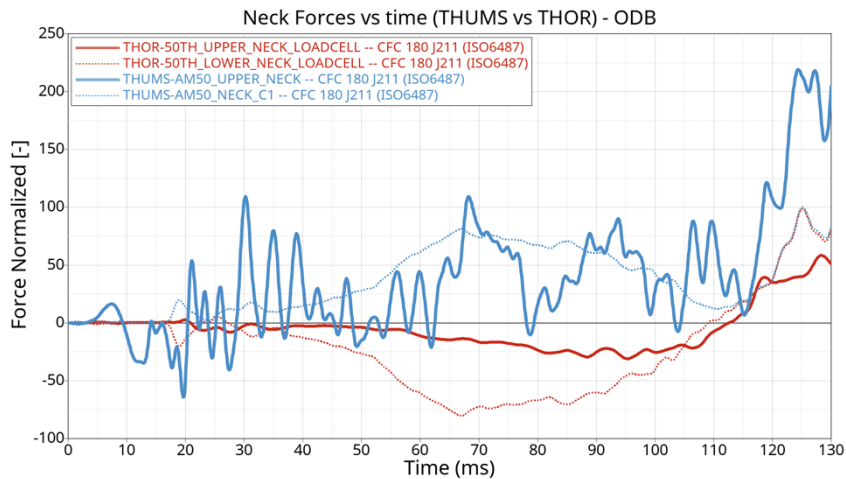


Figure 5.71. Positioned THUMS vs traditional dummy – Upper and Lower (C1) Neck Forces – ODB

As it is possible to notice, the trends of the two curves are comparable. However, as in the FWRB case, the upper neck force obtained from the THUMS model simulation is higher than the

THOR one. Moreover, also the C1 neck forces result to be higher than the ones coming from the THOR dummy simulation

THUMS Thorax signals

In the plots of Figures 5.72 – 5.74, the thorax accelerations, obtained by means of the accelerometers positioned in correspondence of the vertebrae T1, T4 and T12, as in the THOR dummy model, are shown.

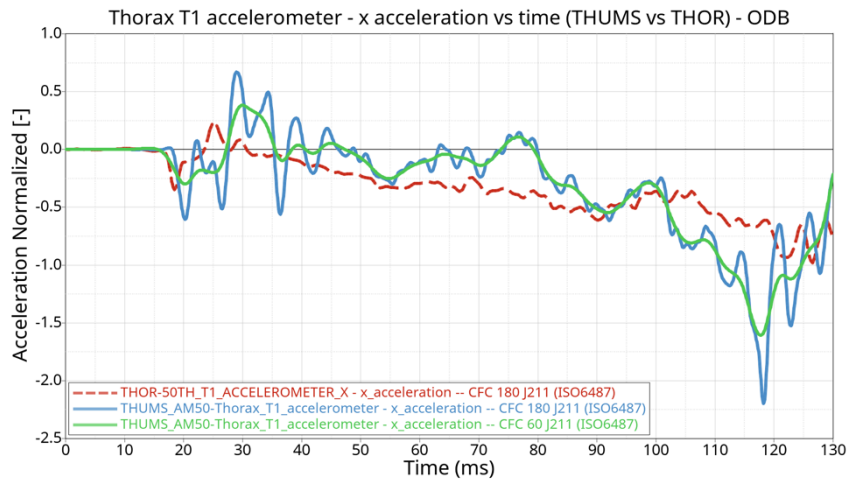


Figure 5.72. Positioned THUMS vs traditional dummy – Thorax T1 – linear x acceleration –ODB

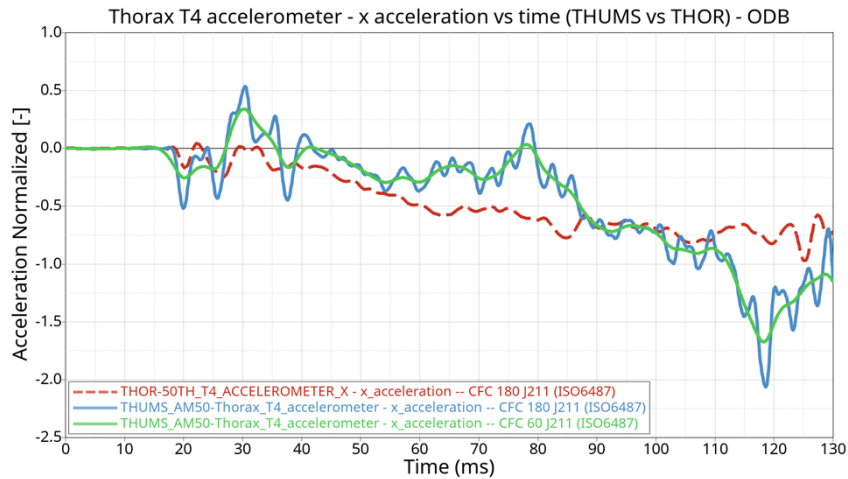


Figure 5.73. Positioned THUMS vs traditional dummy – Thorax T4 – linear x acceleration –ODB

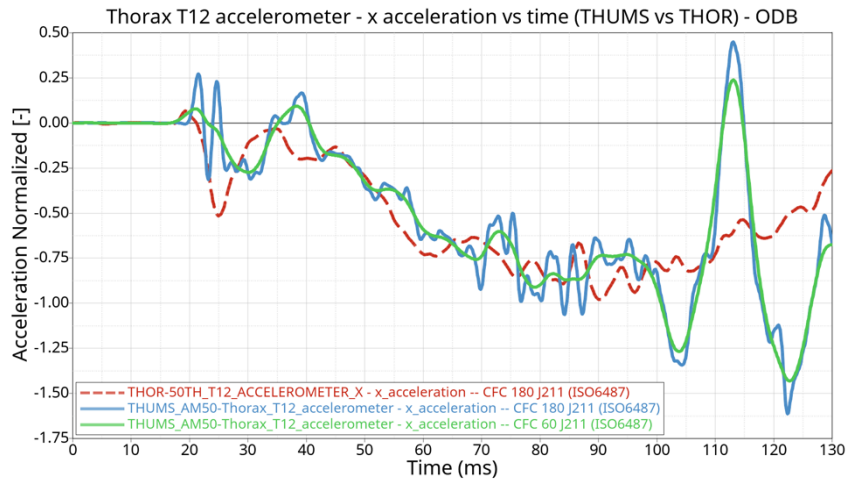


Figure 5.74. Positioned THUMS vs traditional dummy – Thorax T12 – linear x acceleration – ODB

As obtained on the FWRB case, the signals coming from the T1, T4 and T12 vertebra are still affected by oscillations. The difference between the behaviour of the THUMS and the THOR models, however, is mainly due to the different motion of the two bodies. After around 100 ms, till which the accelerations of the two objects have comparable trends, the curves diverge (e.g. Figure 5.74). This finds the explanation by looking at the Figures 5.51 – 5.53: while the backbone deformation of the THOR model does not show any abrupt variation, the one of the THUMS, especially in its lower part, highly deforms during the impact simulation. In particular, the backbone natural curves tend to give way to straighter configuration.

THUMS Pelvis signal

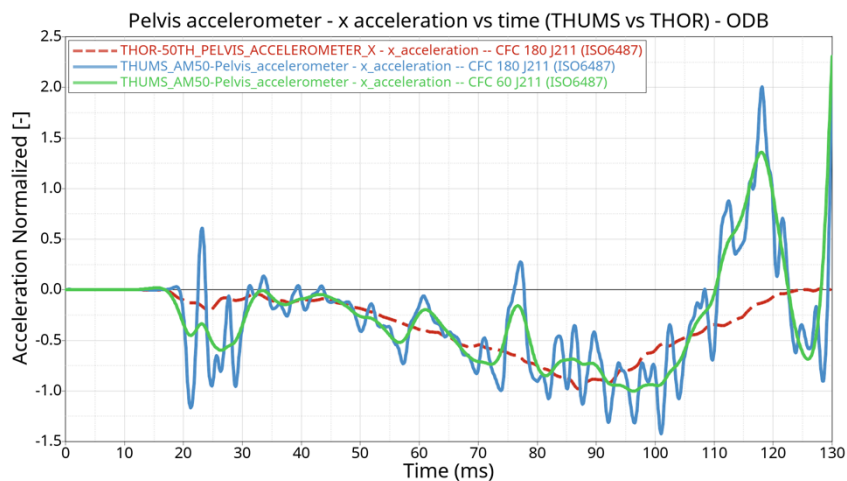


Figure 5.75. Positioned THUMS vs traditional dummy – Pelvis – linear x acceleration – ODB

The signal obtained by means of the pelvis accelerometer (ref. Figure 4.44) has a trend similar to the THOR acceleration, even if, as in the previous plots, it is affected by numerical oscillations.

By referring to Figure 5.75, the main divergence existing between the two curves (in the range 110 – 125 ms), is due to the different motion of the two bodies. By looking at Figures 5.51 – 5.53, it is hence possible to appreciate a large motion of the pelvis bone (i.e. rotation about its y axis) of the HBM. This cannot be said for what the traditional dummy considered in this Thesis work is concerned.

THUMS Legs – Tibia forces

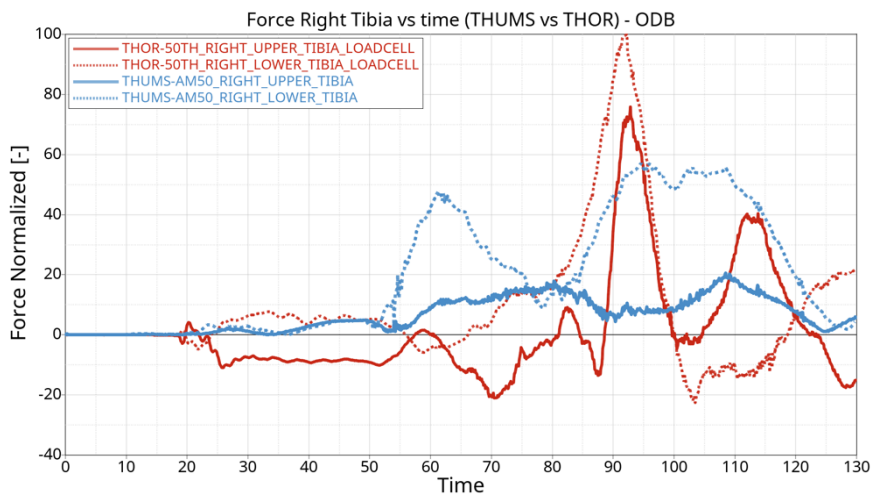


Figure 5.76. Positioned THUMS vs traditional dummy – Right Tibia – Force – ODB

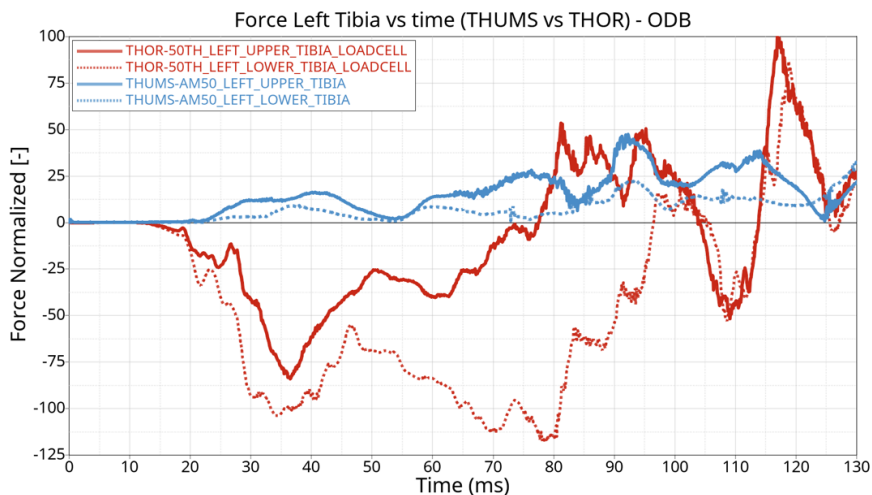


Figure 5.77. Positioned THUMS vs traditional dummy – Left Tibia – Force – ODB

In Figures 5.76 and 5.77, the comparison of the behavior of the THUMS and THOR model in terms of Upper and Lower Tibia forces is reported.

The results obtained from the analysis of both the right and left tibia show that the peak values of HBM are lower than the ones extrapolated from the THOR dummy.

It is therefore possible to observe a significant difference in the obtained curves if they are compared to the same output signals of the FWRB simulation (ref. Figures 5.39).

The maximum values of the upper and lower right tibia forces of the THOR model (80 – 100 ms) finds the confirmation by looking at the frames of Figures 5.49 – 5.51. In those time instants, indeed, the maximum compression of the right leg can be observed (i.e. the minimum distance between the THOR model body and the vehicle dashboard is achieved).

Chapter 6

THUMS in Out-of-Position Configuration - Impact Test Simulations Results

6.1 THUMS in Out-of-Position Configuration

In the Figure 6.0, the complete model used for both the FWRB and ODB impact simulations (§5.1) is shown. This includes all the components implemented in the impact test simulations with the THUMS HBM in conventional driving configuration, with the addition of the vehicle central tunnel.

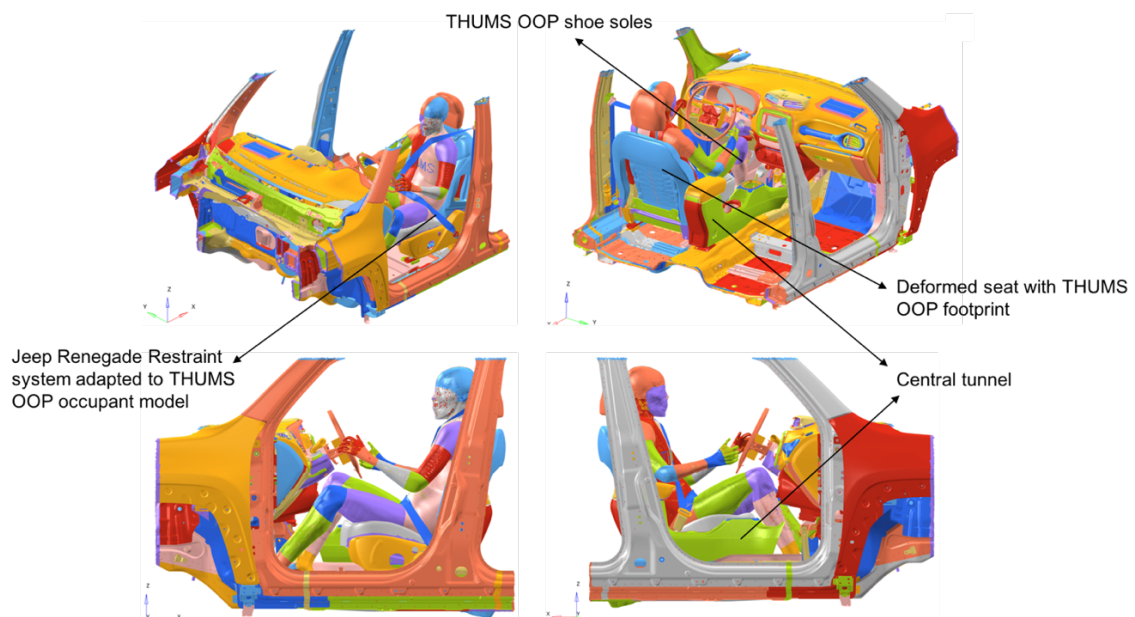


Figure 6.0. THUMS on vehicle FE model – Final simulation setting – OOP Configuration

In this chapter, a description of the results obtained from the simulations including the THUMS in the Out-of-Position (OOP) configuration is reported.

Moreover, the achieved results are compared with the THUMS ones presented in §5.2 and §5.3 and normalized with respect to them.

As for the HBM in conventional driving posture, also in this case the THUMS model correctly behaves inside the vehicle during the impact, as well as the created driver restraint system (ref. §4.3.3). However, the non-conventional seating posture obviously leads to human body motions and displacements which are, generally, not foreseen and not observable in the impact test simulations prescribed by the regulations and performed implementing the traditional dummy FE models.

6.2 Results of the THUMS OOP and comparison with the HBM in conventional driving posture - Full Width Rigid Barrier (FWRB) Impact case

Global Energies

The comparison between the simulation performed in the first part of this Thesis job (ref. *Figure 5.0*) and the one with the THUMS in the OOP configuration (ref *Figure 6.0*) is shown in *Figure 6.1*.

As expected, the change of the THUMS posture does not influence the global energy balance. The disparity between the red and the blue lines of *Figure 6.1*, then, is only due to the additional vehicle component.

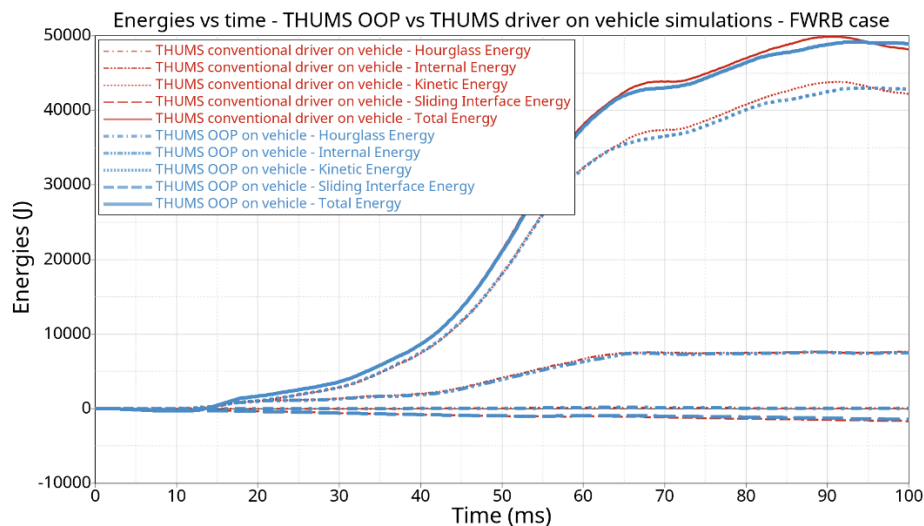


Figure 6.1. THUMS in OOP vs THUMS in driving posture on vehicle – Global Energies – FWRB

THUMS Simulation Frames

Here in the following, the time frames of the simulation of the THUMS in the defined OOP during the FWRB impact are reported.

In Figures 6.2 and 6.3, the lateral xz (left plane) and the isometric views are, respectively, shown.

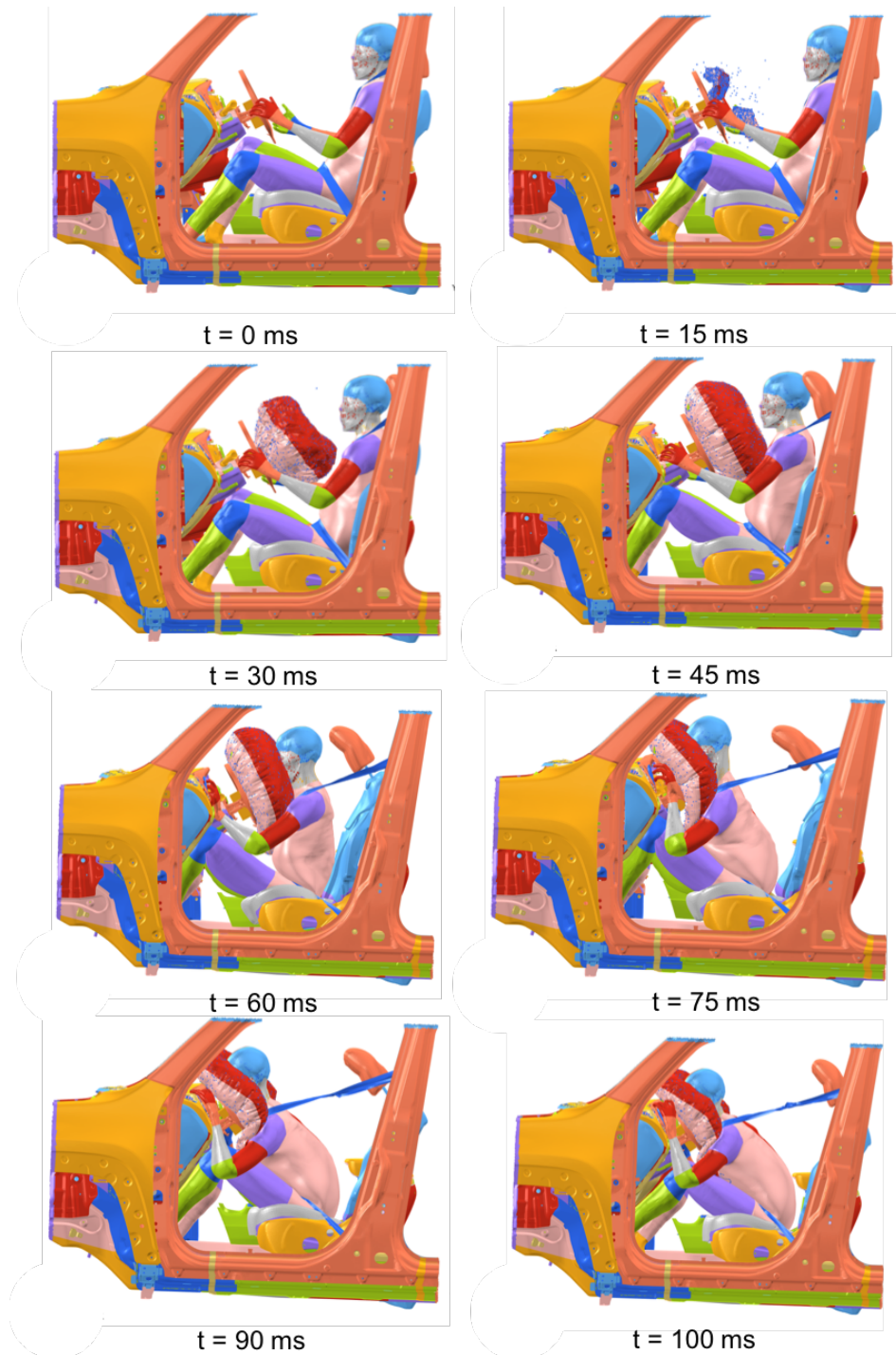


Figure 6.2. THUMS in OOP on vehicle – side xz view - FWRB

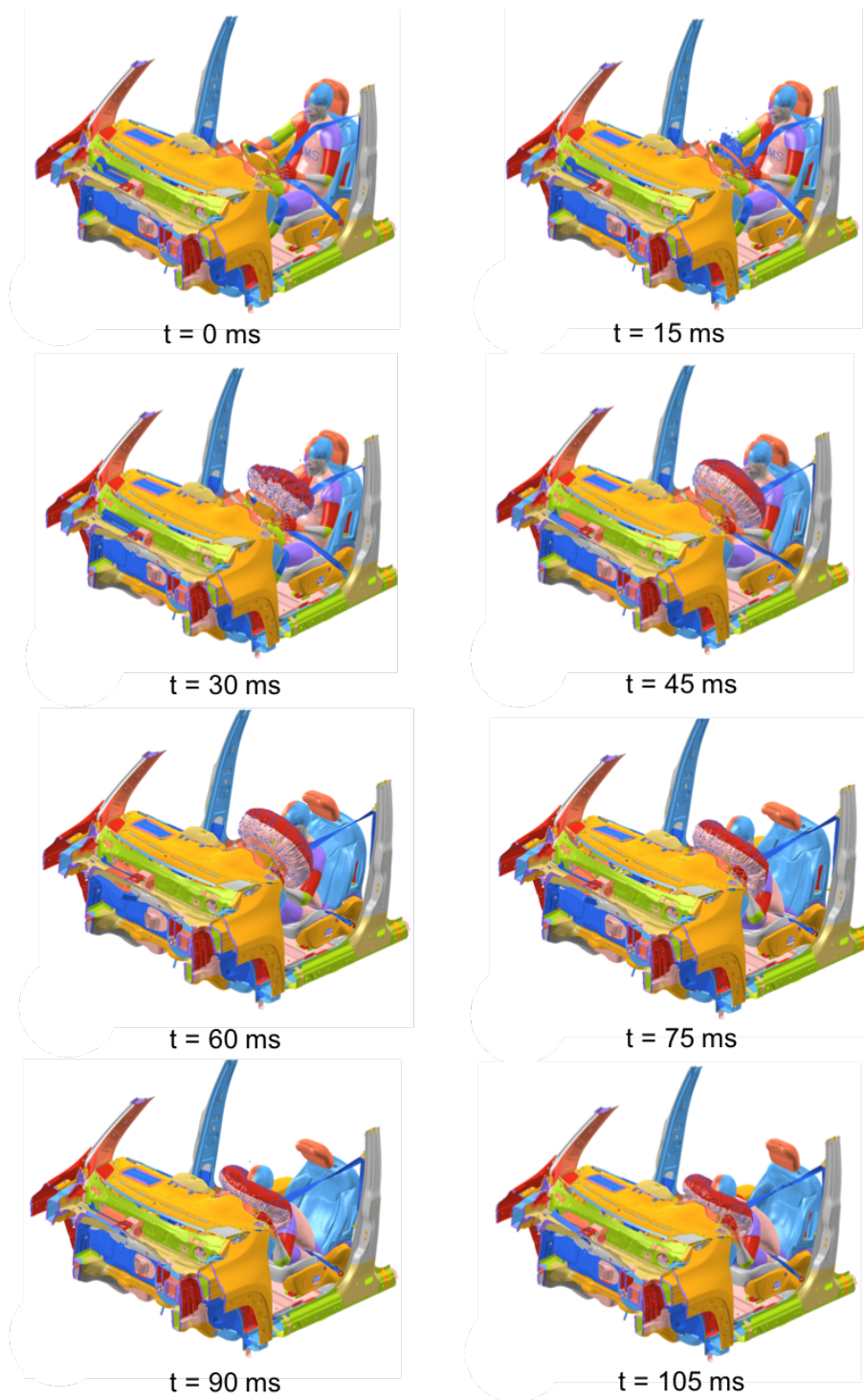


Figure 6.3. THUMS in OOP – isometric view - FWRB

In order to understand the main differences between the THUMS in conventional driving posture and the one in the OOP configuration, a visual comparison is reported in Figures 6.4 – 6.11. In particular, the two models are represented and compared in the same simulation time

instants. The time step used to capture the simulation frames is equal to 15 ms. As it can be noticed in the Figure 6.4, the initial posture of the two FE occupant models is different (ref. §4.2).

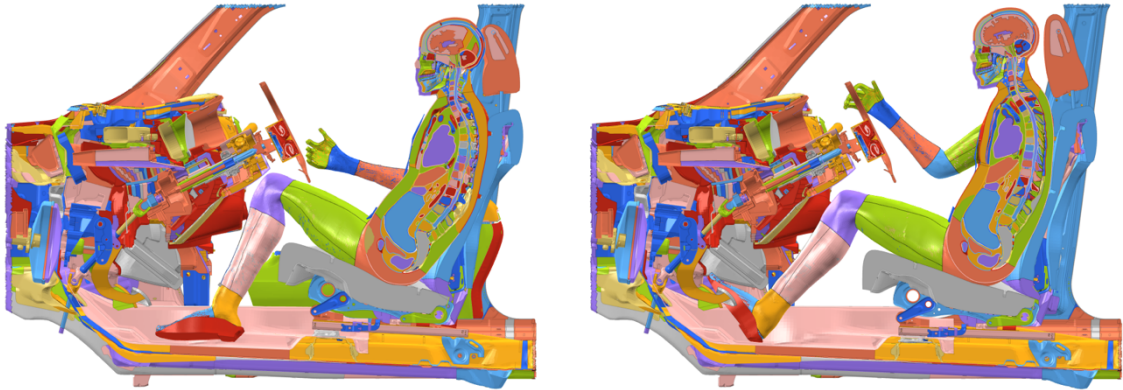


Figure 6.4. THUMS in OOP (left) vs THUMS in driving posture (right) - side xz section view – FWRB – 0 ms

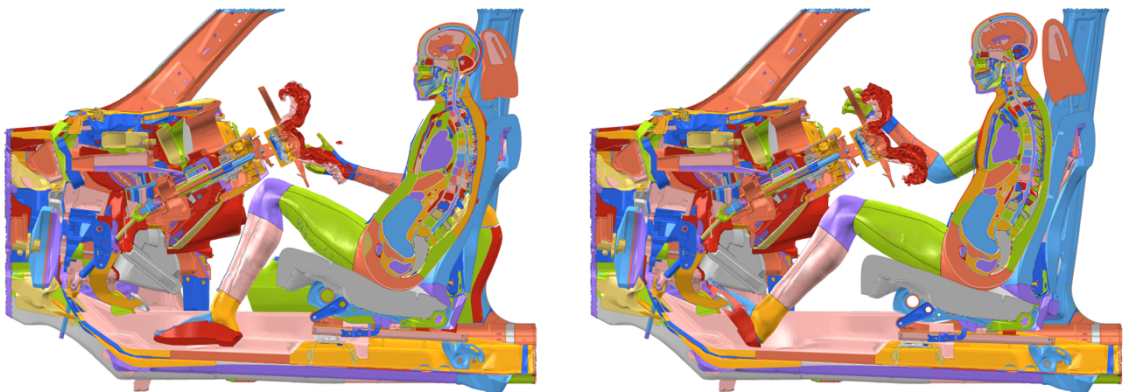


Figure 6.5. THUMS in OOP (left) vs THUMS in driving posture (right) - side xz section view – FWRB – 15 ms

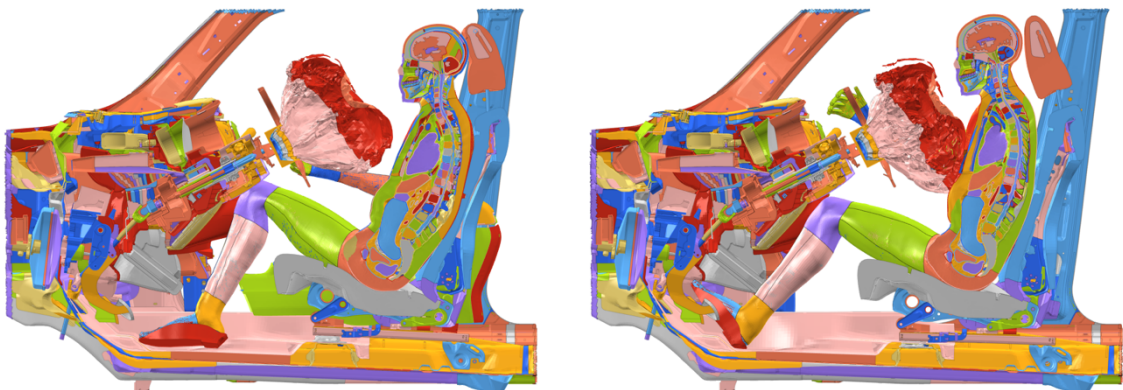


Figure 6.6. THUMS in OOP (left) vs THUMS in driving posture (right) - side xz section view – FWRB – 30 ms



Figure 6.7. THUMS in OOP (left) vs THUMS in driving posture (right) - side xz section view FWRB – 45 ms

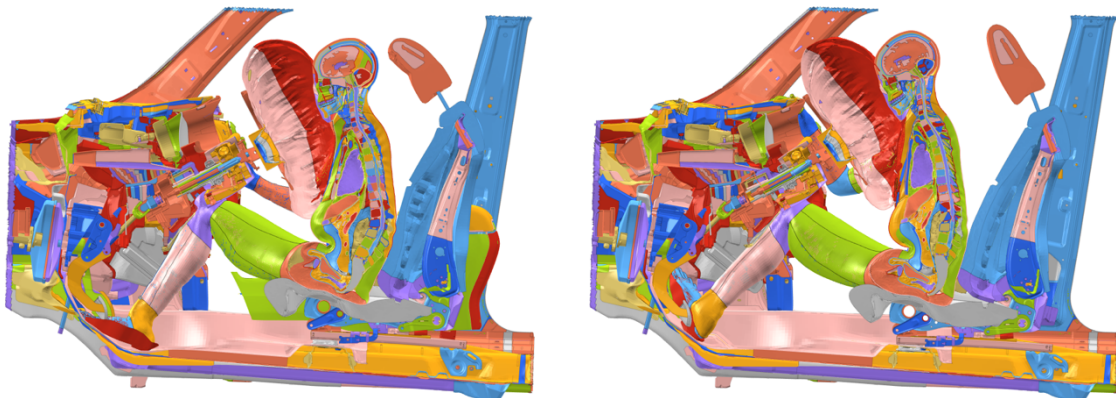


Figure 6.8. THUMS in OOP (left) vs THUMS in driving posture (right) - side xz section view – FWRB – 60 ms



Figure 6.9. THUMS in OOP (left) vs THUMS in driving posture (right) - side xz section view – FWRB – 75 ms



Figure 6.10. THUMS in OOP (left) vs THUMS in driving posture (right) - side xz section view – FWRB – 90 ms

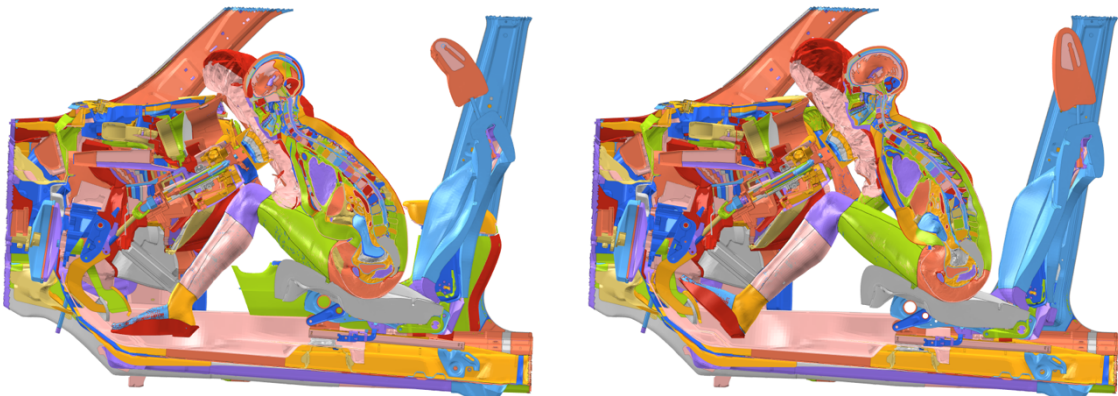


Figure 6.11 THUMS in OOP (left) vs THUMS in driving posture (right) - side xz section view – FWRB – 100 ms

The first difference in the behaviour of the two models can be already appreciated between 30 and 45 ms (Figures 6.6 and 6.7): the Driver Air Bag (DAB) gets in contact with the thorax (at 30 ms) and with the head (45 ms) of the THUMS positioned in the conventional driving posture when the HBM in OOP configuration is still far from it.

This is due to the different backbone inclination of the two models.

Moreover, the head of the THUMS model in the conventional driving posture does not remain straight when touching the DAB: by comparing the Figures 6.7 and 6.8, it is possible to notice that the head negatively rotates around its y axis. This rotational motion can be appreciated in the THUMS OOP simulation by looking, instead, to Figure 6.9, corresponding to 75 ms.

Additionally, a counter rotation of the head is experienced in the THUMS FE model in the usual driving posture configuration: between 90 ms and 100 ms, a positive rotation around its y axis can be noticed (Figures 6.9 – 6.11). The maximum distance between the chin and the upper part of the thorax is, in fact, obtained at the end of the simulation.

Further attention can be focused on the motion of the legs of the two models during the simulation. When the right knee of the THUMS driver hits the lower part of the vehicle dashboard, the leg tends to stretch and the foot slides towards the pedals, by increasing the knee angle. On the contrary, in the case of the THUMS in OOP configuration, the right knee angle tends at first to reduce and, then, increase during the impact. This is due to the initial position of the right foot.

THUMS Head signals

The obtained velocities and accelerations of the head of the OOP THUMS HBM during the crash simulation are here shown. In particular, the linear quantities are presented in Figures 6.12 – 6.19, whereas the rotational ones are included in Figures 6.20 – 6.27. The difference between the two models, shown in the output signal of the linear velocity along the y axis (Figure 6.13) is due to a different rotation of the two HBMs when getting in contact with the DAB.

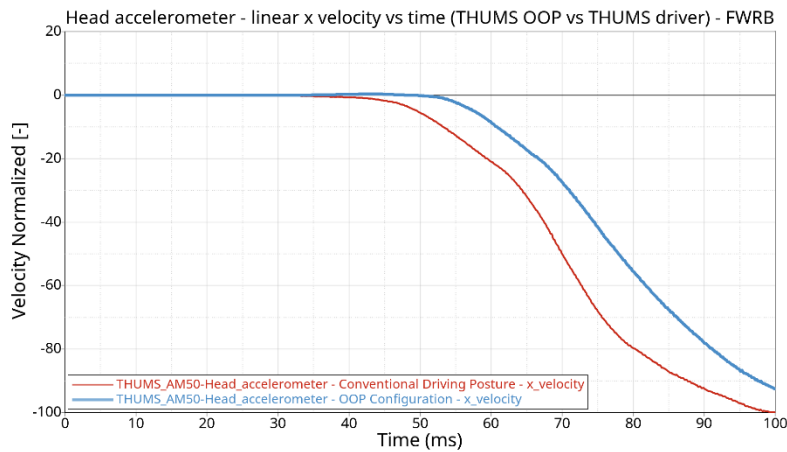


Figure 6.12. THUMS in OOP vs THUMS in driving posture - Head - x linear velocity - FWRB

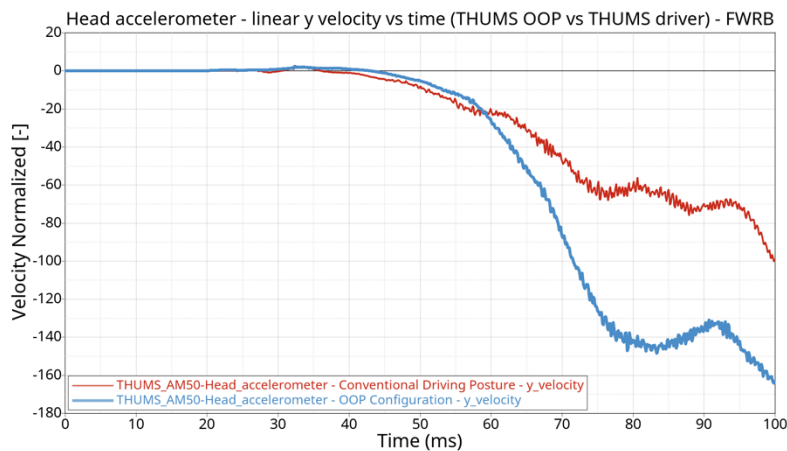


Figure 6.13. THUMS in OOP vs THUMS in driving posture - Head – y linear velocity - FWRB

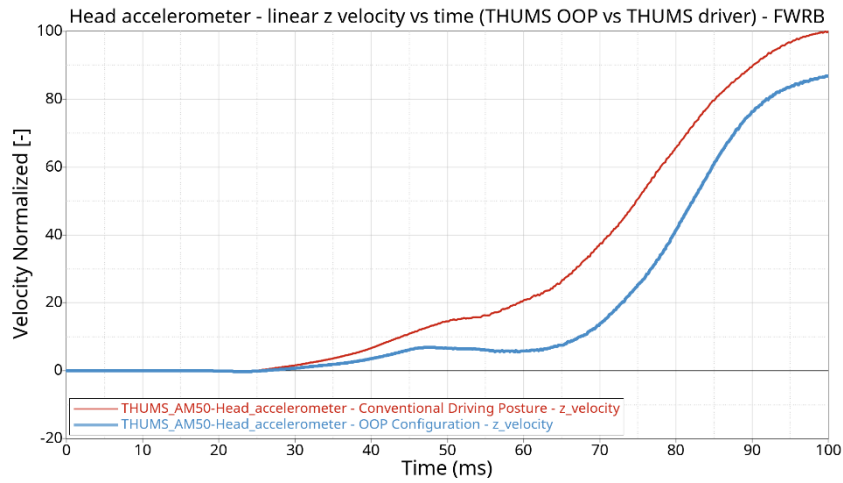


Figure 6.14. THUMS in OOP vs THUMS in driving posture - Head – z linear velocity - FWRB

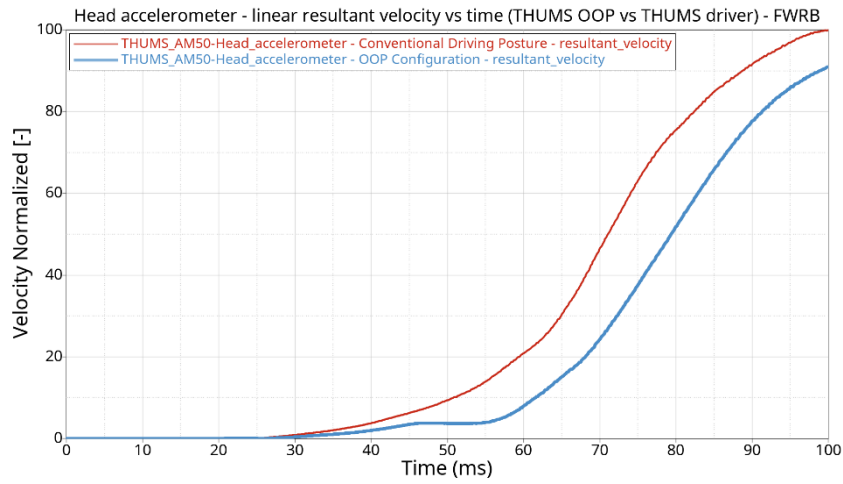


Figure 6.15. THUMS in OOP vs THUMS in driving posture - Head – resultant linear velocity - FWRB

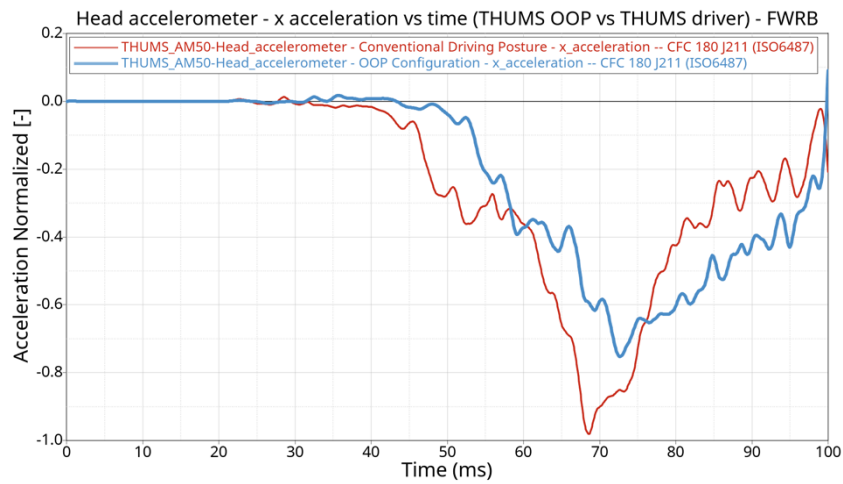


Figure 6.16. THUMS in OOP vs THUMS in driving posture - Head - x linear acceleration - FWRB

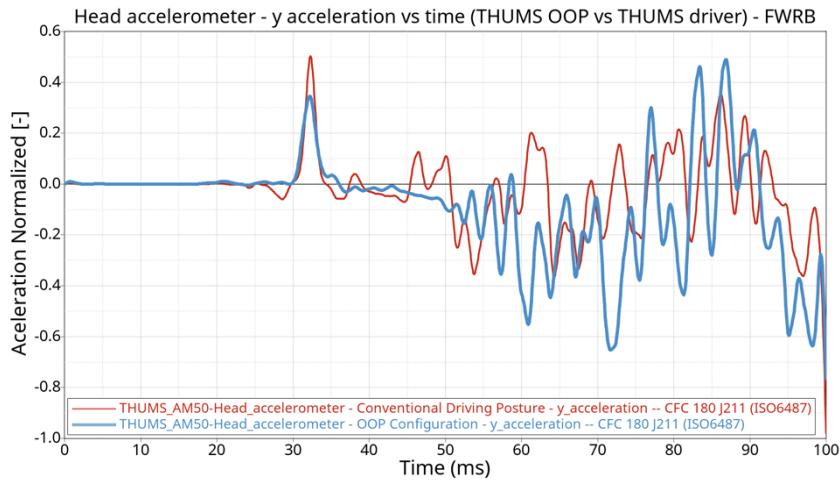


Figure 6.17. THUMS in OOP vs THUMS in driving posture - Head - y linear acceleration – FWRB

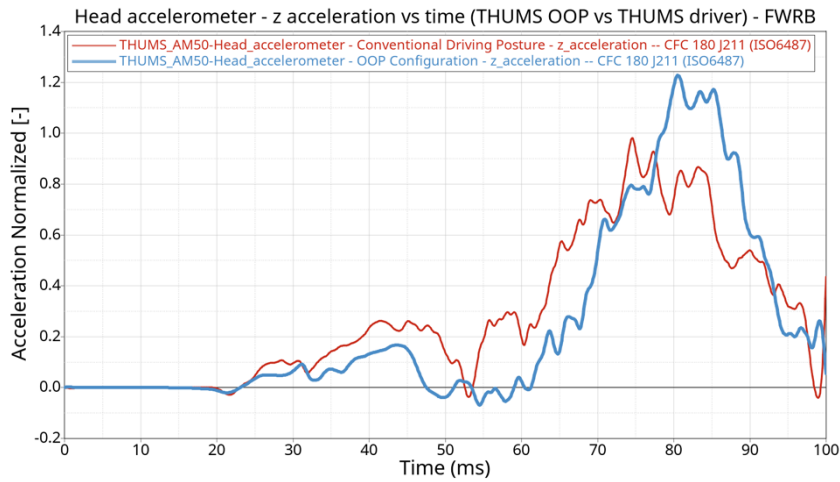


Figure 6.18. THUMS in OOP vs THUMS in driving posture - Head - z linear acceleration – FWRB

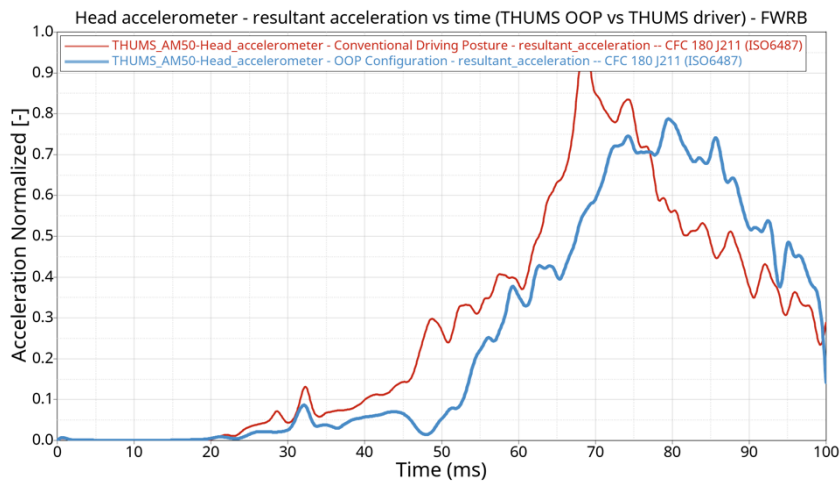


Figure 6.19. THUMS in OOP vs THUMS in driving posture - Head – result. linear acceleration - FWRB

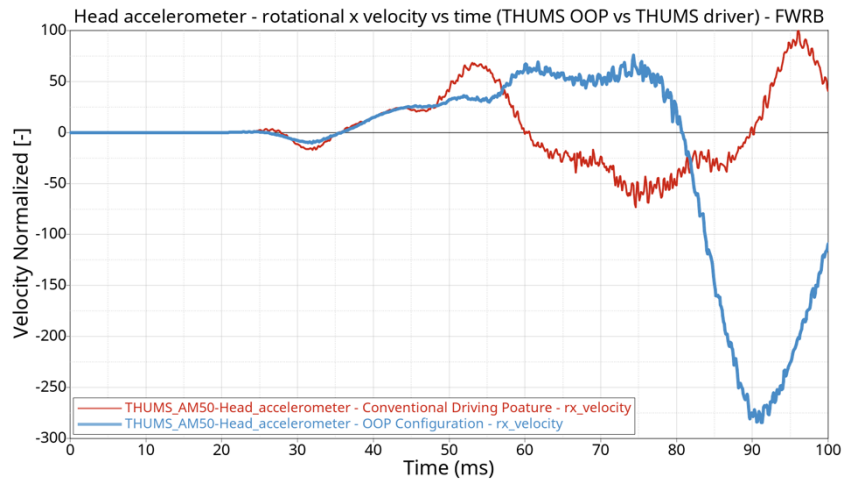


Figure 6.20. THUMS in OOP vs THUMS in driving posture – Head – rot. x velocity – FWRB

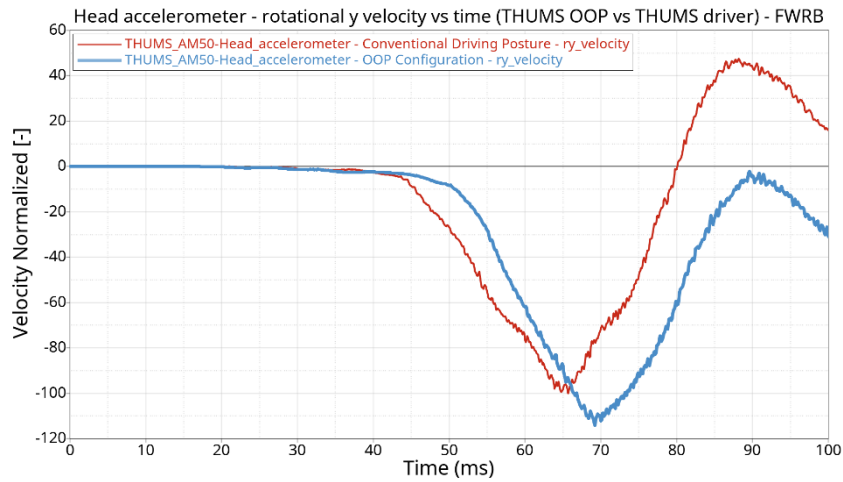


Figure 6.21. THUMS in OOP vs THUMS in driving posture – Head – rot. y velocity – FWRB

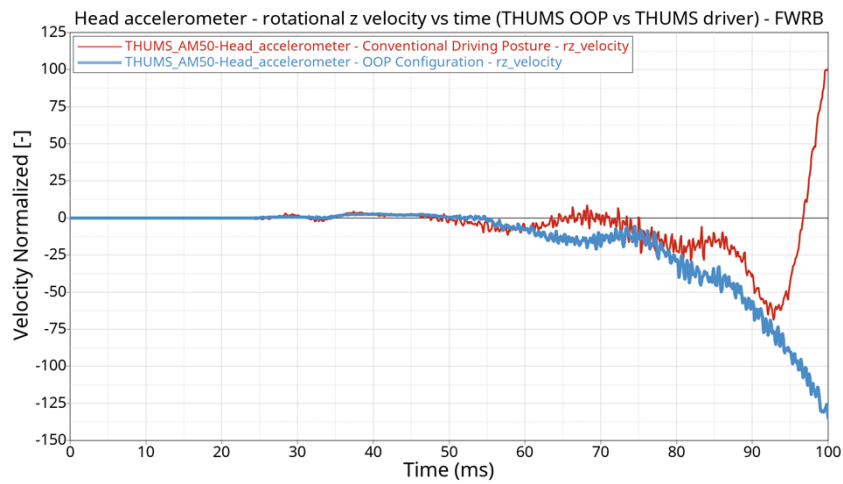


Figure 6.22. THUMS in OOP vs THUMS in driving posture – Head – rot. z velocity – FWRB

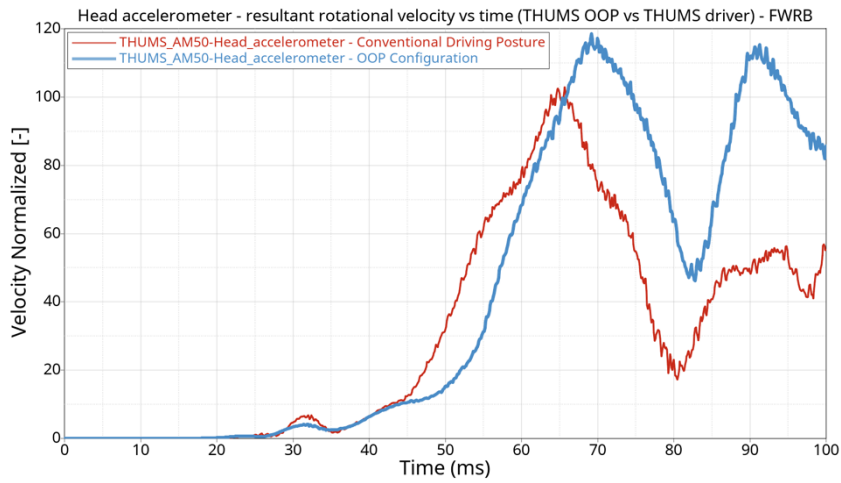


Figure 6.23. THUMS in OOP vs THUMS in driving posture – Head – resultant rot. z velocity – FWRB

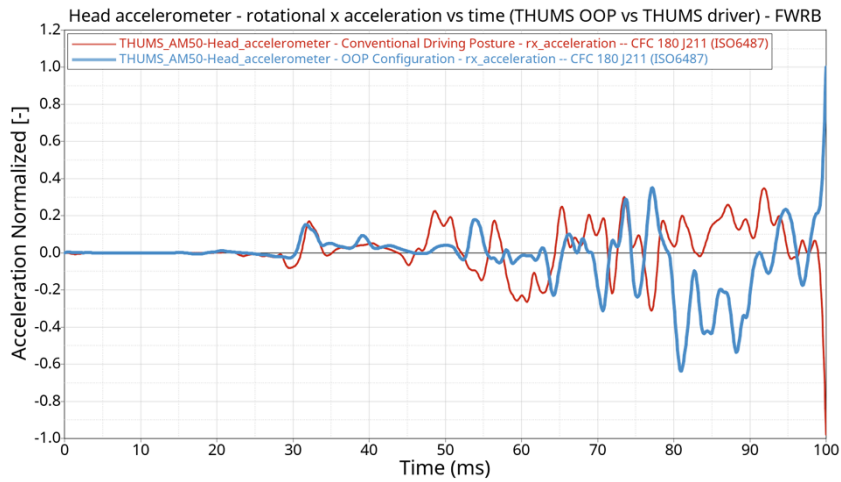


Figure 6.24. THUMS in OOP vs THUMS in driving posture – Head – rot. x acceleration – FWRB

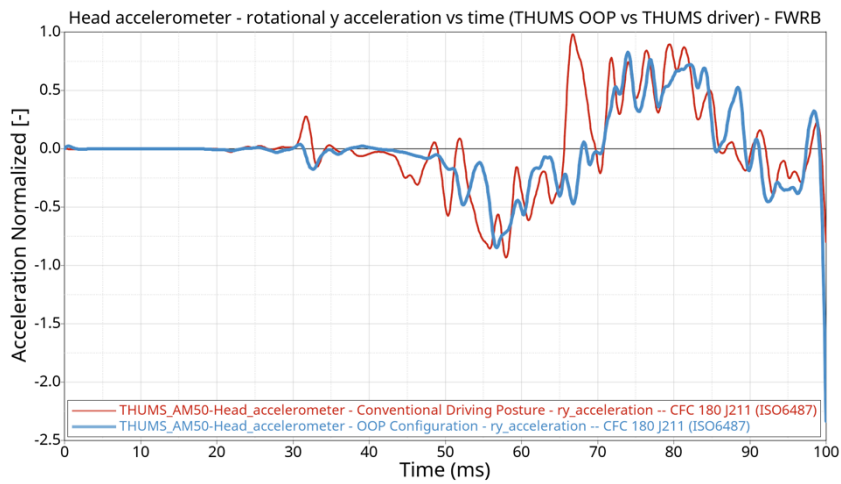


Figure 6.25. THUMS in OOP vs THUMS in driving posture – Head – rot. y acceleration – FWRB

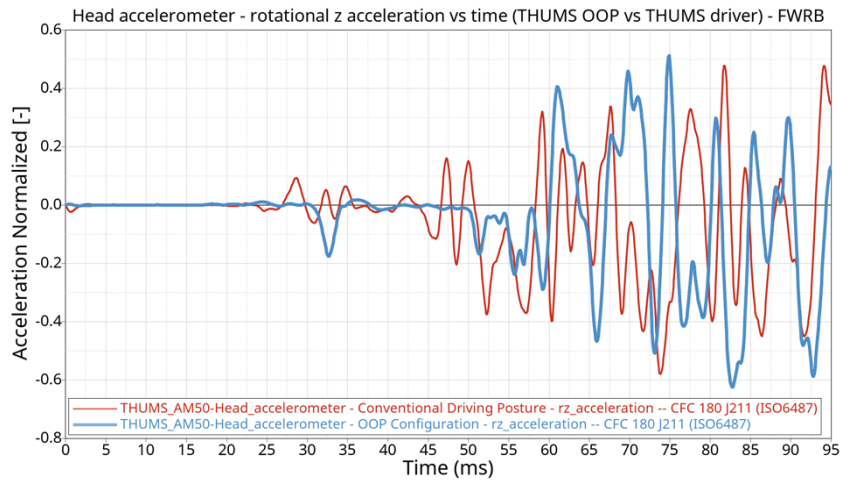


Figure 6.26. THUMS in OOP vs THUMS in driving posture – Head – rot. z acceleration – 95 ms – FWRB

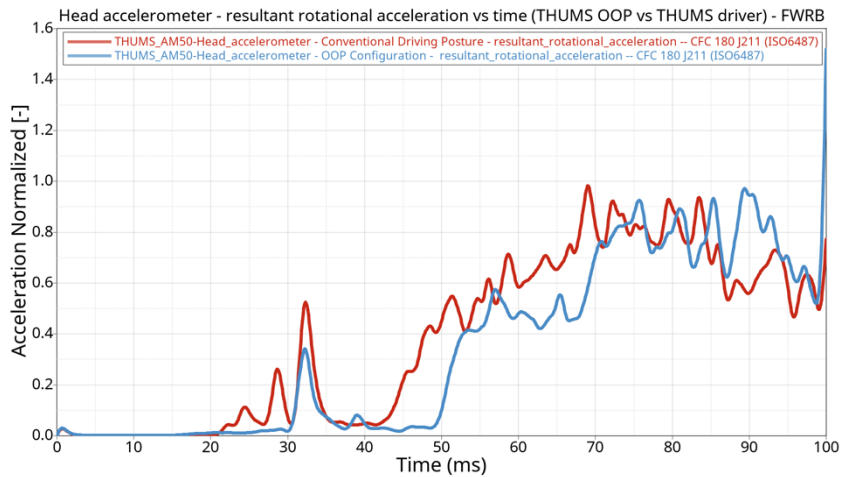


Figure 6.27. THUMS in OOP vs THUMS in driving posture – Head – result rot. acceleration – FWRB

By referring to the curves of Figure 6.16, the THUMS FE model in the conventional driving posture reaches the negative peak before the THUMS in OOP; as also anticipated in the previous pages with reference to the Figures 6.6 – 6.8, the head of HBM driver is the first to get in contact with the DAB and it is, as a consequence, the first to stop and invert its motion.

Since, especially in the rotational accelerations, the filtering action can cause numerical oscillations at the end of the curves (e.g. in Figure 6.25), in the Figure 6.26 the abscissa axis, representing the time (ms), is cut at 95 ms, as done in §5.2.2 and §5.2.3 to better appreciate the ordinate values of the curves.

Head Injury Criteria (HIC)

Also for the THUMS in OOP configuration, the HIC can be calculated, as described in §4.5.1.

Therefore, if the THUMS in-position HIC is assumed to be equal to 100, the computed THUMS HIC value in OOP posture is 89.9.

Brain Injury Criteria (BrIC)

If the THUMS in-position BrIC is assumed to be equal to 100, the computed OOP THUMS BrIC value in the FWRB case is equal to 137.89.

Neck Forces

The comparison between the THUMS and THOR neck forces is reported in Figure 6.28.

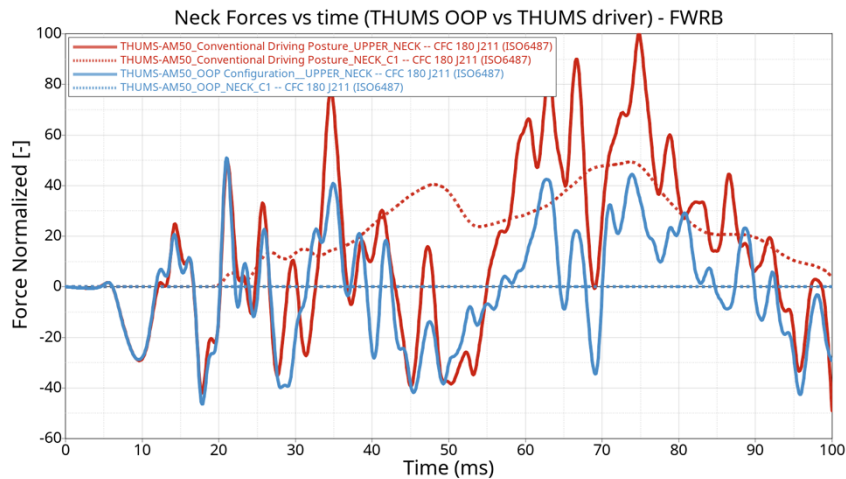


Figure 6.28. THUMS in OOP vs THUMS in driving posture – Upper and Lower (C1) Neck Forces – FWRB

As it is possible to notice, the trends of the upper neck curves are comparable. However, the upper neck force obtained from the OOP THUMS model simulation is lower than the THUMS in driving posture one. The C1 neck forces of the conventional driving posture simulation, moreover, result to be much higher than the ones coming from the THUMS in conventional driving posture.

THUMS Thorax signals

The thorax accelerations, obtained by means of the accelerometers positioned in correspondence of the vertebrae T1, T4 and T12 are shown in Figures 6.29 – 6.31.

As for the head signals, the red thinner lines show the outputs obtained and presented in §5.2.2 and §5.2.3, whereas the blue lines refer to the OOP THUMS.

The similarity between the curves of Figures 6.29 and 6.31 find confirmation by looking at Figures 6.4 – 6.11: even if the initial configuration and inclination of the backbones of the two models is quite different, the motion during the impact is similar, especially for what the T1 and T4 vertebrae are concerned.

The difference between the two curves of Figure 6.31, in the range 60 – 75 ms, is instead due to the different right leg position.

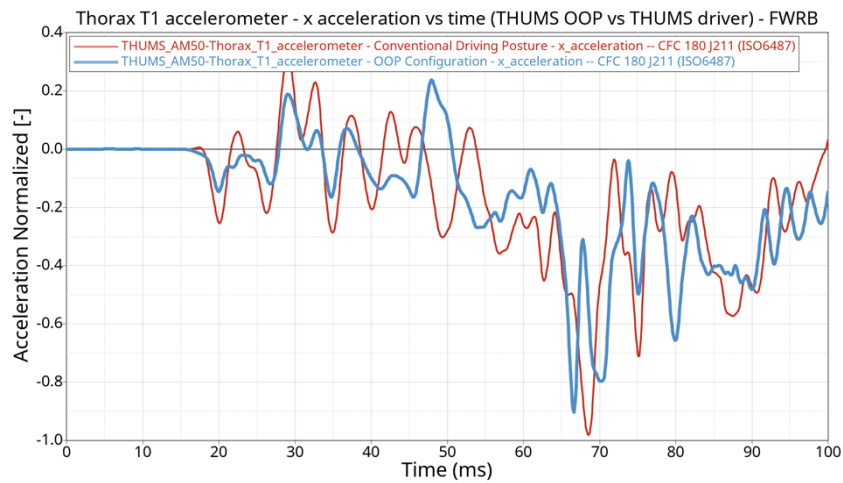


Figure 6.29. THUMS in OOP vs THUMS in driving posture – Thorax T1 – linear x acceleration –FWRB

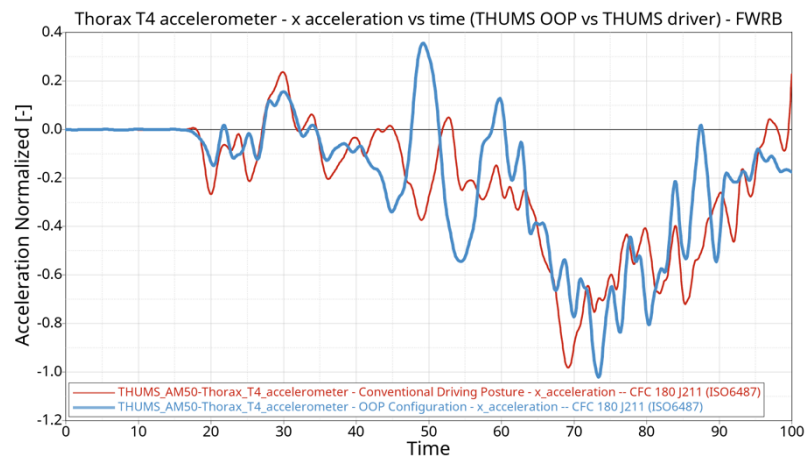


Figure 6.30. THUMS in OOP vs THUMS in driving posture – Thorax T4 – linear x acceleration –FWRB

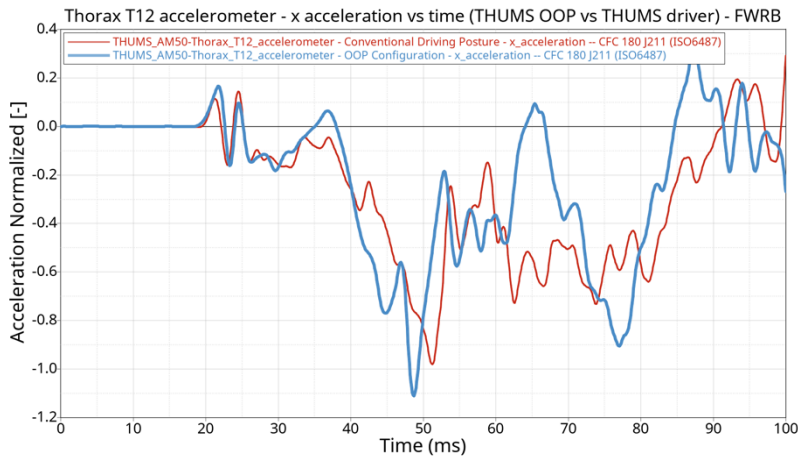


Figure 6.31. THUMS in OOP vs THUMS in driving posture – Thorax T12 – linear x acceleration –FWRB

THUMS Pelvis signal

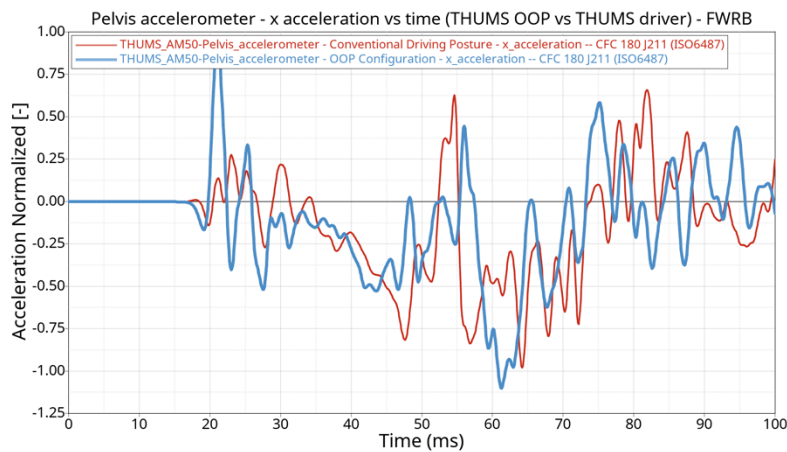


Figure 6.32. THUMS in OOP vs THUMS in driving posture – Pelvis – linear x acceleration –FWRB

In Figure 6.32, it is possible to notice that the x acceleration obtained by means of the pelvis accelerometer is quite similar between the two differently positioned THUMS models, even if numerical oscillations are, also in this case, present.

THUMS Legs – Tibia forces

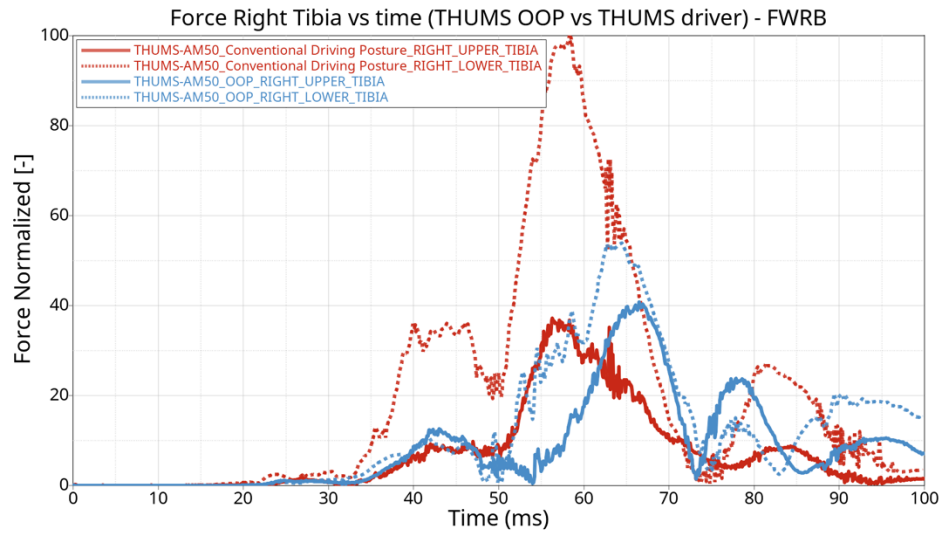


Figure 6.33. THUMS in OOP vs THUMS in driving posture – Right Tibia – Force – ODB

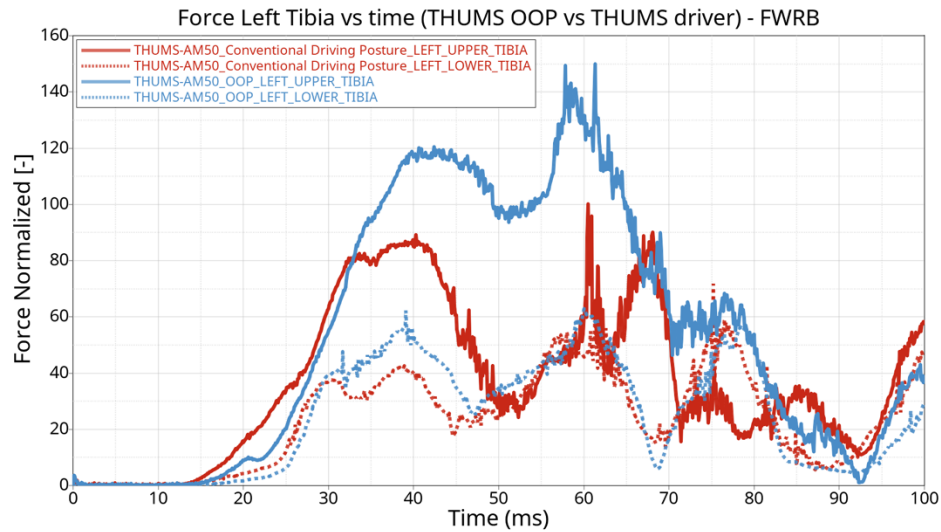


Figure 6.34. THUMS in OOP vs THUMS in driving posture – Left Tibia – Force – ODB

In Figures 6.33 and 6.34, the comparison of the behavior of the THUMS in OOP configuration and the THUMS in conventional standard driving posture models in terms of Upper and Lower Tibia forces is reported.

If the right tibia force is considered, the THUMS in the conventional driving posture undergoes an higher force, especially in the time interval 50 – 70 ms. This finds the confirmation by looking at the figures 6.7 – 6.9: the tibia of the THUMS driver is, in this time interval, compressed between the lower part of the vehicle dashboard and the pedals.

6.3 Results of the THUMS OOP and comparison with the HBM in conventional driving posture – Offset Deformable Barrier (ODB) Impact case

Global Energies

As for the FWRB case (§6.2), the comparison between the simulation performed in the first part of this Thesis job (ref. *Figure 5.0*) and the one with the THUMS in the OOP configuration (ref *Figure 6.0*) for the ODB impact case is shown in Figure 6.35.

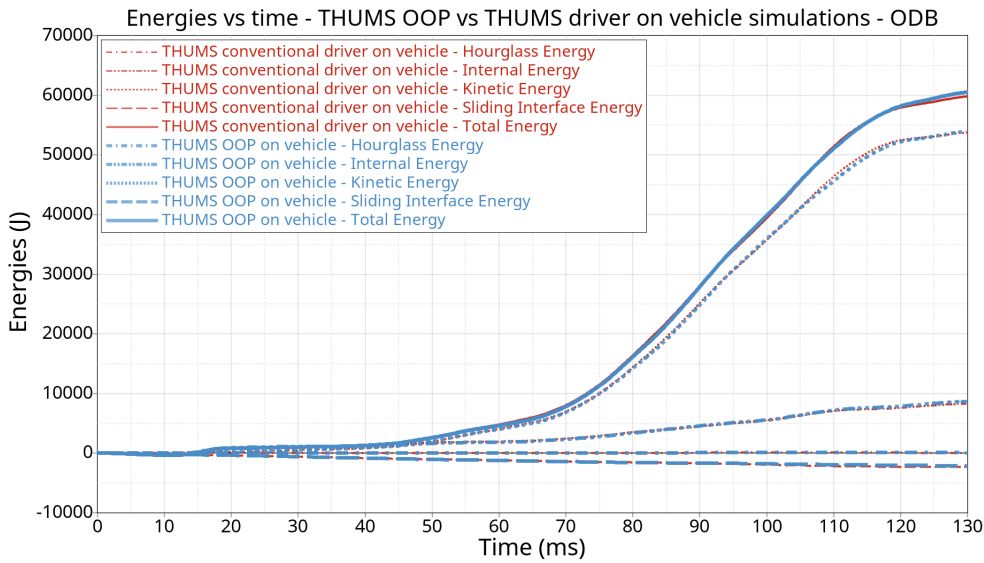


Figure 6.35. THUMS in OOP vs THUMS in driving posture on vehicle – Global Energies – ODB

THUMS Simulation Frames

Here in the following, the time frames of the simulation of the THUMS in the OOP during the ODB impact simulation are reported.

In Figures 6.36 and 6.37, the lateral *xz* (left plane) and the isometric views are, respectively, shown.

In order to understand the main differences in the behaviour of the THUMS in conventional driving posture and of the one in the OOP configuration, a visual comparison is reported in Figures 6.38 – 6.47. The two models are represented and compared in the same simulation time instants. The time step used to capture the simulation frames is equal to 15 ms.

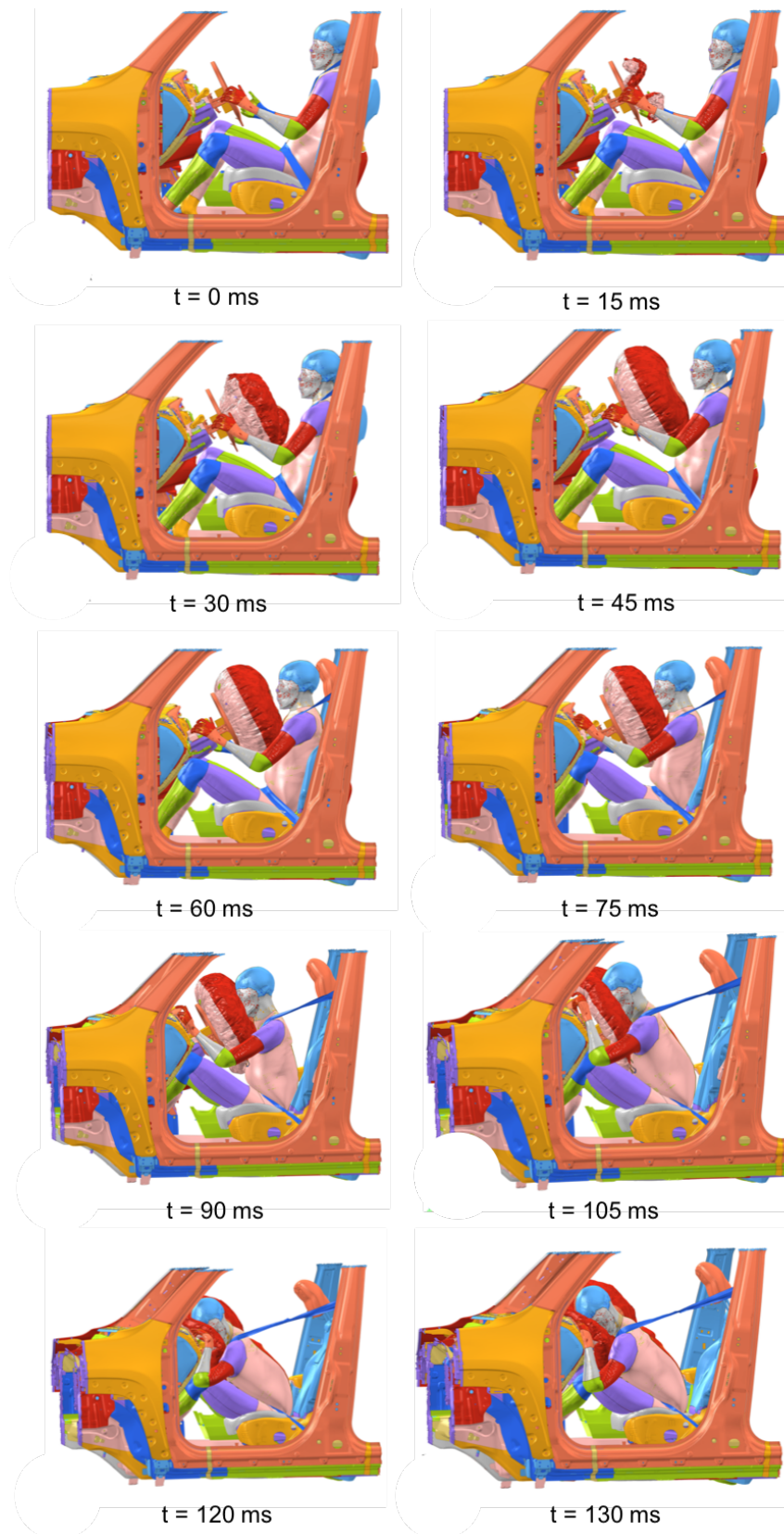


Figure 6.36. THUMS in OOP on vehicle – side *xz* view - ODB

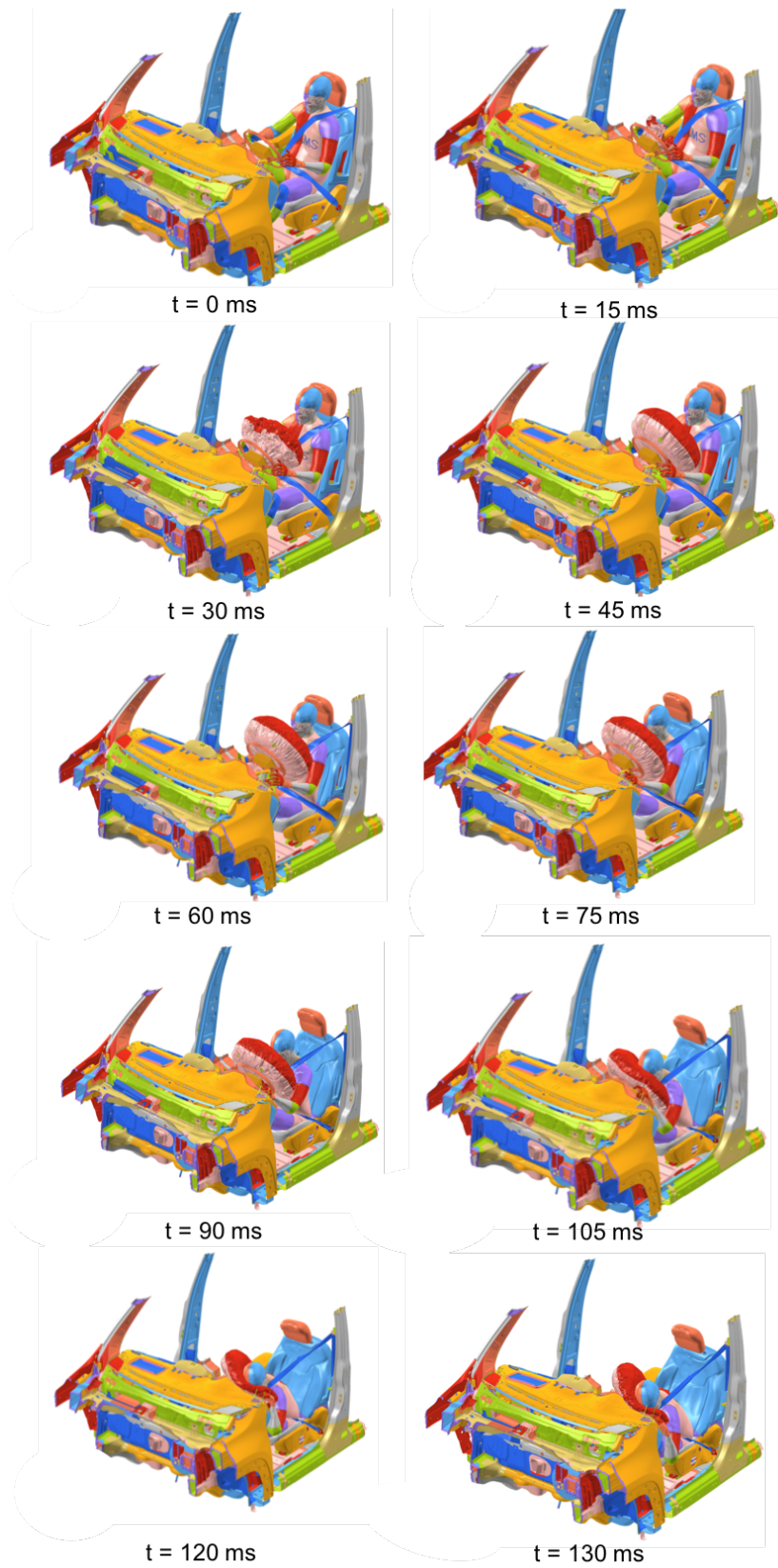


Figure 6.37. THUMS in OOP – isometric view - ODB

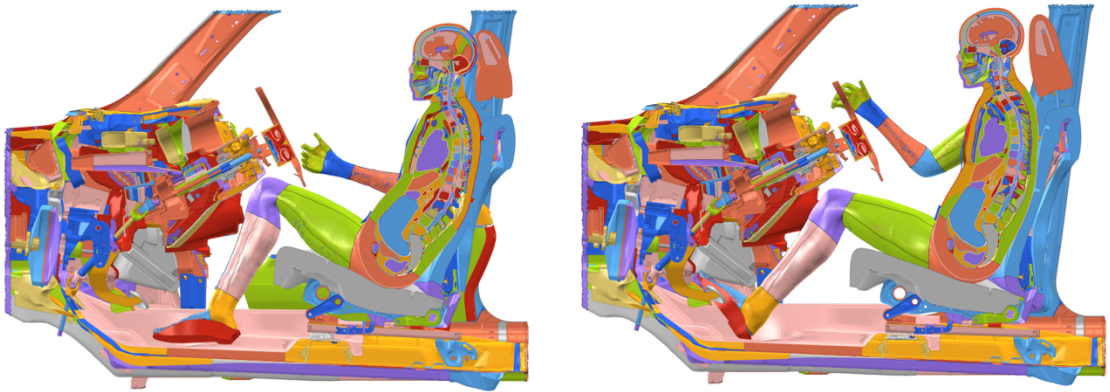


Figure 6.38. THUMS in OOP (left) vs THUMS in driving posture (right) - side xz section view – ODB – 0 ms

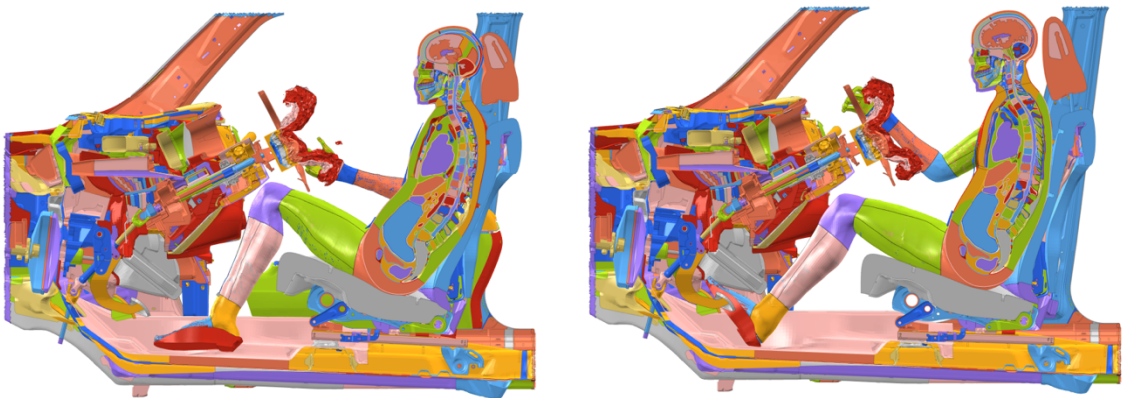


Figure 6.39. THUMS in OOP (left) vs THUMS in driving posture (right) - side xz section view – ODB – 15 ms



Figure 6.40. THUMS in OOP (left) vs THUMS in driving posture (right) - side xz section view – ODB – 30 ms



Figure 6.41. THUMS in OOP (left) vs THUMS in driving posture (right) - side xz section view ODB – 45 ms

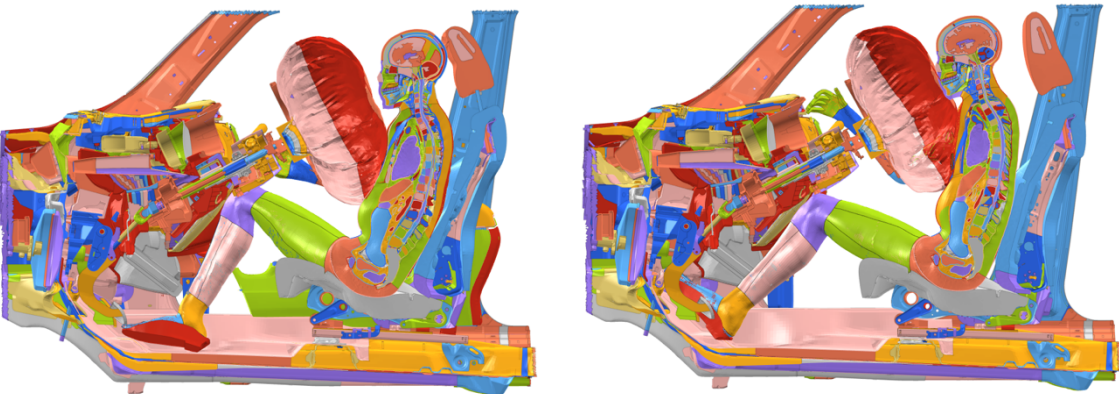


Figure 6.42. THUMS in OOP (left) vs THUMS in driving posture (right) - side xz section view – ODB – 60 ms

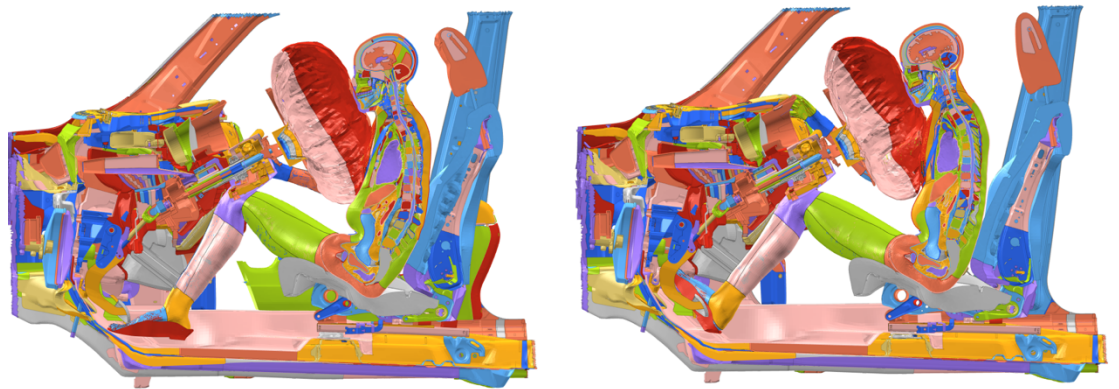


Figure 6.43. THUMS in OOP (left) vs THUMS in driving posture (right) - side xz section view – ODB – 75 ms

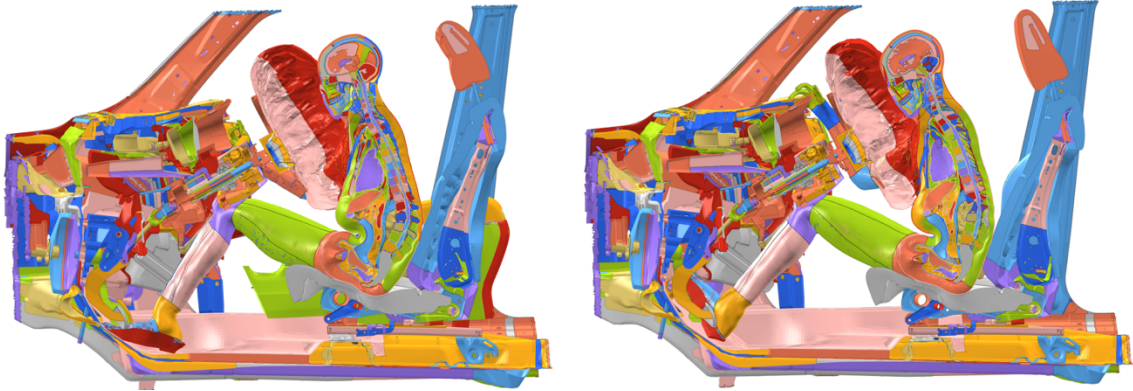


Figure 6.44. THUMS in OOP (left) vs THUMS in driving posture (right) - side xz section view – ODB – 90 ms

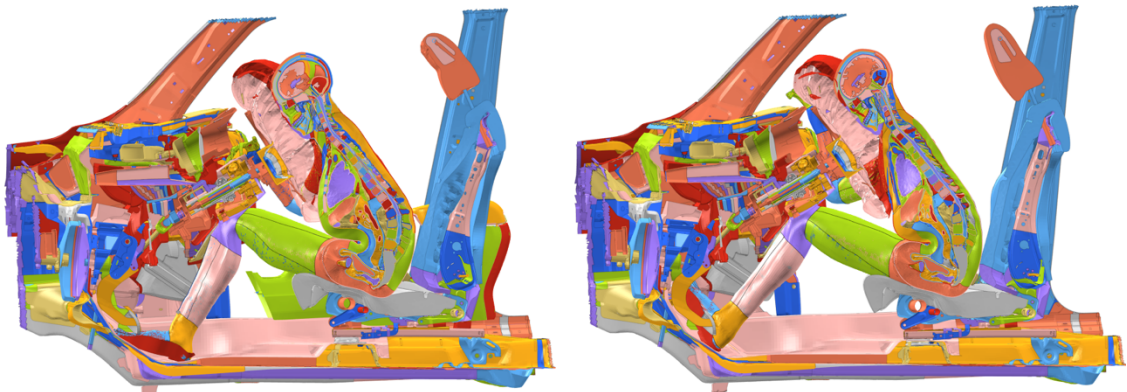


Figure 6.45. THUMS in OOP (left) vs THUMS in driving posture (right) - side xz section view – ODB – 105 ms

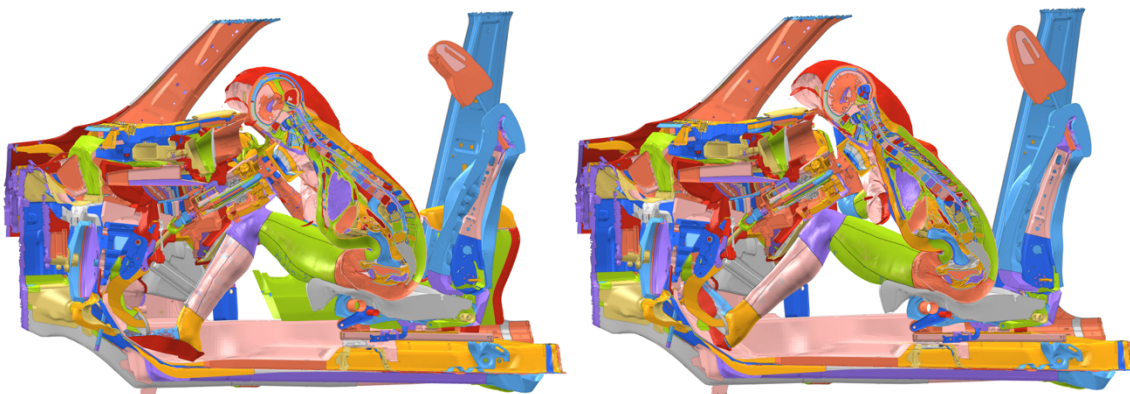


Figure 6.46. THUMS in OOP (left) vs THUMS in driving posture (right) - side xz section view – ODB – 120 ms

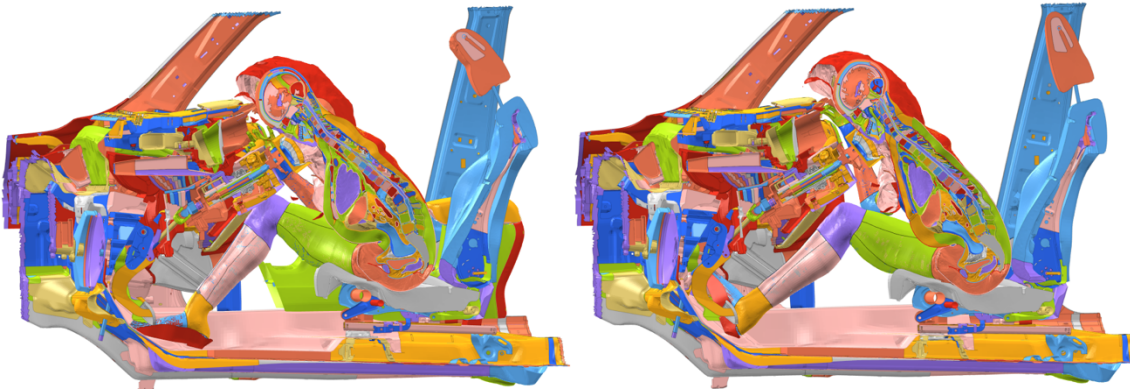


Figure 6.47. THUMS in OOP (left) vs THUMS in driving posture (right) - side *xz* section view – ODB – 130 ms

The first difference in the behaviour of the two models can be already appreciated between 30 and 60 ms (Figures 6.40 - 6.42): due to the different backbone inclination of the two models, the Driver Air Bag (DAB) gets in contact with the thorax and the head of the THUMS positioned in the conventional driving posture when the HBM in OOP configuration is still far from it.

By looking at the Figures 6.45 – 6.47, it is possible to notice that the head of both the models negatively rotates around its *y* axis. Additionally, on the opposite of what is happening in the FWRB impact case, no counter rotation of the head is experienced in the two models.

As in the FWRB simulation, instead, the right knee angle of the THUMS model in OOP configuration tends to reduce and then to increase again during the impact, while the one of the HBM in conventional driving posture simply tends to increase.

THUMS Head signals

The obtained velocities and accelerations of the head of the OOP THUMS HBM during the ODB crash simulation are reported in this section.

The linear quantities are shown in Figures 6.48 – 6.55, whereas the rotational ones are included in Figures 6.56 – 6.63.

By referring to the curves of Figures 6.52 – 6.54, the THUMS FE model in the conventional driving posture and the THUMS in OOP reach the peaks in the same instants; however, the accelerations peaks of the OOP case are higher than the ones of the other simulation.

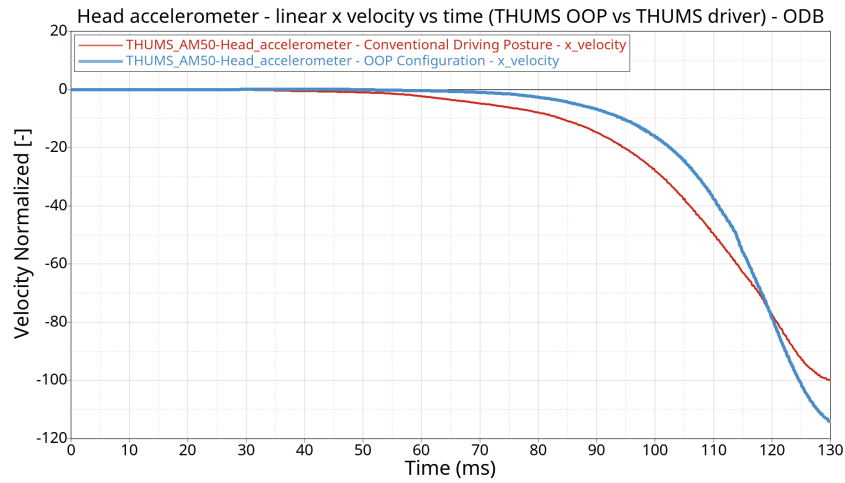


Figure 6.48. THUMS in OOP vs THUMS in driving posture - Head - x linear velocity - ODB

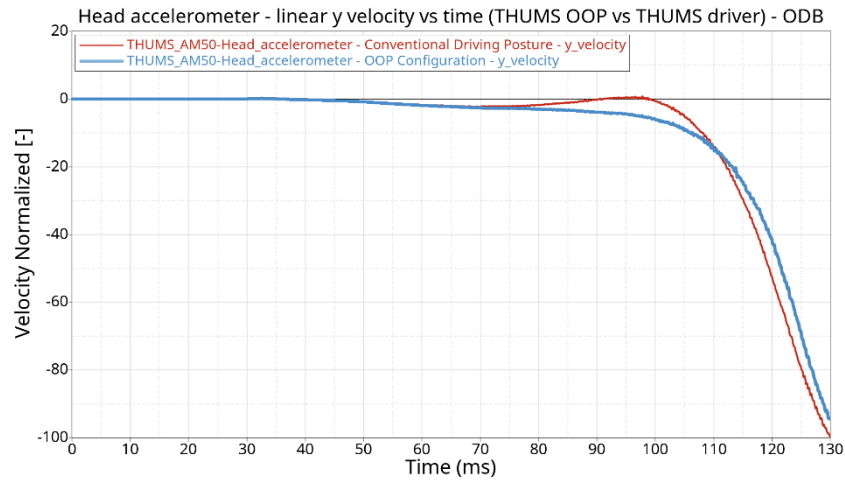


Figure 6.49. THUMS in OOP vs THUMS in driving posture - Head - y linear velocity - ODB

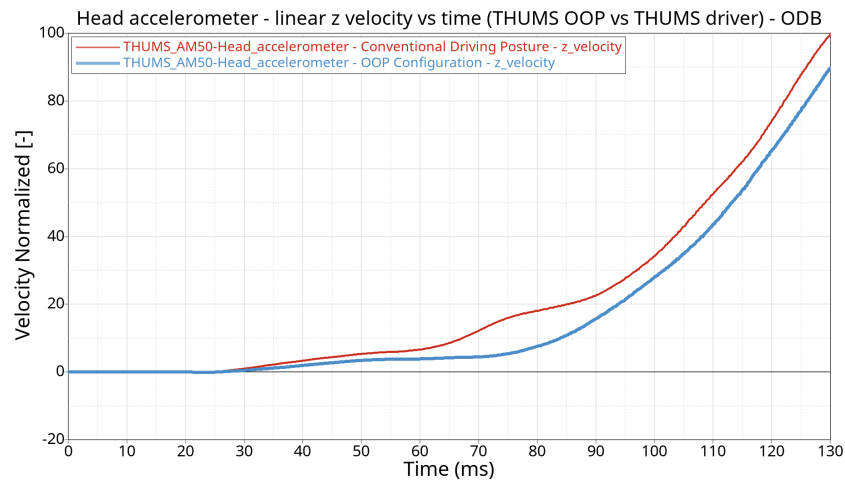


Figure 6.50. THUMS in OOP vs THUMS in driving posture - Head - z linear velocity - ODB

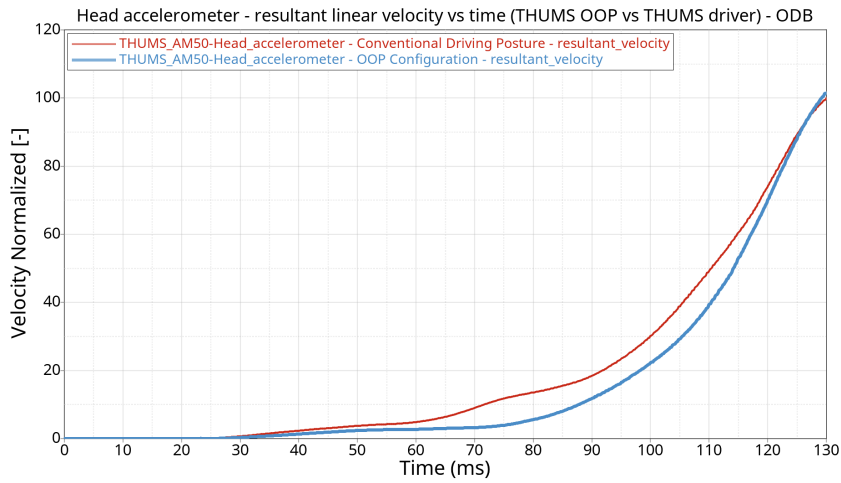


Figure 6.51. THUMS in OOP vs THUMS in driving posture - Head – resultant linear velocity - ODB

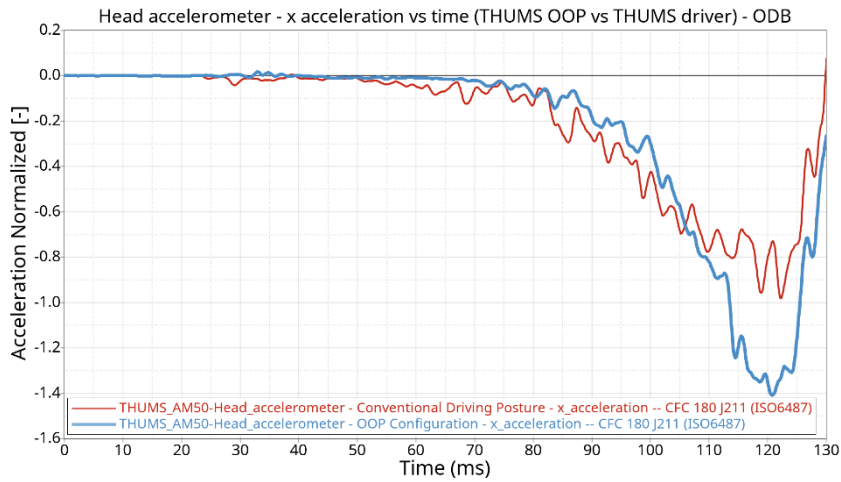


Figure 6.52. THUMS in OOP vs THUMS in driving posture - Head - x linear acceleration - ODB

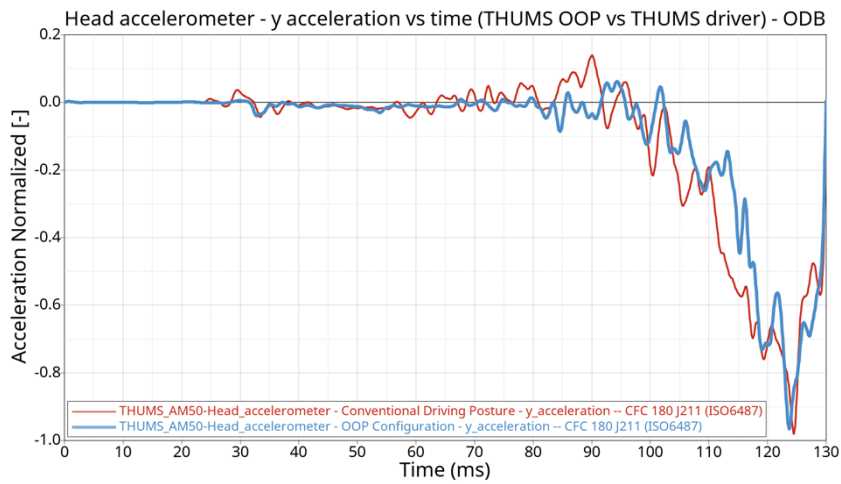


Figure 6.53. THUMS in OOP vs THUMS in driving posture - Head - y linear acceleration – ODB

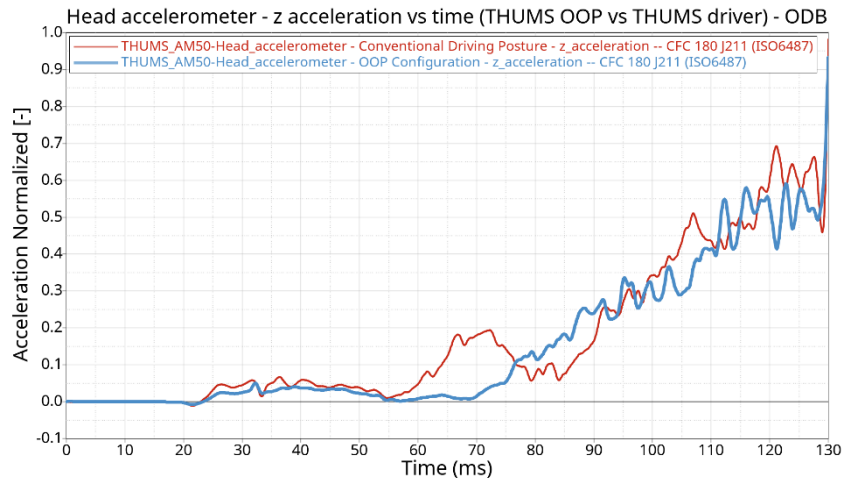


Figure 6.54. THUMS in OOP vs THUMS in driving posture - Head - z linear acceleration – ODB

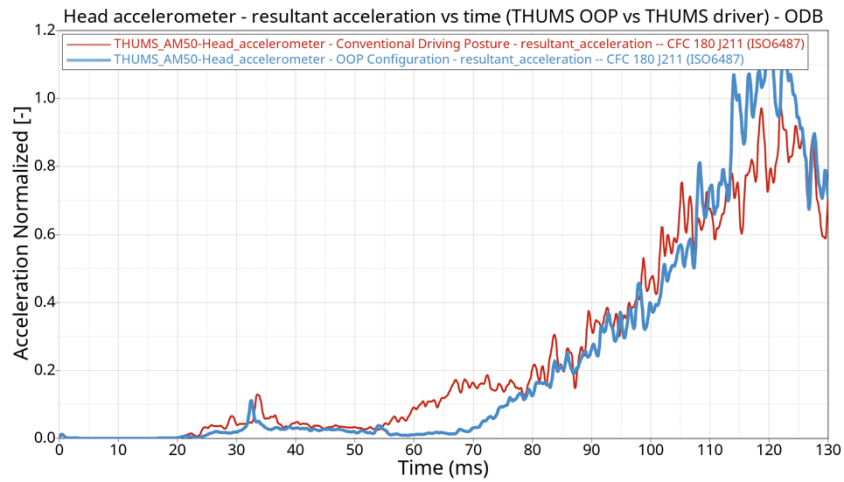


Figure 6.55. THUMS in OOP vs THUMS in driving posture - Head – result. linear acceleration - ODB

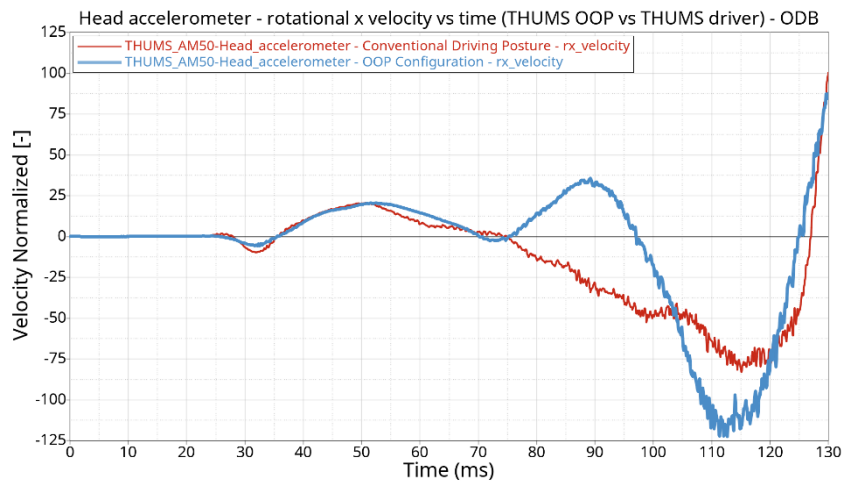


Figure 6.56. THUMS in OOP vs THUMS in driving posture – Head – rot. x velocity – ODB

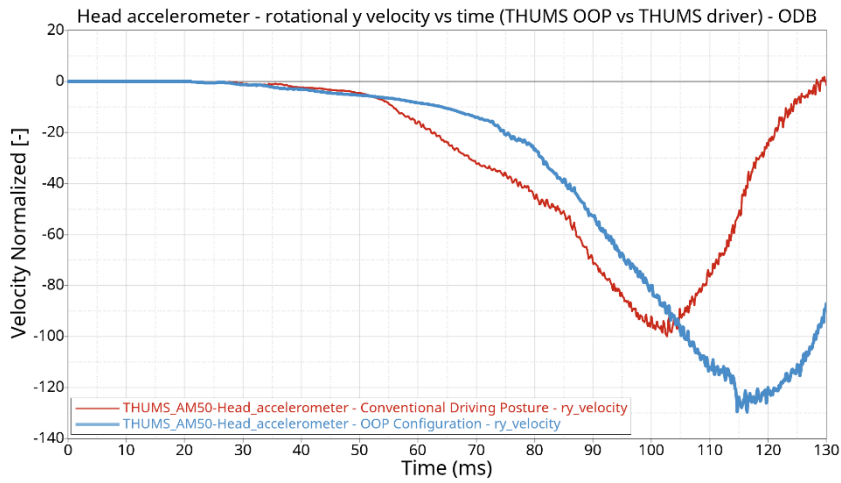


Figure 6.57. THUMS in OOP vs THUMS in driving posture – Head – rot. y velocity – ODB

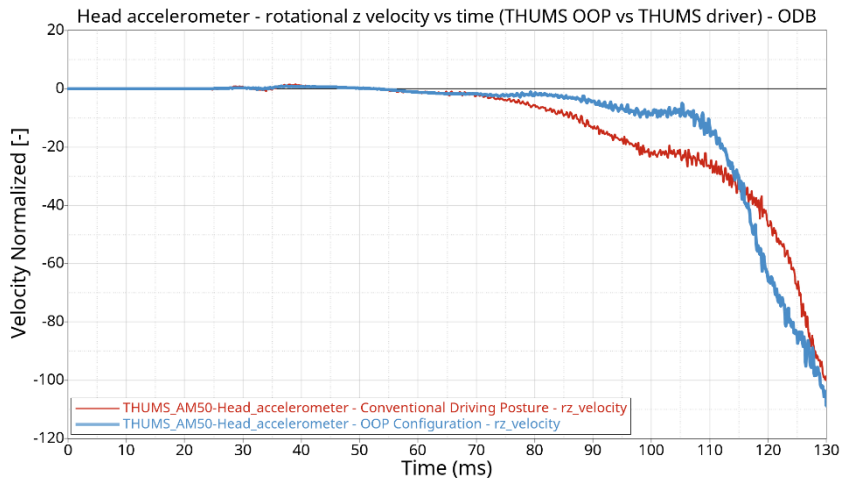


Figure 6.58. THUMS in OOP vs THUMS in driving posture – Head – rot. z velocity – ODB

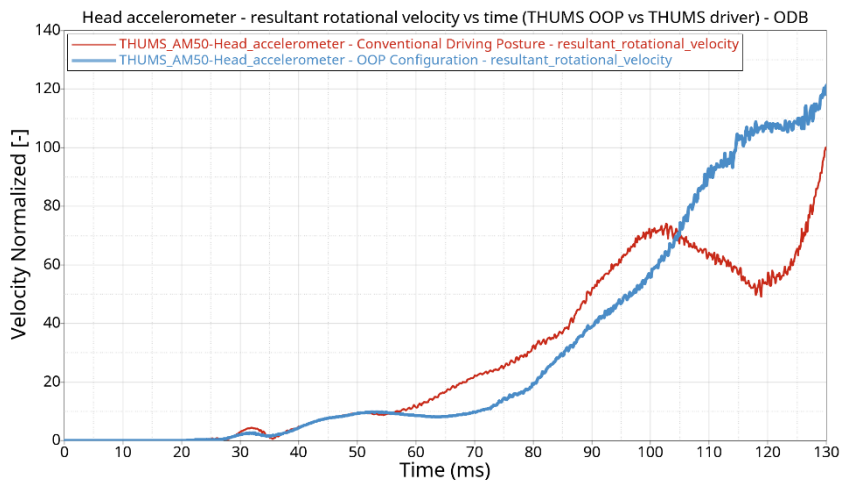


Figure 6.59. THUMS in OOP vs THUMS in driving posture – Head – resultant rotational velocity – ODB

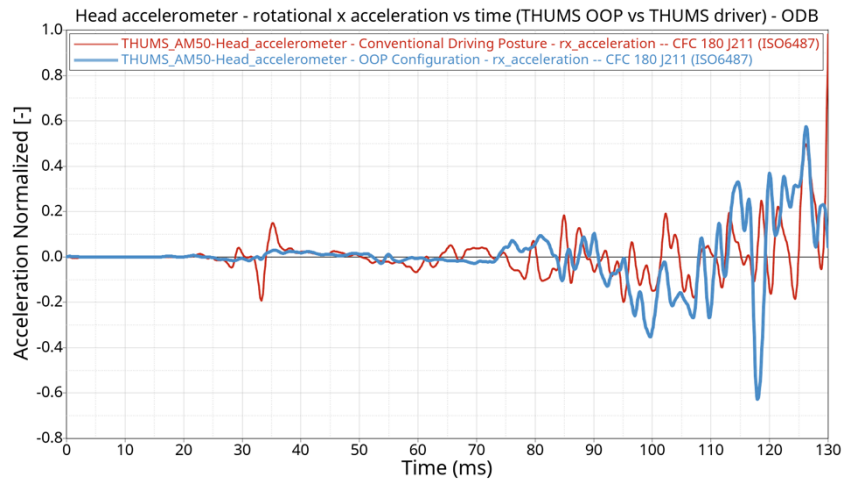


Figure 6.60. THUMS in OOP vs THUMS in driving posture – Head – rot. x acceleration – ODB

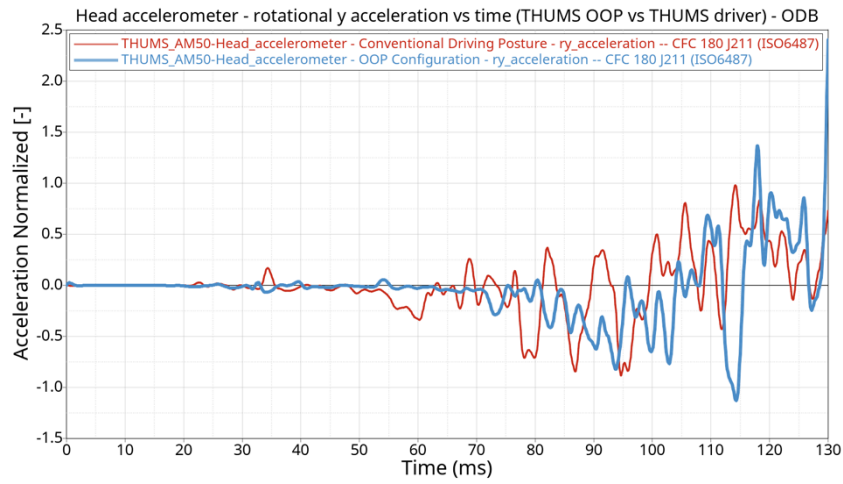


Figure 6.61. THUMS in OOP vs THUMS in driving posture – Head – rot. y acceleration – ODB

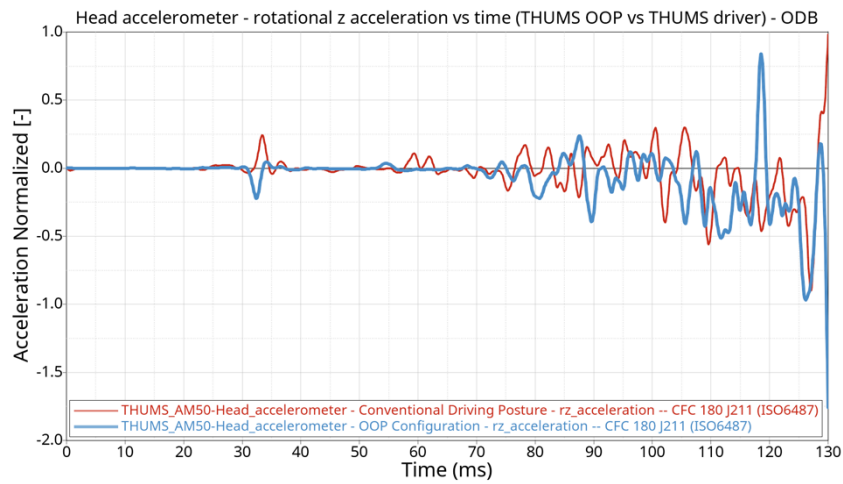


Figure 6.62. THUMS in OOP vs THUMS in driving posture – Head – rot. z acceleration – 95 ms – ODB

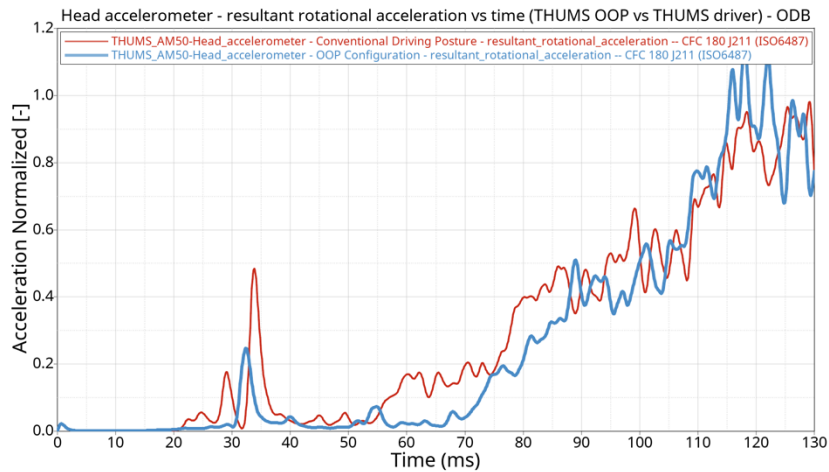


Figure 6.63. THUMS in OOP vs THUMS in driving posture – Head – result rot. x acceleration – ODB

Head Injury Criteria (HIC)

In the ODB impact case, if the THUMS in-position HIC is assumed to be equal to 100, the computed THUMS HIC value in OOP posture is 159.96.

Brain Injury Criteria (BrIC)

The THUMS OOP BrIC is computed as introduced in §4.5.2. As in the FWRB case, by assuming that the BrIC value of the THUMS in standard driving configuration is equal to 100, the THUMS OOP BrIC is 114,25.

Neck Forces

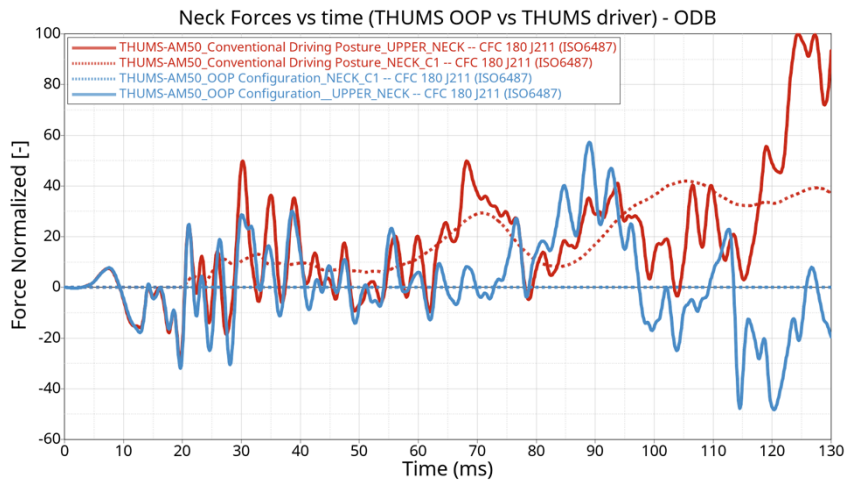


Figure 6.64. Positioned THUMS vs traditional dummy – Upper and Lower (C1) Neck Forces – ODB

The comparison between the THUMS and THOR neck forces is reported in Figure 6.64.

As it is possible to notice, the trends of the two curves are comparable. However, as in the FWRB case, the upper neck force obtained from the THUMS driver model simulation is higher than the OOP one.

THUMS Thorax signals

The accelerations of the vertebrae T1, T4 and T12, obtained by means of the implemented thoracic sensors, are shown in Figures 6.65 – 6.67. The red thinner lines show the outputs obtained and presented in §5.2.2 and §5.2.3, whereas the blue lines refer to the OOP THUMS.

The highest numerical oscillations are observed in Figure 6.65 (T1 accelerometer), in correspondence of about 105 ms.

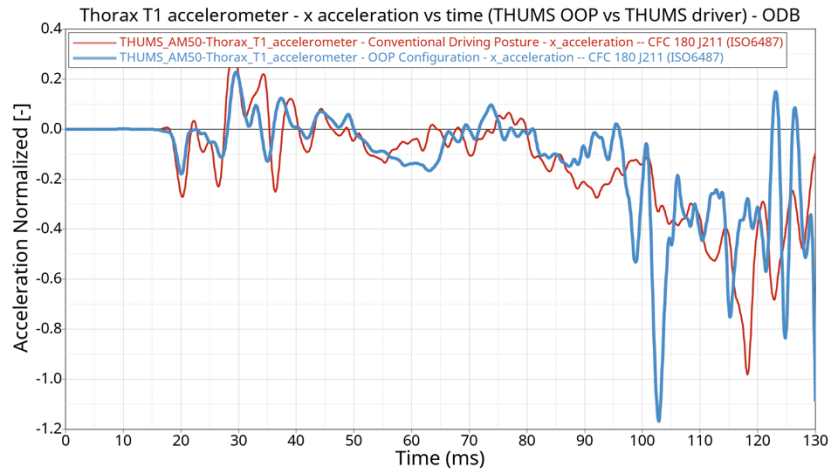


Figure 6.65. THUMS in OOP vs THUMS in driving posture – Thorax T1 – linear x acceleration – ODB

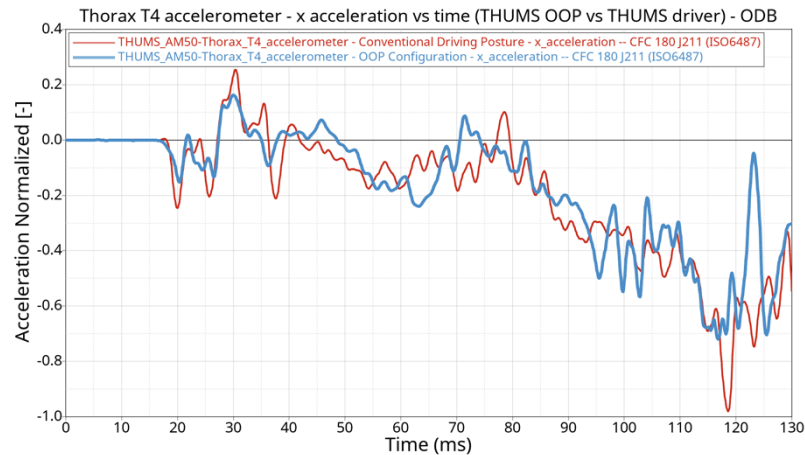


Figure 6.66. THUMS in OOP vs THUMS in driving posture – Thorax T4 – linear x acceleration – ODB

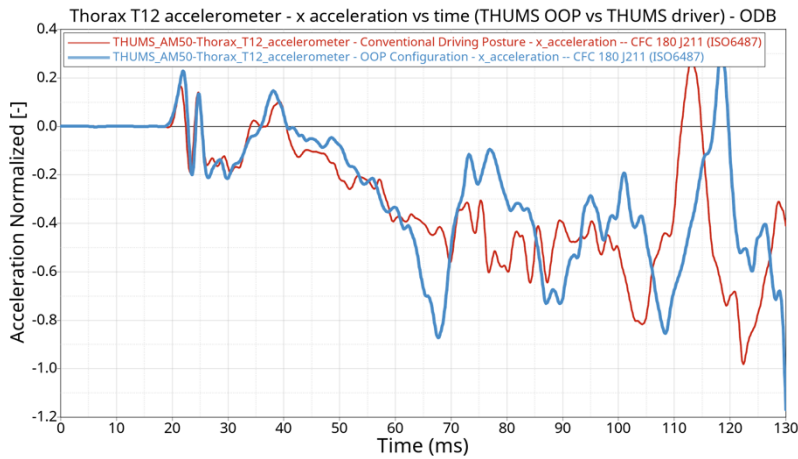


Figure 6.67. THUMS in OOP vs THUMS in driving posture – Thorax T12 – linear x acceleration – ODB

THUMS Pelvis signal

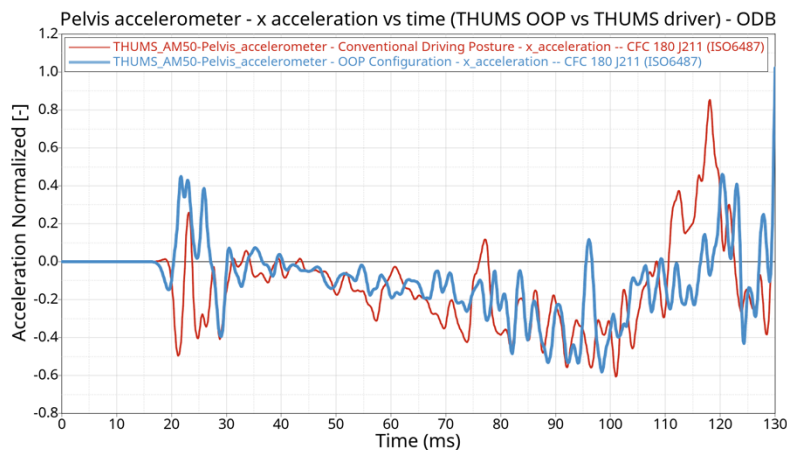


Figure 6.68. THUMS in OOP vs THUMS in driving posture – Pelvis – linear x acceleration – ODB

In Figure 6.68, it is possible to notice that the x acceleration obtained by means of the pelvis accelerometer is quite similar between the two differently positioned THUMS models. Furthermore, the higher values of the pelvis acceleration for the THUMS in conventional driving posture around 110 – 125 ms finds the explanation in Figure 6.47 and 6.48: the pelvis bone performs a negative rotation about its about its y axis, which is not so evident in the THUMS in OOP configuration.

THUMS Legs – Tibia forces

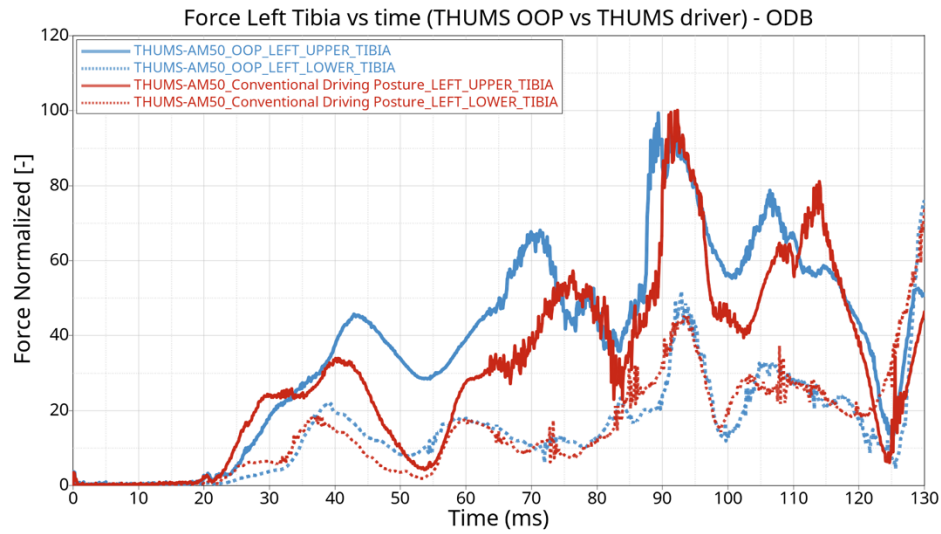


Figure 6.69. Positioned THUMS vs traditional dummy – Left Tibia – Force – ODB

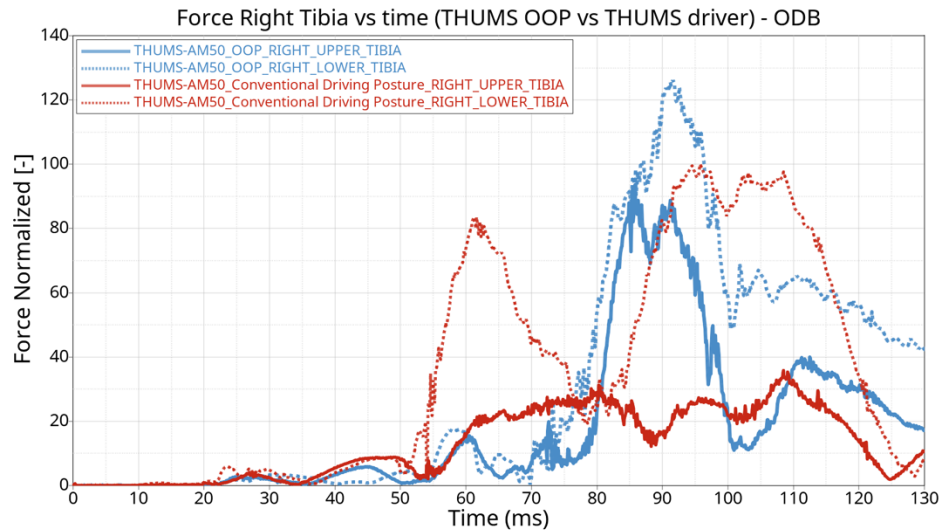


Figure 6.70. Positioned THUMS vs traditional dummy – Right Tibia – Force – ODB

In Figures 6.69 and 6.70, the comparison of the behavior of the tibia forces obtained from the THUMS in-position and OOP models is shown.

With reference to Figure 6.70, the Upper Tibia force of the THUMS in OOP configuration results to be higher (70 – 100 ms) than the one of the HBM in conventional driving posture. This may be caused to the different motion of the two bodies and to the different way in which the right leg hurts the lower part of the dashboard, due to the different initial leg posture.

In particular, since the right foot is initially positioned on the vehicle floor, a discrete displacement of the right leg (knee) towards the +y axis can be observed. This cause a higher tibia bone compression: the lower part of the right leg is contemporary in contact with the vehicle floor and the lower part of the central dashboard.

For what the Figure 6.69 is concerned, no significant variations can be noticed between the two models.

Thesis Final Considerations

In this Thesis work, the use of the Human Body Models for occupant protection evaluation has been investigated, as well as a possible guideline to modify their postures.

The THUMS was positioned in the vehicle internal environment in two different configurations:

- The conventional driving posture
- An Out-of-Position (OOP) configuration, generated basing on statistical researches

The crash impact numerical simulations were based on two frontal reference impact: the Full Width Rigid Barrier (FWRB) and the Offset Deformable Barrier (ODB).

In order to properly set the simulations, additional THUMS FE components have been created (shoe soles, seatbelt, etc.).

In addition, a comparison between the output of the conventional driving posture simulation and of the traditional THOR dummy was performed.

The results reported in this work were obtained by implementing in the HBM the proper sensor system. In the THUMS model, indeed, every physical or biomechanical quantity can be extrapolated and measured. This can be done by applying the sensors in the desired body regions, so as to obtain reliable signals, not influenced by numerical oscillations.

The other great advantage of the HBMs is that they allow the investigation and the analysis of human body postures which are not examinable by using the traditional dummies (e.g. the Out-of-position configuration reported in §4.2 and §6). The second part of this work shows, therefore, that it is possible to position the human body in new and non-conventional occupant postures. Even if the one presented in §4.2 and §6 is not extremely modified with respect to the in-position configuration (i.e. the seat back inclination is unchanged and no seat rotation is applied), it is already possible to observe significantly different results in terms of obtained output quantities and body motion during the impact. As an example, the longitudinal linear head acceleration

measured on the THUMS in OOP configuration during the FWRB impact results to be even lower than the one obtained from the conventional driving posture.

The introduction of those innovative FE models (HBMs) in the automotive safety field is a great improvement, especially if considering the rapid evolutions and innovations implemented in nowadays and future vehicles, also favoured by the introduction of the new technologies (i.e. electrification, automated manoeuvres and computer autopilots, artificial intelligence AI, machine learning techniques etc.)

The occupants' safety remains a fundamental aspect to be evaluated and its study needs to be continuously improved.

In the next future, further advances are planned with reference to this Thesis work, such as the creation of a second THUMS Out-of-Position posture, the implementation of new sensors to obtain supplementary physical and biomechanical data and the different settings of the driver restraint systems.

On the basis of those new analysis it will be even possible to understand if the criteria nowadays used to predict the injuries in the traditional dummies can be still considered useful for the HBMs. In the latter, indeed, the injuries could be directly measured on the models themselves (e.g. rib fractures, thorax deformations, etc.), without the need of implementing equivalent empirical formulae.

On the opposite, even more importantly, in a phase in which the technological development is in rapid evolution (e.g. introduction of Autonomous Vehicles) it will be, probably, more and more important to study and analyse other injury or damage criteria due to the different and new possibilities of "living" the vehicles.

Appendix A

Signals Filtering - SAE Filter J211, Mar 1995 ^[48]

During impact tests, the analysis of the generated acceleration and forces, obtained from sensors implemented in human-like dummies, is generally needed. The methods for assessment of injury potential from impacts are outlined by the Society of Automotive Engineers and the international ISO.

In this Thesis work, the SAE J211 standard is used to filter the analysed accelerations. In particular, this standard “requires signals to be filtered using one of four Channel Frequency Classes (CFC) of low-pass filters and specifies acceptable frequency response for each filter class” [48]. More in details, the CFC 60 and CFC 180 are exploited in this job (ref. Table A.0)

SAE J211, ISO 6487 Filter Classes and Application			
Structural Instrumentation	Accelerometers	Total Vehicle Comparison/Simulations/SLED	CFC 60
		Component Analysis	CFC 600
		Integrations (velocity/displacement)	CFC 180
	Load Cells	Steering Column	CFC 600
		Barrier Force/Seat Belt Load Cells	CFC 60
dummy Instrumentations	Head	Accelerations	CFC 1000
	Neck	Forces	CFC 1000
		Moments	CFC 600
	Thorax	Spine Accelerations	CFC 180
		Rib Accelerations	CFC 1000
		Sternum Accelerations	CFC 1000
		Deflections	CFC 600
	Lumbar	Forces/Moments	CFC 1000
	Pelvis	Accelerations/Forces/Moments	CFC 1000
	Femur/Lower leg	Forces/Moments	CFC 600
Displacements		CFC 600	

Table A.0. SAE J211, ISO 6487 Filter Classes and Applications

Bibliography

- [1] Pictures of the THUMS versions overview: <https://www.greencarcongress.com/2019/02/20190209-thum.html>
- [2] “Development of a Finite Element Model of The Total HUMAN Model for Safety (THUMS) and Application to Injury Reconstruction”, Masami Iwamoto, Yoshikatsu Kisanuki, Isao Watanabe, Katsuya Furusu, Kazuo Miki
Toyota Central R&D Labs., Inc., Aichi, Japan
- [3] “Development of a Finite Element Model of the Human Body”, Kiyoshi Omori, Yuko Nakahira, and Kazuo Miki
Toyota Central R&D Labs., Inc. Nagakute, Aichi 480-1192 Japan
7th European LS-DYNA Users’ Conference – Salzburg 2009
- [4] “Recent advantages in THUMS: development of individual internal organs, brain, small female, and pedestrian model”, Masami Iwamoto, Kiyoshi Omori, Hideyuki Kimpara, Yuko Nakahira, Atsutaka Tamura, Isao Watanabe and Kazuo Miki Junji Hasegawa¹, Fuminori Oshita²
Toyota Central R&D Labs., Inc., Aichi, Japan
¹ Toyota Motor Corporation, Shizuoka, Japan
² Toyota Japan Research Institute, Ltd, Nagoya, Japan
4th European LS-DYNA Users’ Conference – Ulm 2003
- [5] “Documentation - Total Human Model for Safety (THUMS) – THUMS™ - AM50 Pedestrian/Occupant Model Academic Version 4.02_20150527”
May, 2015 TOYOTA MOTOR CORPORATION Toyota Central R&D Labs. Inc.
- [6] “Development of Advanced Human Models in THUMS”, Masami Iwamoto, Yuko Nakahira, Atsutaka Tamura, Hideyuki Kimpara, Isao Watanabe, Kazuo Miki
Toyota Central R&D Labs., Inc. Nagakute, Aichi 480-1192 Japan
6th European LS-DYNA Users’ Conference – Gothenburg 2007
- [7] “Research of the Relationship of Pedestrian Injury to Collision Speed, Car-type, Impact Location and Pedestrian Sizes using Human FE Model (THUMS Version 4)”, Ryosuke Watanabe, Tadasuke Katsuhara, Hiroshi Miyazaki, Yuichi Kitagawa, Tsuyoshi Yasuki, published on *Stapp Car Crash Journal*, Vol. 56 (October 2012), pp. 269-321
Toyota Motor Corporation, Japan
- [8] “Research of Collision Speed Dependency of Pedestrian Head and Chest Injuries using Human FE Model (THUMS Version 4)”, Ryosuke Watanabe, Hiroshi Miyazaki, Yuichi Kitagawa, Tsuyoshi Yasuki, Paper # 11-0043
Toyota Motor Corporation, Japan
- [9] “Development and Validation of the Total Human Model for Safety (THUMS) Version 5 Containing Multiple ID Muscles for Estimating Occupant Motions with Muscle Activation During Side Impacts”, Masami Iwamoto and Yuko Nakahira, published on *Stapp Car Crash Journal*, Vol. 59 (November 2015), pp.53-90
Toyota Central R&D Labs., Inc.

- [10] “*Development and validation of THUMS Version 5 with 1D muscle models for active and passive automotive safety research*”, Hideyuki Kimpara, Member, Yuko Nakahira and Masami Iwamoto
IEEE 2016
- [11] “*Comparison of head and thorax cadaver and Hybrid III responses to a frontal sled deceleration for the validation of a car occupant mathematical model*”, Vezin P., et al. (2001)
Paper presented at 17th ESV Conference, June 4-7, 2011, Amsterdam, The Netherlands
- [12] “*Development of Human-Body Model THUMS Version 6 containing Muscle Controllers and Application to injury Analysis in Frontal Collision after Brake Deceleration*”, Daichi Kato, Yuko Nakahira, Noritoshi Atsumi, Masami Ywamoto
IRCOBI Conference 2018
- [13] “*Development of a Full Human Body Finite Element Model for Blunt Injury Prediction Utilizing a Multi-Modality Medical Imaging Protocol*”, F. Scott Gayzik, Daniel P. Moreno, Nicholas A. Vavalle, Ashley C. Rhyne, Joel D. Stitzel, Virginia Tech – Wake Forest University Center for Injury Biomechanics and Wake Forest University School of Medicine, Department of Biomechanical Engineering
12th International LS-DYNA Users’ Conference – Detroit 2012
- [14] “*Development of the Global Human Body Models Consortium Mid- Sized Male Full Body Model*”, F. Scott Gayzik, Daniel P. Moreno, Nicholas A. Vavalle, Ashley C. Rhyne, Joel D. Stitzel, Virginia Tech – Wake Forest University Center for Injury Biomechanics and Wake Forest University School of Medicine, Department of Biomechanical Engineering, Injury Biomechanics Research
Proceedings of the 39th International Workshop
- [15] “*The VIVA OpenHBM Finite Element 50th Percentile Female Occupant Model: Whole Body Model Development and Kinematic Validation*”, Jonas Östh, Manuel Mendoza-Vazquez, Astrid Linder, Mats Y Svensson, Karin Brodin
IRCOBI Conference 2017
- [16] “*Virtual Vehicle-safety Assessment: Open Source Human Body Models addressing gender diversity (ViVA I)*”, Chalmers Projects
<https://www.chalmers.se/en/projects/Pages/ViVA---Virtual-Vehicle-safety-Assessment---Open-Source-Human-Body-Models-addressing-gender-diversity.aspx>
- [17] “*Implementation and Calibration of the LS-DYNA PID Controller for Female Cervical Muscles*”, Alit Putra, Johan Iraeus, Robert Thomson
Division of Vehicle Safety, Department of Mechanics and Maritime Sciences, Chalmers University of Technology, Gothenburg –Sweden
SAFER – Vehicle and Traffic centre at Chamers – University of Technology
Presentation of Nordic LS-DYNA Users’ Conference, 19 October 2018
- [18] “*Active muscle response using feedback control of a finite element human arm model. Computer Methods in Biomechanics and Biomedical Engineering*”, Osth et al., 2012
- [19] “*Muscle Responses in Dynamic Events- Volunteer Experiments And Numerical Modelling For The Advancement Of Human Body Models For Vehicle Safety Assessment*”, Olafsdottir, 2017
- [20] “*HUMOS: HUMAN Model for Safety – a joint effort towards the development of refined human-like car occupant models*”, Stéphane Robin, LAB PSA Peugeot-Citroën RENAULT, France - Paper number 297
-

- [21] “*Development of a Set of Numerical Human Models for Safety*”, Philippe Vezin, Jean Pierre Verriest¹
*HUMOS2 project coordinator, on behalf of HUMOS2 Consortium
INRETS, Biomechanics and Human Modeling Laboratory, France
- [22] “*Setting the Stage for Autonomous Cars: a Pilot study of Future Autonomous Driving Experiences*”, Ingrid Pettersson¹, I.C. MariAnne Karlsson²
IET Journals, The Institution of Engineering and Technology - Intelligent Transport Systems – Selected Papers from the Vienna Congress (2014) – How to enhance the Sustainable use of ITS
¹ Design & Human Factors, Chalmers University of Technology, Gothenburg 412 96, Sweden
² Volvo Car Corporation, Digital User Experience, Sweden
- [23] “*A Preliminary Analysis of Real-World Crashes Involving Self-Driving Vehicles*”, Brandon Schoettle, Michael Sivak, University of Michigan Transportation Research Institute, UMTRI-2015-34, October 2015
- [24] “*Autonomous Vehicle Safety: An Interdisciplinary Challenge*”, Philip Koopman (Carnegie Mellon University, Pittsburgh PA 15217), Michael Wagner (Edge Case Research LLC)
IEEE - Intelligent Transportation Systems Magazine – Spring 2017
- [25] “*Automated Vehicles, On-Demand Mobility, and Environmental Impacts*”, Jeffery B. Greenblatt¹, Susan Shaheen²
Transportation (MV CHESTER, Section Editor) – Published Online: 21 July 2015, © Springer International Publishing AG 2015
¹ Energy Analyst and Environmental Impacts Division, Lawrence Berkeley National Laboratory, Berkeley, USA
² Transportation Sustainability Research Center, University of California, Berkeley, USA
- [26] “*Autonomous Cars and Society*”, Forrest A. and M. Konca, Worcester Polytechnic Institute, 1 May.
<http://www.wpi.edu/Pubs/E-project/Available/E-project-043007-205701/unrestricted/IQPOVP06B1.pdf> (2007)
- [27] “*Automatic vehicle guidance: the experience of the ARGO autonomous vehicle, World Scientific*”, Broggi A., M. Bertozzi, A. Fascioli and G. Conte, ISBN 981-02-3720-0, pp. 250
<http://millemiglia.ce.unipr.it/ARGO/flyer.pdf> (1999).
- [28] “*Dynamic vision for perception and control of motion*”, Dickmanns E. D., Springer, ISBN 978-1-84628-638-4, 474 pp.
<http://www.springer.com/engineering/mechanical+engineering/book/978-1-84628-637-7> (2007).
- [29] “*EUREKA Network. Programme for a European traffic system with highest efficiency and unprecedented safety (PROMETHEUS)*”, Brussels, Belgium.
[http://www.eurekanetwork.org/project/-/id/45\(2013\)](http://www.eurekanetwork.org/project/-/id/45(2013)). Accessed 20 October 2013..
- [30] “*Human Factors Evaluation of Level 2 and Level 3 Automated Driving Concepts – Concepts of Operation*”, Andrew Marinik, Richard Bishop, Vikki Fitchett, Justin F. Morgan, Tammy E. Trimble and Myra Blanco, NHTSA (www.nhtsa.gov) U.S. Department of Transportation – Technical Report No. DOT HS 812 044, July 2014

- [31] “*Taking Over Control from Highly Automated Vehicles in Complex Traffic Situations: the Role of Traffic Density*”, Christian Gold, Moritz Korber, David Lechner and Klaus Bengler, Institute of Ergonomics, Technical University of Munich, Germany
“Human Factors” – Vol 58, No. 4, June 2016, pp 642-652, Copyright © 2016, Human Factors and Ergonomics Society
- [32] “*Investigating User Needs for Non-Driving-Related Activities During Automated Driving*”, Bastian Pfleging¹, Maurice Rang², Nora Broy³
^{1,2} LMU Munich – Munich, Germany
³ BMW Group – Munich, Germany
- [33] “*Shifting Gears: User Interfaces in the Age of Autonomous Driving*”, A. L. Kun, S. Boll and A. Schmidt
IEE *Pervasive Computing* 15, 1 (Jan 2016), 32-38. DOI: <http://dx.doi.org/10.1109/MPRV.2016.14>
- [34] “*How Will the Driver Sit in an Automated Vehicle? – The Qualitative and Quantitative Descriptions of Non-Driving Postures (NDPs) when Non-Driving-Related-Tasks (NDRTs) are Conducted*”, Yucheng Yang¹, Jan Niklas Klinkner¹, Klaus Bengler¹
¹Chair of Ergonomics, Technical University of Munich, Boltzmannstr. 15, 85747 Garching, Germany
- [35] “*A longitudinal simulator study to explore driver’s behavior during highly-automated driving*” – “*Design Implications of Drivers’ Engagement with Secondary Activities During Highly- Automated Driving – A Longitudinal Simulator Study*”, David R. Large¹, Gary Burnett¹, Andrew Morris², Arun Muthmani², Rebecca Matthias³
Loughborough Institutional Repository, 2017
¹ Human Factors Research Group, University of Nottingham, Nottingham, UK
² Human Loughborough Design School, Loughborough University, Loughborough, UK
³ Jaguar Land Rover Research, International Digital Laboratory, University of Warwick, Coventry, UK
- [36] “*Seating Positions and Activities in Highly Automated Cars – A Qualitative Study of Future Automated Driving Scenarios*”, Sofia Jorlov, Katarina Bohman, Annika Larsson
IRCOBI Conference 2017
- [37] “*Transformation Smoothing to use after Positioning of Finite Element Human Body Models*”, Tomas Janak¹, Yoann Lafon², Philippe Petit³, Philippe Beillas⁴
IRC-18-33, IRCOBI Conference 2018
¹ PhD student in Biomechanics, LBMC, UMR_T9406, Université Claude Bernard Lyon 1 – Ifsttar in Lyon, France
² PhD, Assistant Professor, LBMC, UMR_T9406, Université Claude Bernard Lyon 1 – Ifsttar in Lyon, France
⁴ PhD researcher at the LBMC, UMR_T9406, Université Claude Bernard Lyon 1 – Ifsttar in Lyon, France
³ PhD Research Engineer at the LAB PSA Groupe – Renault in Nanterre, France
- [38] “*PIPER Software Framework and Application: User Guide*”, Version 1.0.1 – July 19, 2017
Position and Personalize Advanced Human Body Models For Injury Prediction (PIPER). Project 605544- 2013-2017.
Project founded by the European Commission within the 7th Framework Programme
- [39] “*The Automotive Body – Volume II: System Design*”, L. Morello, L. R: Rossini, G. Pia, A. Tonoli, ed. Springer
-

- [40] “EuroNCAP Technical Bulletin – Pedestrian Human Model Certification”, Version 1.1 – October 2018 – TB 024, C. Klug, J. Ellway
Application date: January 2019
- [41] “Comparison of Hybrid III and Human Body Model in Head Injury Encountered in Pendulum Impact and Inverted Drop Tests”, Benedetta Arosio, PhD, Politecnico di Milano
TRB First International Roadside Safety Conference, S. Francisco, 14 June 2017
- [42] “Impact Response of Restrained PMHS in Frontal Sled Tests: Skeletal Deformation Patterns Under Seat Belt Loading”, Greg Shaw¹, Dan Parent¹, Sergey Purtsezov, David Lessley¹, Jeff Crandall¹, Richard Kent¹, Herve Guillemot¹, Stephen A. Ridella², Erik Takhounts², Peter Martin², published on *Stapp Car Crash Journal*, vol. 53 (November 2009), pp. 1-48
¹ University of Virginia Center for Applied Biomechanics
² National Highway Traffic Safety Administration
- [43] EuroNCAP Technical Bulletin TB021– “Data format and Injury Criteria Calculation”, Version 2.0, R. Scharam, March 2017:
- [44] “Development of Brain Injury Criteria (BrIC)”, Erik G. Takhounts, Matthew J. Craig, Kevin Moorhouse, Joe McFadden, national Highway Traffic Safety Administration, published on the *Stapp Car Crash Journal*, Vol. 57 (November 2013), pp. 243-266:
- [45] “Crash Analysis Criteria description”, Vers. 1.6.1, Measured data processing vehicle safety workgroup, Algorithm workgroup: D. Cichos (bast), D. de Vogel (Ford), M. Otto (TUV Rheinland), O. Schaar (Delphi), S. Zolsch (National Instruments), in cooperation with the Task Force ISO TS 13499 (ISO-MME), April 2004
- [46] EuroNCAP website:
<https://www.euroncap.com/en/vehicle-safety/the-ratings-explained/adult-occupant-protection/full-width-rigid-barrier/>
- [47] EuroNCAP website:
<https://www.euroncap.com/en/vehicle-safety/the-ratings-explained/adult-occupant-protection/offset-deformable-barrier/>
- [48] “DADiSP / CFC – CFC Channel Frequency Class Module”
DADiSP – The Ultimate Engineering Spreadshit
<https://www.dadisp.com/cfc1.htm>

